Ingo Machenbach

Drinking Water Production by Coagulation and Membrane Filtration

Thesis for the degree doktor ingeniør

Trondheim, September 2007

Norwegian University of Science and Technology
Faculty of Engineering Science and Technology
Department of Hydraulic and Environmental Engineering

NTNU
Innovation and Creativity

NTNU
Norwegian University of Science and Technology

Thesis for the degree doktor ingeniør

Faculty of Engineering Science and Technology
Department of Hydraulic and Environmental Engineering

ISBN 978-82-471-3831-1 (printed version)
ISBN 978-82-471-3845-8 (electronic version)
ISSN 1503-8181

Doctoral theses at NTNU, 2007:175

Printed by NTNU-trykk

Abstract

Drinking water production with low-pressure hollow-fibre membranes is becoming increasingly more widespread as replacement for conventional separation technology. Upstream coagulation can mitigate fouling layer formation on membranes and allows removal of colloidal and soluble compounds smaller than the membrane pores. However, integrating membrane systems with coagulation bears the risk of impaired system performance due to unfavourable aggregate characteristics. This is of particular importance when treating humic substances due to their strong dependence on the solution environment.

The experimental work in this study aimed at finding optimal coagulation, flocculation, and membrane operating conditions for treating a typically Nordic surface water with high humic content. Commercial aluminium-based coagulants and chitosan were applied in the pre-treatment step. Short, controlled flocculation was achieved by using a pipe, jet-mix, or packed-bed flocculator. An outside-in operated ultrafiltration system based on a polymeric hollow-fibre was used as separation unit.

The study showed that optimized coagulation conditions are crucial to successful operation of the membrane unit. For the applied raw water (colour 50 mg Pt/L), a specific aluminium dosage of 3 mg Al/L and a coagulation pH in the range of 6–6.5 were found optimal with respect to permeate quality, membrane operation, and metal residuals. Coagulant dosages exceeding the optimal dosage and a pH drop increased hydraulically not-reversible fouling significantly. Chitosan neither met the expectations for NOM removal for the investigated raw water nor did its use seem favourable in combination with a polymeric membrane.

Controlling floc aggregation can reduce pressure increase rates on the hollow-fibre membrane provided that flocculators are designed for low velocity gradients ($G<30\ s^{-1}$). The packed-bed flocculator outperformed the other floccu-

lators. However, flocculation times longer than 5 minutes should be applied to avoid rapid backwash pressure increases on the membrane.

The membrane system was operated with fluxes in the range of 45–75 LMH during filtration and a 1.5 times higher value during backwashes. Forward filtration without air scouring proved feasible. To improve detachment of fouling layers, vigorous air scouring was used during backwashes. A filtration cycle of 30–60 minutes followed by a backwash interval of about 30 seconds gave good results. Increasing coagulant dosage and flux were the two most significant contributors to hydraulically non-reversible fouling. Water recovery only had a minor effect on the pressure development of the membrane. However, the results suggest that efficient sludge removal from the immersion tank is of importance. Operation at lower NOM concentrations left pressure increase rates unchanged, rendering the application potential of the system highest for NOM-rich surface waters.

Acknowledgements

This thesis is the result of the research work I carried out in the period of 2001–2007 at the Department of Hydraulic and Environmental Engineering, Norwegian University of Science and Technology (NTNU). Over the years, many people have accompanied and supported me. I wish to express my gratitude to everyone who has made this work possible.

In particular, I would like to thank Prof. Hallvard Ødegaard for giving me the opportunity to work in his group, for supervising this research, and for sorting out matters during troublesome times. I also thank Prof. TorOve Leiknes for many fruitful discussions about membrane technology.

To my colleagues at the Department of Hydraulic and Environmental Engineering and SINTEF Water and Environment, thank you for your support and friendship. A special thanks to all administrative, technical, and laboratory staff for their assistance.

Funding for this research was provided by the Norwegian University of Science and Technology and The Research Council of Norway.

I am forever indebted to my parents and my sister for their unconditional support and encouragement whenever I needed it.

And finally, my deepest gratitude to Maja for your love, your endless patience, and for putting up with my seemingly neverending story.

Trondheim, August 2007

Ingo Machenbach

Errata

Page 65, paragraph 3: 10 m/s should read 10m/h

Contents

List of Figures

List of Tables

Abbreviations

AOC	Assimilable organic carbon
ASTM	American Society for Testing and Materials
ATP	Adenosine triphosphate
BDOC	Biodegradable organic carbon
BW	Backwash
CA	Cellulose acetate
CF	Constant flux
Chi	Chitosan
CI	Confidence interval
CIP	Cleaning-in-place
CP	Constant pressure
Da	Dalton
DBPs	Disinfection by-products
CFD	Computational fluid dynamics
DOC	Dissolved organic carbon
EPS	Extracellular polymeric substances
Exp(s)	Experiment(s)
HIV	Human immunodeficiency virus
HS	Humic substances
ICP	Inductively-coupled plasma-emission
I–O	Inside-out
JMF	Jet-mix flocculator
LMH	Membrane flux, expressed as $\mathrm{L\,m^{-2}\,h^{-1}}$
MBR	Membrane bioreactor
MF	Microfiltration
MFI	Modified fouling index
MW	Molecular weight
MWCO	Molecular weight cut-off
NF	Nanofiltration
NOM	Natural organic matter

NTU	Nephelometric turbidity units
O–I	Outside-in
PA	Polyamide
PACl	Polyaluminium chloride
PAH	Polynuclear aromatic hydrocarbons
PAN	Polyacrylonitrile
PBF	Pack-bed flocculator
PCB	Polychlorinated biphenyls
PCR	Polymerase chain reaction
PDADMAC	Polydiallyldimethyl ammonium chloride
PF	Pipe flocculator
PLS	Partial least-squares (projection to latent structures)
PP	Polypropylene
PS	Polystyrene
PSf	Polysulfone
PVC	Polyvinyl chloride
PWP	Pure water permeability
rms	Root-mean-square
rpm	Rounds per minute
TOC	Total organic carbon
SEM	Scanning electron microscope
SDI	Silt density index
SS	Suspended solids
SUVA	Specific UV absorption
TMP	Transmembrane pressure
UF	Ultrafiltration
UV_{254}	Ultraviolet light (subscript denotes wavelength in nm)
UVA	UV absorption
WHO	World Health Organization

Nomenclature

Latin letters

A	m^2	Area
b	various dimensions	Regression coefficients
c	mg L^{-1}	Concentration
D	m^{-1}	Diffusivity
d	m	Diameter
E	W m^{-2}	Area-specific power consumption
$\widehat{E}$	W m^{-3}	Permeate-specific power consumption
f	dimensionless	Hydraulic efficiency
J	L m^{-2} h^{-1}	Membrane flux
G	s^{-1}	Root-mean-square velocity gradient
K	various dimensions	Factor
K'	dimensionless	Factor
k	dimensionless	Number of predictors
L	L m^{-2} h^{-1} bar^{-1}	Permeability
M	kg $kmol^{-1}$	Average molecular weight
m	mbar d^{-1}	Pressure increase rate (slope)
$\dot{m}$	kg s^{-1}	Mass flow
n	dimensionless	Number of observations
P	bar	Pressure
p	dimensionless	Fraction, probability
Q	m^3 h^{-1}	Flow rate
R	m^{-1} *or* J kg^{-1} K^{-1}	Resistance *or* ideal gas constant
$\widehat{R}$	m^{-2}	Specific resistance
r	m	Radius
s	dimensionless	Weighting factor for PLS regression
S	m^{-1}	Specific surface area
T	K	Absolute temperature
t	s	Time

V	m^3	Volume
v	$m\ s^{-1}$	Velocity
w	dimensionless	Water recovery
X	various dimensions	Predictor (independent variable)
x	dimensionless	Specific humidity ratio
Y	various dimensions	Response (dependent variable)
z	m	Ordinate perpendicular to membrane surface

Greek letters

$\dot{\gamma}$	s^{-1}	Shear rate
Δ	dimensionless	Difference, e.g. used for pressure ΔP
δ	m	Thickness
∂	dimensionless	Derivative
ϵ	dimensionless	Fractional porosity, residual error
η	dimensionless	Efficiency
μ	$N\ s\ m^{-2}$	Dynamic water viscosity
ν	dimensionless	Adiabatic factor
ρ	$kg\ m^{-1}$	Density
τ	dimensionless	Tortuosity factor
Φ	dimensionless	Log-removal

Sub- and superscripts

0	Bulk or initial
20°C	Normalized to a temperature of 20°C
$*$	Steady state
a	Dry air
bw	Backwash
B	Brownian
c	Cake
cp	Concentration polarization layer
cr	Critical
f	Filtration
L	Inertial lift
m	Membrane
ma	Moist air
S	Shear-induced
s	Air scouring
t	Tangential or target

p	Pore, particle, or permeate
w	Wall, water, or weighted

Chapter 1

Introduction

1.1 Background

Balancing the risks from microbial pathogens and disinfection by-products (DBPs) confronts water suppliers with a major challenge. While protection from pathogenic organisms is of primary importance in water treatment, DBPs pose health risks during long-term exposure. In view of increasing surface water concentrations of natural organic matter (NOM) in Northern Europe, many water utilities are forced to rethink and enhance their systems. At the same time, focus is drawn on multi-barrier treatment concepts to protect the population from an ever-increasing number of emerging pathogens. The fact that pathogens often have different resistances for chemical disinfectants renders physical removal of microorganisms preferable to chemical inactivation.

Membrane filtration already plays an important and irreplaceable part in drinking water treatment. Owing to unique retention capabilities and versatility, there is good reason to believe that the number of membrane applications in drinking water treatment will increase utterly in the future. With respect to pathogen rejection, unlike other unit processes the barrier function of a membrane commonly remains unimpaired even during suboptimal operation of upstream processes or the membrane unit itself. Consequently, membrane processes are likely to become the barrier-backbone in future water works.

Coagulation-assisted membrane filtration represents an interesting intermediate between the two most prevalent NOM-removal processes, coagulation/rapid media filtration and nanofiltration. Combining coagulation with low-pressure membrane filtration has the potential of alleviating many of the

drawbacks encountered with both conventional NOM-removal methods. Low-pressure membranes represent practically complete barriers to bacteria and larger microorganisms, while virus retention depends mainly on the membrane. Although low-pressure membranes are prone to performance deterioration caused by fouling just as other membranes, the hollow-fibre configuration offers various methods to counteract fouling along with high robustness and compactness.

1.2 Scope and objectives

This research comprises an applied study on low-pressure membrane filtration with upstream coagulation for a surface water with high coagulant demand. The type of raw water chosen for this study resembled the typical characteristics of lake water in the Nordic countries, i.e. elevated NOM concentration, low turbidity, and low buffer capacity. Commonly applied commercial coagulants were used for coagulation. An immersed hollow-fibre membrane operated in outside-in mode formed the core of the separation step. The investigated process scheme involves a number of interdependent variables that affect the treatment efficiency or result. Tab. 1.1 lists the main operating parameters identified and addressed.

The study pursued two primary research goals. Firstly, to establish reasonable operating conditions and performance values for the membrane. When this research was initiated, no experiences with coagulation/immersed hollow-fibre filtration had been reported of in the Nordic countries. In comparison to the most prevalent methods used for NOM-removal in Norway, the investigated process combination has numerous advantages but is not widely applied. One ambition was thus to arrive at recommendations for sound operation and to enable a comparison of this process combination with other methods. The second goal was to investigate the inter-dependencies between the main process variables (Tab. 1.1). The weakest point of this process combination is the coagulation step. In a real-life applications, the raw water quality can be subject to seasonal or sudden variations with the result of inadequate coagulation. Such events may not only affect the permeate quality but also cause a pronounced loss of membrane performance. Knowing the effects of varying pre-treatment conditions on membrane filtration ultimately helps to avoid pitfalls in design and excessive performance loss during operation.

Table 1.1: Variables in coagulation-assisted membrane filtration

Pre-treatment	Membrane separation
Coagulant type and dosage	Apparent forward filtration flux
Coagulation pH	Backwash frequency
Flocculation conditions	Use of air scouring
	Water recovery
	Chemical cleaning

1.3 Structure

Chapter 2 introduces the main contaminants in surface water relevant to this research study, identifies their sizes and properties, and discusses pertinent regulatory aspects of drinking water treatment.

Chapter 3 reviews the salient aspects of membrane filtration, rejection and fouling mechanisms, coagulation and flocculation as well as the rationale of integrated membrane processes. The review focusses on coagulation-assisted low-pressure membrane processes and emphasizes hollow-fibre systems.

Chapter 4 presents the rationale of the study and elucidates the primary advantages of coagulation-assisted membrane filtration compared to direct media filtration and nanofiltration. The objectives and the hypotheses for the study are formulated.

Chapter 5 describes and explains the experimental set-up and protocols in detail. Methods for data evaluation and analytical methods are introduced.

Chapter 6 describes and discusses the results of a preliminary assessment of the raw water and the membrane experiments. Membrane behaviour is further evaluated by statistical modelling.

Chapter 7 concludes the study with a revision of the hypotheses set forth in Chapter 4 and recommendations for operating a coagulation/immersed membrane filtration unit.

Chapter 8 suggests topics for further research.

Chapter 2

Surface water contaminants and treatment

2.1 Natural organic matter

2.1.1 Origin and formation

Surface waters contain diverse types of natural organic matter produced in various environmental systems. NOM maybe washed into water bodies from other ecosystems (allochthonous NOM), for instance by leaching from soils or peat bogs, or originate within a water body (autochthonous NOM), e.g. from release by plankton and bacteria.

A large fraction of NOM present in surface water consists of *humic substances*, which result from the decomposition of plant and animal residues in the hydrological cycle. Formation theories commonly include pathways of microbial transformation, condensation reactions involving polyphenols and quinones, and partial lignin degradation. The chemical nature of humic substances varies considerably with the location. Factors such as soil and vegetation type, climate, topography, and human activity affect the composition and concentration of humic substances in natural waters. The humic fraction of NOM can vary from 35% to 70% between water sources. Humic substances are ubiquitous in the aquatic environment and impart a yellow-brownish colour in water.

The remaining NOM fraction, also called *non-humic substances*, only contributes marginally to colour and constitutes between 30% and 65% of the organic matter in natural water.

2.1.2 Chemical characterization and properties

Humic substances represent a broad class of structurally complex macromolecules. Aquatic humic substances are non-volatile, hydrophobic biopolymers composed of aromatic and aliphatic structures, which contain three main functional groups: carboxylic acid (COOH), phenolic and alcoholic hydroxyl (OH), and methoxy carbonyl groups (C=O) (Thurman 1985). The carboxylic and the phenolic groups have pK_a values between 4 and 6, and between 9 and 11, respectively. Deprotonation of these functional groups renders humic substances negatively charged over the whole pH range relevant to water treatment. Humic substances are operationally divided into three crude fractions based on their solubility in aqueous acids and bases:

Fulvic acids are soluble at any pH and appear light yellow to yellowish-brown in solution. The typical molecular weight range of fulvic acids is 300 to 10 000 Dalton. Fulvic acids constitute the dominating part of humic substances.

Humic acids are insoluble under acidic conditions and precipitate at pH values below 2. Double bonds in the molecular structure are the dominating reason for the strong greyish-brown colour of humic acids. The molecular weight of humic acids ranges from 500 to about 100 000 Dalton.

Humin is the fraction of humic substances that is insoluble in water and black in colour.

The intensity of colour reflects the chemical properties of each of these fractions. The degree of polymerization, the molecular weight, and the carbon content increase with increasing colour intensity. In contrast, the oxygen content, the anionic charge density, and the degree of solubility decrease with increasing colour intensity (Stevenson 1994). Chromophoric groups in the molecular structure are responsible for producing colour. If these groups are present in conjugations, intense colour will develop.

Non-humic substances are predominantly hydrophilic components, such as polysaccharides, lipids, amino acids, and other low molecular weight compounds. Their molecular weight varies from below 1 000 to about 50 000 Dalton. The aromaticity of non-humic substances is lower than that of fulvic and humic acids.

2.1.3 Influence of solution chemistry

The molecular shape of natural organics is strongly affected by solution properties, such as organic concentration, pH, and ionic strength. Ghosh and Schnitzer (1980) reported two common molecular shapes: rigid spherocolloids and flexible linear molecules. Above a critical DOC concentration of 3.5 to 5 g/L, the authors found humic substances to exist as spherocolloids, which they explained by steric size effects.

The ionic strength of the solution affects both size and shape of humic substances. On increasing ionic strength, humic molecules change from the linear to the spherical form and the structure becomes more coiled (Ghosh and Schnitzer 1980). Several investigators demonstrated that the molecular size of humic substances decreases with increasing ionic strength, which can be explained by charge depression (Cornel *et al.* 1986, Jucker and Clark 1994).

The solution pH affects the conformation of humic substances due to its influence on the charge density. Increasing pH increases the charge density due to the dissociation of functional groups. This increases intramolecular repulsion and causes humic molecules to expand in more linear structures. Consequently, the molecular size of humic substances increases with the pH (Cornel *et al.* 1986, Shaw *et al.* 1994). At low pH, contraction occurs due to charge reduction and the humic molecule attains a coiled, spherical shape.

2.1.4 Interactions with solutes

The presence of metal cations, such as Ca^{2+} and Mg^{2+}, affects the speciation and the size of humic substances. Natural organics act as chelating agents for metal ions or bind cations weakly via a charge shielding effect. These interactions become stronger as the charge of the organics increases. In water treatment processes, multivalent cations are applied to effect aggregation of humic substances by charge neutralization (coagulation). The influence of calcium on the size of humic substances depends on the organic concentration. Engebretson and von Wandruszka (1994) found aggregation preferentially to take place in concentrated solutions. At lower concentrations the authors observed smaller molecular sizes, which they attributed to intramolecular contractions.

Humic substances play an important role in the transport and fate of pollutants in natural ecosystems. Trace metals and heavy metals can form soluble complexes with humic substances or associate with organics as colloids. Furthermore, humic substances bind to hydrophobic micropollutants, such as pesticides and herbicides, and can increase their solubility (Hiraide 1992, Österberg *et al.* 1993, Leenheer 1994).

2.1.5 Interactions with inorganic colloids

The colloidal state represents a condition intermediate between true solution, where water constituents are of ionic or molecular dimension, and particulate suspensions, where constituents are sufficiently large to settle under the influence of gravity. The colloidal range extends approximately from 1 nm to 1 µm in particle diameter.

Inorganic colloids in surface water include the oxy/hydroxides of Mn, Fe, Al, and Si, as well as clays (Thurman 1985). Colloids have a high specific surface area and their behaviour in suspension is largely determined by their surface properties and the solution chemistry. At low ionic strength, colloid behaviour is dominated by double-layer interactions. NOM can stabilize colloids due to electrostatic or steric interactions (Tiller and O'Melia 1993). Surfaces of inorganic colloids, such as clays and metal oxides, provide adsorption sites for NOM. Adsorption of NOM occurs under most conditions but decreases with increasing solution pH.

2.1.6 Analytical characterization methods

A common way of assessing the concentration of NOM is to determine the total or dissolved organic carbon (TOC/DOC) content of a water sample. Organic carbon represents a bulk parameter that does not distinguish organic matter by type but can be determined with good accuracy. Two parameters used to assess the biostability of water are based on DOC measurements: (1) biodegradable organic carbon (BDOC), a measure of the immediately degradable DOC fraction upon inoculation with a bacteria culture, and (2) assimilable organic carbon (AOC), the DOC fraction degraded by two specific bacteria strains under non-limiting nutrient conditions.

UV absorbance and colour are colligative properties measured as light absorbency in the UV and visible wavelength range, respectively. UV absorbance is commonly determined at a wavelength of about 254 nm and can be mainly related to the amount of double bonds in aromatic rings. Light absorption in the range of 410–450 nm is used to determine colour. Both spectrophotometric methods are affected by the solution pH resulting in increased absorbencies on increasing pH. In a study including eight Norwegian surfaces waters, Ratnaweera *et al.* (1999) found colour, UV absorbency, and DOC content to be inter-correlated regardless of water source and molecular size fraction.

The ratio of UV absorbance to dissolved organic carbon concentration is referred to as specific UV absorption (SUVA). SUVA can be used as a surrogate

Table 2.1: Nature of NOM and expected removal based on SUVA

SUVA	NOM characteristics	Coagulation	Typical DOC removal*
≥ 4	Mostly aquatic humics High hydrophobicity High MW	NOM controls	>50%
2–4	Aquatic and other NOM Hydrophobic/–philic NOM Mixture of MW	NOM influences	25–50%
<2	Mostly non-humics Low hydrophobicity Low MW	NOM has little influence	<25%

* coagulant-dependent, iron-based coagulants are typically slightly more effective

parameter to characterize the aromatic nature of the dissolved organic carbon. Typical SUVA values range between 2 and 5, a lower ratio indicating a higher content of non-humic substances (Tab. 2.1).

Molecular size or weight fractionation provides essential information as diffusion coefficients and removal efficiencies depend on the size of a solute. Within the wide variety of techniques, chromatographic methods and sequential ultrafiltration are the most commonly applied methods. Chromatographic techniques, such as gel permeation chromatography and size exclusion chromatography, depend on a set of standards, eluents, detectors, and the actual method which can make the comparison of results difficult. UF fractionation is limited by uncertainties with respect to the true MWCO of available membranes and possible membrane-solute interactions (Egeberg *et al.* 2002). A general drawback of fractionation techniques is the partial solute removal that may cause changes in the solution chemistry and thus affect NOM conformation.

Other techniques aim at characterizing NOM with respect to its fractions of different hydrophobicity and charge. Using a sequence of non-ionic, cationic, and anionic resins, Bolto *et al.* (1998) distinguished (1) a very hydrophobic fraction ascribed to humic acids, (2) a weakly hydrophobic fraction ascribed to fulvic acids, (3) a hydrophilic charged fraction ascribed to proteins, amino acids and anionic polysaccharides, and (4) a hydrophilic neutral fraction ascribed to carbohydrates, aldehydes, ketones, and alcohols.

2.1.7 Natural organics in drinking water treatment

NOM may impart an aesthetically undesirable colour, taste, and odour in water but no conclusive evidence has been published as to whether NOM has adverse effects on human health. However, NOM interferes with treatment processes during which potentially harmful compounds may be formed.

In coagulation processes, presence of NOM causes the dominant coagulant demand. In comparison, the charge density of a clay mineral ranges between 0.1 to 1 µeq/mg clay whereas the total charge on aquatic fulvic acid is about 10 to 15 µeq/mg DOC (Van Benschoten and Edzwald 1990*b*).

NOM causes fouling of membranes, reducing the overall process performance and resulting in higher frequency of backwashing and cleaning membrane systems. If activated carbon is used for the removal of micropollutants (e.g. taste and odour, algal toxins, pesticides), NOM competes for adsorption sites, decreasing the efficiency of the adsorption process (Fettig 1999).

In disinfection processes, oxidation of NOM increases the required disinfectant dose and causes formation of disinfection by-products. Typical DBPs formed during chlorination are trihalomethanes, haloacetic acids, and chlorophenols. The formation potential of halogenated DBPs is directly proportional to the aromatic content of the organics and thus correlates well with UV absorption (Singer 1999, Gallard and von Gunten 2002). A number of organochlorine DBPs have been associated with bladder and other cancer forms (Morris *et al.* 1992). The US Environmental Protection Agency issued new regulations in 1998 for controlling the concentration of DBPs in drinking water (US EPA 1998). Unless properly controlled, DBPs and low molecular weight NOM can cause heterotrophic growth in water distribution systems. Due to its lower molecular weight and less complex chemical structure, the non-humic fraction may contribute to a relatively greater part of the BDOC and appears to be difficult to remove.

Furthermore, the efficiency of oxidation processes for removal of iron and manganese can decline at elevated concentrations of NOM (Heinicke *et al.* 2000). Also, corrosion of copper piping may increase as humic substances enhance the solubility of copper corrosion products (Broo *et al.* 1999). As noted earlier, NOM can mobilize heavy metals and organic xenobiotics by complexation reactions. Ultimately, these compounds might be carried through to the consumer.

Removal of NOM can be achieved by a variety of treatment processes and their combinations. The main unit operations may be summarized as:

Enhanced coagulation and floc separation. The most prevalent coagulants are iron and aluminium salts. Polyelectrolytes are applied both as sole coagulant (e.g. chitosan) and flocculation aid. Typical floc separation processes include conventional sedimentation, granular media filtration, dissolved air flotation, and membrane processes with open pore structures (micro- and ultrafiltration).

Membrane filtration. Membranes with tight pore structures (pore size 1–5 nm or MWCO 1–20 kDa) can be applied to achieve direct NOM removal without coagulation. A fundamental study on this topic has been presented by Thorsen (1999).

Ozonation and biofiltration. Ozone oxidizes organic matter to low molecular weight compounds, decreasing colour and UV absorbance almost instantly. However, an appreciable DOC-removal is only obtained in a biologically active filter, which also improves the biostability of the finished water (Camel and Bermond 1998).

Sorption processes. Several different sorbent materials have been investigated and applied for NOM removal with varying success. The most prevalent media are granular activated carbon, anion exchange resins, and a number of metal oxides (Fettig 1999).

2.2 Turbidity

Raw water may contain silts, clays, algae as well as other particulate and colloidal matter that causes turbidity (cloudiness). Turbidity is a measure for the relative sample clarity. Since this optical parameter is inexpensive to determine and measurable online, turbidity is widely used to monitor filtrate quality in filtration plants and commonly included in drinking water standards. Turbidity is undesirable for three principal reasons:

- Particulate matter and colloids that cause turbidity may have pathogens associated with them.
- Turbidity decreases the efficiency of disinfection techniques by shielding pathogens from chemical or thermal damage.
- Inorganic colloids provide attachment sites for heavy metals such as cadmium, mercury, and lead, as well as many toxic organic contaminants such as PCBs, PAHs, and pesticides.
- A hazy or cloudy appearance makes water unappealing to drink and is therefore not accepted by the public.

2.3 Pathogenic microorganisms

Microorganisms present in water include algae, bacteria, crustaceans, helminths, protozoa, rotifiers, and viruses. The commonly recognized waterborne pathogens consist of several groups of viruses, bacteria, and protozoa. Although pathogens have not been investigated in this research, a brief review is given due to their importance for the selection of treatment technology. With respect to coagulation and flocculation, most bacteria and protozoa can be considered as particles, and most viruses as colloidal organic particles.

Infectious diseases caused by pathogenic organisms are the most common and widespread health risk associated with drinking water (World Health Organization 2006). The list of infectious waterborne pathogens and the diseases they cause is quite extensive but the most common manifestation is a mild to acute gastrointestinal illness. However, the consequences of a microbial infection can be dramatic, even lethal, to immunocompromised persons, such as those infected with HIV and patients receiving immunosuppressive therapy (e.g. cancer, chronic rheumatological disease), as well as elderly or very young people whose immune systems are not as active as in healthy adults. Several new pathogens have arisen as problems in drinking water production and distribution in recent years. Changes in human demographics, eating habits, microbial adaptation, and changes in livestock farming practices contribute to the reemergence of waterborne infectious diseases (Theron and Cloete 2002). Meanwhile, consumer immunities to pathogens are declining due to better sanitary conditions, which increases the susceptibility of disease upon failures of water treatment and distribution systems.

Viruses are obligate cell parasites that can only live and reproduce in susceptible host cells. A protein coat (capsid) surrounds the nucleic acid molecule (genome) and provides protection from environmental hazards. Viruses linked to waterborne diseases range from 25 to about 80 nm in size (Tab. A.1). Pathogenic viruses invade cells and take over their machinery, disrupting cell functions or causing death of the cell. Waterborne pathogenic viruses include naturally occurring enteroviruses, rotaviruses, and Hepatitis A. More recently identified pathogens are the enteric adenoviruses, astroviruses, caliciviruses, and the Norwalk family of agents. The predominant viral infections are hepatitis, gastroenteritis, and poliomyelitis.

Bacteria are unicellular, prokaryotic microorganisms that multiply by binary fission. Their cell is enclosed within a membrane of about 100 nm

in thickness. Fundamental cell shapes are circular (coccus), rod (bacillus), curved (vibrio), and spiral (spirillum). Pathogenic bacteria range in length from approximately 0.3 to 20 µm and 0.1 to 1.5 µm in width (Tab. A.2). Waterborne bacterial pathogens include species in the genera *Legionella*, *Salmonella*, *Shigella*, *Vibrio*, *Campylobacter*, *Yersinia*, and toxigenic strains of *Escherichia coli*. Emerging bacterial pathogens are among others non-tuberculous mycobacteria and *Helicobacter pylori*. Bacteria cause a wide range of diseases, such as cholera, typhoid fever, salmonellosis, legionellosis, and various diarrheal diseases.

Protozoa are unicellular eukaryotic microorganisms that lack a cell wall. They have a relatively complex internal structure and pass through several stages during a life cycle. The stages of most protozoa that actively feed and multiply are frequently called trophozoites. In parasitic species this is the stage usually associated with pathogenesis. To survive harsh environmental conditions, some species secrete a protective covering and form a metabolically dormant stage called a cyst, oocyst, or a spore. Encystment protects protozoa from drinking water disinfection efforts and facilitates the spread of disease. Ingestion of cysts or spores can trigger protozoal infections in humans. The smallest waterborne protozoal cysts that can cause disease measure only 3 to 6 µm (Tab. A.3). Key protozoa being studied as agents of waterborne disease are *Giardia lamblia*, *Cryptosporidium parvum*, and *Entamoeba histolytica*. Emerging pathogenic protozoa are microsporidia and *Cyclospora cayetanensis*. Diseases caused by waterborne pathogenic protozoa include amoebic dysentery, amoebic meningoencephalitis, and flagellate diarrhea.

Helminths are worm-like parasites. These invertebrates are characterized by elongated, flat or round bodies and can be separated into flukes (trematodes), tapeworms (cestodes), and roundworms (nematodes). Helminths develop through egg, larval, and adult stages. Although helminths are relatively large (>1 mm long), their eggs and larvae typically have the size of protozoa. Infection is most common and most serious in developing countries with *Ascaris lumbricoides* being one of the prominent species. Generally speaking, infection by waterborne helminths is not a significant risk throughout Europe, but it is of potential concern following the use of untreated wastewater in agricultural irrigation.

In contrast to bacterial pathogens, human enteric viruses and protozoal parasites are environmentally stable, resistant to methods employed to control bacterial pathogens, and have notably low infectious doses. Unlike most viral

and bacterial infections, protozoan diseases are often chronic, lasting months or years. Hence, physical removal of pathogens is an important disinfection issue together with chemical inactivation.

2.4 Water quality standards

Drinking water standards and regulations are in a continuous state of evolution as more research results become available. Notwithstanding considerable differences in regulatory practice and enforced standards between countries, a certain level of agreement is evident with respect to maximum contaminant levels.

2.4.1 Microbial aspects

The first priority of water treatment is to ensure the microbial quality of drinking water. Outbreaks of diseases transmitted by drinking water affect a large number of people within very short time, placing entire communities at risk.

Most pathogens transmitted by water are fecal in origin. With a few exceptions, pathogens usually do not grow and proliferate outside their host, but many survive for long times in water. Water quality monitoring standards commonly include limits for indicator organisms of bacterial and fecal contamination, such as total and thermotolerant coliform bacteria, *E. coli*, enterococci, and aerobic bacteria (colony count). However, no indicator serves to predict the occurrence of all pathogens and the use of indicators is contested. Particularly the presence of protozoan cysts and viruses may remain undetected, since these pathogens are more persistent in the environment than most indicator organisms. In addition to traditional indicators, the Norwegian drinking water regulations employ the spore forming bacterium *Clostridium perfringens* as indicator for environmentally resistant pathogens. New methodologies are emerging to detect both specific pathogens and indicator organisms. Among these are methods based on antibody techniques, gene probes, PCR, flow cytometry, and biosensors.

2.4.2 Chemical aspects

A growing number of chemical contaminants have been regulated over the last decades. As chemical contaminants are normally associated with adverse

health effects only after long-term exposure, they are placed in a lower priority category than microbial contaminants (World Health Organization 2006). Chemical contaminants of relevance in drinking water may have different origin:

- natural sources – arsenic, chromium, fluoride, manganese;
- industrial and anthropogenic sources – heavy metals, volatile organic compounds, and chemicals in treatment additives, linings, and coatings;
- agricultural sources – nitrate, nitrite, and pesticides;
- water treatment – disinfectant and coagulant residuals, DBPs, corrosion products;
- pesticides used for public health purposes; or
- cyanobacterial toxins – for instance microcystin-LR posing a health hazard mainly during bacterial overgrowth events.

2.4.3 Acceptability aspects

Consumers will judge drinking water quality primarily by parameters they are able to perceive with their own senses. Turbidity, colour, smell or taste make water unappealing to drink. Even if such characteristics may not necessarily imply a health risk, they increase public awareness and suspicion towards water supply and supplier. Aesthetic parameters that may give rise to consumer complaints fall into one of these categories:

- taste and odour caused by substances of biological or chemical origin;
- appearance such as colour, turbidity, pH, iron, and manganese; and
- temperature.

The threshold level at which aesthetic parameters are objectionable to consumers varies largely. Unless such parameters are of implicit health significance, acceptability standards are usually enforced at lower priority. However, consumer satisfaction and confidence are important driving forces behind water quality regulations and treatment practice.

2.4.4 Radiological aspects

Radiological contamination of drinking water can originate from naturally occurring radioactive species, technological processes involving naturally radioactive materials, and man-made radionuclides. Compared to all other natural and man-made sources of ionizing radiation, radon (^{222}Rn) in indoor air causes the highest radiation dosage to the public. Elevated, yet not excessively high concentrations of radon have been measured in Norwegian bedrock groundwater. Surface water samples only contained negligible amounts of radon (Strand *et al.* 1998). Current guidelines for radionuclides are based on an effective dose equal to 0.1 mSv from one-year consumption of drinking water (World Health Organization 2006, Norwegian Ministry of Health and Care Services 2001).

2.4.5 Concept of multiple hygienic barriers

Provision of safe drinking water requires careful consideration of measures, from watershed protection to specific water treatment operations and final distribution. The concept of multiple hygienic barriers compiles all aspects of drinking water safety into a holistic water quality management strategy for risk minimization. A hygienic barrier may be generally defined as any measure that

- removes or kills pathogenic agents,
- dilutes or removes chemical or physical constituents, or
- decomposes chemicals or changes their physical condition

to such an extend that their presence no longer poses a risk to human health (Krogh and Hofshagen 1998). The example presented in Tab. 2.2 elucidates the effect of a multiple barrier solution. All three systems achieve a nominal 6-log removal[a] of contaminants. However, as long as only one barrier is present, the integrity of this barrier rather than its removal efficiency determines the safety level. Assuming a 1%-relative annual failure time per barrier, consumers will experience a complete barrier failure (0-log removal) for a total time of about 4 days a year. Each additional barrier reduces the complete barrier failure time by two orders of magnitude regardless of its removal efficiency. Furthermore, the remaining safety level upon a failure event remains higher in return for a small compromise in the time at which the nominal design performance is achieved. The combined action of many barriers with a low removal efficiency may outperform systems having fewer barriers with a higher removal efficiency.

[a] Log removal $\Phi = \log \frac{c_0}{c}$.

Table 2.2: Performance of different barrier systems with a 6-log nominal removal. Example calculated for a relative annual failure time of one percent per barrier (p=0.01)*

Log-removal	One barrier à 6-log	Two barriers à 3-log	Three barriers à 2-log
0	5256.0 min	52.6 min	0.5 min
2			157.7 min
3		175.2 h	
4			262.8 h
6	361.4 d	357.7 d	353.9 d

*p is the average over the total length of all failure events divided by 365 days.

Evaluation of hygienic barriers requires the identification of potential hazards and possible preventive measures, removal efficiencies in water treatment operations, and a risk assessment for barrier failure. All water treatment operations discussed in section 2.1.7 consitute hygienic barriers to a certain extend. However, unit processes differ in efficiency and robustness. Process design criteria for obtaining desired microbial barrier effects are not well-defined. Imposing barriers against chemical pollutants further complicates design issues, since processes removing microbial contaminants do not necessarily address chemical pollutants.

Disinfection, a process for the deliberate reduction of infective agents, usually constitutes the final – and in many cases the only – barrier against pathogenic agents. The most prevalent chemical agents for disinfection are chlorine compounds, chlorine dioxide, and ozone. The theoretical basis for design of chemical disinfection processes is the CT-value, the effective disinfectant concentration c multiplied by the contact time t based on the most resistant pathogen. UV irradiation is receiving increased attention, particulary due to its higher disinfection efficiency with respect to chlorine resistant protozoan cysts. UV disinfection doses are described in terms of emitted lamp power per unit of fluid under irradiation (Ws/m^2). The efficacy of disinfection depends on raw water variables, such as pH, turbidity, and temperature, on mixing conditions, and the pathogen itself. Each type of pathogen may have a different resistance to each disinfectant (Gerba *et al.* 2003). As a result, the barrier effect of disinfection processes is subject to variations and requires the existence of preceding barriers that physically remove pathogens. In his review

on a century with chemical disinfection to suppress the spread of waterborne pathogens Schoenen (2002) concludes:

> "Disinfection of drinking water cannot replace filtration. Disinfection should be used to minimize the residual risk due to the presence of pathogens in water but cannot be used for bringing faecally contaminated water into a hygienically sound condition."

For more than a century, filtration processes have played a significant role in drinking water treatment with respect to pathogen removal. Pathogens are known to attach to particles rendering particle removal an essential aspect of disinfection. Apart from ensuring complete particle removal, membranes are capable of rejecting pathogens directly. Membrane separation therefore constitutes an integral component in a multi-barrier approach for safe drinking water production.

Chapter 3

Membrane filtration of surface water

3.1 Classification of membranes and rejection characteristics

Membrane separation covers the entire size range of water constituents, from particulate matter to mineral salts and dissolved organics (Fig. 3.1). Selection of the suitable membrane process in a given situation involves numerous considerations including an evaluation of the required separation efficiency with respect to present and possible future water quality standards, impacts of possible pre- and posttreatment processes, operating conditions, management of residuals, and treatment cost.

Pressure-driven membrane processes are distinguished by the amount of pressure required to achieve separation and the size of contaminants removed. Micro- and ultrafiltration (MF/UF) are low-pressure processes based on porous membranes, typically operated below 3 bar or up to 0.8 bar of suction pressure. Nanofiltration (NF) relies on semipermeable membranes with further capabilities to remove dissolved compounds. With operating pressures above 3 bar, NF is considered a high-pressure process. Low-pressure membranes are loosely distinguished by their pore size, whereas high-pressure membranes are typically characterized by molecular weight cut-off (MWCO) or salt rejection. The type and number of rejection mechanisms involved in membrane separation varies substantially. Rejection is generally expressed as the fraction of a constituent removed, or

$$R = 1 - \frac{c_p}{c_f} \tag{3.1}$$

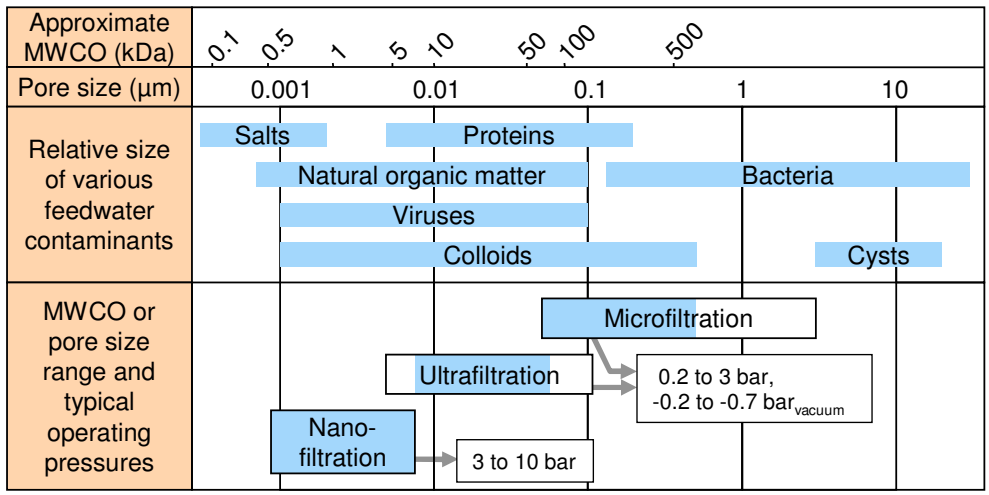

Figure 3.1: Contaminant sizes and membrane processes

where c_p and c_f are the permeate and feed concentrations of the constituent, respectively. Low-pressure MF and UF membranes are intended to separate particulate and colloidal material. Their dominant rejection mechanism is mechanical sieving, although electrostatic interactions, dispersion forces near the pore wall, and hydrophobic bonding strongly affect rejection of materials with dimensions similar to the membrane's pore size (Taylor and Wiesner 1999). Assuming pores of cylindrical geometry and spherical particles, the rejection of particles by physical straining can be estimated as a function of the non-dimensional particle diameter $\lambda = d/d_{pore}$

$$R = \begin{cases} 1 - (1-\lambda)^2 \left[2 - (1-\lambda)^2\right] G & \lambda \leq 1 \\ 1 & \lambda > 1 \end{cases} \tag{3.2}$$

where G is a lag coefficient, empirically estimated as:

$$G = \exp(-0.7146\,\lambda^2) \tag{3.3}$$

It should be noted that cake or gel layers forming on top of the membrane alter the apparent rejection characteristics. Suspended material transported towards a cake may be removed by a straining mechanism at the top. However, material entering the cake may deposit within it due to mechanisms similar to packed-bed filtration, with previously deposited particles acting as particle collectors.

3.1.1 Microfiltration

MF membranes achieve a practically complete removal of suspended solids at higher permeabilities than UF and NF. The pore size of MF membranes ranges from 0.05 to 5 µm (macropores) with a typical pore size between 0.1 and 0.2 µm. Pore size properties above 0.1 µm are assessed by a standard bubble point and mean flow pore test (e.g. ASTM F316-03). MF membranes do not reject dissolved compounds unless they are adsorbed to particles. Hence, removal of NOM is low and depends on the pore size and the membrane material.

Removal of pathogens is limited to bacteria and larger microorganisms. Suchecka *et al.* (2005) determined the pore size properties of 26 commercially available MF membranes and found the maximum pore size 3-4 times larger than the average pore size. Cells were able to penetrate pores significantly smaller than the cell. The maximum rather than the nominal pore size was indicative of cell rejection capabilities. Jacangelo *et al.* (1995) exposed three MF membranes with nominal pore sizes of 0.1 µm and 0.2 µm to MS2 bacteriophages, two bacteria (*P. aeruginosa* and *E. coli*), and two protozoan cysts (*G. muris* and *C. parvum*). The selected membranes removed bacteria and protozoan cysts to less than detection limits. However, rejections of MS2 bacteriophages were less than 1-log and decreased on increasing fluxes. In another pilot study, Karimi *et al.* (1999) studied removal of cyst-sized particles with 0.2-µm MF membranes. Depending on the spiking particle concentration, removal of *Giardia*-sized (5–15 µm) and *Cryptosporidium*-sized (2–5 µm) particles averaged 3.3–4.4 logs and 2.3–3.5 logs, respectively. MF is capable of considerable virus removals depending on membrane and solution properties. Herath *et al.* (1999) studied the removal of four coliphages on two MF membranes with a nominal pore size of 0.05 µm and 0.2 µm. Virus removals varied between 20% and 80% although the average membrane pore measured twice the size of the respective virus. Mono-cultures exhibited the highest retention at a solution pH near the isoelectric point of the species and the lowest removals at alkaline pH. The authors explained this by virus-virus coagulation, which increased slightly in mixed virus cultures. The ionic strength of the feed did not influence virus rejection. Hou *et al.* (1980) reported a 54%-removal of poliovirus from tap water by a 0.22-µm rated cellulose nitrate membrane. Removal increased to 99% by using a positively charged membrane and decreased to 35% for a negatively charged membrane. Additional sieving capabilities of a cake layer and fouling may enhance the extend of virus removal from surface water. Madaeni *et al.* (1995) found the presence of biomass and turbidity in the feed to increase virus removal on a hydrophobic 0.22-µm membrane. SEM micrographs showed that viruses were retained by adsorption onto the membrane

and by formation of a deposit matrix on and within the membrane. The rejection of poliovirus varied with time; after an initial 100%, rejection dropped to 91% and eventually increased again.

3.1.2 Ultrafiltration

UF retains particles, colloids, and macromolecules mainly by size exclusion. Commercial UF membranes typically have pore sizes in the range of 10-50 nm (mesopores) and are frequently characterized by MWCO. Standard methods for assessing the nominal MWCO (e.g. ASTM E1343-90) are based on 90%-retention figures for specific macromolecular solutions. However, results depend strongly on the solute employed for determination, its concentration, solvent characteristics, and flow conditions. In water treatment, the nominal MWCO is a rather inconclusive parameter while the *absolute* cut-off value is decisive for assessing the barrier effect of a membrane (Jacangelo *et al.* 1995). Retention by size exclusion is rather probabilistic in character, since it depends on the size distribution of substances in the feed, the pore size distribution on the membrane surface, and the possibility that potentially permeable species never encounter a large enough pore. In addition, the actual rejection mechanisms involved also depend on the solution chemistry, the nature and type of particles present in suspension, and the operating conditions. Anselme and Jacobs (1996) identified the main rejection mechanisms involved in ultrafiltration:

- physical straining (by membrane, cake and/or gel layer)
- electrostatic repulsion
- adsorption on or in the membrane
- hydraulic factors (flow regime, transmembrane pressure)

Rejection of NOM by UF membranes thus represents a complex issue. Solution parameters that affect conformation of NOM (section 2.1.3) may also affect membrane properties, for instance pH influencing surface charge. Separation of surface water NOM thus differs from that of pure macromolecular solutions. Thorsen (1999) estimated that the true molecular weight of soft-water NOM ranges between 25% and 35% of the given MWCO specification. UF membranes remove significant fractions of NOM depending on their properties.

As long as the membrane integrity is not compromised, UF represents a complete barrier against bacteria and larger microorganisms. Viruses removal

capacities due to sheer size exclusion may be enhanced by similar phenomena as discussed in the previous section. In pilot-scale, Jacangelo *et al.* (1995) observed >6-log removal of MS2 bacteriophages for a 100-kDa membrane, regardless of applied shear forces and operating pressure. Decisive for retention of the smallest pathogenic viruses (25-30 nm) seems to be the existence of abnormally large pores and minor membrane defects. Urase *et al.* (1996) reported less than 2-log removal of 23-nm coliphages in mono-culture at pore size ratings of 20 nm and above. UF membranes with a MWCO of 20 kDa and below exhibited 3 to 6-log removal but never removed the virus completely. The authors explained this by virus leakage through large pores that are not reflected in pore size distributions.

3.1.3 Nanofiltration

The MWCO range of NF membranes extends approximately from 200 to 2 000 Dalton. NF membranes are almost non-porous and solute mass transport is diffusion-controlled. Charge and valency determine the permeability of a solute. Generally, multivalent ions are rejected stronger than monovalent ions. NF membranes are used for softening purposes to remove calcium and magnesium species.

NF processes achieve a separation of NOM from surface water on the order of 90%. Hem and Efraimsen (2001) found the BDOC fraction in NF permeate significantly reduced but measured low retention of compounds contributing to AOC, possibly due to nutrient limitation, particularly phosphorous, in the chosen surface waters.

Theoretically, full rejection of pathogenic species should be anticipated in NF. However, integrity loss and membrane imperfections can cause breakthrough of microorganisms.

3.2 Module configurations

Membranes are assembled into modules that are mounted into pressure vessels or racks. Four major types of modules exist on the market, all of which are used in NOM removal processes. Rotating disc and cylinder modules are more recent designs and not commonly applied. Tab. 3.1 compares advantages and disadvantages of commercially available membrane modules (Aptel and Buckley 1996).

Table 3.1: Comparison of different module types

Criteria	Plate and frame	Spiral-wound	Tubular	Hollow fibre (UF/MF)	Rotating disc or cylinder
Packing density	+	++	–	++(+)	–
Ease of cleaning					
– in situ	+	–	++	–	+
– by backwash	– [1]	–	–	+++	–
Cost of module	+	+++	–	+++	–
Pressure drop	–	++	+++	++	+++
Hold-up volume	+	+	–	++	–
Quality of pre-treatment required	+	–	+++	++	+++

+++ clear advantage

– clear disadvantage

[1] certain modules tolerate backwashing

Hollow-fibre modules are the most prevalent membrane configuration in low-pressure MF and UF processes for surface water treatment. On the basis inner diameter, Mulder (1998) defines hollow fibres (d_i<0.5 mm), capillary (0.5<d_i<10 mm) and tubular membranes (d_i>10 mm). However, membrane manufacturers frequently do not distinguish between the former two categories. Instead, a hollow-fine fibre with inner fibre diameters below 0.1 mm is defined. Although specific dimensions vary by manufacturer, approximate ranges for fiber dimensions are (US EPA 2005):

- Outside diameter: 0.5–2.0 mm
- Inside diameter: 0.3–1.0 mm
- Fiber wall thickness: 0.1–0.6 mm
- Fiber length: 1–2 m

Depending on the permeate flow direction, hollow-fibres are classified as either *inside-out* (I–O) or *outside-in* (O–I) membranes (Fig. 3.2). The I–O flow mode resembles that of a tubular membrane, whereas in O–I, or transversal flow

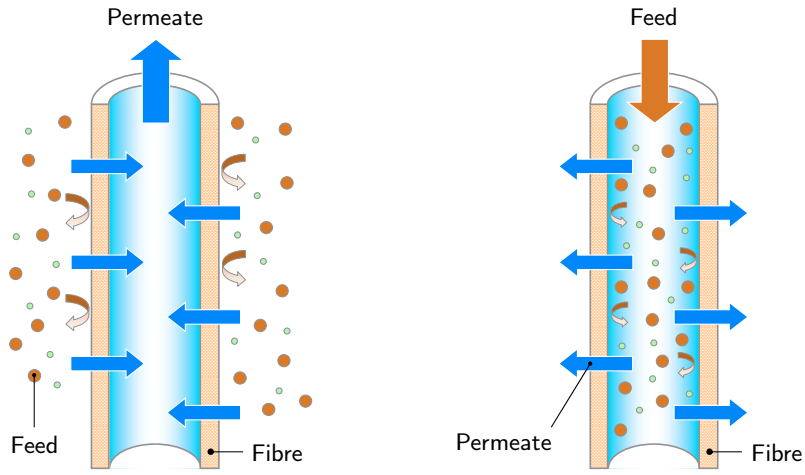

(a) Outside-in (b) Inside-out

Figure 3.2: Types of hollow fibre membranes

mode, permeate is collected on the lumen side. *Encased systems* use modules that consist of fibres sealed into a cylindrical casing with separate connectors for the shell and tube side. Permeate is forced through the membrane at a constant shell or tube side pressure. *Immersed systems* use modules containing O–I fibre bundles mounted loosely on racks that are submerged in a feed tank. Permeate is withdrawn under negative pressure (vacuum), commonly at a constant flow rate.

3.3 Fouling

Membrane systems are prone to fouling, a decrease in permeability over time due to the accumulation of compounds on the membrane surface or within its pores. The hydraulic resistance of the fouling layer often controls permeation, yet its development is generally difficult to predict quantitatively. Substances that cause a permeability decline are collectively called *foulants* and fall within the categories

- *organic* – humic substances, polysaccharides, proteins but also organic polymers used in water treatment processes;
- *biological* – cell debris, microorganisms and associated compounds, including extracellular polymeric substances; and

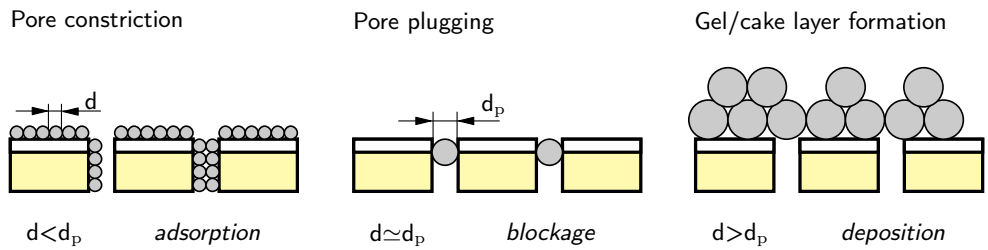

Figure 3.3: Fouling mechanisms in dependence of foulant size

- *inorganic* – clays and silts, precipitates of metals (e.g. iron, manganese), coagulants, and sparingly soluble salts, as well as silicates.

3.3.1 Mechanisms

The pure water flux J across an unfouled membrane can be described by Darcy's law:

$$J = \frac{\Delta P}{\mu\, R_m} \tag{3.4}$$

where ΔP is the transmembrane pressure (TMP), μ is the dynamic water viscosity, and R_m the hydraulic membrane resistance. Convective permeate transport across MF and UF membranes can be modelled assuming Poiseuille flow through a parallel array of uniform capillaries. The resistance of a membrane with an effective pore radius of r_p is then described by

$$R_m = \frac{8\,\delta_m\,\tau}{\epsilon\,{r_p}^2} \tag{3.5}$$

where δ_m is the effective membrane thickness, τ a pore tortuosity factor, and ϵ the membrane porosity. From Eqs. (3.4) and (3.5) it is apparent that (1) temperature affects flux due to its influence on the water viscosity, (2) the membrane resistance decreases with larger pores, and (3) the permeate flux increases proportionally with the TMP. In the presence of foulants, however, deviation from the linear pressure-flux relationship occurs due to blocking or constriction of pores and formation of a layer that causes additional flow resistance (Fig. 3.3). A foulant may be involved in several fouling mechanisms that occur simultaneously.

Adsorptive fouling. Adsorption and deposition of foulants in membrane pores decreases ϵ or r_p and thus increases R_m (Eq. 3.5). The propensity of natural organics to adsorb to membranes depends on their characteristics, the prevailing solution environment, and membrane properties.

Since hydrophobic compounds tend to adhere to surfaces to minimize water contact, adsorption should increase with the hydrophobicity of NOM. Jucker and Clark (1994) reported greater adsorption of the more hydrophobic humic acid than of fulvic acid. Similarly, Schäfer *et al.* (2000) found humic acid to foul a MF membrane faster than fulvic acid. However, in other studies the hydrophilic NOM fraction exhibited the highest fouling potential (Carroll *et al.* 2000, Lin *et al.* 2000). Studies aimed at identifying the molecular size fraction responsible for fouling gave conflicting results. Assuming that solubility is inversely proportional to molecular size, higher molecular weight organics should cause greater adsorption. While some investigators found this hypothesis confirmed (Yuan and Zydney 1999*b*, Lin *et al.* 2000), Carroll *et al.* (2000) identified the low molecular (neutral hydrophilic) NOM fraction to be the major contributor to fouling.

Solution conditions that may exacerbate adsorptive fouling include decreased pH, increased ionic strength, and the presence of divalent cations (Hong and Elimelech 1997). At ambient natural water conditions, NOM and membrane surfaces are negatively charged. Changes in solution pH alter the charge of both and thus influence electrostatic repulsion. At low pH, the charge density of humic substances and the membrane declines, reducing the repulsive forces and allowing greater adsorption (Jucker and Clark 1994, Yoon *et al.* 1998, Jones and O'Melia 2001). Calcium cations may enhance adsorption by reducing the solubility of NOM, by forming intermolecular bridges between humic substances, or by forming salt bridges between negatively charged sites on the membrane (or fouling layer) and NOM (Jucker and Clark 1994, Yuan and Zydney 1999*a*). Yoon *et al.* (1998) attributed increased adsorption at high pH in the presence of calcium to the latter mechanism. Increasing ionic strength compresses the electrical double-layer, which facilitates contact between NOM and membrane surfaces.

Membrane charge arises from the ionization of the membrane polymer's functional groups and is pH-dependent. Higher charge density on the membrane surface is associated with greater membrane hydrophilicity as measured by a contact angle test. Laîné *et al.* (1989) observed that lake water fouled hydrophilic membranes considerably less than hydrophobic ones. Adsorption is generally highest at a pH near the membrane's isoelectric point. Surface modification can render membrane polymers more hydrophilic and less prone

to fouling. After graft-polymerization with polyacrylic acid, Meier-Haack *et al.* (2003) found the flux decline of a modified MF membrane substantially lower than that of the original PP membrane when filtering of a soft surface water with high NOM content.

Colloidal fouling. Suspended particles and colloids are known to foul membranes by depositing onto the upstream face or entering the pores. The rejection of species transported towards the membrane by convection (permeation drag) results in a concentration gradient in the boundary layer. The increasing concentration in this so called *concentration polarization layer* generates a backdiffusion of species into the bulk solution (film theory). Belfort *et al.* (1994) identified three main backtransport mechanisms:

1. *Brownian diffusion*, the random motion of particles due to collisions with surrounding molecules resulting in movement from a region of higher to one of lower concentration
2. *Shear-induced diffusion*, the particle motion originating from random particle-particle interactions and motion in the shear flow of a concentrated suspension.
3. *Inertial lift*, a wall effect that causes a particle in a velocity field to migrate away from both the membrane surface and the flow axis (axial and lateral movement).

At steady state, the convection of solids towards the membrane surface is balanced by backtransport away from the membrane, transmission of solids through the membrane, and the convective flow of particles tangential to the membrane. Neglecting bulk concentration gradients along the feed-side of the membrane and permeation of species, this mass balance may be expressed as

$$J\,c = \underbrace{(D_B + D_S)\,\frac{\partial c}{\partial z} + v_L\,c}_{\text{backtransport}} + J_t\,c \tag{3.6}$$

where D_B and D_S are the Brownian and the shear-induced diffusivity, respectively, v_L the inertial lift velocity, and J_t is a tangential flow component representing transport alongside the membrane. Integration of Eq. (3.6) with the boundary conditions $z = 0 : c = c_0$ and $z = \delta_{cp} : c = c_m$ gives

$$J = \frac{(D_B + D_S)}{\delta_{cp}}\,\ln\frac{c_m}{c_0} + v_L + J_t \tag{3.7}$$

Table 3.2: Backtransport at the membrane-solution interface

Mechanism	Dependency on shear rate $\dot{\gamma}_w$ and particle diameter d_p	Conditions under which dominating
Brownian diffusion	$D_B \equiv K_B \, {d_p}^{-1}$	Low shear, $d_p < 0.1$ µm
Shear-induced diffusion	$D_S \equiv K_S \, {d_p}^2 \, \dot{\gamma}_w$	Intermediate shear, $d_p > 1$ µm
Inertial lift	$v_L \equiv K_L \, {d_p}^3 \, {\dot{\gamma}_w}^2$	High shear, $d_p \gg 1$ µm

where δ_{cp} is the thickness of the boundary layer and c_0, c_m are the concentrations in the bulk and at the membrane surface, respectively. The particle size and the hydrodynamic conditions determine the dominating backtransport mechanism for a particle (Tab. 3.2). It must be noted that other factors influence mass transport in the boundary layer, for instance the solids concentration and the suspension viscosity, which are omitted here. Eq. (3.7) predicts that under mass-transfer-limited conditions the flux performance of a membrane is controlled by the rate at which foulants are transferred *back from* the membrane surface into the bulk fluid. Such conditions will prevail in the higher flux region. Attempting to increase the flux, without providing a compensating mechanism to increase the rate of backtransport, will lead to an accumulation of material on the membrane and in turn decrease the permeability. In the lower flux region, the linear pressure-flux relationship according to Eq. (3.4) applies.

Membrane characteristics that affect colloidal fouling include the relative size of pores to feedwater colloids and the membrane surface topography. If the size range of colloids falls within the same order of magnitude as the membrane pores, pore plugging can occur resulting in rapid permeability decline. Although larger membrane pore size translates into higher initial permeability, the long-term productivity can be lower than for a tighter membrane due to more rapid colloidal fouling. This phenomenon has been observed in numerous studies (Marshall *et al.* 1993) and is further discussed in section 3.4.3. As a rule of thumb, Cheryan (1998) suggested a particle size to pore size ratio of 10 to reduce fouling. Fouling may also be related to surface roughness. Protuberances on the membrane surface can act as "hooks" for colloidal matter and microorganisms, thus leading to greater fouling compared with smooth and uniform surfaces.

The silt density index (SDI) and the modified fouling index (MFI) are well documented methods to assess the colloidal fouling potential of a feed. In both tests, water is filtered through a 0.45-µm membrane in dead-end flow at constant pressure. Boerlage *et al.* (2002) developed a refined protocol of the latter test based on a 13-kDa UF membrane (MFI-UF) to capture smaller particles. However, neither of these tests take shear-dependent backtransport into account and may thus provide misleading results with respect to particle deposition. Furthermore, in membrane systems that allow hydraulic backwashing, the long-term system productivity depends on the fouling removal efficiency.

Biological fouling. Microorganisms may actively colonize the membrane surface and form a biofilm. Bacteria accumulate on surfaces by adhesion and growth and feed on easily assimilable organics. Bonding to the membrane increases with time due to the biosynthesis of adhesive extracellular polymeric substances (EPS). Within the EPS matrix, bacteria concentrate nutrients and trace organics enabling them to survive even in low nutrient environments. The EPS matrix forms a gel-layer that suppresses turbulent mixing at the membrane surface, resulting in enhanced concentration polarization, whereby retained material is captured in the gel (Ridgway and Flemming 1996). Additionally, the flocculated bacteria themselves impart a resistance to filtration. Biofouling is a widespread problem in membrane systems treating surface water and wastewater. Apart from reducing a membrane's productivity, biofouling causes an increased chemical cleaning demand and may reduce the module lifetime.

Biofouling in drinking water applications may be predicted using methods similar to those applied for assessing growth potential in distribution systems. While AOC and BDOC give an indication of the easily biodegradable organic fraction, the actual growth conditions on the membrane surface may not be resembled in a bioassay. A more accurate method to predict biofouling has been introduced by van der Kooij *et al.* (2003). This method entails growing a biofilm on glass rings in a continuous-flow reactor and monitoring the specific biological activity over time (pg ATP cm^{-2} d^{-1}).

Inorganic fouling. All types of membranes may be fouled by the precipitates of metal species, including the oxides/hydroxides and carbonates of calcium, magnesium, iron, and aluminium. Fouling by salts and metal species generally occurs by two processes: (1) precipitation or (2) flocculation on or within the porous structure of the membrane. Precipitation or scale formation on the membrane occurs when solubility limits of salts are exceeded on the feed side.

Scaling is of particular importance in membranes processes capable of rejecting solutes, such as NF and reverse osmosis. A detailed analysis is given by Rautenbach and Albrecht (1989). In integrated membrane processes for drinking water treatment, coagulants may contribute to inorganic fouling depending on their speciation (see 3.4). Changes in the solution environment on the feed side or across the membrane with respect to temperature or pH may lead to precipitative fouling.

Modelling. In practice, the aforementioned fouling mechanisms will occur simultaneously. The *resistance-in-series model* generalizes the Darcy-equation to the case where resistance to filtration is produced by both the membrane and foulants accumulated in, on, or near the membrane. Assuming that osmotic pressure effects are negligible, Eq. (3.4) can be modified

$$J \equiv \frac{1}{A}\frac{dV}{dt} = \frac{\Delta P}{\mu\,(R_m + R_{cp} + R_p + R_c)} \tag{3.8}$$

to include the resistances due to concentration polarization (R_{cp}), internal pore fouling (R_p), and cake formation (R_c). The predominant causes of permeability loss in MF and UF membranes are cake formation, pore blockage, and adsorptive fouling. Its key role in the formation of cake and gel layers notwithstanding, concentration polarization typically exerts a negligible resistance to flow in low-pressure MF and UF, i.e. $R_{cp} \ll R_c$. The resistance of the cake may be expressed as

$$R_c = \widehat{R}_c\,\delta_c \tag{3.9}$$

where $\widehat{R}_c$ is the specific cake resistance and δ_c the cake thickness. Using the Carman-Kozeny equation, $\widehat{R}_c$ of an incompressible cake composed of uniform particles can be estimated:

$$\widehat{R}_c = \frac{K'\,(1-\epsilon_c)^2\,{S_c}^2}{{\epsilon_c}^3} \tag{3.10}$$

where ϵ_c is the cake porosity, S_c the specific surface area per unit particle volume ($S_c = 6/d$ for rigid spherical particles), and the constant $K' \approx 5.0$. Eqs. (3.10) and (3.9) predict that the cake resistance decreases on increasing cake porosity. This partly explains the rationale for feed pretreatment to affect the particle size distribution prior to membrane filtration (section 3.4.3); large particles in the feed form a cake of higher porosity and also respond better to shear-induced backtransport processes (section 3.2). In MF and UF of particle suspensions, however, the cake resistance may quickly exceed the membrane

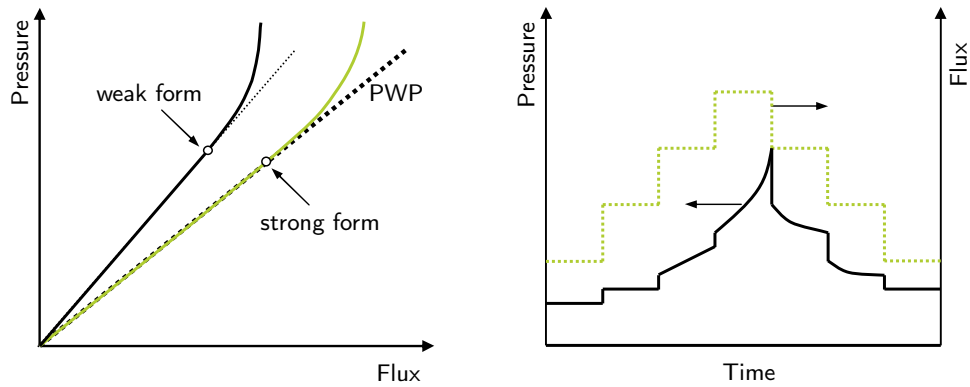

(a) Forms of critical flux (b) Flux-stepping experiment

Figure 3.4: Critical flux

resistance. The cake layer will then act as a "secondary membrane" limiting the overall permeability. In particle filtration, the difference in long-term permeability between MF and UF might therefore be quite small.

3.3.2 Concept of critical flux

In accordance with fundamental particle migration theories discussed in section 3.3.1, a *critical flux* J_{cr} has been defined as a practical criterion for the transition between concentration polarization and fouling. Field *et al.* (1995) first introduced this concept stating that: "The critical flux hypothesis for microfiltration is that on start-up there exists a flux below which a decline of flux does not occur; above it, fouling is observed". Two distinct forms of the concept have been introduced: (1) The *strong form*, referring to the highest attainable flux inducing the same TMP as pure water and (2) the *weak form*, describing the highest flux in the linear flux-pressure region, even if the required TMP is higher than for pure water filtration (Fig. 3.4a). Alternatively, Howell (1995) defined subcritical flux operation as stable filtration at constant permeability for an extended period of time.

In practice, most feed waters contain substances that adsorb to the membrane surface. Adsorptive fouling reduces the membrane permeability quickly and requires chemical cleaning for removal. Consequently, the *weak form* of the critical flux is the more amenable concept in real systems. The most common way of determining J_{cr} experimentally is to increase the flux step-wise for a fixed duration in each step, giving a constant TMP at low fluxes but an

ever-increasing rate of TMP increase beyond J_{cr} (Fig. 3.4b). However, variables influencing such measurements include step duration, step height, initial state of the membrane, feed characteristics, and system hydraulics (Le Clech *et al.* 2003).

Most critical flux studies are concerned with cross-flow MF of larger colloid suspensions (Metsämuuronen *et al.* 2002), particularly biomass suspensions. Chen *et al.* (1997) investigated cross-flow MF and UF of colloidal silica suspensions. Once J_{cr} was exceeded, the authors obtained significant TMP hysteresis when stepping the flux up and down, which they attributed to cake formation. At subcritical conditions, little (MF) or negligible (UF) TMP hysteresis occurred. Kwon *et al.* (2000) found J_{cr} to increase with increasing particle size and increasing cross-flow velocity in MF of spherical PS latex particles. Although varying membrane pore size had virtually no effect on J_{cr}, the authors observed a higher fouling rate at fluxes above J_{cr} for membranes of larger pore size. Higher suspension concentrations reduced J_{cr}. Increasing shear rate promotes backtransport processes and reduces the boundary layer thickness, which in turn can enhance J_{cr}. Choksuchart *et al.* (2002) found air scouring to enhance J_{cr} in immersed UF of coagulated clay suspensions.

Many commercial MF and UF systems are operated without a cross-flow. In these cases, permeability decline is primarily dependent on the transmembrane pressure and the efficacy of the periodic backwashing procedure (Wiesner and Chellam 1999).

3.3.3 Constant pressure vs constant flux filtration

Pressure-driven membrane filters can be operated in either constant pressure (CP) or constant flux (CF) mode (Fig. 3.5). In CF mode, the transmembrane pressure is increased to maintain a preset flow rate across the membrane as it gets fouled. Once a specified terminal pressure is reached, the unit is shut down for recovery cleaning. Since drinking water treatment plants are normally specified by a design flow rate, MF and UF plants are frequently operated in CF mode with periodic backwashing. The disadvantages of CF operation are that increasing pressure may lead to membrane and/or cake compression and decreasing backwash effectiveness. Alternatively, the operating pressure can be held constant, resulting in declining flux. Operation in CP mode may require a larger installed membrane area to meet peak water demands.

Wetterau *et al.* (1996) studied the effects of fouling on cross-flow UF of groundwater and found no significant difference between the two modes of operation. For O–I hollow-fibre MF of a high quality surface water, however,

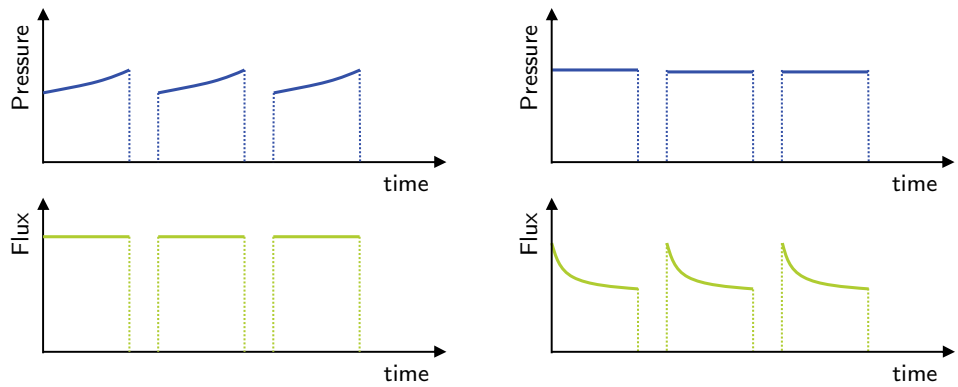

(a) Constant flux (b) Constant pressure

Figure 3.5: Pressure and flux development during different types of membrane operation.

Chellam and Jacangelo (1998) identified CP as the preferred mode of operation based on the cumulative volume filtered per unit membrane between chemical washes. The authors used a direct-flow system, in which the water recovery depended on the backwash frequency. In CF mode, the set flux did not influence the permeability decline of the membrane for a constant recovery. The authors calculated that operation in CF mode increases energy demands but also reduces membrane area significantly compared to CP mode. Tarabara *et al.* (2002) compared both operation modes for cross-flow NF using PS beads in the range of 20-650 nm. Their results indicated the preferential use of CP mode for particle diameters below 100 nm.

3.3.4 Fouling control

Membrane fouling may be reversible or irreversible. *Reversible fouling* refers to the productivity loss that can be restored by hydraulic (backwashing or flushing) or chemical means. In contrast, a permanent loss in productivity is termed *irreversible fouling*. The instantaneous permeability L, often called specific flux, is a suitable parameter for state-monitoring of membranes with respect to fouling:

$$L = \frac{J}{\Delta P} = \frac{1}{\mu \sum_i R_i} \tag{3.11}$$

where $\sum_i R_i$ is the total resistance to filtration. After a certain conditioning phase, the reference permeability L_0 or pure water permeability (PWP) of a

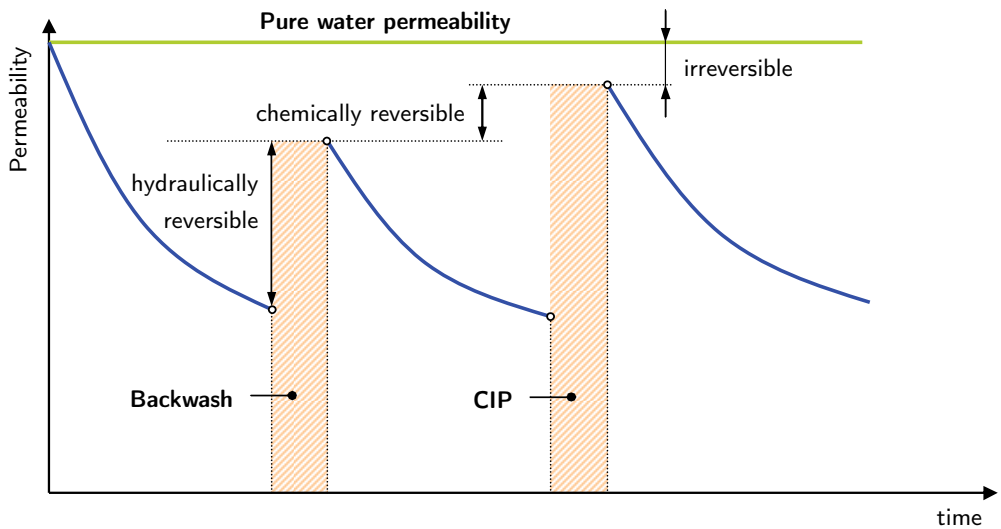

Figure 3.6: Permeability decline and recovery

new membrane is recorded, which allows to resolve fouling into a hydraulically reversible, a chemically reversible, and an irreversible part (Fig. 3.6).

Low-pressure membrane systems employ two methods to control or counteract reversible fouling: backwashing and cleaning-in-place (CIP). For backwashing, the direction of filtrate flow is reversed to dislodge accumulated foulants on the membrane. At the same time, shear forces are created on the feed side to sweep foulants away from the membrane. This may be accomplished by flushing the membrane surface, air scouring, or a combination of both. In some cases or events, chemicals are added to the permeate to increase backwash efficiency or prevent biological growth, which is referred to as chemically enhanced backwash. However, frequent backwashing – typically conducted every 10 to 60 minutes – is not 100% effective. The productivity of the membrane thus decreases with time until a CIP has to be performed. During a CIP, parts of the membrane system are removed from service and exposed to a concentrated cleaning solution. Chlorine, citric acid, and caustic soda are the most common cleaning agents but proprietary detergent solutions are also used. A CIP may consist of several soak cleaning steps to remove chemically reversible fouling. As opposed to backwashing, which is performed automatically and only lasts a few seconds, a CIP requires operator intervention and takes up to 24 hours to complete. Depending on the fouling characteristics of the feed, a CIP is performed once every several weeks and more commonly at greater

than monthly intervals (Malmrose 2003).

Fouling control represents an intricate optimization problem. Backwashing reduces the hydraulic efficiency of a membrane system and CIP causes system-downtime as well as waste disposal cost. The key economic factor in membrane operations is not the operating flux per se, but productivity, expressed as total permeate volume V_p produced between chemical cleanings:

$$V_p = f \int_0^T JA \, \mathrm{d}t \tag{3.12}$$

where T is the time between two chemical cleanings. The hydraulic efficiency f, defined as the ratio of net flux over instantaneous flux, corrects for the permeate volume lost during a backwash (Côté *et al.* 1998):

$$f = \frac{t_f - R\, t_{bw}}{t_f + t_{bw}} \tag{3.13}$$

where t_f and t_{bw} are the durations for filtration and backwashing, respectively, and R is the ratio of backwash to filtration flux. As evident from Eq. (3.12), increasing flux increases the produced permeate volume, though at the expense of more frequent CIP. The increased waste disposal cost and system downtime for a CIP must be valued against the lower investment cost for less installed membrane area.

3.3.5 Fouling issues of hollow-fibre membranes

The aspect ratio (diameter to length) of hollow fibres commonly ranges between 10^{-4} and 10^{-3} to achieve a high packing density, and to prevent fibre collapse during filtration and backwash. However, flow inside low aspect-ratio fibres is associated with a high internal pressure drop, which depends on the inner diameter and the length of the fiber. The change in internal pressure along the fibre leads to an axially dependent flux profile, which in turn gives a non-uniform pattern of foulant deposition (Carroll and Booker 2000, Chang and Fane 2001). The fibre geometry and - in case of O–I fibres - the inter-fibre hydrodynamic environment are important design aspects for module optimization.

The hydrodynamic environment of O–I fibres may be influenced by the liquid velocity and air injection on the feed side. The preferred fibre orientation in such case is vertical, with feed/air flow axial to the fibre (Chang and Fane 2000*b*, Chang and Fane 2000*a*). Bubbles introduced at the bottom end of a

vertically mounted fibre bundle rise due to the buoyancy force and form a slug flow between the fibres. The increasing bubble velocity promotes turbulence alongside the fibre. Chang and Fane (2000*b*) reported enhanced fouling control when combining air injection and axial liquid circulation, which they assumed to be due to

- wall shear caused by two-phase flow;
- turbulence caused by the falling film in the bubble wake;
- fibre shaking caused by bubbling.

However, two-phase filtration was only effective at low liquid velocities. At high liquid flow rate, fibre shaking and filtration performance decreased. In filtration of a yeast suspension, Chang and Fane (2001) observed a lower permeability decline with smaller fibres, which they attributed to enhanced shaking and fibre movement. On the other hand, calculations with a flow model showed that the flux distribution becomes significantly more inhomogeneous with decreasing fibre diameter and longer fibres. In addition, the required suction pressure for maintaining the same average membrane flux increases with a decrease in fibre diameter. In a later publication, Chang *et al.* (2002) applied the previously developed flow model to optimize fibre length and diameter for productivity, packing density, and pressure drop. They calculated an optimal inner fibre diameter between 0.4 and 0.7 mm for fibre lengths from 0.5 to 3 m.

During O–I filtration of suspensions with increased solids concentration, particles may settle in the lower potted end of the fibre bundle or are driven into the top end by the upward liquid velocity, sometimes referred to as *sludging*. Such sludge layers may be difficult to remove by backwashing or CIP. To circumvent this problem, one-header modules have been developed, where only one fibre end is potted into a module element while the other end of each fibre is individually sealed and floats freely in the feed (Voßenkaul and Schäfer 2002).

3.4 Integrated membrane systems with coagulation

Membrane processes can be either used either as stand-alone treatment systems or combined with other processes, such as coagulation, oxidation, or further separation processes based on membranes. The combination of membranes with non-membrane processes is referred to as *integrated membrane system*.

3.4.1 Coagulation

In water treatment, coagulation is used to increase the rate of particle aggregation. Particles suspended in water usually carry a negative charge due to ionization of surface groups, specific adsorption of ions, or ion substitution (isomorphic replacement). The primary particle charge is believed to be balanced by a rigid layer of oppositely charged counterions close to its surface (Stern layer) and an outer *diffuse layer* of broadly distributed ions. The electric potential at the outer surface of the Stern-layer is called *zeta potential*. Together, the surface charge and associated counterion charge constitute the *electrical double layer*. As particles in suspension approach one another, they are affected by repulsive forces from overlapping of their diffuse counterion layers and attractive van der Waals forces. In a stable suspension, repulsive forces prevail over attractive forces and little aggregation occurs. Addition of a coagulant destabilizes a suspension by one or several of these mechanisms:

- *Charge neutralization.* Oppositely charged coagulant species are adsorbed to the particle surface, thereby reducing the thickness of the diffuse counterion layer and thus the repulsive forces. Similarly, surface deposition of a particle on another of opposite charge can give charge neutralization, also called heterocoagulation.
- *Sweep coagulation.* Mechanism specific to hydrolysing metal salt coagulants at pH 6–8 and dosages that exceed the coagulant demand for charge neutralization. Negatively charged particles or NOM become enmeshed in the growing amorphous hydroxide precipitate.

In the destabilization phase, numerous chemical reactions may take place within fractions of a second. Therefore coagulants must be dispersed rapidly and uniformly in water. Initial *flash mixing* is crucial to optimal coagulant performance and utilization. Owing to the low typical coagulant to feed volume ratio on the order of 1:50 000 flash mixers require a proficient engineering design (Kawamura 2000).

Hydrolysing metal salt coagulants. The trivalent salts of aluminium and iron, are widely used in NOM removal processes, with aluminium sulphate $[Al_2(SO_4)_3 \cdot n\,H_2O]$ being the most extensively used agent. In aqueous solution, trivalent metal salts react with alkalinity species to soluble hydrolysis species, according to the sequence

$$Me^{3+} \longrightarrow Me(OH)^{2+} \longrightarrow Me(OH)_2^+ \longrightarrow Me(OH)_3 \longrightarrow Me(OH)_4^-$$

and an amorphous hydroxide precipitate $Me(OH)_{3(am)}$ depending on pH and temperature. These hydrolysis products can adsorb on many particulate surfaces or bind with functional groups of NOM. Pre-hydrolysed coagulants have been used increasingly for several years, particularly polyaluminium chloride (PACl). PACls are produced by controlled neutralization of $AlCl_3$ solutions and characterized by their relative basicity:

$$\text{Basicity}(\%) = \frac{100}{3} \cdot \frac{[OH^-]}{[Al]} \tag{3.14}$$

The basicity affects aluminium speciation and alkalinity consumption upon PACl addition. On increasing basicity, the total Al-fraction in form of a polymeric Al_{13} species increases, which is believed to be highly effective for charge neutralization (Shen and Dempsey 1998). Although their mode of action is not well understood, PACl products outperform alum at low temperatures and are also claimed to have a lower specific sludge production. Since PACl is a partially neutralized coagulant, the water pH is less affected during coagulation, which is of importance when treating soft, low-alkalinity surface waters. Dynamic studies with hydrolysing coagulants have shown that PACls give more rapid flocculation and stronger flocs than alum at equivalent dosages (Gregory and Dupont 2001, Duan and Gregory 2003, Zouboulis and Traskas 2005).

Metal-based coagulants are known to preferentially remove hydrophobic rather than hydrophilic compounds, charged rather than neutral compounds, and high-molecular weight (>10 000 Da) rather than low molecular weight compounds (Carroll *et al.* 2000). Typical TOC removals achieved in coagulation of NOM range between 40% and 60% with the residual TOC being largely composed of low molecular weight, non-polar, neutral compounds. Gregor *et al.* (1997) showed that TOC removal is greater in the pH range for charge-neutralization than in the sweep coagulation range. When using metal-based coagulants for drinking water treatment, the solubility of the hydroxide precipitate must be considered to minimize residual metal concentrations. This is most pronounced for aluminium-based coagulants due to the higher solubility of $Al(OH)_{3(am)}$ in the relevant pH range for water treatment. For alum coagulation, Al is least soluble at pH 6 to 6.3 at 25°C. At decreasing water temperature, minimum solubility shifts towards higher pH in the region 6.5 to 7 (Van Benschoten and Edzwald 1990*a*). For coagulation with PACl, minimum Al solubility occurs near pH 6.5 and minimum solubility is less affected by decreasing temperature.

Polymers. The use of cationic polymers as primary coagulants for NOM removal is well documented in the literature (Bolto *et al.* 1998, Kam and Gregory 2001). Synthetic as well as natural polymers are applied in water treatment processes. Chitosan is the most prominent natural polymer used in water treatment, which is obtained by full or partial deacetylation of chitin. Chitosan is a low to medium-MW heteropolymer consisting of uncharged $N-$acetyl$-\alpha-\text{D}-$ glucosamine and $\alpha-\text{D}-$ glucosamine, which is positively charged below pH 7 due to deprotonation of the amino group. A comprehensive review of water treatment polymers is given by Bolto (1995).

Polymers act as destabilizing agents via a charge neutralization and precipitation mechanism (Bolto 1995). The efficacy of a polymer is primarily determined by its charge density, whereas molecular weight is of subordinate significance. Decreasing pH lowers the charge density of humic substances and can give improved dose efficiencies for NOM removal. Although a colour removal of up to 95% and UVA-removal of 60% can be achieved, TOC removal is usually on the order of 50% (Kvinnesland 2003). Inorganic particles, such as clays, metal oxides and hydroxides, present in water or formed in situ can aid NOM removal due to their adsorption capacities. Combined use of metal-based coagulants and polymers has been shown to give synergistic removal effects. Kawamura (1991) found low dosages of chitosan and sodium alginate to improve turbidity removal in combination with alum. For water from two different sources, Bolto *et al.* (2001) obtained the same removal for colour and UV absorbers when replacing 67% of the alum dose with 0.5 mg/L or 1 mg/L PDADMAC.

The advantages of polymer coagulants include their lower optimal dosage compared to metal-based coagulants, no consumption of alkalinity, decreased sludge production, and less pH-dependent process results. Among the disadvantages of polymer use are a potentially lower NOM removal capability, toxicity concerns of residual monomer concentrations, and cost.

3.4.2 Flocculation

Flocculation refers to a process during which the prevailing hydrodynamic environment promotes interparticle collision for aggregation of primary particles to flocs. Various mechanisms can effect flocculation:

- *Brownian motion* is relatively unimportant in systems with mixing and convection except for very small particles. The particle interaction this mechanism causes is called *perikinetic flocculation.*

- *Differential settling* leads to aggregation in quiescent water, where denser particles settle faster than less dense ones and collide.
- In *laminar shear* particles suspended in a faster moving shear layer are carried into the neighbourhood of particles in the adjacent, slower moving shear layer and eventually come into contact. This process is called *orthokinetic flocculation*.
- In *turbulent flow*, the fluctuating motion of the fluid forms eddies that vary in size. The presence of time-varying velocity gradients within these eddies causes relative motion of entrained particles, which leads to particle collisions.

In flocculators, water is agitated either by paddles (mechanical) or by a routing water through a specific geometry that induces turbulence, for instance pipes, baffled channels, or pebble beds (hydraulic). The jet-mix or submerged jet flocculator is a simple, energy-effective design that has been tested as part of this thesis. A jet-mix flocculator consists of several compartments that are separated by perforated plates. Turbulence is induced by an inlet nozzle creating a water jet in the first chamber and by acceleration of the liquid in the holes of the perforated plates. The principle of submerged jet flocculation has been incorporated previously in treatment processes for drinking water (Sobrinho *et al.* 1996, Jang *et al.* 2005) and wastewater (Watanabe *et al.* 1998). Camp and Stein (1943) developed the root-mean-squared (rms) velocity gradient to quantify mixing in turbulent flocculation by analogy with the shear rate in a simple, one-dimensional, laminar shear flow. Their rms velocity gradient, or G *value*, is given by

$$G = \sqrt{\frac{P}{\mu V}} \tag{3.15}$$

where P is the net power dissipated in the fluid, V is the fluid volume in the vessel, and μ is the dynamic fluid viscosity. Flocculation may be seen as a stepwise process. Following destabilization, G-values in the range of 200–500 s^{-1} are selected to achieve rapid formation of primary particles. In this phase, floc size is relatively unimportant. After about 30 seconds, aggregation of more than 90% of suspended particles will have been effected. Once primary particles have formed, excessive shear forces prevail over the cohesive interparticle forces and thus prevent further aggregation. Hence, to achieve aggregation to flocs lower G-values and longer detention times are required (Tab. 3.3).

The validity of G as a design and scale-up parameter is disputed because it only describes the overall intensity of fluid motion. However, the rate of

Table 3.3: Coagulation and flocculation conditions

Step	Velocity gradient G $[s^{-1}]$	Detention time t_D [s]
Flash mixing[1]	600 – 1 000	1 – 2
Aggregation to microflocs[2]	200 – 500	15 – 30
Aggregation to macroflocs[2]	20 – 50	300 – 1 000

[1] Kawamura (2000), [2] Grohmann (1985)

flocculation also depends on the spatial distribution of a fluid's kinetic energy over the size of the eddies. Furthermore, the local rate of energy dissipation may vary widely with the location, and over several magnitudes. Theoretical calculations by Han and Lawler (1992) showed that fluid shear only controls flocculation at a particle size above 1 µm, while Brownian diffusion controls the relative motion when smaller particles interact. More recent flocculation research has been directed at macroscopic parameters pertaining to floc growth, particularly the transient fractal dimension. However, the current level of understanding of the factors affecting fractal dimension is limited to well-defined model flocculating systems (Thomas *et al.* 1999).

3.4.3 Rationale of membrane filtration with coagulation

Early research on coagulation as pretreatment to low-pressure membrane filtration was conducted by Wiesner *et al.* (1989) and Lahoussine-Turcaud *et al.* (1990). However, many studies focussed on membrane performance enhancement, not NOM removal. In view of colloidal fouling and backtransport mechanisms, several authors hypothesized that coagulation and flocculation increased particle size and charge, reducing pore penetration and deposition on the membrane surface and forming a more porous and reversible fouling layer upon deposition (Fig. 3.7). In the presence of NOM, coagulation reduces adsorptive fouling if the organics are amenable to coagulation. On the other hand, positively charged coagulant species or coagulant-NOM complexes may exacerbate fouling in a similar manner as calcium.

3.4.4 Effect of coagulation on membrane performance

Several authors observed significant improvement of membrane performance after coagulation. Laîné *et al.* (1989) investigated the effect of coagulation on

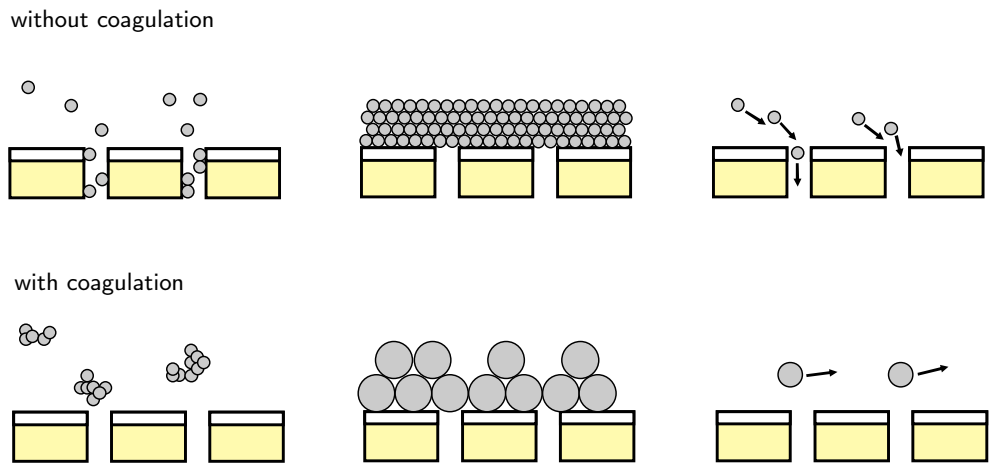

(a) reduced pore fouling (b) more porous cake (c) enhanced backtransport

Figure 3.7: Possible mechanisms for membrane performance enhancement by coagulation

a hydrophilic regenerated CA membrane and a hydrophobic PAN membrane for a reconstituted lake water. The membranes were operated in constant pressure mode. For untreated raw water, the fluxes declined to 20% and 5% of the initial flux for the hydrophilic and hydrophobic membrane, respectively. After coagulation with 60 mg/L PACl, the terminal fluxes were 60% and 10% of the initial membrane flux for the hydrophilic and hydrophobic membrane, respectively. Lahoussine-Turcaud *et al.* (1990) studied coagulation of river water with ferric chloride and PACl before cross-flow UF. Coagulation reduced short-term reversible fouling of a PSf-membrane but did not affect the extend or rate of irreversible fouling. The authors suggested that coagulation redistributes flux decline from chemically to hydrodynamically reversible fouling and attributed irreversible fouling to low MW polysaccharides. Peuchot and Ben Aïm (1992) studied cross-flow filtration of bentonite solutions flocculated with PACl in a stirred filtration cell fitted with a 0.2-µm cellulose ester membrane. Within the studied bentonite concentrations (100 to 500 mg/L), the authors found a 10-fold increase in permeate flux when they applied the optimal flocculant dose as determined in jar-tests and a flocculation G-value of 130 or 200 s^{-1}. No effect of the feed concentration on the permeate flux and quality became apparent in this study although the system was sensitive to flocculant overdosing at low bentonite concentrations. Jack and Clark (1998) treated water

from an agricultural watershed using a powdered activated carbon-UF system. Significant fouling problems occurred as the raw water quality deteriorated. However, addition of 14 mg/L ferric chloride to the UF recirculation loop restored membrane performance to near normal operation. Bian *et al.* (1999) investigated filtration of PACl-coagulated river water (pH 7) with a 150 kDa CA hollow fibre operated in I–O mode and a crossflow velocity of 0.5 m/s. Flux decline was highest for untreated raw water and lowest for a low specific Al-dosage of 1 mg Al/L. Increasing coagulant dosage increased flux decline. Carroll *et al.* (2000) found coagulation of river water to reduce the fouling rate on a PP hollow fibre operated in constant pressure O–I mode. Settling prior to membrane filtration had no effect.

In some studies on NOM removal, coagulation had a detrimental effect on membrane performance. Maartens *et al.* (1999) investigated UF of a surface water with a NOM concentration of 85 mg C/L using an I–O hollow-fibre PSf-membrane with a MWCO of 40 kDa. After coagulation at pH 4.5 with $AlCl_3$ or $CaCO_3$ (1 g/L), the clarified effluent caused more extensive fouling than untreated raw water. Schäfer *et al.* (2001) studied the influence of coagulation on membrane performance for removal of humic and fulvic acid in a stirred cell apparatus. Increasing the iron chloride dosage exacerbated fouling on MF and UF membranes, but reduced the fouling of NF membranes. The authors explained this by the fact that foulants are bound to precipitates that are too large to foul the NF membranes. Based on an economic analysis the study concluded that NF was superior to MF with pre-coagulation for organics removal.

Neither of the cited studies ascertained the mechanisms by which coagulation improved or worsened membrane performance. The usefulness of results obtained in stirred cell experiments is limited for membrane systems with flow conditions that differ largely from the test cell. Furthermore, the raw water matrix influences test results rendering it difficult to compare membrane performance between locations.

3.4.5 Coagulation conditions

The solution environment and coagulant dose affect the size and charge of particles being formed, which in turn influences rejection mechanisms at the membrane surface. Wiesner *et al.* (1989) studied the suspension behaviour of PACl-coagulated humic acid solutions in an unstirred MF-cell. At a specific dosage of 6.8 mg Al/L and below pH 7, particles formed after flocculation were relatively small ($<$0.5 µm). Above pH 7 particle size increased, reaching

a maximum near pH 8. At a lower specific dosage (2.7 mg Al/L), the particle size was consistently larger than 0.5 µm at low pH and reached a maximum near pH 7. The maxima in particle size occurred at minimum zeta potential. Comparing the cumulative filtrate volumes produced over time, increases in pH up to a value of 7.7 increased filtrate production at any time for the higher coagulant dosage (6.8 mg Al/L). Beyond pH 7.7 a reverse trend became apparent. At the lower dosage filtration was most favourable at pH 7.1 producing more filtrate than the best filtrate curve obtained at higher dosage. Veerapaneni *et al.* (1992) studied the performance of a tubular zirconia membrane for filtration of a high-TOC surface water. The optimal coagulation pH for flux increase was about 6 and 5–6 for alum and ferric sulphate, respectively. Lee *et al.* (2000) found alum coagulation in the charge neutralization regime (10 mg/L alum at pH 5) to be more favourable for MF through O–I hollow fibres than sweep floc coagulation (100 mg/L alum at pH 7.5). For cross-flow MF, however, no effect of physicochemical floc properties became apparent. Permeability decline was similar in both coagulation regimes. Judd and Hillis (2001) investigated I–O hollow fibre MF of surface water coagulated with iron salts. Within the dosing range of 1–4 mg Fe/L, the specific cake resistance and the residual cake resistance after backflushing declined on increasing dosage. The authors showed that the effect of iron dosage on cake resistance was more significant than the pH effect for coagulation with PACl reported by Wiesner and co-workers. Pikkarainen *et al.* (2004) coagulated humic water with iron- and aluminium-based coagulants and compared clarification and MF for subsequent particle separation. The iron-based coagulants gave the highest NOM removal around pH 5, outperforming the Al-based coagulants at their optimal pH of 6. Compared to clarification, membrane filtration increased DOC removal for all coagulants except ferric sulphate. Neither the presence of a cake layer nor flocculation affected DOC passage through the membrane. The specific cake resistance decreased with increasing coagulant dose, corroborating earlier findings of Judd and Hillis (2001).

Howe and Clark (2002) compiled the results of a several studies addressing coagulation effects on membrane filtration. All testing was performed in a dead-end filtration cell at constant pressure. Coagulated suspensions were settled and prefiltered through a glass-fibre filter (nominal rating 0.2–0.6 µm) to study fouling of the remaining submicron aggregates after coagulation isolated from particulate fouling effects. Low alum doses exacerbated fouling rates significantly compared to uncoagulated water. Membrane performance improved when a coagulant was dosed in sufficient amounts to remove DOC. Beyond this dosage, fouling decreased on increasing DOC removal (reduced UV absorbance). SEM images showed that less material deposited on the membrane

on increasing coagulant dosage. Rinsing the fouled membrane surface with reagent-grade water was taken to be indicative of the extend of hydraulically reversible fouling. Although coagulation retarded fouling, the proportion of hydraulically reversible flux to total flux remained unchanged for hydrophilic membranes. However, the rinsing procedure did not resemble proper backwashing as in the case of hollow-fibre membranes. Alum, ferric sulphate, and PACl altered membrane performance in a similar manner. A combination of alum and a low dosed cationic polymer (PDADMAC) improved DOC removal and membrane performance. When coagulated suspensions were not prefiltered, fouling was generally reduced. The authors theorized that submicron aggregates become entrapped in a porous cake layer that acts as a dynamic membrane and prevents them from fouling the membrane. Adjusting the coagulation pH to the optimal value for DOC removal generally improved membrane performance. However, in a series of tests with one source water, coagulation at an optimized pH for DOC removal dramatically increased fouling.

3.4.6 Colloidal fouling theory

Following a series of NOM-fractionation and membrane filtration experiments, Howe and Clark (2002) were able to isolate components fouling low-pressure membranes and remove them completely. Foulants did not pass through a 3-kDa regenerated CA-membrane while most of them passed through a 100-kDa CA-membrane. The authors postulated that the physical dimensions of water constituents in general are the key to their fouling propensity in MF and UF processes:

- *Molecular matter (<3 kDa)* is too small to cause a significant reduction in flow path given the pore size of low-pressure membranes.
- *Colloidal matter* of organic and inorganic origin is small enough to enter the membrane pores and large enough to constrict them. Colloids mainly responsible for fouling fall within the approximate size range between 3 nm and 20 nm with larger colloids having a progressively smaller impact. Since the characteristic diffusion time of colloids is up to several orders of magnitude shorter than their detention time in the pore, there is sufficient time for diffusion and adsorption to the pore walls. Multilayer adsorption may explain why MF membranes with large pores can lose capacity very rapidly. The characteristics of the membrane material play an important part for membrane fouling caused by this fraction.

- *Particulate matter (>0.2 µm)* is too large to enter membrane pores but forms cake structures on the membrane surface. The mechanisms for obstructing flow by cake formation are discussed in 3.3.1.

According to this theory, coagulation reduces membrane fouling only if the concentration of small colloids is reduced. Low coagulant doses may exacerbate fouling by either partially reducing the repulsive forces between colloids and membrane thus facilitating adsorption, or by converting non-fouling solutes to small colloids constituting a fouling effect. The theory is consistent with findings of previous research:

1. Humic acid causes more membrane fouling than fulvic acid (Jucker and Clark 1994, Schäfer *et al.* 2000). Fulvic acids are less than 2 nm in size, whereas humic acids are larger and extend across the entire critical size range.

2. Activated carbon adsorption does not reduce fouling (Laîné *et al.* 1989, Carroll *et al.* 2000, Lin *et al.* 2000). A significant part of the adsorption surface exist within micropores of less than 2 nm, which are inaccessible to critical colloids.

3. Pre-settling of solids has no effect on fouling (Carroll *et al.* 2000). Critical colloids have very low settling velocities and will not be removed.

4. Using a series of fractionation steps, Sundaramoorthy *et al.* (2005) removed specific NOM fractions from a bulk surface water. The individual fractions contained either particulate (P), colloidal (C), or dissolved (D) constituents in several combinations. A fouling potential in the order (C)>(C+D)>(bulk water)=(P+C)>(D) became apparent after exposing the coagulated fractions to an immersed hollow-fibre membrane, demonstrating the high fouling potential of colloidal matter.

5. Colligative NOM properties (e.g. DOC, colour, UVA) alone do not serve as predictors for fouling behaviour.

On the other hand, foulants exhibit different affinities for a given membrane material independent of their size. Compounds with a high affinity for the membrane will have a higher tendency to foul the membrane irreversibly, while those with lower affinity may be removed during hydraulic or chemically-enhanced backwashes. Several researchers have identified hydrophilic colloidal and macromolecular organic matter with non-humic properties as major contributor to fouling (Cho *et al.* 1999, Carroll *et al.* 2000, Fan *et al.* 2004). Since

this organic fraction is less amenable to coagulation, irreversible fouling may remain largely unaffected after coagulation pretreatment. Lee *et al.* (2004) found the flux recovery of fouled UF membranes to be higher than that of MF membranes and suggested that fouling of UF membranes is caused mainly by cake/gel layer formation while MF membranes are affected more by pore blockage. These findings favour the use UF membranes in integrated membrane systems based on coagulation.

Chapter 4

Rationale and hypotheses

4.1 Rationale

Surface water is the major raw water source for about 90% of the population in Norway. Many water works treat water from a nearby lake. Due to climatic conditions, Norwegian lake water is generally characterized by low turbidity (<1 NTU), low alkalinity (<0.5 meq/L), low hardness (<5 mg Ca/L), high colour (30–80 mg Pt/L), and high total organic carbon (3–6 mg C/L) (Ødegaard *et al.* 1999). Water works have to ensure final concentrations of colour and TOC lower than 20 mg Pt/L and 5 mg C/L, respectively, to comply with Norwegian and European quality standards for drinking water. Additionally, Norwegian regulations impose the existence of two independent hygienic barriers in each water supply system, one of which must ensure disinfection or other treatment to remove, inactivate, or kill infective agents. A treatment step that qualifies as hygienic barrier shall give inactivation or removal of 99.9% (3-log) for bacteria and viruses and 99% (2-log) for parasite cysts (Norwegian Ministry of Health and Care Services 2001). The two most widely spread technologies for treatment of surface water with elevated NOM concentrations are coagulation/rapid media filtration and nanofiltration. If either of these NOM removal process shall act as hygienic barrier, more stringent rules apply. Coagulation-based systems shall comply with the limits described in Tab. 4.1, while for nanofiltration a maximum nominal pore size of 10 nm and a sufficient cross-flow velocity are required.

Table 4.1: Norwegian drinking water quality standards (selected parameters)

Parameter	Unit	General	Coagulation-based systems*
Colour	mg Pt/L	<20	<10
TOC	mg C/L	<5	<3
Turbidity	NTU	<1	<0.2
Iron	mg/L	<0.2	<0.15
Alumininium	mg/L	<0.2	<0.15

*standards apply for approval as hygienic barrier

4.1.1 Immersed hollow-fibre systems with coagulation

Low-pressure membrane filtration for drinking water production is a fast-growing marked worldwide. In 2004, about 500 plants were in operation with an installed production capacity exceeding 5 million m^3 per day. The largest treatment plants based on low-pressure membranes treat more than 200 000 m^3 of drinking water per day. However, most applications aim primarily at removal of turbidity and microorganisms.

Coagulation and low-pressure membrane filtration of surface water combines aspects of both major NOM removal processes applied in Norway and alleviates many of the drawbacks with each. The technology is slowly extending to the Nordic countries. In 2004, about 60 coagulation-assisted membrane filtration plants were in operation worldwide with an installed capacity of over 1 million m^3 per day.

Due to the high coagulant demand of NOM-rich surface waters, the membrane system has to cope with high suspended solids concentrations in feed and concentrate. However, few membrane configurations tolerate high particle loadings. The call for high packing densities and compactness of membrane systems results in module designs with thin feed flow channels that are prone to clogging. Robust designs, such as tubular modules, tolerate concentrated feeds but have low packing densities (<100 m^2/m^3) and high friction losses. Hollow fibres offer a solution to this dilemma: hollow-fibre membrane systems tolerate high particle concentrations, achieve relatively high compactness, and have low friction losses. Immersed hollow-fibres (O–I) are highly tolerant of particulates, rendering them particularly suitable for treating water with high

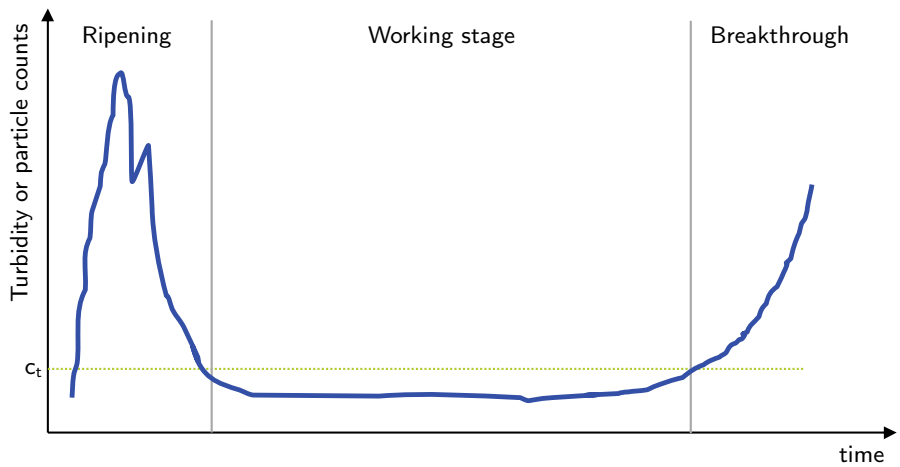

Figure 4.1: Evolution of filtrate quality over a filter cycle in direct filtration (c_t denotes target turbidity or particle counts)

coagulant demand. O–I operated fibres are often reinforced by a braided support that prevents rupture at high shear and increases the fibre ruggedness.

4.1.2 Coagulation-UF versus rapid media filtration

Most Norwegian coagulation-based plants for NOM removal use direct filtration in rapid media filters. Common coagulants are aluminium sulphate (alum), different polyaluminium chlorides, and iron chloride. Non-ionic polymers are frequently applied in low doses to increase the filtration rate and/or filter run time. Replacing a rapid media filter with a hollow-fibre membrane has a number of advantages:

Consistently high permeate quality. Fig. 4.1 shows the typical evolution of filtrate turbidity over a run cycle of a rapid media filter. After an initial spike in turbidity or particle counts, the filter undergoes a ripening period, a working stage, and breakthrough. Filter-to-waste is a common procedure during the ripening period until a desired effluent quality is reached. Filtrate quality can vary during the production period and is affected by several parameters including water pH, coagulant dose, and filtration rate. In comparison, a low-pressure membrane delivers a constant permeate quality with a turbidity of c_{min} or lower during the entire production period. Although the productivity of the membrane system may decline, the retention of particles and large colloids remains unaffected.

High water recovery. Despite water losses occurring during backwashes and filter ripening, rapid media filters usually achieve high water recoveries (>90%). The length of filter run times can be optimized by parameters such as coagulant type and dose, filter aids, composition of the filter bed, filtration rate, and backwash procedures. However, water recovery decreases on increasing coagulant demand, representing a particular problem for treatment of NOM-rich surface waters. The practical water recovery of low-pressure hollow-fibre systems is to a much lesser degree dependent on coagulant dose. Commonly, a net recovery of 95% is achieved, even for treatment of highly coloured surface water.

Simpler backwash procedure. Optimizing backwash procedures for rapid media filters has been a topic of numerous research studies. The backwash procedure strongly affects the filter ripening period, which is rather complex in nature and still not fully understood. The increased passage of particles into the finished water supply during ripening is not typically well-managed. In membrane systems, the permeate quality is unaffected by backwashes. Backwashing is time-controlled, not quality controlled, and the relative backwash time is shorter than in rapid media filtration. However, the fact that permeate is used for backwashing increases water losses and downtime for CIP needs to be taken into account for assessing system availability.

Increased barrier effect. Well-designed and operated direct filtration processes may achieve >3-log removal of protozoan cysts, bacteria and viruses. During ripening, removal is typically moderately lower (0.5–1 log) than during stable operation. However, coagulation failures may severely compromise removal capacity, underscoring the importance of well-controlled coagulation for maintaining the barrier height. Emelko *et al.* (2003) reported increasing passage of oocyst-surrogate particles during the early (0.1–0.3 NTU) and late (>0.3 NTU) breakthrough phase, which indicates that a safety margin should be applied to the practical length of the filter working stage. Rapid media filtration systems have been accredited for 2-log and 1-log removal of protozoan cysts and viruses, respectively. Without upstream coagulation, low-pressure UF systems have received 4-log removal credits for protozoan cysts and bacteria while virus removal credits range between 2 and 3-log (California Department of Health Services 2001). Upstream coagulation can increase virus removal to >4-log (Fiksdal and Leiknes 2004). Consequently, a low-pressure membrane system constitutes an integral barrier within a water treatment plant independent of preceding unit processes. However, microbial reduction figures

deteriorate during breaches of membrane integrity. Sensitive and reliable integrity monitoring is essential to maintaining the barrier height. No single method available to date fulfils all integrity monitoring requirements (Farahbakhsh *et al.* 2003).

4.1.3 Coagulation-UF versus nanofiltration

With over 100 plants in operation, nanofiltration based on spiralwound membrane modules is state-of-the-art technology for surface water treatment in Norway. Plant sizes vary from below 1 000 to 16 000 m^3/d. The membrane unit is preceded by a 50-µm automatically backwashed microsieve or cartridge filter and less commonly by a rapid sand filter. Typically, 8"-spirals in lengths of 1 or 1.5 m are mounted into 4–6 m long element housings. Most plants use CA membranes with nominal pore sizes of 1–5 nm. In comparison, potential advantages of low-pressure hollow-fibre systems with upstream coagulation are:

Higher water recovery. In practice, the water recovery of NF systems is limited to about 75%. Higher recovery exacerbates fouling and increases energy demand for pumping in the recirculation line utterly. In comparison, net recoveries of hollow-fibre systems typically range from 85 to 98%.

Lower energy consumption. NF spirals require a feed pressure of 3–6 bar. To achieve a reasonable water recovery and cross-flow velocity, a large amount of concentrate has to be recycled. The flow in the recirculation line may be as high as the feed flow. Given a specific module pressure drop of 0.2–0.3 bar/m, a significant amount of energy is consumed for pumping. Hollow-fibre systems operate at feed pressures well below 1 bar and without a cross-flow. However, energy savings are offset by coagulant usage, both from point of view of economical as environmental aspects.

Less installed membrane area. Sustainable fluxes achieved on low-pressure hollow-fibre systems filtering coagulated surface water range between 40 and 80 LMH. Compared to common sustainable fluxes of 15–17 LMH for nanofiltration of surface water (Thorsen 1999), low-pressure membrane applications require less installed membrane area, reducing effort for integrity testing and membrane replacement.

Increased fouling control. Spiralwound membranes do not tolerate backwashing. The only fouling control measure during normal operation is the feed cross-flow, which in the case of the Norwegian plants is kept at velocities of 0.1–0.2 m/s. Poor and varying raw water quality may reduce

membrane performance significantly. Manufacturers of spiralwound membranes recommend a maximum feed turbidity of 1 NTU and a maximum feed SDI of 5. Consequently, feed pretreatment is a salient issue in NF applications. Commercial hollow-fibre systems tolerate high particle concentrations and may be backwashed with permeate to remove deposits as discussed in 3.3.4. Chemicals may be dosed into the backwash water to increase the backwash efficiency. Additionally, many hollow-fibre membranes used for surface water filtration consist of polymers with notably higher chlorine resistance (>250 ppm) than CA.

Less frequent chemical cleaning. Spiralwound membrane modules require frequent chemical cleaning and sanitizing. Norwegian NF systems commonly use a daily CIP cycle, which is automatically activated during nighttime and lasts for 1–2 hours. Typical chemicals applied during CIP are chlorine as well as acidic and caustic detergents. Depending on the CIP procedure, the waste volume generated during chemical cleaning corresponds to 0.2–0.5% of the produced permeate volume. In low-pressure hollow-fibre systems, a CIP is performed no more than once every 2 weeks and more commonly at greater than monthly intervals. A CIP cycle requires the system to be removed from service for a duration of 4–12 hours. Monthly CIP wastes are less than 0.05% of the plant flow (Malmrose 2003).

4.2 Hypotheses

Object of this study was an immersed hollow-fibre filtration process with upstream coagulation. One of the objectives of this study was to establish "good practice" operating parameters for a NOM-rich surface water. Furthermore, many of the research studies reviewed in chapter 3.4 have given contradictory results. A straightforward application of previous research to O–I filtration with immersed hollow fibres is thus not possible. To emphasize the main objectives of this research, the following hypothesis were formulated:

A Operation without continuous air scouring is feasible.

While continuous air scouring is a requirement in MBR applications, it is a costly fouling control method in drinking water filtration. Furthermore, air scouring induces turbulence in the immersion tank, which interferes with aggregate formation and settling processes. Although the rate of particle deposition during filtration decreases with continuous air scouring, filtration in the absence of turbulence may promote particle aggregation and thus formation of

a more porous cake that is easily removed by backwashing. Additionally, the immersion tank would serve as settling tank, which allows to withdraw a more concentrated retentate.

B Coagulant dosage requirements decrease.

For aluminium-based coagulants, the practicable pH range for coagulation of humic surface water is primarily determined by the aluminium solubility. According to current Norwegian regulations, residual metal concentrations in the product water must be lower than 0.15 mg/L (Tab. 4.1). In direct filtration with rapid media filters, however, decreasing coagulant dose narrows the practicable pH range for coagulation with respect to aluminium residuals (Eikebrokk 1999), which has been attributed to the formation of alumino-humic colloids that are not retained in the filter bed. Consequently, a minimum threshold dosage must be applied even if a lower dosage would be sufficient with respect to TOC and colour removal.

A 40-nm UF membrane should be capable of separating alumino-humic colloids, rendering the issue of high residual metal concentrations at low coagulant dosages less eminent. Hence, a lower coagulant dosage may be applied that just meets the removal requirements. Studies on the effect of coagulant dosage and coagulation pH on membrane fouling have given conflicting results (section 3.4.5). Furthermore, fouling effects obtained with immersed hollow fibres may differ from other membrane configurations and need to be assessed.

C Chitosan is a suitable coagulant for pre-coagulation.

Sludge production and associated disposal cost are the main disadvantage of using low-pressure membrane technology in combination with coagulation. Although chitosan is costly when treating water with high coagulant demand, sludge production is reduced by some 90% because no hydroxide formation occurs. As opposed to chemical sludges that require landfilling, chitosan sludge is of purely biological nature and may be returned to the environmental cycle, for instance as ingredient in soil amendment or fertilizer products. Compared to aluminium-based coagulants, use of chitosan also circumvents the potential problem of metal residuals in the product water.

D Flocculation has an impact on long-term fouling.

In coagulation-assisted membrane filtration, the objective of flocculation is no longer to create a settleable floc. Flocculation may rather be used to reduce the fouling propensity of the destabilized suspension by influencing particle size and shape. One problem is, however, that the hydrodynamic conditions

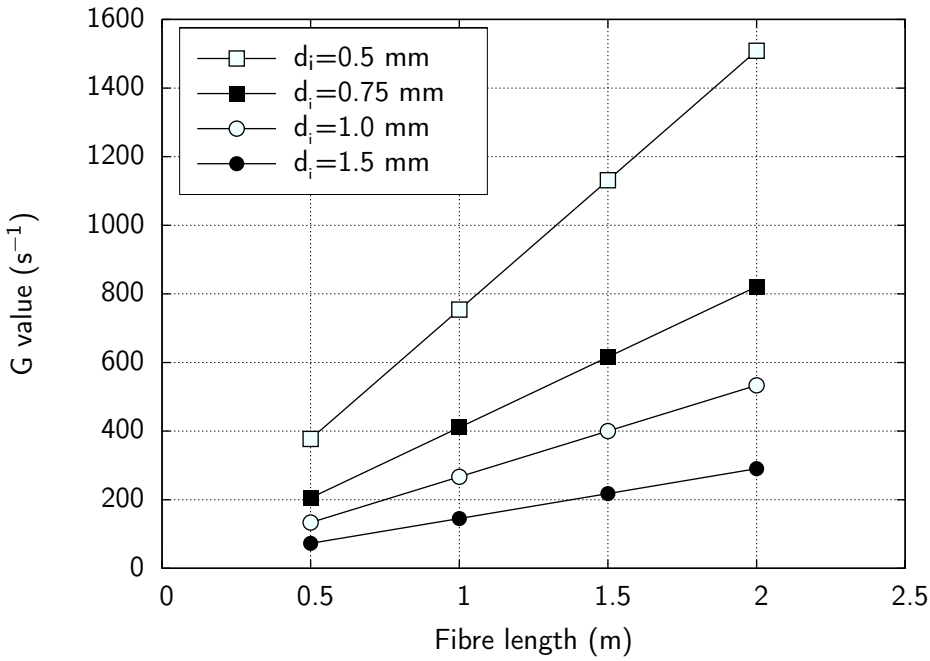

Figure 4.2: Shear conditions at the entrance of I–O fibres in dependence of fibre dimensions (Flux J=30 LMH, operation in dead-end mode).

for flocculation are frequently predetermined by the module or fibre geometry. While efficient flocculation requires low-shear conditions for aggregation to macroflocs (Tab. 3.3) and to prevent floc break-up, many membrane module designs rely on high-shear flow conditions to control particle deposition. Even in the case of dead-end operated I–O fibres, high shear conditions prevailing at the fibre entrance may limit the maximum floc size (Fig. 4.2). Consequently, many studies concluded that flocculation conditions do not influence membrane filtration. On the other hand, Watanabe and Yonekawa (2007) showed that flocculation occurred in within the flow channels of a ceramic membrane despite the small channel diameter (2.5 mm) and short flocculation time (50 s).

In case of immersed O–I fibres, flocculation conditions may have a more pronounced effect. In the absence of air scouring, the flocculated suspension is held at low-shear conditions in the immersion tank, which may promote further aggregation. Larger flocs may increase the porosity of the filter cake that forms on the membrane surface and thus improve backwash effectiveness (Fig. 3.7). Increasing particle size also increases the settling velocity of particles that are eventually withdrawn from the tank bottom. However, since it is difficult

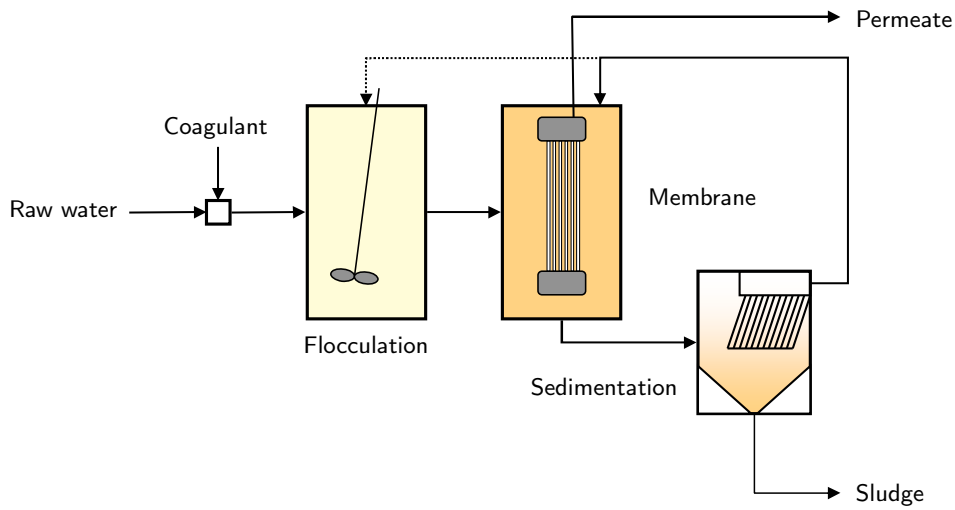

Figure 4.3: Immersed membrane system with post-sedimentation

to optimize hydrodynamic conditions in the immersion tank for flocculation, efficient aggregation of particles will have to occur in a flocculator.

E Water recovery does not influence long-term fouling.

Reducing water recovery decreases fouling in certain membrane applications due to lower concentrations of rejected material in the retentate (see also section 5.2.4). Lower convection of particles towards the membrane will reduce the particle fouling rate, i.e. the pressure increase during a filtration cycle. To maintain a high overall system water recovery (>95%), the retentate could be settled in a compact settling unit (e.g. lamella settler) and the clear phase recycled to the immersion tank or an earlier unit process. In the treatment scheme shown in Fig. 4.3, the membrane would still produce all clean water but with reduced suspended solids exposure.

However, to what extend cake fouling detaches during backwashes depends largely on particle characteristics, which are affected by coagulation and flocculation conditions. The long-term pressure increase rate should therefore remain less influenced by water recovery.

F The optimal coagulation conditions correspond to those for direct media filtration.

Coagulation of surface waters using aluminium-based coagulants has to meet two requirements: (1) adequate removal of NOM, and (2) a residual aluminium

concentration of 0.2 mg/L or less. The dosage minimum to fulfill the former requirement falls within the pH range between 5 and 6, while the lowest aluminium solubility occurs between pH 6 and 7. Similar to rapid media filters, low-pressure membranes practically do not retain dissolved aluminium. Hence, the normal coagulation pH will be between 6 and 7. However, aggregate characteristics change even within this narrow pH range and may thus influence long-term membrane fouling.

G Operation at low NOM concentrations does not decrease fouling rates.

At lower NOM concentrations coagulant demand decreases and so does the particle volume fraction after coagulation. However, particle charge after coagulation/flocculation depends mainly on pH and the specific coagulant dose per unit charge in solution. Assuming that particle characteristics rather than particle concentrations are decisive for long-term fouling, membrane performance should remain largely unaffected when filtering raw water with low NOM concentration through an O–I hollow fibre after optimal coagulation.

4.3 General assumptions

MF versus UF. The study was based on a membrane with a nominal pore size of approximately 40 nm. According to the size ranges depicted in Fig. 3.1, this membrane may be classified as an "open" ultrafiltration membrane. Principally, a membrane in the microfiltration size range would be sufficient to retain aggregates formed upon coagulation of humic water. However, the difference in applied suction pressures between a 40-nm UF and a 0.2-µm MF hollow fibre membrane becomes very small when operated in O–I mode, particularly because the fouling layer will dominate the resistance to flow in a high-solids application. The advantages of using a UF membrane with a lower cut-off are increased retention figures for viruses, increased surface porosity, and a lower risk of pore clogging by particles in the same size range as the membrane pores. Recent findings by Matsushita *et al.* (2005) show that the virus log-reduction for coagulation/microfiltration decreases on increasing pore size from 0.1 µm to 1 µm, which supports the use of UF.

No chemically enhanced backwashes. The membrane unit was operated without chemical addition during backwashes. For immersed systems, chemical use during backwashes may cause formation of unwanted by-products in the immersion tank and thus require more frequent tank drains. Ultimately,

such practice leads to a significant increase of waste volumes and was considered impractical.

Use of a pre-hydrolysed coagulant. The main coagulant used throughout the study was a low-basicity polyaluminium chloride. Chapter 3.4.1 discusses the advantages of pre-hydrolysed coagulants over conventional metal-based coagulants. The water temperature affects performance of PACl to a lesser extent than alum. Since the water temperature varied throughout the experimental period, PACl was considered preferable with respect to reproducibility of data. Nevertheless, a comparison between alum and PACl on some issues was performed.

Iron-based coagulants were not investigated in this study. Ferric chloride is capable of removing a somewhat larger fraction of organic carbon than aluminium-based coagulants. However, the optimum pH for coagulation of humic substances with ferric chloride ranges between 4–5 and is thus lower than the recommended pH range for the membrane used in the study (Tab. D.2). Although certain ferric coagulants are less expensive than aluminium-based ones, sludge production is higher with ferric coagulants at equivalent NOM removal ratios.

Chapter 5

Materials and methods

5.1 Preliminary bench-scale study

5.1.1 Raw water

A NOM-rich, reconstituted natural raw water resembling Nordic surface water conditions was prepared by adding a NOM concentrate to local (Trondheim) tap water in an approximate dilution of 1:350. The concentrate was the spent alkaline regenerant solution from an inland water works using anion exchange for NOM removal. Water treatment at the local water works includes CO_2 addition and filtration through calcium carbonate bed for corrosion control as well as chlorine disinfection. The composition of local tap water (diluant) and the humic raw water after concentrate addition are shown in Tab. 5.1. Due to a salinity of about 95 mS/cm in the NOM concentrate, the conductivity increased by a factor of 3.5 over that of tap water. Raw water was adjusted to pH 7 with concentrated HCl. A fresh 25-L batch of raw water was prepared for each set of jar-tests.

5.1.2 Coagulants

Three commercial coagulants were used throughout the study, two metal-based coagulants and one organic biopolymer:

1. Aluminium sulphate, granulated (Kemira ALG), abbreviated *alum*.
2. Polyaluminium chloride, low basicity (Kemira PAX-16, OH/Al ratio 1.05), abbreviated *PACl*.

Table 5.1: Composition of raw water compared to tap water

Parameter	Unit	Tap water	Raw water
Colour*	mg Pt/L	13 ± 1	50 ± 3
UV_{254} absorption*	m^{-1}	8.9 ± 0.25	31 ± 1.1
DOC	mg C/L	2.4 ± 0.3	6.3 ± 0.25
Alkalinity	mmol/L	1	1
SUVA	m^{-1} mg^{-1} L	3.7	4.9
Conductivity	µS/cm	133	470
Turbidity	NTU	0.2	<0.3

*values measured at pH 7

3. Ground chitosan (Primex ChitoClear™, degree of deacetylation 94%, approximate MW 80 000 g/mol, charge density 4.5 meq/g at pH 6).

Granulated alum was dissolved in distilled water to give a specific aluminium concentration of 0.83% in the working solution. PACl was diluted 1:3 in distilled water to obtain a working solution. A 1-g/L chitosan working solution was prepared by slowly adding ground chitosan to tap water. For rapid dissolution, the pH was kept in the range of 3.5–4 using 0.1 M hydrochloric acid. Working solutions were freshly prepared for each set of jar tests.

5.1.3 Jar-test protocol

Coagulant performance was assessed using a lab-scale batch flocculator system (Kemira flocculator model 90). The paddle speed programme was set to an initial 60 s of rapid mixing at 400 rpm followed by 20 min of slow mixing (flocculation) at 30 rpm. A subsequent sedimentation step was omitted. Raw water was filled into 1-L jar-test beakers and adjusted with an adequate amount of 0.1 M HCl to obtain final coagulation pH values of 6.2–6.3 and 5 for the aluminium coagulants and chitosan, respectively. Coagulant was dosed with an automatic pipette near the paddles to achieve rapid dispersion during the early phase of rapid mixing (Korpijärvi *et al.* 2000).

Immediately after flocculation, a 50-mL sample was withdrawn for zeta potential measurements. Depending on coagulant dosage, 100–200 mL of the

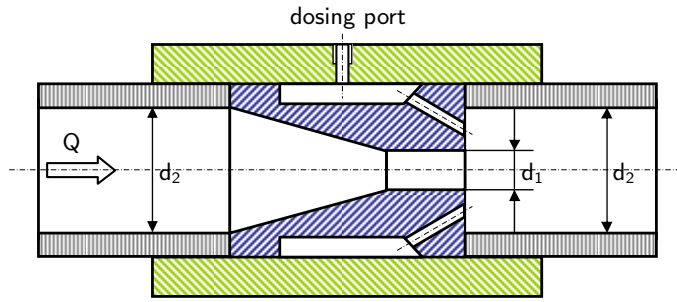

Figure 5.1: Design of static mixer for coagulant dosing (d_1=6 mm, d_1=16 mm)

flocculated suspension were decanted into a measuring cylinder for suspended solids determination. Approximately 200 mL of the remaining sample were passed through a 0.45-µm membrane filter and analysed for colour, UV_{254} absorption as well as DOC.

5.2 Pilot-scale continuous filtration experiments

5.2.1 Raw water

The same raw water as described in Tab. 5.1 was prepared continuously in a 120-L tank by dosing NOM concentrate into a tap water flow of 420 L/h using a peristaltic pump. A centrifugal pump supplied a flow of 400 L/h from the raw water tank to the coagulation step and mixed the tank contents by recirculation. Excess raw water went to an overflow drain. The raw water temperature varied between 7°C and 12°C during the experimental period.

5.2.2 Coagulation and flocculation

Acid for pH control (1 M HCl) and coagulant were fed into two inline mixers by high-precision peristaltic pumps (Alitea –XV). In both inline mixers, chemicals were mixed with the feed at turbulent flow conditions (Re>15 000, G>10 000 s^{-1}) in a contracted pipe section (Fig. 5.1). Working solutions of the coagulants were prepared as described in section 5.1.2, except that PACl was used in dilution 1:5.

The flocculation step of the pilot unit was designed for compact treatment with short hydraulic retention time. Five different flocculation conditions were applied: (Tab. 5.2):

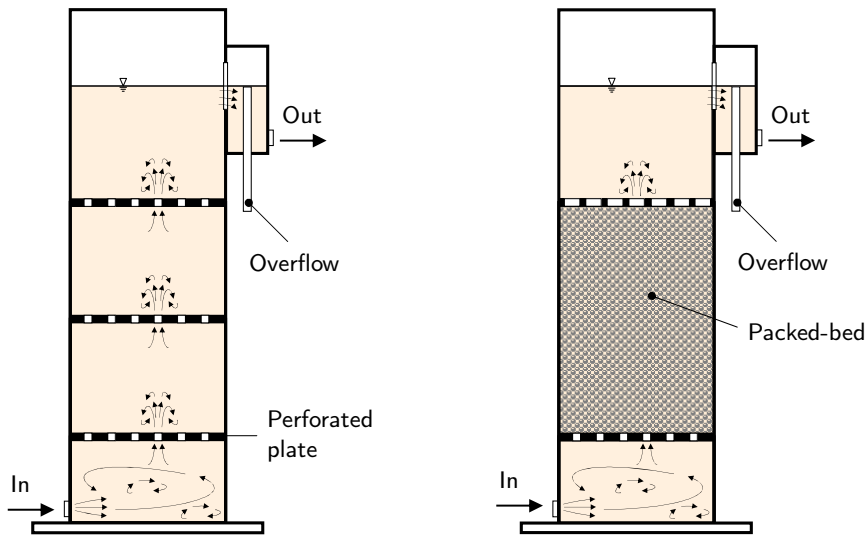

(a) Jet-mix flocculator (b) Packed-bed flocculator

Figure 5.2: Schematics of the flocculator types used in the study.

Table 5.2: Flocculation conditions tested before membrane filtration

Flocculator type	Abbr	G[1] [s]	t_d [min]	Remarks
None	No			
Pipe	PF	400	0.5	braided PVC hose
4-chamber jet-mix with uniform jet-velocity	JMF1	15	5	v_{jet}=10 cm/s
4-chamber jet-mix with decreasing jet-velocity	JMF2	15	5	v_{jet}=10→5→1 cm/s
Packed-bed	PBF	10	5	plastic media[2]

[1] approximate global rms velocity gradient based on head loss
[2] modified AnoxKaldnes K1 media (see Fig. 5.3a)

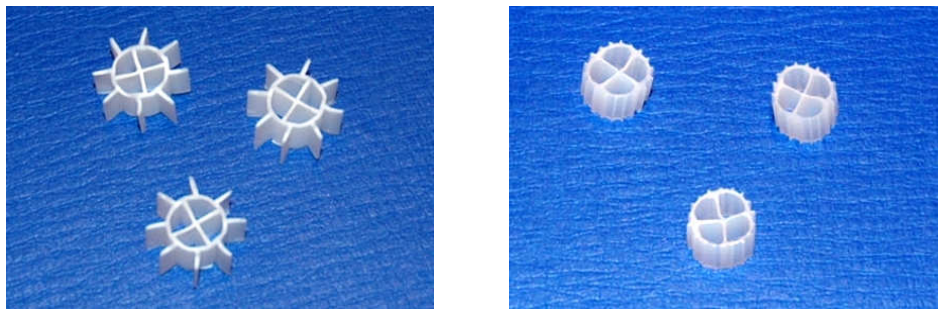

(a) Modified K1 media (b) Regular K1 media

Figure 5.3: Modified AnoxKaldnes K1 media used in the packed-bed flocculator compared with regular K1 media used in the MBBR™ process.

- *No flocculation.* The coagulated suspension was pumped directly into the immersion tank with a detention time of less than 5 seconds in the pipes.
- *Pipe flocculator.* Following design calculations described by Grohmann (1985), a braided PVC hose (inner diameter 16 mm, length 16.5 m) was used to flocculate coagulated raw water at an approximate G-value of 400 s^{-1} for 30 seconds. A high G-value was chosen to effect efficient aggregation to microflocs. Before filtration, the flocculated suspension was passed through an empty upflow tank with a hydraulic detention time of 5 min.
- *Jet-mix flocculator, design 1.* The jet-mix flocculator was designed for an upward flow velocity of 10 m/s through four compartments and had a total detention time of 5 min. In configuration 1, the jet velocity in the holes of all 3 perforated plates was 10 cm/s. Fig. 5.2a shows a schematic of the flocculator, pictures are found in the appendix.
- *Jet-mix flocculator, design 2.* In configuration 2, the design was modified to obtain different hydraulic conditions in each compartment. The jet velocity was decreased from 10 cm/s in the second compartment to 5 and 1 cm/s in the last two compartments. It was anticipated that decreasing jet velocities would avoid possible destruction of aggregates formed in a previous compartment.
- *Packed-bed flocculator.* The packed-bed flocculator was constructed by removing the second perforated plate of the jet-mix flocculator and filling the 50-cm void volume between the first and third plate with an irregular bed of modified AnoxKaldnes K1 plastic media (Fig. 5.2b). Compared to the commercial K1 media used in the MBBR™ process (Fig. 5.3b), the

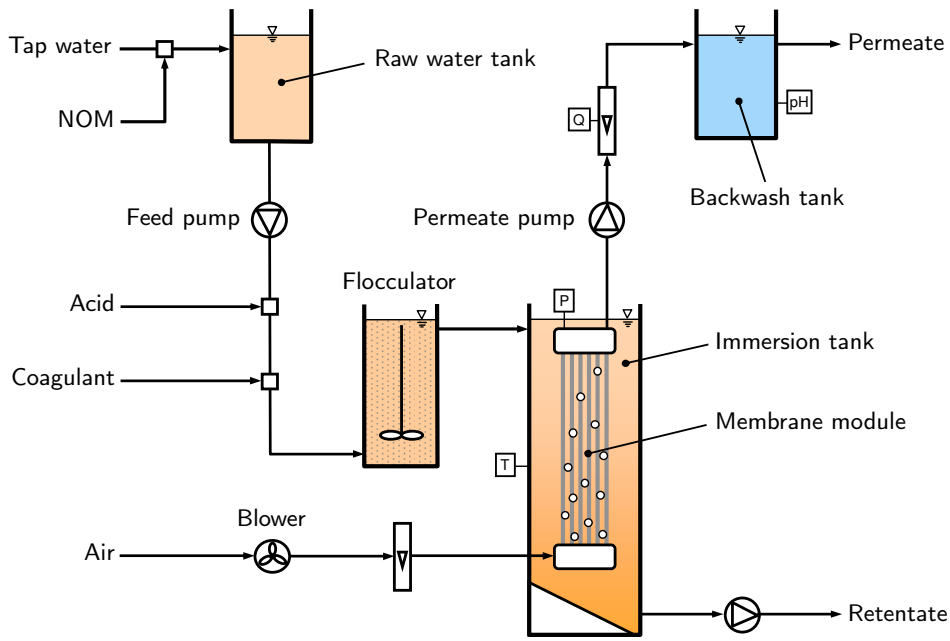

Figure 5.4: Flowsheet of the pilot plant

modified media had fewer (8 instead of 18) and longer (3 mm instead of 1 mm) outer fins giving a larger void volume in a packed bed (Fig. 5.3a). The outer diameters measure about 14 and 10 mm for the modified and the regular media, respectively. Since the media reduced the flocculator volume by some 20%, the flow rate through the coagulation/flocculation step was reduced to 300 L/h to maintain a flocculation time of 5 min.

5.2.3 Membrane unit

The flocculated suspension was passed into a cylindrical immersion tank via an overflow arrangement, which maintained a constant liquid level in the tank. Excess suspension went to waste. In the bottom of the tank, an inclined plate was installed for efficient sludge withdrawal. The approximate working volume of the immersion tank was 20 L.

The tank contents were filtered using an immersed Zenon Zeeweed® hollow fibre membrane. According to manufacturer specifications, this O–I operated membrane achieves a 40 nm nominal size cut-off with no pore larger than 0.1 µm. The ZW-10 module used in the experiments contained about 300

hollow fibres with an approximate surface area of 1 m^2 (see Appendix D). A doubled-headed piston pump (FMI QV-1) was used to withdraw permeate from the top header of the module at a constant flow rate. After a preset filtration time, a programmable time controller reversed the pumping direction to effect backwashing of the membrane with permeate from a holding tank. During backwashes, compressed air was injected through nozzles in the bottom module end. Four process parameters were continuously recorded using a data acquisition system (Grant Squirrel 1000 series): (1) the permeate/backwash flow rate (Macnaught M2RSP-1H oval gear flowmeter), (2) the suction pressure in the top header of the module (ESI GS4103 pressure transmitter), (3) the temperature in the immersion tank (JUMO 90281F55 Pt-100 element), and (4) the permeate pH (Prominent Dulcotest PHEX 112 SE electrode).

5.2.4 Start-up considerations

Before each experiment, sodium hypochlorite solution was pumped into the membrane module in backwash mode to give a final chlorine concentration of 250 ppm Cl_2 in the immersion tank. After a 12-hour soak period the tank was drained, rinsed, and filled with distilled water. The pure water permeability was determined at various fluxes to ensure that each experiment started at similar conditions.

The time t^* required to attain the system's steady-state concentration of suspended solids c^* is obtained from the mass balance around the immersion tank. For a completely mixed system, it may be assumed that steady state conditions prevail once 95% of c^* is reached (Jensen 2001). Integration of the mass balance gives

$$t^* = \frac{V}{Q_p} \frac{w}{1-w} \ln \frac{w}{1-p} \tag{5.1}$$

where V is the immersion tank volume, Q_p the permeate flow rate, w the water recovery, and p the fraction of c^* to be reached. Eq. (5.1) shows that increasing water recovery and decreasing flux prolong the start-up time significantly. To attain steady state conditions rapidly, the system was operated in dead-end mode for the first hours of each experiment. Thereafter, retentate was withdrawn continuously from the bottom of the immersion tank to obtain a water recovery of 95%. A filtration experiment ended after 48–72 hours of continuous operation.

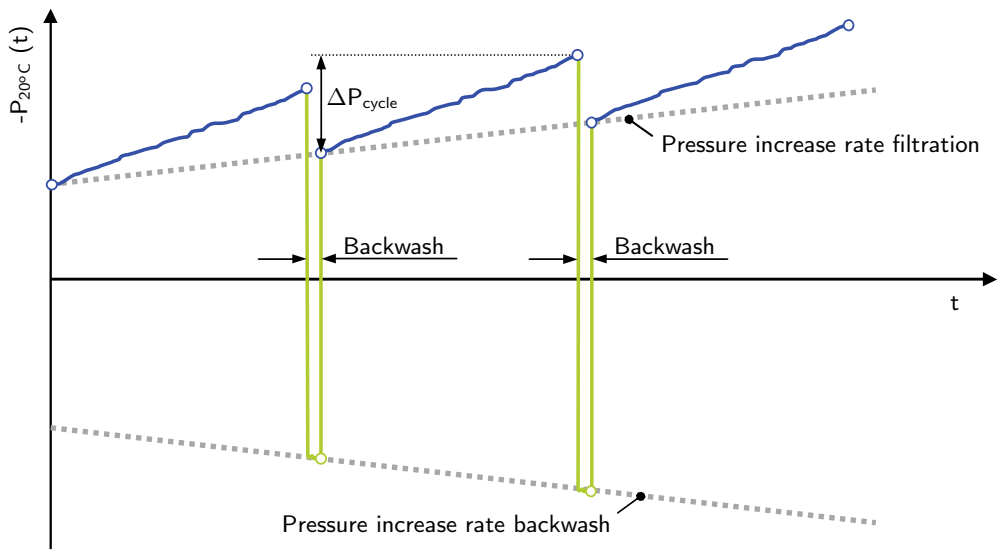

Figure 5.5: Pressure development and determination of fouling rates for forward filtration and backwashing based on pressure increase rates (ordinate shows operating pressure with inverse sign, cf. Eq. 5.2)

5.2.5 Evaluation of fouling rates

The gradual increase of the operating pressure measured immediately *after* a backwash was interpreted as hydraulically not reversible fouling. Once steady-state conditions prevailed in the membrane tank, this pressure increased linearly from cycle to cycle except for periods with temperature variations. Pressure values were normalized for a temperature of 20°C by correcting for the changes in water viscosity using Eq. (5.2). The slope of the linear regression line through the normalized pressure points measured *after* a backwash was taken to be the fouling rate for forward filtration (Fig. 5.5).

$$P_{20^\circ C}(t) = P(t)\ \frac{\mu_{20^\circ C}}{\mu(T)} \tag{5.2}$$

During backwashes, permeate is pumped into the membrane module at higher flow rates, resulting in higher absolute pressures for backwashing than for forward filtration. Hence, the backwash pressure reaches the membrane's terminal operating pressure of about 550–600 mbar first and determines when recovery cleaning (CIP) must be performed.[a] Similar to the aforementioned determi-

[a] In certain cases the forward filtration pressure before backwashing, i.e. the highest pressure during forward filtration, is used to estimate cleaning intervals.

nation of the fouling rate for forward filtration, a backwash fouling rate was calculated based on the highest pressure measured during a backwash. Both fouling rates were calculated based on the absolute values of pressure, i.e. as positive values. In the regression analyses, data points from the initial period without retentate withdrawal were excluded if the pressure development was non-linear. The 95% confidence limits of the regression parameters were determined based on the two-tailed Student's t-distribution with $n - 2$ degrees of freedom.

Under well-controlled conditions, the pressure increase during a filtration cycle ΔP_{cycle} remains relatively constant. During the course of each experiment, the value of ΔP_{cycle} normalized to 20°C was monitored to identify possible fluctuations in operating conditions.

5.2.6 Experimental design

Coagulation conditions were varied within practically relevant limits as determined by jar-test experiments. Compared to normally recommended practice, the membrane unit was challenged to a higher extent. This was mainly to increase the differences in performance between the various treatment conditions. The following operating parameters were controlled in these ranges:

- Raw water colour: 30 or 50 mg Pt/L
- Coagulants: alum, polyaluminium chloride, or chitosan
- Coagulant dosage: 2–5 mg Al/L or 5 mg Chi/L
- Coagulation pH: 6.3 or 7.0 for Al, 5.0 for Chi
- Flocculation conditions: no, PF, JMF1, JMF2, PBF
- Flux: 45–75 LMH
- Backwash frequency: 1–4 times per hour
- Water recovery: 85% or 95%

Experiments were carried out in 3 blocks with one type of coagulant at a time. Tab. 5.3 gives an overview of all documented experiments grouped by coagulant and flocculation conditions. It should be noted that the experimental schedule did not necessarily follow this order.

Table 5.3: Experimental design

Id	Coag	Colour (mg Pt/L)	Dosage (mg/L)	pH	Floc	#BW (h^{-1})	Flux (LMH)	w (%)
A01	Alum	50	5	6.1	PF	2	60	95
A02	Alum	50	3.75	6.2	PF	2	60	95
A03	Alum	50	5	6.1	PF	4	60	95
A04	Alum	50	5	6.1	PF	1	60	95
A05	Alum	50	5	6.1	PF	2	60	95
C01	Chitosan	50	5	5.0	None	2	60	95
P01	PACl	50	5	6.3	PF	2	60	95
P02	PACl	50	3.5	6.3	PF	2	60	95
P03	PACl	50	5	6.3	PF	4	60	95
P04	PACl	50	3	6.3	None	2	60	95
P05	PACl	50	5	6.2	None	2	60	95
P06	PACl	50	5	6.3	JMF1	2	45	95
P07	PACl	50	5	6.3	JMF1	2	60	95
P08	PACl	50	5	6.3	JMF1	2	75	95
P09	PACl	50	5	6.3	PF+JMF1	2	60	95
P10	PACl	50	3	6.3	JMF2	4	60	95
P11	PACl	50	3	6.4	JMF2	2	60	95
P12	PACl	50	3	6.3	JMF2	1	60	95
P13	PACl	50	5	6.3	JMF2	2	60	95
P14	PACl	50	3	6.4	JMF2	2	45	95
P15	PACl	50	3	6.2	PBF	1	45	95
P16	PACl	50	3	6.2	PBF	2	60	95
P17	PACl	50	3	6.2	PBF	2	75	95
P18	PACl	50	5	6.2	PBF	4	60	95
P19	PACl	50	5	6.1	PBF	2	60	95
P20	PACl	50	2	6.2	PBF	2	60	95

continued on next page

Table 5.3: Experimental schedule (continued)

Id	Coag	Colour (mg Pt/L)	Dosage (mg/L)	pH	Floc	#BW (h^{-1})	Flux (LMH)	w (%)
P21	PACl	50	3	6.2	PBF	2	60	85
P22	PACl	50	5	6.2	PBF	2	60	85
P23	PACl	50	3	6.2	PBF	2	75	85
P24	PACl	50	5	6.2	PBF	2	75	85
P25	PACl	50	3	7	PBF	2	60	95
P26	PACl	50	5	7	PBF	2	60	95
P27	PACl	30	1.5	6.2	PBF	2	60	95
P28	PACl	30	2	6.2	PBF	2	60	95

5.3 Analytical methods

pH was measured using a Radiometer PHM 83 ion meter fitted with a PHC 2701-7 combined pH electrode. During the pilot-scale experiments, a handheld pH meter (Hanna instruments HI8915 ATC with HI1230 electrode) was used to check the pH after the different stages of treatment. Both used electrodes gave rapid stable readings in samples with low ionic strength.

Colour was determined at a wavelength of 410 nm on a Hitachi U-3000 spectrophotometer using a 50-mm glass cuvette. An inter-laboratory comparison between Nordic countries showed that absorption measured gives the highest precision (Hongve and Akesson 1996). Absorption values were converted to milligrams platinum equivalents per litre (mg Pt/L) based on a K_2PtCl_6 standard curve.

UV_{254} absorption was determined in 3 replicates at a wavelength of 254 nm using a 10-mm quartz cuvette.

Dissolved organic carbon (DOC) determination was performed on a Tekmar Dohrmann Apollo 9000 combustion analyser. Samples were filtered through a 0.45-µm membrane filter, acidified with one drop of PA-grade phosphoric acid, and stored in glass vials at 4℃ until automated analysis could be performed.

Suspended solids concentrations were determined gravimetrically by filtration of a 50–200 mL sample through a 0.45-µm membrane filter. Filters were covered and left to air-dry for at least 48 hours before weighing.

Turbidity values were measured with a Hach 2100N turbidimeter in ratio mode. In the pilot-scale experiments, a *residual turbidity* was determined for retentate samples drawn immediately after a backwash. After 30 minutes settling in a 1-L jar, 3 aliquots of the clear phase were withdrawn by pipette and analysed on a Hach 2100A turbidimeter.

Zeta-potential was analysed by Laser Doppler velocimetry on a Coulter 440SX. The settings for determination programme were 120 s runtime, electric field on and off times of 4 and 0.4 s, respectively, voltages of 30 or 40 V, and a frequency range of 500–1000 Hz.

NOM fractionation after molecular weight was performed using a 400-mL pressure filtration cell (Amicon 8400) fitted with Amicon YM1, YM10 and XM50 membranes. The YM1 and YM10 membranes were made of regenerated cellulose and had a MWCO of 1 and 10 kDa, respectively. The active layer of the XM50 membrane consisted of poly(acrylonitrile-co-vinyl chloride) with an approximate MWCO of 50 kDa. Before use, membranes were washed in a 0.1 M NaOH solution and rinsed with deionized water. Size distributions were determined by parallel processing of samples. Serial filtration results in larger errors and requires larger volumes to be filtered (Logan and Jiang 1991). For each filtration step, the cell was filled with 350 mL of 0.45-µm pre-filtered sample and pressurized to 3 bar. To avoid an excessive increase in the feed concentration, permeation was stopped after of a volume of 50 mL was passed. Permeate samples were analysed for TOC, colour, and UV_{254} absorption.

Aluminium and calcium concentrations were analysed by high-resolution inductively coupled plasma-mass spectrometry (HR-ICP-MS). Samples were acidified with 65%-HNO_3 and sent to an external laboratory for analysis.

Normally, analyses were performed shortly after sample collection. During the pilot-scale experiments, raw water and permeate samples were stored at 4–6°C in dark 250-mL glass bottles and analysed within 4 days after sample collection.

Chapter 6

Results and discussion

6.1 Raw water NOM characterization

The ion exchange eluate used to enrich the tap water NOM concentration increased the specific UV absorption (SUVA) of raw water (Tab. 5.1), indicating that the eluate contains a larger percentage of complex aromatic NOM compounds than tap water. To ensure that the model raw water after NOM enrichment resembled other natural surface waters, NOM characteristics were determined after titration and membrane fractionation. Fig. 6.1 shows that colour and UV absorption increase with the pH in a similar manner as in other surface waters. In the pH range from 5.5–9 colour and UV_{254} absorption increase by some 38% and 15%, respectively, independent of NOM concentration. For UV absorption, the increase is most pronounced below pH 7 and above pH 9. Throughout the study, raw water colour and UV absorption values were determined after neutralization to pH 7, while permeate values were measured at the respective coagulation pH. Consequently, the calculated removal efficiencies are slightly offset by a pH factor, which can be estimated using Fig. 6.1. However, deviations become negligible at low NOM concentrations such as in permeate samples.

Membrane fractionation of raw and tap water samples at pH 7 resulted in fairly similar NOM distributions in all four size ranges investigated (Fig. 6.2). Compared to tap water, compounds imparting colour increased in the size range above 50 kDa and decreased in the range from 10–50 kDa. UV_{254} absorption values differed marginally between both samples, although in the size range above 50 kDa the value was lower after NOM enrichment. The DOC concentration below 1 kDa increased after addition of the NOM concentrate,

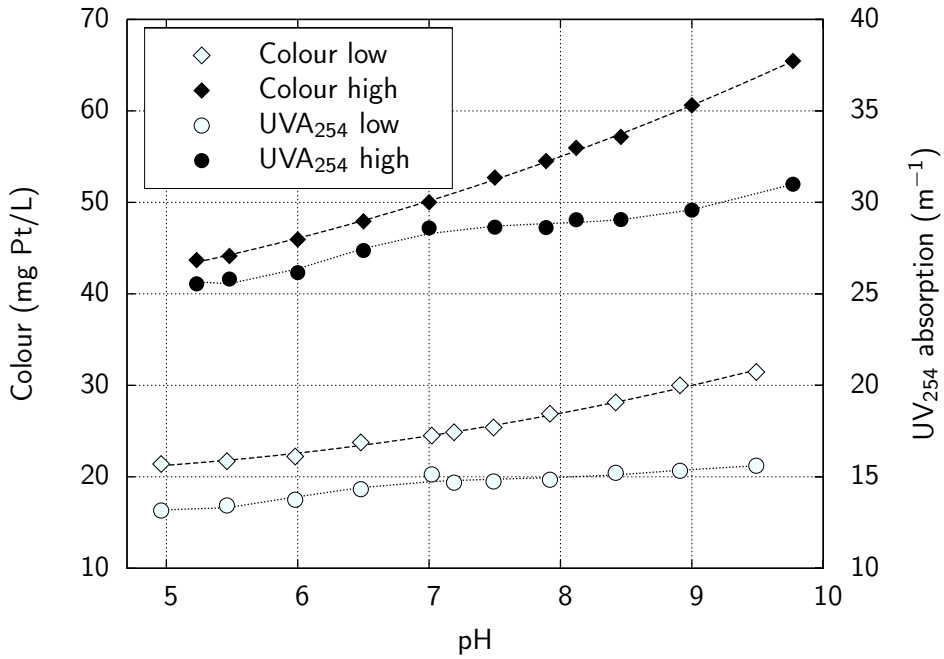

Figure 6.1: Dependence of colour and UV_{254} absorption on pH for two different NOM concentrations

however, the DOC percentage in that size range decreased as indicated by the higher SUVA value. Equivalently, the DOC percentage in the range from 10–50 kDa increased.

The results show that the addition of NOM concentrate to tap water leads to a relatively unbiased increase of organics. The strongly alkaline NOM concentrate increased the raw water conductivity (see Tab. 5.1) without affecting the molecular size distribution notably. SUVA ratios larger than 4 indicate a high proportion of aquatic humic substances with high hydrophobicity and molecular weight. Coagulation of such NOM-rich waters typically results in DOC removals larger than 50% (Edzwald and Tobiason 1999). Furthermore, based on the MW distributions it can be estimated that the 40-nm UF-membrane used in the pilot experiments will not achieve any relevant NOM removal without upstream coagulation. Previous research results suggest the same: Egeberg *et al.* (2002) introduced a molecular weight correlation based on diffusivity: $D = a\,\mathrm{MW}^b$ ($a = 51.94 \cdot 10^{-10}$ m^2 s^{-1}, $b = -0.397$). This relationship predicts average molecular sizes smaller than 10 nm for practically all NOM components present in the raw water.

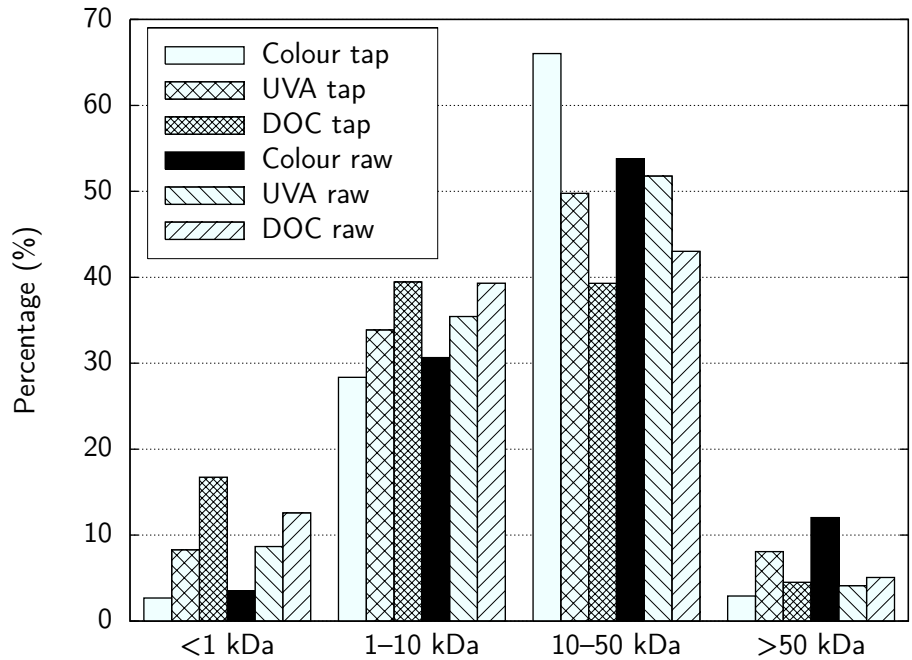

Figure 6.2: NOM size distributions in tap and raw water (colour 50 mg Pt/L) measured at pH 7

6.2 Preliminary coagulation experiments

6.2.1 Dosage determination

The performance results obtained in jar tests for all 3 coagulants used in the study are given in Tab. 6.1–6.3. As expected, both aluminium coagulants achieved satisfactory treatment results with respect to NOM removal. Alum was slightly more efficient at removing colour, UV_{254}-absorbing compounds, and particularly DOC. No visible floc formation occurred at a specific dosage of 2 mg Al/L for either coagulant, which is reflected in the low values for suspended solids. In both cases, the flocculated suspensions caused a high resistance to filtration during 0.45-µm filtration, indicating a large fraction of colloidal particles. Nevertheless, suspended solids formation was notably higher for PACl at this dosage which may be attributed to the better flocculation properties of the pre-hydrolysed coagulant. Otherwise, the dosage specific sludge production was slightly higher for alum. For both aluminium coagulants, near-zero zeta potential was measured at a specific dosage of about

4 mg Al/L. However, a dosage of 3 mg Al/L already resulted in a filtrate colour below 10 mg Pt/L. Subsequently, dosages of 3–5 mg Al/L were applied in the pilot experiments.

Chitosan performed notably poorer than the metal-based coagulants. At a dosage of 7 mg/L, DOC removal was lower than 40% and filtrate colour exceeded 10 mg Pt/L. For the same raw water, Kvinnesland (2003) found removals to increase utterly at higher chitosan dosages. However, the flocculation properties of the formed aggregates started to decrease beyond a dosage of 7 mg/L. Compared to the metal-based coagulants with a specific sludge production of 5.7 and 6.5 mg SS/mg Al for PACl and alum, respectively, coagulation with chitosan resulted in a significantly lower sludge production (<1.7 mg SS/mg chitosan). Surprisingly, positive zeta potentials were measured in all flocculated suspensions, suggesting complete charge neutralization at the lowest chitosan dosage. However, floc formation only became apparent at dosages above 2 mg/L. On the other hand, the coagulation mechanisms of chitosan differ widely from those of metal-based coagulants. For a raw water with a natural colour >100 mg Pt/L, Vogelsang (2001) showed that colour removal increased linearly far beyond the dosage giving zero zeta potential, suggesting that charge neutralization was not the dominating coagulation mechanism. Consequently, near zero zeta potential does not serve as condition to find the optimal chitosan dosage. It must be noted, though, that zeta potential determination by electrophoretic light scattering is prone to several error sources, for instance electroosmosis, which may have affected the measurements with chitosan suspensions. For the pilot experiments, a dosage of 5 mg/L was chosen, resulting in an average removal of colour and DOC near 70% and 30%, respectively.

6.2.2 Removal of NOM fractions

Fractionation of filtered samples coagulated with PACl and chitosan were carried out to further investigate the differences between both types of coagulants. For practical reasons, permeate samples from the membrane pilot unit were used for fractionation.

The removal efficiencies for colour and DOC measured in the PACl permeate corresponded to established figures discussed in section 3.4.1. Colour removal was high in all molecular weight ranges except for substances below 1 kDa. PACl achieved a high removal of DOC and UV-absorbing compounds larger than 10 kDa, but removal efficiencies dropped markedly below 10 kDa.

Table 6.1: Jar test results PACl (raw water 50 mg Pt/l, coagulation pH 6.3)

Dosage (mg Al/L)	Colour removal (%)	UVA_{254} removal (%)	DOC removal (%)	Zeta potential (mV)	Sludge production (mg SS/L)
2	72.3	60.4	44.1	−11.7	9.2
3	84.3	72.9	51.5	−6.9	19.7
4	91.5	80.8	60.4	+1.3	23.9
5	94.3	85.0	64.7	+10.4	28.3

Table 6.2: Jar test results alum (raw water 50 mg Pt/l, coagulation pH 6.3)

Dosage (mg Al/L)	Colour removal (%)	UVA_{254} removal (%)	DOC removal (%)	Zeta potential (mV)	Sludge production (mg SS/L)
2	76.9	63.6	46.3	−10.7	2.2
3	87.3	74.9	59.7	−5.6	20.6
4	93.3	82.4	68.7	+3.4	26.8
5	94.6	84.7	72.1	+8.7	32.6

Table 6.3: Jar test results chitosan (raw water 50 mg Pt/l, coagulation pH 4.9)

Dosage (mg/L)	Colour removal (%)	UVA_{254} removal (%)	DOC removal (%)	Zeta potential (mV)	Sludge production (mg SS/L)
2	47.5	23.6	11.8	+3.9	2.7
3	58.0	32.9	18.2	+7.3	4.4
4	65.4	40.2	23.7	+12.0	6.6
5	72.4	47.5	30.4	+14.4	n/a
7	76.4	53.6	37.6	+16.8	n/a

Table 6.4: NOM removal efficiency by molecular weight range for PACl (dosage 3 mg Al/L, pH 6.3) and chitosan (dosage 5 mg/L, pH 5)

MW range	Colour removal (%)		UVA removal (%)		DOC removal (%)	
(kDa)	PACl	Chitosan	PACl	Chitosan	PACl	Chitosan
<1	47.9	0.9	52.0	−41.4	0	−85.8
1–10	84.9	37.0	71.4	−17.8	55.3	−34.2
10–50	99.0	91.7	92.9	69.2	80.2	54.6
>50	88.6	99.6	92.1	92.6	95.3	100.0

*Fractionation carried out with permeate samples from the pilot unit

The pronounced difference in removal efficiencies for colour and DOC using chitosan gives rise to two assumptions: (1) chitosan is less efficient at removing low molecular weight organics, and (2) the polymer itself increases the DOC concentration. The fractionation results support these assumptions. Substances imparting colour were largely removed down to a MW of 10 kDa. In the range of 10–50 kDa both UV_{254} and DOC removals were significantly lower than for PACl. With an average molecular weight of about 80 kDa, one may expect a potential DOC contribution of chitosan in the higher MW range. Interestingly, the concentration of compounds contributing to UV_{254} and DOC values below 10 kDa increased after coagulation with chitosan, suggesting that the residual organics after coagulation with chitosan might pose a problem with respect to DBP formation potential or biostability. However, the reason for an organic contribution in the low MW range is unclear and needs to be verified using other molecular weight fractionation techniques.

6.3 Pilot-scale membrane filtration experiments

6.3.1 Effect of air scouring

Continuous air scouring can reduce particle deposition on the membrane surface and the associated pressure increase during forward filtration. Flux stepping experiments were carried out to quantify the effect of air scouring for raw water coagulated with 5 mg Al/L alum. Once the membrane rig had attained the steady-state suspended solids concentration, the rate of pressure increase over a 10-minute forward filtration cycle was measured for fluxes between 30

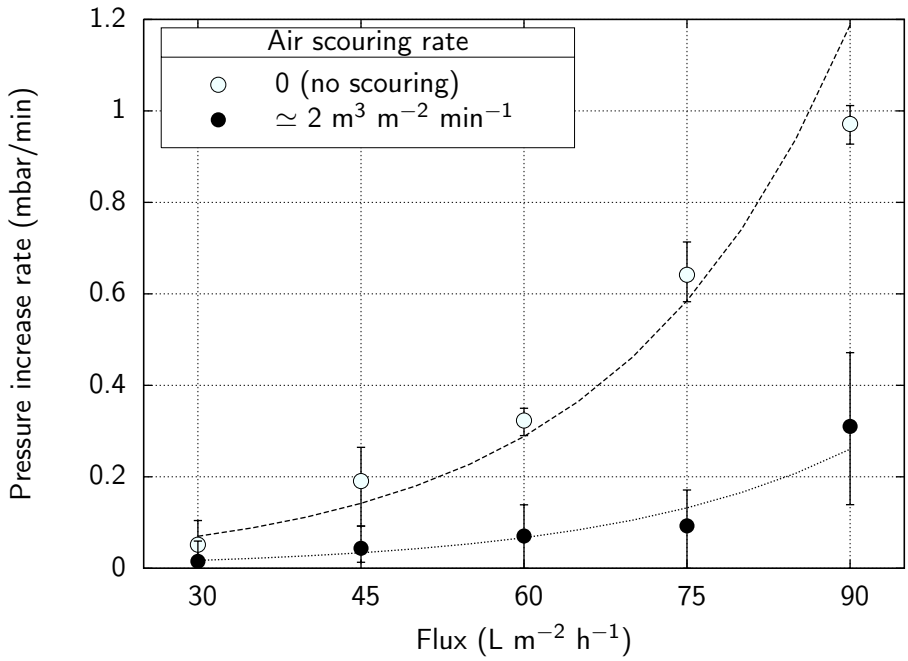

Figure 6.3: Effect of air scouring on the pressure increase rate during a filtration cycle caused by particle deposition (suspended solids concentration 300–400 mg/L)

and 90 LMH with and without gentle air scouring (2 $m^3 m^2_{footprint} min^{-1}$)[a]. Before stepping the flux up or down, the membrane was backwashed for 30 seconds using a backwash flux of 105 LMH combined with vigorous air scouring. Since the pressure increased linearly during a 10-minute cycle, the rate of pressure increase was determined by linear regression.

Results from replicate experiments show a pronounced effect of air scouring on the pressure increase rate above a flux of 45 LMH (Fig. 6.3). For a system with gentle air scouring, elevated pressure increase rates were only measured for the highest flux of 90 LMH. On the other hand, relatively low pressure increase rates were measured without air scouring up to a flux of 60 LMH. Sedimentation of suspended particles was clearly visible after a few minutes of filtration, indicating that the immersion tank can serve as settling unit to a certain extent in the absence of air scouring.

Continuous air scouring does not affect the fouling propensity of particles

[a]Footprint refers to the projectional floor area occupied by a module.

per se but merely reduces deposition. In other words, even with continuous scouring, the system will require efficient hydraulic backwashes to remove deposited material. A rough estimation of energy demand shows that continuous air scouring may consume up to 10 times as much energy as permeate pumping and backwashing:

Energy demand of air scouring. For the investigated membrane system, the airflow rate per m^2 installed membrane surface area to effect air scouring is assumed to be in the range of

$$Q_{\text{air}} = 0.5 \ldots 1.0 \text{ m}^3 \text{ m}^{-2} \text{ h}^{-1}$$

Values in the upper range are more typical for MBR applications (Judd 2002), while aeration demand may be lower in drinking water applications. The density of moist air can be estimated using

$$\rho_{ma} = \frac{p}{R_a \, T} \, \frac{1+x}{1 + x \cdot R_w / R_a} \tag{6.1}$$

where p is the partial pressure of air (Pa), T the absolute temperature (K), $R_a = 287.1$ J/(kg K) and $R_w = 461.5$ J/(kg K) are the ideal gas constants for dry air and water vapour, respectively, and x the specific humidity ratio. At normal ambient temperature and pressure and an average moisture content of 0.015 $\text{kg}_{\text{water}}/\text{kg}_{\text{air}}$, the density of air falls in the range of $\rho_{ma} = 1.2 \ldots 1.25$ kg/m^3. The required mass flow of air thus amounts to

$$\dot{m} = 0.6 \ldots 1.2 \text{ kg m}^{-2} \text{ h}^{-1}$$

Assuming adiabatic compression, the specific power demand E_s (W/m^2) required to compress air may be calculated by

$$E_s = \frac{\dot{m} \; R \; T}{M_{\text{air}} \; \nu \; \eta} \left[\left(\frac{P}{P_0} \right)^{\nu} - 1 \right] \tag{6.2}$$

Due to the water pressure at bottom of the immersion tank, friction losses in piping and the diffusors, a minimum compression of air to P=2 bar will be required. With the values described in Tab. 6.5, a specific power demand per unit membrane surface area in the range of

$$E_s = 11 \ldots 25 \text{ W/m}^2$$

Table 6.5: Values used to estimate required aeration energy

Definition	Symbol	Unit	Value used
Specific air mass flow	$\dot{m}$	kg m^2 s^{-1}	$1.6 \ldots 3.5 \cdot 10^{-4}$
Ideal gas constant	R	kJ kmol^{-1} K^{-1}	8.314
Air temperature	T	K	288
Average MW of air	M_{air}	kg kmol^{-1}	28.9
Adiabatic factor	ν	–	0.283
Compressor efficiency	η	–	0.9
Compression ratio	P/P_0	–	2
Net membrane flux	J_{net}	L m^{-2} h^{-1}	$40 \ldots 60$

is calculated. For continuous air scouring and typical net membrane fluxes in the range of $40 \ldots 60$ L m^{-2} h^{-1}, the specific energy demand per volume produced permeate roughly amounts to

$$\widehat{E}_s = 0.2 \ldots 0.6 \text{ kW/m}^3$$

In comparison, if air scouring is used only to assist backwashes, the energy demand is reduced to about 1/20 to 1/60 of the above value depending on backwash frequency and duration.

$$\widehat{E}_s^* = 0.005 \ldots 0.03 \text{ kW/m}^3$$

Energy demand of permeation and backwashing. The specific amount of energy E_f consumed per unit membrane surface to withdraw permeate can be estimated using the equation

$$E_f = \frac{1}{\eta} \, \bar{J} \, \Delta P \tag{6.3}$$

where $\bar{J}$ is the gross flux across the membrane, ΔP the pressure difference, and η the pump efficiency. The gross flux may be calculated by

$$\bar{J} = \frac{1}{f} \, J_{net} \tag{6.4}$$

Table 6.6: Values used to estimate pumping energy

Definition	Symbol	Unit	Value used
Net membrane flux	J_{net}	L m^{-2} h^{-1}	40 . . . 60
Hydraulic efficieny	f	–	0.95
Pump efficiency	η	–	0.85
Pressure difference	ΔP	bar	0.55

where f is the hydraulic efficiency (see Eq. 3.13). For simplicity, the operating pressure of the membrane unit is assumed to be at its maximum value at all times (worst case), here $\Delta P = 0.55$ bar. Using the values in Tab. 6.6, a specific power demand per unit membrane surface area in the range of

$$E_f = 0.8 \ldots 1.1 \text{ W/m}^2$$

is calculated. Choosing the same net fluxes as before, the (maximum) specific energy demand per volume produced permeate roughly amounts to

$$\widehat{E}_f = 0.02 \ldots 0.03 \text{ kW/m}^3$$

and is thus approximately one order of magnitude lower than the energy demand for continuous air scouring. For a system with air scouring only during backwashes, the amount of energy required to compress air falls within the same range as the energy demand for pumping.

Backwash protocol. During all further experimental work, the immersed membrane system was challenged to operate solely with an effective hydraulic backwash procedure:

- no air scouring during forward filtration, saving 95–99% aeration energy depending on backwash frequency and duration;
- backwashing at 1.5 times the forward filtration flux for a total time of one minute per hour, resulting in a hydraulic efficiency of about 96%;
- vigorous air scouring during backwashes at a specific airflow rate of 6–7 m^3 $m^{-2}_{\text{footprint}}$ min^{-1}. For comparison, the common (continuous) airflow rate used in full-scale MBR applications based on the immersed membrane system used in the study is in the vicinity of 5 m^3 $m^{-2}_{\text{footprint}}$ min^{-1} (Judd 2002).

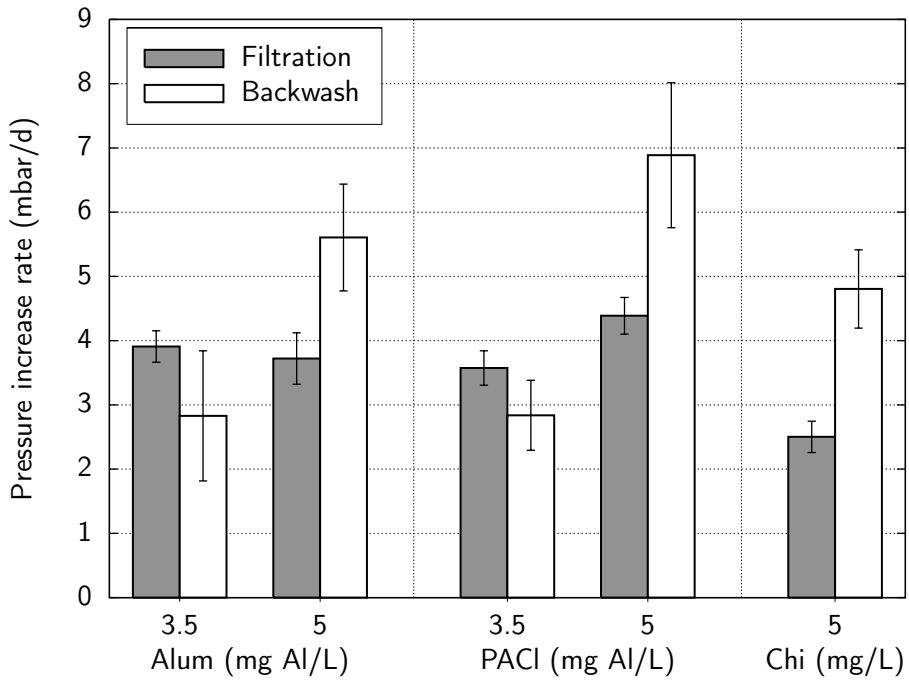

Figure 6.4: Effect of coagulant dosage on pressure increase rates (Pipe flocculator, J=60 LMH, t_f=29.5 min, t_{bw}=0.5 min, error bars indicate 95%-confidence intervals). Data from Exps. A02, A01, P02, P01, and C01

6.3.2 Effect of coagulant and dosage

Deposition of foulants on the membrane surface may be influenced by coagulant type and dosage. Taking the NOM removal efficiency into consideration, fouling rates were determined for all three coagulants used throughout the study to establish a reference for comparison. The pre-treatment conditions were pipe flocculation at high G-value (PF) followed by membrane filtration at a flux of 60 LMH with 2 backwashes per hour lasting 30 seconds each.

Alum and polyaluminium chloride. For the aluminium-based coagulants, a specific dosage in the range of 3–5 mg Al/L achieved satisfactory to high NOM removal. Two dosages were tested to simulate different coagulation conditions (Exps. A01–A02, P01–P02). At a coagulation pH of 6.3, both primary destabilization mechanisms will prevail, i.e. charge neutralization and sweep coagulation. However, a specific dosage of 3.5 mg Al/L just meets the coagulant

demand for complete charge neutralization. Consequently, charge neutralization will be the dominating mechanism at this dosage. Due to higher hydroxide precipitation, sweep coagulation will presumably dominate at a dosage of 5 mg Al/L.

The pressure increase rates measured for both aluminium-based coagulants differed only marginally from each other (Fig. 6.4). At 3.5 mg Al/L, no statistically significant differences could be established between alum and PACl. The pressure increase rates for backwashing are lower than those for filtration. On the other hand, at a specific dosage of 5 mg Al/L the pressure increase rates for backwashing increased strongly for both coagulants, exceeding the values for forward filtration. Due to large data variation, the apparent difference in the backwash pressure increase rates between both coagulants was not statistically significant. Interestingly, the pressure increase rates for forward filtration were similar to those obtained at the lower dosage. Normally, the backwash pressure should increase at a lower or equal rate as the forward filtration pressure. A faster inclining backwash pressure indicates an additional resistance in reverse flow mode, which may originate from deposits forming on the permeate side of the fibre. During a backwash, these deposits are forced into the fibre matrix and exert an additional resistance to flow. In the subsequent filtration cycle, these deposits are partially removed with the permeate. The permeation pressure is therefore affected to a lesser degree. In practice, this phenomenon has been observed also in pilot studies on immersed membrane filtration with upstream coagulation (Zenon 2005).

Residual aluminium concentrations were determined in a total of 15 randomly drawn permeate samples during the initial experiments with alum and PACl (A01–A05, P01–P03). The permeate aluminium concentration varied from 10 to 30 µg Al/L and was thus well below the Norwegian standard of 150 µg Al/L. No statistically significant increase over the raw water aluminium concentration was measured.

Backwashing with chlorine solution followed by a short soaking period (5 hours) removed foulants completely in all cases with no measurable decline in the membrane's pure water permeability, i.e. no irreversible fouling occurred.

Chitosan. A dosage of 5 mg Chi/L was chosen to achieve acceptable colour removal (Exp. C01). The permeate quality corresponded to the results obtained in the jar tests. Fig. 6.4 shows that the pressure increase rate for forward filtration was some 30% lower than for the aluminium-based coagulants (3.5 mg Al/L). However, fouling was dominated by a notably higher backwash pressure increase rate, which exceeded the values obtained with alum

and PACl. The results presented in section 6.2.2 indicate that the permeate contains chitosan residuals, which can form deposits in the fibre lumen and increase the resistance to flow during backwashes.

The suspended solids concentration in the immersion tank was comparatively low (≃150 mg/L). Flocs visible in the immersion tank had a voluminous, fragile appearance and settled slowly. The residual turbidity measured in the immersion tank increased notably over the value after coagulant addition. Poor sedimentation characteristics may explain partially why the pressure increase over a 30-minute filtration cycle (ΔP_{cycle}) attained almost the same high value as for the aluminium coagulants despite the lower suspended solids concentration (Figs. C01c and C01d).[b]

Over time, a gelatinous layer formed on the membrane surface, which seemed resistant to air scouring and backwashing. Being a cationic biopolymer, chitosan and its aggregates potentially adsorb to the negatively charged membrane polymer and form relatively strong bonds. Chitosan fouling required more than 12 hours soaking in chlorine solution to detach. However, the CIP efficiency could be significantly accelerated if the membrane was backwashed first with a 1 g/L citric acid solution. In an acidic environment, chitosan fouling layers loosened from the membrane and settled in large flakes. However, deposits near the potted ends of the fibre were very difficult to remove. Subsequent soaking in chlorine solution was still necessary to restore the membrane's pure water permeability. Replicate experiments (results not shown) confirmed the pressure development and removal issues observed during CIP for chitosan fouling. Due to unsatisfactory permeate quality and recalcitrant fouling layers, chitosan was not used for further experimentation.

6.3.3 Effect of flocculation

Good flocculation requires hydrodynamic conditions optimized for particle collision. This is normally achieved by a flocculator. In an immersed membrane system, several operating variables will affect post-flocculation, including coagulant dosage, filtration flux, water recovery, and use of air scouring. The interdependencies between flocculation and membrane operation were studied to find optimal pre-treatment conditions for coagulation with PACl.

Dosage dependence. Figs. 6.5 and 6.6 compare the pressure increase rates for filtration and backwash after different flocculation treatments. A pronounced effect of flocculation is evident at the lower specific aluminium dosage

[b] Experimental data presented in Appendix B from page 131.

of 3 mg/L. Compared to treatment without a flocculator, the jet-mix (JMF2) and the packed-bed flocculator (PBF) reduce the pressure increase rate for filtration markedly. However, in all cases fouling is dominated by the backwash pressure increase. Only use of the PBF lowers the increase rate of the backwash pressure. At 5 mg Al/L, no statistically significant effect of flocculation could be established for the pressure increase rate during filtration, except for a combination of PF and JMF1, which gave a somewhat reduced pressure increase. After jet-mix flocculation, the backwash pressure increase rates attained similar values as for filtration. However, flocculation using a PF or a PBF lead to higher backwash pressure increases. In case of the PF, the same negative effect on backwash pressure was observed for coagulation with alum at 5 mg Al/L (Fig. 6.4). This indicates that short flocculation times with a PF designed for high G-values can exacerbate fouling at aluminium dosages exceeding the optimal dosage for adequate colour removal. Although the difference in backwash pressure increase rates between treatment without flocculation and PBF is not statistically significant, fouling remains backwash-dominated in case of the PBF.

In cold, low-turbidity surface waters, flocculation kinetics of metal-based coagulants may be retarded because of slower nucleation and low particle content. Three categories of nucleation processes are commonly discerned (Dirksen and Ring 1990):

- *Primary homogeneous nucleation* takes place in a particle-free supersaturated solution in the absence of any solid interface.
- *Primary heterogeneous nucleation* is induced by foreign solid interfaces, such as surfaces of other solids, stirrers, or reactor walls. Nucleation on a foreign surface, which has a lower surface energy than that of a new solute particle, takes place at a lower critical supersaturation.
- *Secondary nucleation* refers to several mechanisms of nuclei formation from the growing precipitate.

During coagulation of surface water, the latter two nucleation processes are likely to be dominant. For treatment of low-turbidity surface water with low coagulant dosages, flocculation in a PBF may be favourable. As opposed to the other hydraulic flocculators, the suspension is passed over a large surface, which promotes primary heterogeneous nucleation. For comparison, microsand is added in the Actiflo® process after rapid mixing of a coagulant to enhance nucleation/flocculation kinetics and sedimentation velocity. Since some deposition of solids occurs in the interstitial volume of the packed bed,

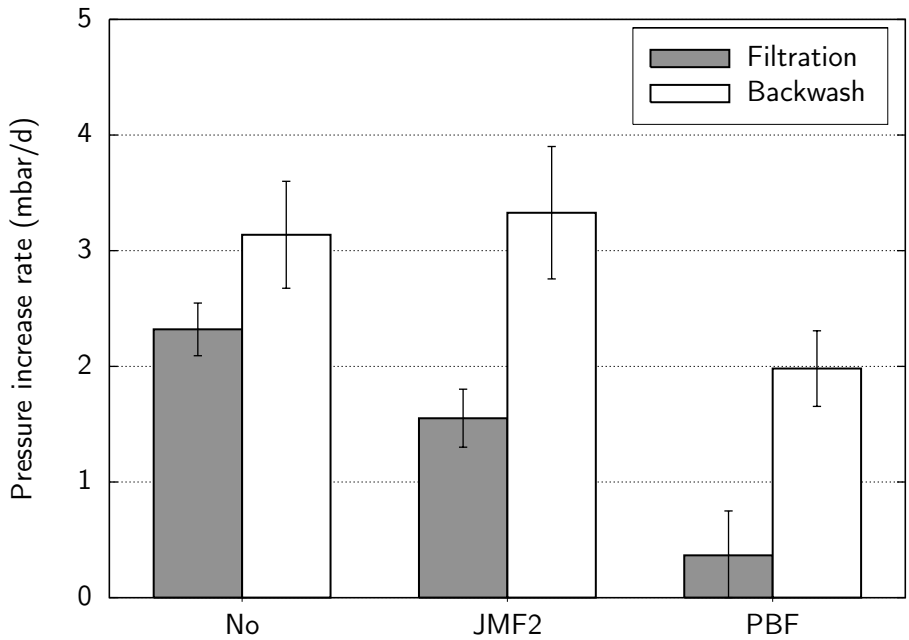

Figure 6.5: Flocculation effects at a PACl dosage of 3 mg Al/L (J=60 LMH, t_f=29.5 min, t_{bw}=0.5 min, error bars indicate 95%-confidence intervals). Data from Exps. P04, P11, and P16

secondary nucleation processes may be promoted as well. In addition, the suspension is routed through a complex flow geometry providing good particle collision. The compartmentalized jet-mix flocculator achieves better plug-flow conditions compared to an empty tank, promotes fluid agitation, and avoids short-circuiting, which improves aggregation of flocs. Compared to the PBF, however, no additional surface for nucleation is provided. Neither flocculation treatment at 3 mg Al/L resulted in lower pressure increase rates for backwashing than for filtration, suggesting that either the flocculation time was too short or that other conditions in the immersion tank affected backwashing adversely.

Flocculation kinetics generally increase with the particle concentration due to higher collision frequency. On increasing dosage, flocculation with metal-based coagulants improves due to higher hydroxide precipitation and secondary nucleation, which explains the small differences between the flocculators at the higher coagulant dosage. On the other hand, the results suggest that under unfavourable flocculation conditions the backwash pressure will increase

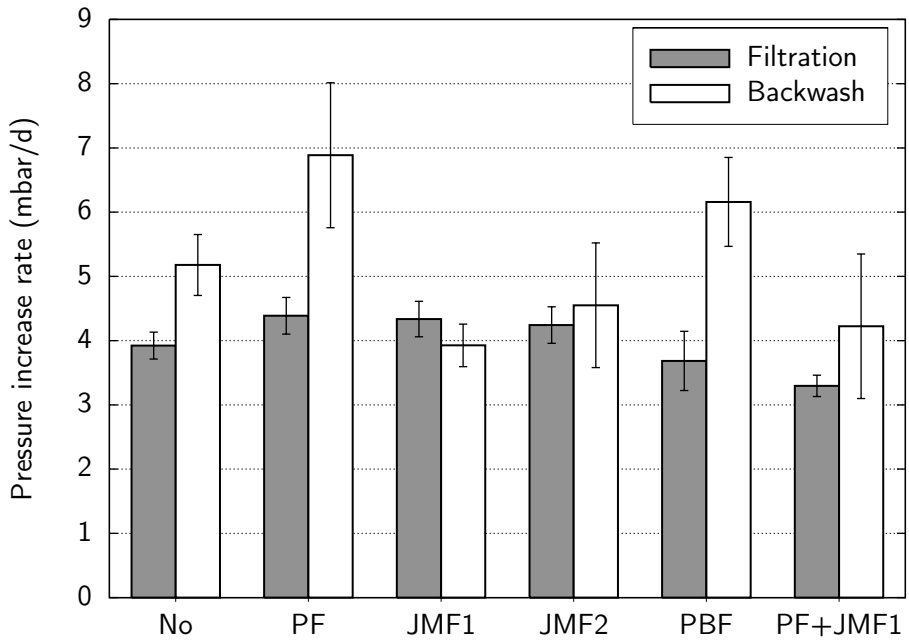

Figure 6.6: Flocculation effects at a PACl dosage of 5 mg Al/L (J=60 LMH, t_f=29.5 min, t_{bw}=0.5 min, error bars indicate 95%-confidence intervals). Data from Exps. P05, P01, P07, P13, P19, and P09

notably faster than the forward filtration pressure. The JMFs performed best in both configurations at the higher coagulant dosage (Fig. 6.6). It is interesting to note that the combination of 30-sec pipe flocculation with JMF1 gave a better performance with respect to backwash pressure increase than PF alone. However, it remains unclear why the backwash pressure increase rate after the PBF attained a relatively high value.

Under similar flocculation conditions, the pressure increase rate for filtration was strongly dosage dependent. Using a PBF, the pressure increase rate for filtration increased with the coagulant dosage (Fig. 6.7). At 2 mg Al/L, forward filtration resulted in practically no pressure increase rate. The backwash pressure increased rapidly at 2 mg Al/L while backwash pressure increase rates were lower at higher dosages. This behaviour may be explained with particle charge effects and precipitation kinetics. The lowest dosage does not meet the coagulant demand for complete destabilization and the forming precipitate is thus negatively charged. Accordingly, aggregation to flocs is poor, resulting in smaller particle size and higher cake resistance. The relatively high

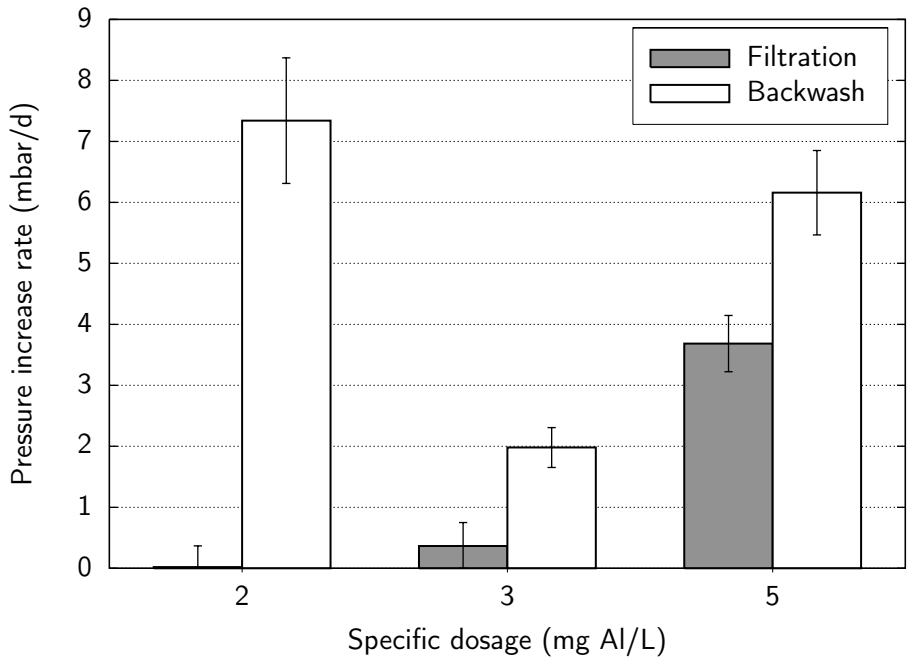

Figure 6.7: Fouling rates after packed-bed flocculation at different aluminium dosages (J=60 LMH, t_f=29.5 min, t_{bw}=0.5 min). Data from Exps. P20, P16, and P19

residual retentate turbidity of 14 NTU (Fig. P20f) and an average ΔP_{cycle} of 12–14 mbar (Fig. P20c) support this assumption. Due to opposing charges, the cake layer forming at 2 mg Al/L detaches easily from the membrane during a backwash. On increasing dosage, particles may attach stronger to the membrane owing to reduced charge repulsion forces. When low shear conditions prevail in the immersion tank, particles may enter interior surfaces of the membrane unhindered an form resistant fouling layers. Slow precipitation kinetics with subsequent precipitate formation in the fibre lumen may explain a higher backwash pressure increase rate in case of the lowest aluminium dosage. It must be noted, though, that the backwash pressure data from experiment P20 (Fig. P20b) have inconsistencies, which have affected the calculation of the backwash pressure increase rate. However, the generally higher pressure increase rate for backwashing points towards too short flocculation times.

Flux dependence. Increasing flux exacerbates membrane fouling because the permeation drag force acting on a particle increases with the flux. However,

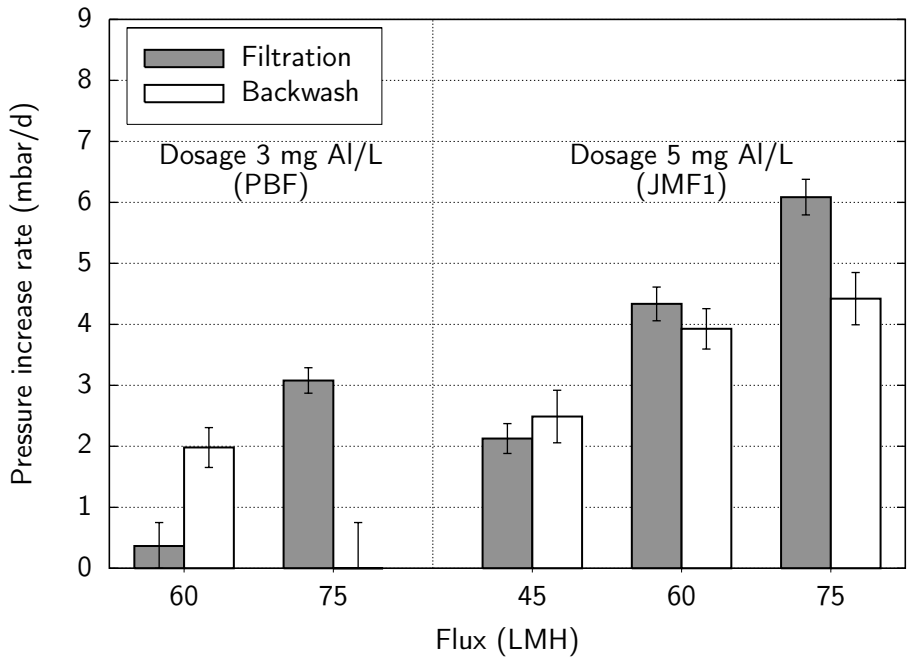

Figure 6.8: Flux-dependent fouling rates at two aluminium dosages (Flocculation in PBF and JMF1, t_f=29.5 min, t_{bw}=0.5 min). Data from Exps. P16–P17, P06–P08

since coagulation conditions influence particle characteristics, an interdependency between dosage and flux must be expected.

Fig. 6.8 compares pressure increase rates at optimal and slightly overdosed coagulation conditions for different fluxes. Increasing flux exacerbated fouling rates for both investigated dosages. However, the marked difference in system performance for both dosages indicates that dosage optimization is important. Given that full-scale systems normally operate at fluxes in the range of 40 to 60 LMH, a flux of 75 LMH is relatively high. Nevertheless, the pressure increase rates at 75 LMH and 3 mg Al/L were lower than the respective values at 60 LMH and 5 mg Al/L. A direct implication of these results is that variations in water quality will affect system performance if coagulant is dosed proportionally to flow.

Backwash dependence. Backwashing with permeate constitutes the most important method to control fouling of the membranes. The backwash protocol

is defined by an optimal configuration of

- reverse flux,
- aeration rate,
- backwash duration, and
- backwash frequency.

The backwash procedure described in section 6.3.1 relies on vigorous air scouring during backwashes, which disturbs settling and floc formation in the immersion tank. Provided that adequate flocculation improves the system performance, too frequent backwashes may have an adverse effect. Furthermore, more frequent backwashing decreases the system availability and increases water losses. On the other hand, too long filtration cycles may result in more non-hydraulically reversible fouling.

During all experiments, a backwash flux 50% above the forward filtration flux was applied. Although lower values are commonly used in practice, a high backwash flux was chosen to avoid limitations in backwash efficiency. With the exception of one experiment (2×10 s), backwash duration and frequency were adjusted in 3 different combinations to give a total backwash time of one minute per hour (4×15 s, 2×30 s, 1×60 s) and thus the same overall system productivity. The underlying assumption for this backwash strategy was that longer filtration cycles require longer backwash cycles.

Fig. 6.9 shows the effect of backwash frequency for a system with pipe flocculation. For alum coagulation at 5 mg Al/L, a trend towards better system performance becomes apparent with longer filtration cycles, i.e. less frequent backwashing. A backwash cycle once every 30–60 minutes gave lower pressure increase rates than backwashing every 15 minutes. On the other hand, coagulation with PACl at the same Al-dosage resulted in practically no significant difference in performance for the two tested backwash frequencies. Although the previous results showed that flocculation is not retarded at 5 mg Al/L, the reason for the difference in performance of both coagulants may lie in their flocculation behaviour. Flocculation kinetics with alum are slower than with PACl (section 3.4.1). An alum-coagulated feed may thus benefit from post-flocculation in the immersion tank to a larger extend than a PACl-coagulated feed. The performance obtained after alum coagulation with the shortest backwash cycle (2×10 s) was not poorer compared to the experiments with longer backwash duration (2×30 s and 1×60 s). Short, efficient backwash cycles are therefore preferable, which contradicts the assumption that the backwash cycle length should increase with the filtration cycle length. Interestingly, the

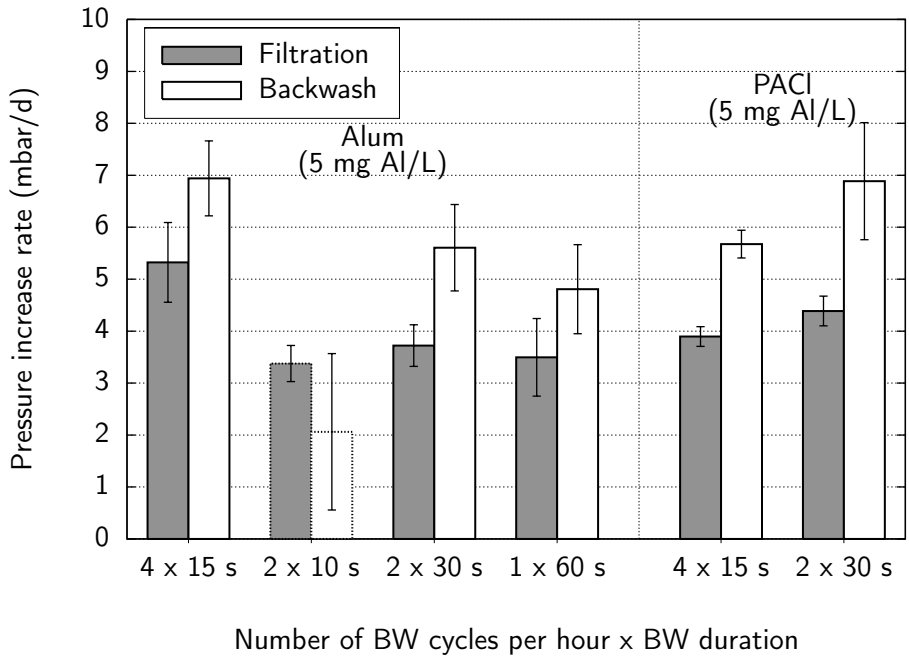

Figure 6.9: Influence of backwash frequency on pressure increase rates (Flocculation in PF, Flux J=60 LMH). Data from Exps. A03, A05, A01, A04, and P03, P01

shortest backwash cycles resulted in the lowest backwash pressure increase rate. However, the backwash pressure data show a considerable amount of scatter (Fig. A05b). The low regression value for the backwash pressure increase rate may therefore be misleading.

Following treatment in a flocculator with low G-value, the effect of backwash frequency was dosage-dependent (Fig. 6.10). Pressure increase rates for filtration decreased with the backwash frequency at a specific dosage of 3 mg Al/L (PACl). When applying a dosage of 3 mg Al/L, the residual retentate turbidity ranged from 25 to 28 NTU, indicating a relatively high fraction of small, slowly settling particles (Figs. P10d–P12d). Small particles are likely to cause more pore plugging, particularly after a high-turbulence backwash that can cause floc break-up. No clear effect on the backwash pressure increase rate became apparent. Only the highest backwash frequency (4 × 15 s per hour) resulted in a lower pressure increase rate for backwashing than for filtration. The results suggest that more frequent backwashes at this coagulant dose do not improve performance. Given the relatively low suspended solids

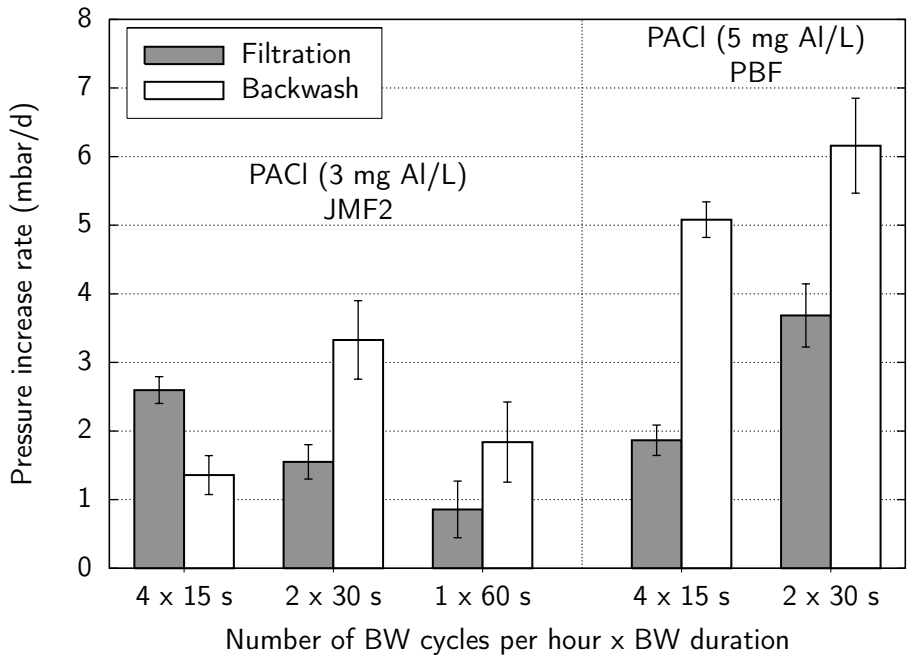

Figure 6.10: Influence of backwash frequency on pressure increase rates (Flocculation in JMF2/PBF, Flux J=60 LMH). Data from Exps. P10–12 and P18–19

concentration in the process tank, a backwash every 30–60 minutes is sufficient. It should be noted, however, that the average ΔP_{cycle} increased from 6–8 mbar per cycle for a 4 × 15 s protocol to about 18–20 mbar per cycle for a 1 × 60 s protocol (Figs. P10c–P12c). Although these differences seem small, longer filtration cycles render the system more vulnerable to performance loss caused by sudden changes in coagulation conditions.

The opposite effect occurred at a dosage of 5 mg Al/L. Backwashing every 30 minutes nearly doubled the pressure increase rate for filtration compared to backwashing every 15 minutes. Assuming stronger particle attachment due to lower charge repulsion at this coagulant dosage, longer filtration cycles allow for higher accumulation of solids on the membrane surface and in pores. Backwashing with permeate alone does not sufficiently remove deposits. The low residual retentate turbidity ($\simeq$ 10 NTU) indicates a larger particle size after flocculation at this dosage (Figs. P18f and P19f). Consequently, the cake porosity increases, explaining the lower pressure build-up during a filtration cycle ΔP_{cycle} compared to 3 mg Al/L. Compared to experiments P01 and

P03, conducted under similar conditions as P18 and P19 but with a pipe flocculator, pressure increase rates for filtration and backwashing are lower, which may be attributed to better flocculation using a PBF. However, in all cases, the backwash pressure increase rate was notably higher than that for filtration.

In summary, the results presented in this section show that flocculation plays an important but intricate part in fouling for an O–I system. Fouling exacerbates in the absence of controlled flocculation, particularly at short detention times. However, since some of the operating parameters discussed in the following sections influence particle behaviour in the immersion tank, it is difficult to distinguish post-flocculation effects from upstream flocculation.

6.3.4 Effect of water recovery

Experiments P21 through P24 aimed at assessing the effects of reducing the water recovery to 85% for two different dosages (3 and 5 mg Al/L) and fluxes (60 and 75 LMH).

At a set flux of 60 LMH, the most significant observation was the lower backwash pressure increase rate at 85% water recovery (Fig. 6.11). Removing retentate faster from the system reduces the solids retention time and thus the possibility of interactions between aluminium aggregates and the membrane. In experiments with 95% recovery, the low retentate flow rate resulted in an accumulation of a sludge layer in the bottom of the immersion tank, which was re-suspended during a backwash. While this effect can improve post-flocculation in the immersion tank, re-suspension of settled matter induced by air scouring will cause particle erosion and possibly partial dissolution of the amorphous precipitate. For a short period of time after a backwash, a precipitate may form on the lumen side of the fibre due to supersaturation of aluminium species, which increase the backwash pressure for a constant backwash flux over time. Re-suspension of settled particles occurred to a much lesser degree at 85% recovery and may explain the lower backwash pressure increase rate. On the other hand, the pressure increase rates for filtration were either somewhat higher or as high as for 95% recovery. As expected, the lower suspended solids concentration in the immersion tank at 85% recovery slightly reduced the pressure build-up during a filtration cycle of 30 minutes (Figs. P21b and P22b). Compared other experiments with specific aluminium dosages of 5 mg/L (e.g. P05, P13, P18–19), the residual retentate turbidity increased at 85% recovery. However, neither of these observations seemed to have had an influence on the filtration pressure increase rate or backwash efficiency.

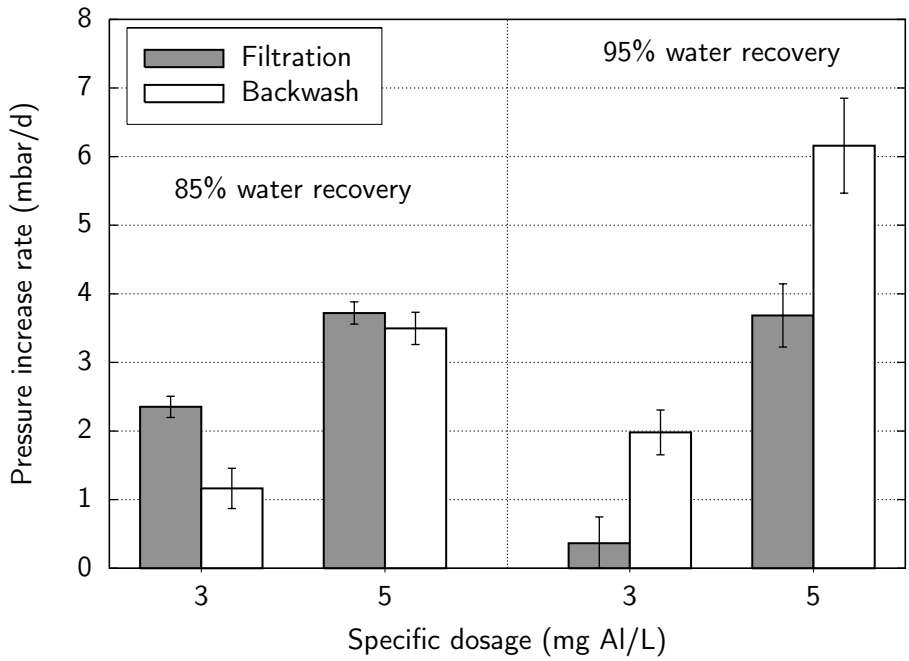

Figure 6.11: Effect of water recovery on pressure increase rates (Flux J=60 LMH, Flocculation in PBF). Data from Exps. P21–22, P16, and P19

At a flux of 75 LMH, again practically no difference in pressure increase rates between filtration and backwash was observed at 85% water recovery (Fig. 6.12). Compared to the experiments at 60 LMH, the effect of coagulant dosage on the fouling rates was even less pronounced at 85% recovery. No benefit of operating at lower water recovery was evident at a dosage of 3 mg Al/L, although the backwash pressure increase rate measured at 95% water recovery (Exp. P17) was unexpectedly low and may be an outlier. On the other hand, lower water recovery improved performance at 5 mg Al/L. Assuming that flocculation is not retarded at this dosage, it is unlikely that the different choice of flocculator (PBF vs. JMF1) affected the result to such a high extent. The increased downflow velocity and improved solids removal at 85% are a more likely explanation for the better performance.

Lowering the water recovery gave more stable and lower backwash pressure increase rates. However, the seemingly poorer performance at 95% recovery may be explained by inefficient sludge removal. Sludge withdrawal could have been improved either by withdrawing retentate batch-wise at increased flow

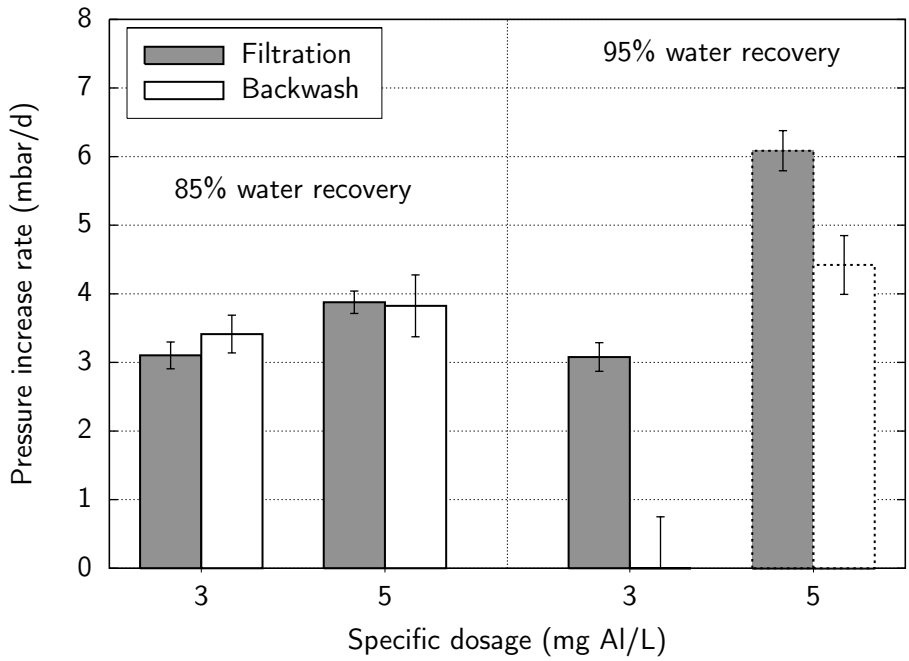

Figure 6.12: Effect of water recovery on pressure increase rates (Flux J=75 LMH, Flocculation in PBF, dashed line denotes flocculation in JMF1). Data from Exps. P23–24, P17, and P08

rates shortly before a backwash or by an optimized design of the tank bottom (e.g. sedimentation cone). However, neither of these options were tested. At 85% recovery, the residual retentate turbidity increased notably at higher specific coagulant dosage, indicating a higher fraction of small particles with low settling velocities. This renders subsequent retentate sedimentation as suggested in Fig. 4.3 less efficient and may pose a problem in terms of particle return load to the membrane unit. Consequently, fouling rates at 85% water recovery may increase over the value obtained in these experiments. For the optimal dosage of 3 mg Al/L, no significant improvement of reducing water recovery became apparent.

6.3.5 Effect of coagulation pH

In a parallel study on contact filtration based on the same raw water, Saltnes *et al.* (2001) measured minimum aluminium solubility for alum and PACl at pH 6.3–6.4 (Fig. 6.15). The coagulation pH throughout most experiments (P01–

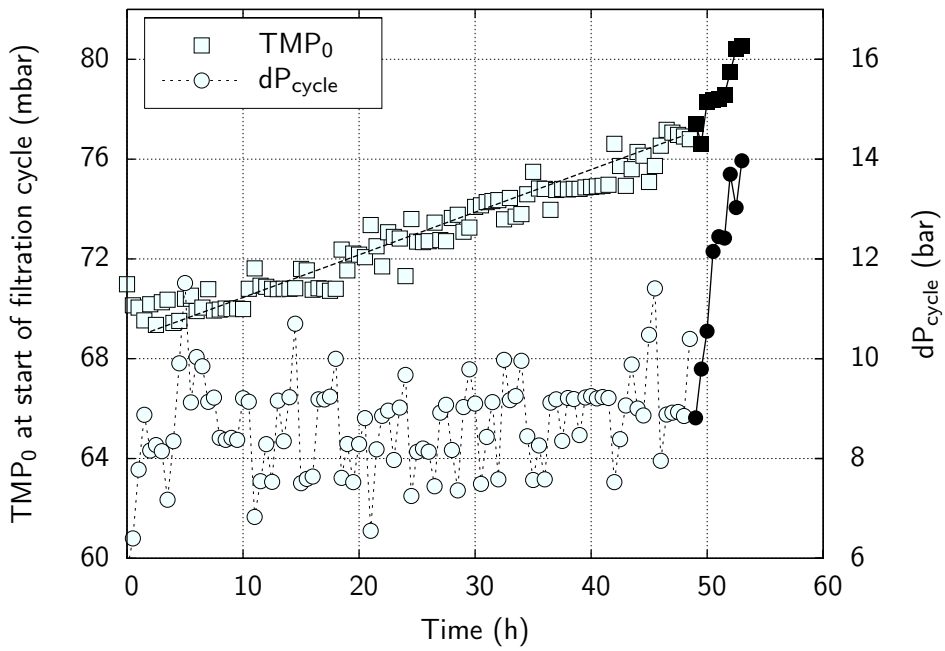

Figure 6.13: Effect of sudden pH drop (Flux J=60 LMH, 5 mg Al/L, open symbols pH 6.2, filled symbols pH 5.6).

P24) was therefore held at 6.3 ± 0.1 to remove as much as possible of the added coagulant with the precipitate. Experiments with pH outside this range were conducted for two reasons:

- *Faulty pH control* can cause sudden pH changes, which affect membrane performance. Since chemical addition is prone to disturbances, the consequential effects must be evaluated.
- *Coagulation at higher pH* increases particle size. Zouboulis and Traskas (2005) also showed that flocculation occurs more rapidly at pH 7 than at pH 6. Although coagulant demand and residual aluminium concentrations increase, fouling may decline as a result of different aggregate structure and charge.

Low pH coagulation. Fig. 6.13 illustrates the response of a simulated pH drop after two days of normal operation. Following a low and linear pressure incline, a sudden pH drop causes a steep increase of the filtration pressure.

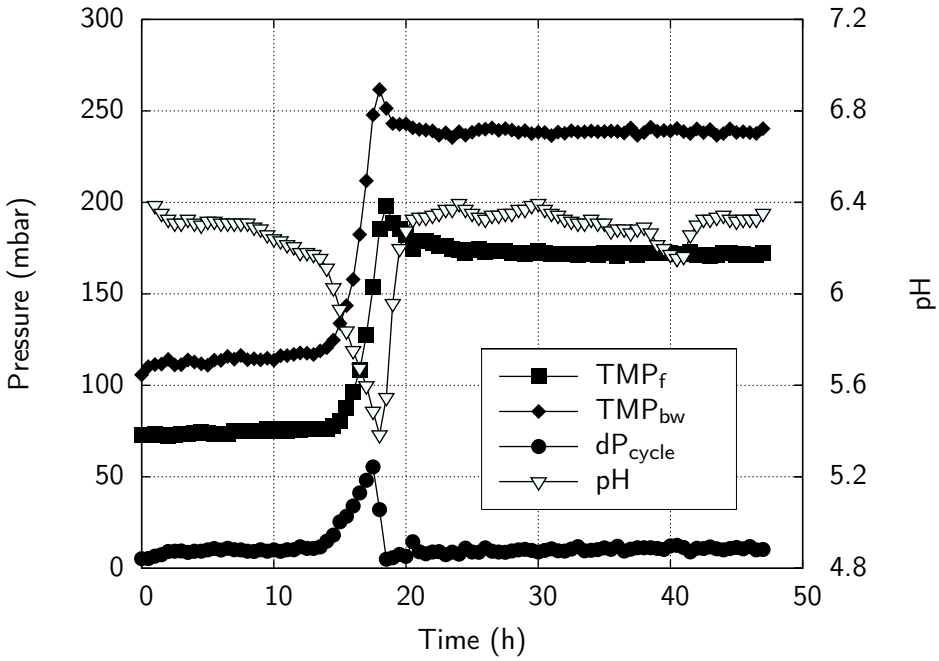

Figure 6.14: Pressure recovery after a sudden pH drop (Flux J=60 LMH, 5 mg Al/L). The pH incident occurred approximately 15 hours after start-up and lasted for about 3 hours.

Similarly, the average ΔP_{cycle} increases by roughly 60%, indicating a significantly reduced permeability of the cake layer. A pH drop only becomes visible after a certain delay due to the residence time of the system. These findings are consistent with research on I–O filtration of PACl-coagulated surface water presented by Lerch *et al.* (2005). The explanation for this behaviour lies in the changed aggregate characteristics. Coagulation at lower pH leads to a higher prevalence of polyvalent, cationic aluminium species and reduces the charge on the functional groups of humic substances. Aggregates formed under these conditions are smaller in size and carry higher charge. Consequently, reduced charge repulsion causes them to bind stronger to a negatively charged membrane surface, thus building dense and resistant fouling layers. A normal CIP with chlorine solution removed all foulants completely and restored the clean water permeability of the membrane.

A follow-up experiment conducted under similar conditions allowed to assess the recovery of system pressures after the coagulation pH was restored. Fig. 6.14 shows that only the pressure build-up during a filtration cycle ΔP_{cycle}

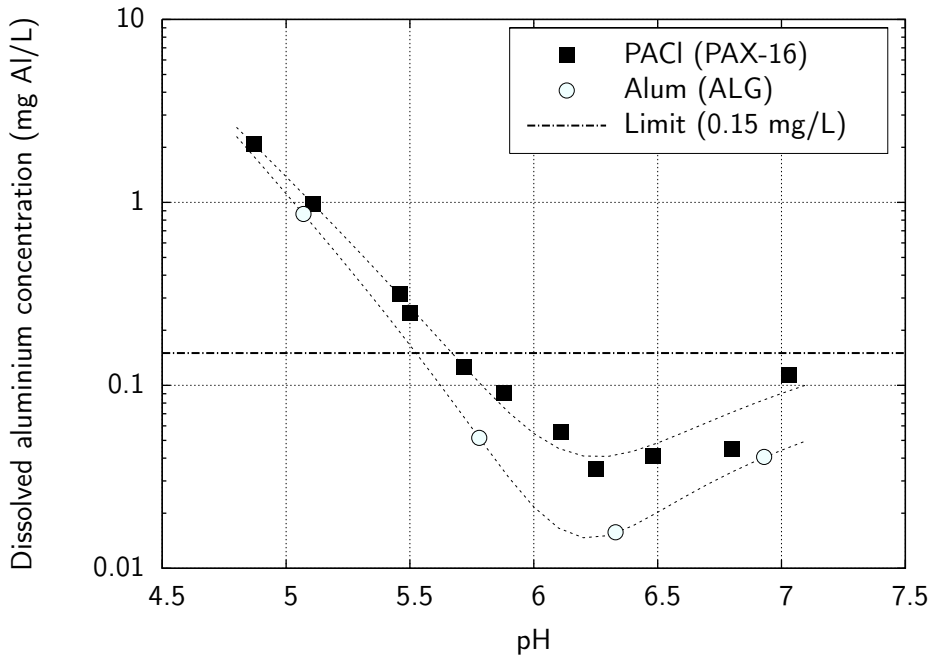

Figure 6.15: Residual aluminium concentration vs. coagulation pH established for the raw water used throughout the study (adapted from Saltnes *et al.* (2001)).

attains the same value as before the pH incidence, while the filtration and backwash pressures sustain permanent losses. However, a certain recovery from the highest pressure points became apparent for both pressures and pressure increase rates stabilized once the coagulation pH returned to its set value. The likely explanation for this behaviour is the sudden change in coagulation conditions after a pH drop. Particles forming under coagulation conditions in the charge-neutralization regime (low pH) cause more pore fouling and less permeable cake layers. Surface layers on the membrane detach during air scouring-assisted backwashes after the pH is restored, explaining the moderate decrease in filtration pressure after the pH incident. On the other hand, pore fouling does not respond to backwashes and thus exerts a resistance to filtration also after the coagulation pH returns to its set value of 6.3. Minor pH variations above pH 6 did not affect filtration pressures to any significant extent.

The results show that even a short pH drop severely reduces system performance due to formation of hydraulically not reversible fouling, which underscores the importance of pH control. Hillis (2006) made similar observations in

a pilot study based on the same membrane system but with ferric sulphate as coagulant. The system responded with a steep incline in filtration pressure to pH control failures. However, in contrast to the results presented here, pressure recovery was notably better once the target coagulation pH of 4.5 was restored. From point of view of permeate quality, a moderate pH drop will not necessarily have negative consequences. Colour removal increases with decreasing pH and turbidity removal remains unaffected. On the other hand, soluble aluminium concentrations also increase as shown in Fig. 6.15. Outside the optimal pH range of 5.6–7.0, residual aluminium concentrations do not comply with the maximum permissible limit in Norway (0.15 mg Al/L).

High pH coagulation. At pH 7, flocculation conditions changed visibly due to more sweep coagulation. Voluminous, "fluffy" flocs were apparent in the flocculator and in the immersion tank. The suspended material settled quickly, resulting in a lower residual turbidity in the immersion tank than observed at pH 6.3 (Figs. P25f and P26f). The fouling layer on the hollow fibres was dark brown and appeared gelatinous, while at pH 6.3 a yellow-brownish colour and a grainy appearance was typical.

A comparison of pressure increase rates reveals a trend towards lower long-term fouling at pH 7 and higher specific aluminium dosage. For a coagulant dosage of 3 mg Al/L no statistically significant difference was established (Fig. 6.16). However, the lower coagulant dosage at pH 6 (3 mg Al/L) gives a better permeate quality in terms of colour and UVA than the higher dosage (5 mg Al/L) at pH 7. If the treatment goal is to achieve a permeate colour below 10 mg Pt/L, coagulant consumption and sludge production increase by about 60% at pH 7. However, contrary to the findings of Lee *et al.* (2000), coagulation at pH 7 did not increase long-term fouling as observed in this study at pH values well below 6. The average pressure increase per cycle (ΔP_{cycle}) was higher at pH 7, presumably due to a lower permeability of the cake layer forming on the membrane (Figs. P25c and P26c).

In summary, coagulation in the transition regime between charge neutralization and sweep coagulation is optimal with respect to keeping filtration pressures low, using low coagulant concentrations, and obtaining low metal residuals. These coagulation conditions correspond largely to those used in direct media filtration. Because charges on humic substances increase with the pH, organic removal is more efficient in the pH range of 6–6.5 than at pH 7 and above. Below pH 6 hydraulically not reversible fouling increases dramatically, while low pressure increase rates were observed in the pH range of 6–7.

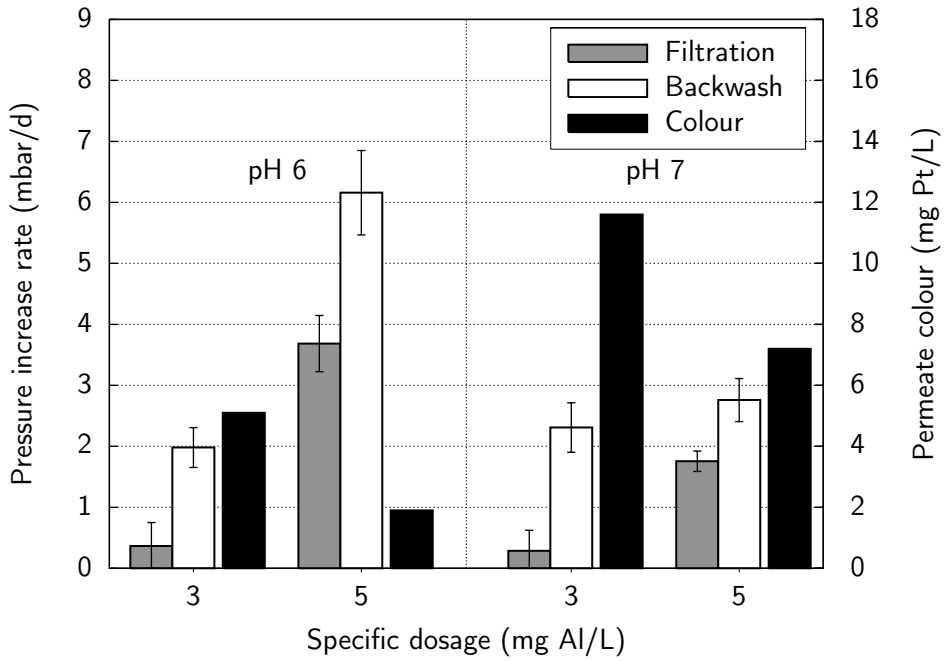

Figure 6.16: Pressure increase rates at pH 6 and 7 and permeate colour concentration (Flux J=60 LMH, Flocculation in PBF). Data from Exps. P16, P19, and P25–26

6.3.6 Effect of NOM concentration.

Experiments P27 and P28 assess the membrane performance at a lower raw water NOM concentration of 30 mg Pt/L. Coagulant dosages were reduced to 1.5 and 2.0 mg Al/L to achieve similar NOM removal as in the previous experiments. Despite lower sludge production and thus lower solids concentration in the immersion tank (Figs. P27d and P28d), ΔP_{cycle} attained values in the same range (9 ± 3 mbar) as before. This shows that the pressure increase due to cake fouling is significantly affected by particle characteristics and that the retentate solids concentration alone does not serve to predict ΔP_{cycle} (see also section 6.4).

As anticipated, the pressure increase rates for filtration and backwash at colour 30 mg Pt/L climbed to similar values as measured for higher raw water colour. The backwash pressures increased at a slightly higher rate than the filtration pressures, which may be attributed to the short flocculation time as mentioned earlier. However, comparing the results of both raw water NOM

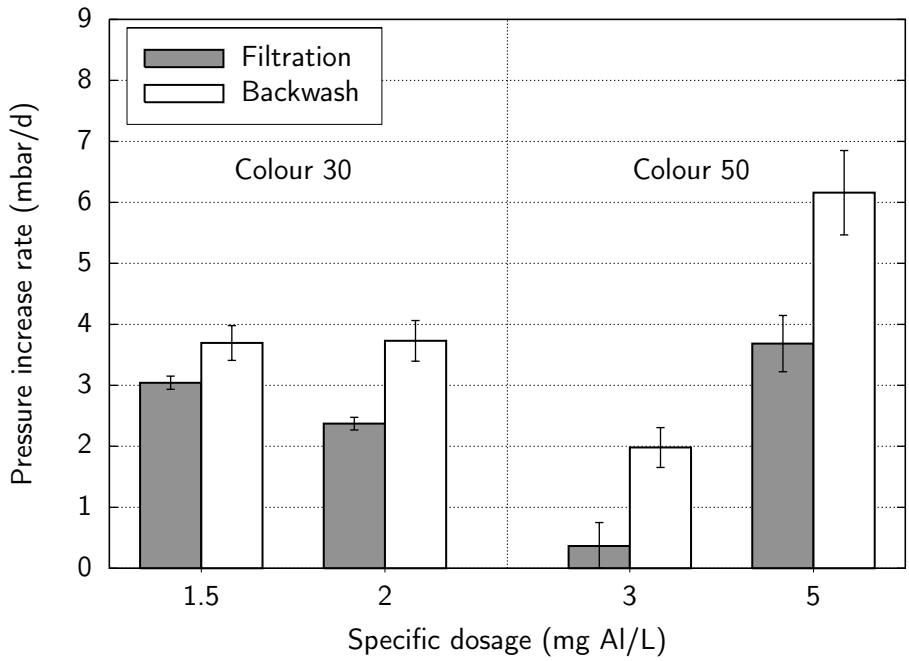

Figure 6.17: Effect of NOM concentration on pressure increase rates (Flux J=60 LMH, Flocculation in PBF). Data from Exps. P27–28, P16, and P19. Colour given as mg Pt/L

concentrations, it is noteworthy that a coagulant dosage of 3 mg Al/L at higher colour gave slightly lower pressure increase rates than all values obtained at lower colour (Fig. 6.17). The reason for this is likely to be generally improved flocculation kinetics at higher coagulant dosages/solids concentrations.

Both experiments at lower raw water colour resulted in a very stable performance in terms of pressure increase rates, ΔP_{cycle}, suspended solids, and residual turbidity. Due to lower solids production and thus lower solids concentration in the immersion tank, sludge withdrawal was effective so that no resuspension of settled matter could occur during backwashes. As observed in experiments with reduced water recovery, backwash pressure increase rates stabilized and attained values close to those for filtration.

In summary, the results from Exps. P27–P28 show that the performance of the membrane unit remains relatively unchanged when treating raw waters with lower NOM concentration.

6.4 Multivariate analysis of effects

The multitude of effects occurring during coagulation and immersed membrane filtration makes an overall quantitative comparison of operating conditions quite complex. Multivariate analysis allows separating the different treatment conditions from each other and comparing their individual influence on membrane performance quantitatively. Furthermore, the analysis offers a possibility to identify potential outliers in the results.

A subset of experimental data was evaluated using partial least squares (PLS) regression, a technique that generalizes and combines features from principal component analysis and multiple regression. This method is particularly useful when predicting a set of dependent variables from a large set of independent variables.

Notations. Every experiment represents one *observation* of process behaviour as the result of chosen operating parameters. The following conventions are made to organize the data set for analysis:

$$\begin{aligned} \text{Operating conditions} &= \textit{Predictors} = \text{independent variables } (X) \\ \text{Measured process behaviour} &= \textit{Response} = \text{dependent variable(s) } (Y) \end{aligned}$$

In case of only one dependent variable[c], the response Y exists as vector with i observations. The values of k predictor variables collected on these observations are stored in the $i \times k$ predictor matrix X (see Appendix C).

General principles. The goal of PLS regression is to predict Y from X and to describe their common structure. PLS regression is based on linear transition from a large number of original predictors to a new variable space defined by a small number of orthogonal factors, called PLS components or *latent vectors*. In other words, PLS components are mutually independent linear combinations of the original predictors. By performing a simultaneous decomposition of X and Y, the PLS algorithm determines these components iteratively in such a way that the first PLS component explains most of the covariance between X and Y, the second components explains the maximum share of the residual covariance, and so on. Unlike similar approaches (e.g. principal component

[c]There are two PLS algorithms, PLS1 for problems with a univariate response variable, and PLS2 for problems with multivariate response variables. In this study, only PLS1 was used.

regression), PLS regression avoids focussing on large variations in the predictor variables that are of minor importance for explaining the variation in the response variable(s). Regressions are accompanied by a validation procedure to find the optimal number of PLS components and test models for robustness.

Data pre-processing. Pre-processing of data aims at reducing "noise" introduced by background effects, different measurement units, different variances in variables, etc. For all analyses, two data preprocessing options were chosen: centering and weighting. *Centering* involves subtracting the average from each variable (mean-centering). This ensures that all results will be interpretable in terms of variation around the mean. *Weighting* is a special form of scaling, which becomes important when variables have largely different value ranges. All variables were multiplied with the reciprocal of their respective standard deviations $1/SDev$. In this way, each variable has the same variance and thus the same chance to influence the estimation of the PLS components. Response values were not weighted.

Instead of pH values, the respective molar concentration of dissociated hydrogen $[H^+] = 10^{-pH}$ was used for modelling to circumvent the use of a predictor variable with a logarithmic scale.

Model and Output. Response values are approximated by a linear combination of the predictors. In its simplest form, a PLS model specifies a linear relationship between the response variable Y and a set of predictors X

$$Y = b_0 + b_1X_1 + b_2X_2 + \ldots + b_kX_k + \epsilon \tag{6.5}$$

where b are the regression coefficients and ϵ the residual error. If a predictor is weighted, the regression coefficient b contains the weighting factor s:

$$b = s \cdot b_w \tag{6.6}$$

The weighted regression coefficient b_w can be used to compare the influence of predictors against each other. In the following sections, b_w is therefore used as a relative measure of individual effects on the pressure development during membrane filtration.

The main results of PLS regression include scores and loadings plots, predicted Y-values, residuals, error measures, and regression coefficients. Scores and loadings plots serve to diagnose the regression, to identify outliers, etc. A comprehensive explanation is given by Martens and Næs (1989). An important

error measure is the *residual Y-variance*, which expresses how much variation remains in the observed response after the modelled part is taken out. The residual Y-variance is an overall measure of misfit. The complement value is called *explained Y-variance*. Both values are expressed as percentage of the total Y-variance and their sum equals to unity.

PLS regressions were performed using version 7.5 of the software package The Unscrambler by Camo Software AS (`http://www.camo.com`). Modelling parameters and result plots are summarized in Appendix C.

6.4.1 Pressure increase rates

The pressure increase rates obtained in Exps. P01–P26 were submitted to PLS regression. In the remaining data set, experimental conditions differed significantly due to either use of a different raw water or a different coagulant. The latter data was therefore excluded from PLS regression. As a starting point, a total of 9 predictors was chosen:

- Four different flocculators (PF, JMF1, JMF2, PBF)
- Dosage (specific aluminium dosage)
- Backwash frequency (#BW per hour)
- Water recovery (w)
- Flux
- Coagulation pH (as $10^{-\mathrm{pH}}$)

Using flocculation conditions in terms of flocculation time and rms velocity gradient (G-value) as predictor proved unsuccessful because the values of these variables varied little between experiments. Neither did the residual turbidity measured in retentate samples serve as adequate predictor for flocculation, partly because of missing values. Instead of introducing a quantitative measure of flocculation, each type of flocculator was assigned a variable with two levels: "1" for flocculator used and "0" for flocculator not used. In experiments without controlled flocculation, all four flocculator variables were set to zero (see Tab. C.7).

Filtration pressure. The pressure increase rates for filtration (m_f) were set as response variable and subjected to PLS regression. No particular outliers were identified in the data set. The weighted regression coefficients for 2 predictor sets are shown in Fig. 6.18.

Including all 9 predictors in a regression explained 73% of the variance in Y (residual Y-variance of 27%). Validation suggested that one PLS component described the data set optimally. Flux and dosage were the two strongest predictors explaining 64% of the Y-variance alone. This means that the other 7 predictors as a group conveyed little information. Hence, the b_w values (white bars in Fig. 6.18) only serve as a first indication of a predictor's influence. The results suggest that flocculation could reduce the pressure increase rate for filtration. Increasing water recovery also gave a slight reduction of the response. All other predictors, particularly increasing coagulant dosage and flux, lead to higher pressure increase rates. It must be borne in mind that using $10^{-\mathrm{pH}}$ as predictor instead of pH inverts the sign of the regression coefficient. Thus a positive value of b_w for this predictor implies that increasing pH *decreases* the pressure increase rate for filtration. The results obtained with the regression model coincide well with the observations described in the previous section. However, the weighted regression coefficients (b_w) could not be tested for significance. The possibility of large uncertainty limits therefore renders their absolute values not robust for direct comparison.

In order to find the significant effects and establish more confidence in the result, PLS regressions were run iteratively with subsets of the predictor variables to minimize the residual Y-variance. The best predictor set consisting of only PBF, coagulant dosage, water recovery, flux, and $10^{-\mathrm{pH}}$ explained 81% of the variance in the response, thus reducing the residual Y-variance to 19%. These 5 predictors were subsequently considered significant and the remaining ones omitted from regression. The revised b_w-values are plotted with grey bars in Fig. 6.18.

In descending order, dosage, flux, and the presence of a PBF came out as the strongest predictors. As anticipated, coagulant dosage optimization remains of vital importance for the successful operation of the membrane system. In comparison, the influence of the coagulation pH within the range of 6.3–7.0 is significantly lower. Since the model predicts a lower contribution of flux to pressure increase than dosage, a dosage-optimized system can operate at higher flux than an overdosed system to reach the same pressure increase rate. It is noteworthy that the presence of a PBF reduced the pressure increase rate. This result highlights the benefit of controlling flocculation conditions in a coagulation assisted membrane system with immersed membranes. However, the choice of flocculator seems important since the PBF outperformed the other flocculators. On the other hand, neither the pipe flocculator (PF) nor the jet-mix flocculators (JMF1/2) remained in the set of significant predictors due to too high uncertainty in these variables. Particularly the effect of the JMF1/2

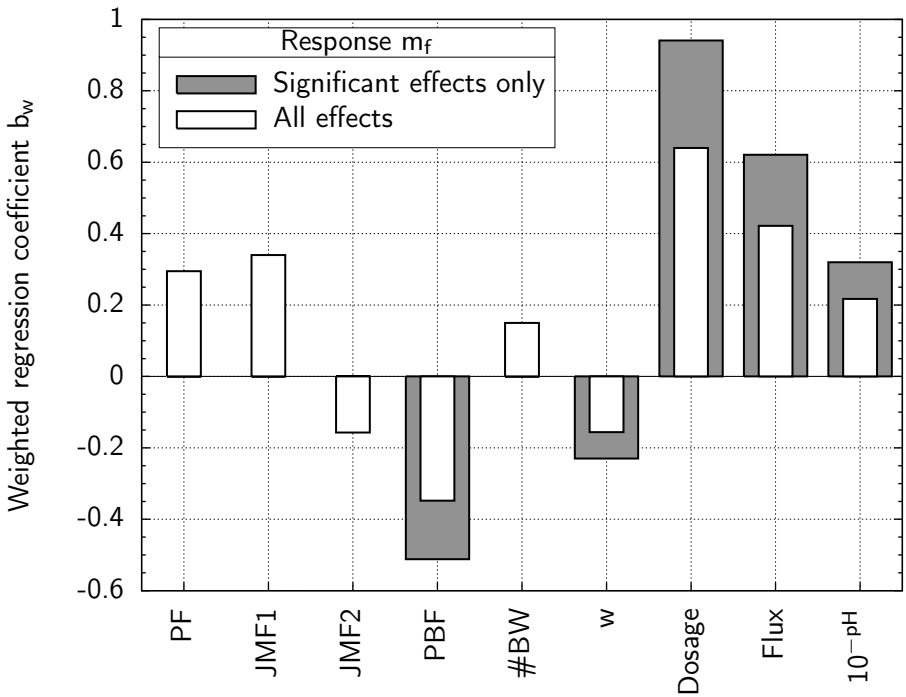

Figure 6.18: Relative influence of predictors on the filtration pressure increase rate m_f for two predictor sets.

may therefore be underrated. The negative contribution of water recovery to pressure increase suggests that operation at higher recovery is favourable.

Backwash pressure. The same procedure as above was applied to the backwash pressure increase rates (m_{bw}). Two response values obtained in Exps. P17 and P20 could be identified as outliers. Both values were suggested as possible outliers in the previous section. PLS regression thus confirmed them as outliers and both values were subsequently excluded from further analysis.

Also in this case, validation showed that one PLS component described the backwash pressure increase rate optimally. A PLS regression model based on all 9 predictors explained 66% of the Y-variance. Coagulant dosage and flux alone explained 59% of the Y-variance, while most of the remaining predictors influenced the Y-variance to a lesser degree (white bars in Fig. 6.19). Since the backwash pressure data was generally more scattered, a higher residual Y-variance and larger uncertainty limits for the b_w-values had to be expected.

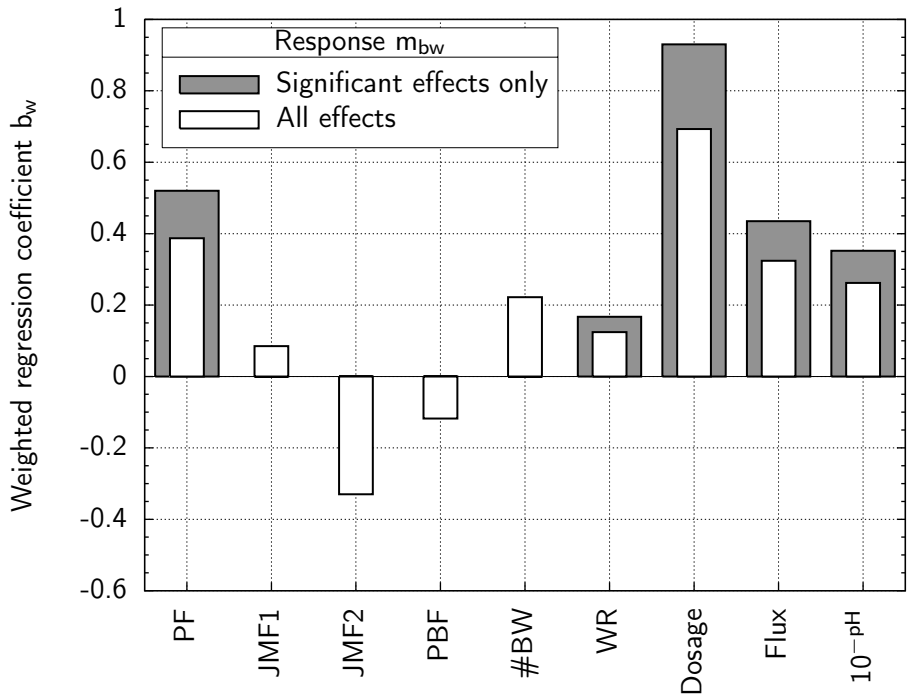

Figure 6.19: Relative influence of predictors on the backwash pressure increase rate m_{bw} for two predictor sets.

Five predictors were identified as significant: (1) dosage, (2) presence of a pipe flocculator, (3) flux, (4) 10^{-pH}, and (5) water recovery. PLS regression using only these five predictors increased the explained Y-variance to 72%. Coagulant dosage was also the strongest predictor for the development of the backwash pressure. For practical application, this shows clearly that overdosing coagulant will shorten the run time between two CIPs. Evidently, the filtration and backwash pressures will not develop independently as assumed here. However, the clear and nearly equally strong influence of the coagulant dosage on both pressure increase rates makes dosage optimization imperative. The b_w-value for the pipe flocculator (PF) conceals a large uncertainty interval because of few response values. In principle, flocculation conditions were not expected to influence the backwash pressure increase rate. Nevertheless, the positive contribution of this predictor reflects the fact that flocculation at high G-values did either not improve or worsen pressure increase compared to a system with no controlled flocculation. The PLS regression model also predicts a slightly higher backwash pressure increase rate at higher water recovery.

As mentioned earlier, less efficient solids removal in experiments with higher recovery may have caused this influence. On the other hand, water recovery is a minor predictor for the backwash pressure increase rate and may thus be neglected. The coagulation pH influenced the development of the backwash pressure moderately and to a similar extent as the filtration pressure. Higher pH decreased both pressure increase rates slightly but also resulted in poorer permeate quality.

6.4.2 Pressure increase per filtration cycle

Due to its "early-warning-potential", the pressure increase in each filtration cycle is a valuable process control parameter. The primary reason for increasing pressure during filtration is cake formation. Under stable operating conditions, ΔP_{cycle} remains relatively constant. Any sudden changes in operating conditions will affect ΔP_{cycle} first, which gives the plant operator time to remedy faults before extensive hydraulically irreversible fouling occurs on the membranes. To compare and analyze the influence of operating parameters on cake formation, a similar procedure as described in the previous chapter was applied to the average[d] pressure increase per filtration cycle.

The resistance-in-series model presented in Eq. 3.8 represents a mechanistic approach to describing the pressure increase per filtration cycle. However, assessing the resistance of the cake layer by models such as described by Eqs. 3.9–3.10 is cumbersome because values for the model parameters may not be available. Using the resistance-in-series model as a basis, the cake resistance and thus the average pressure increase per filtration cycle may be described by a PLS model. Provided that only the accumulating cake layer and the membrane exert a resistance to flow, ΔP_{cycle} can be derived from Eq. 3.8:

$$\Delta P_{cycle} = \mu \cdot J \cdot R_c \tag{6.7}$$

The cake resistance will be a function of several operating parameters and shall be described by a PLS model. Since the flux J enters as multiplier, the structure of Eq. 6.7 differs from that of a PLS model (Eq. 6.5). Dividing by the flux and grouping constants leaves R_c as modelling object with the response

$$\frac{\Delta P_{cycle}}{J} = b \cdot R_c \tag{6.8}$$

[d] Average of all ΔP_{cycle}-values measured at steady-state conditions.

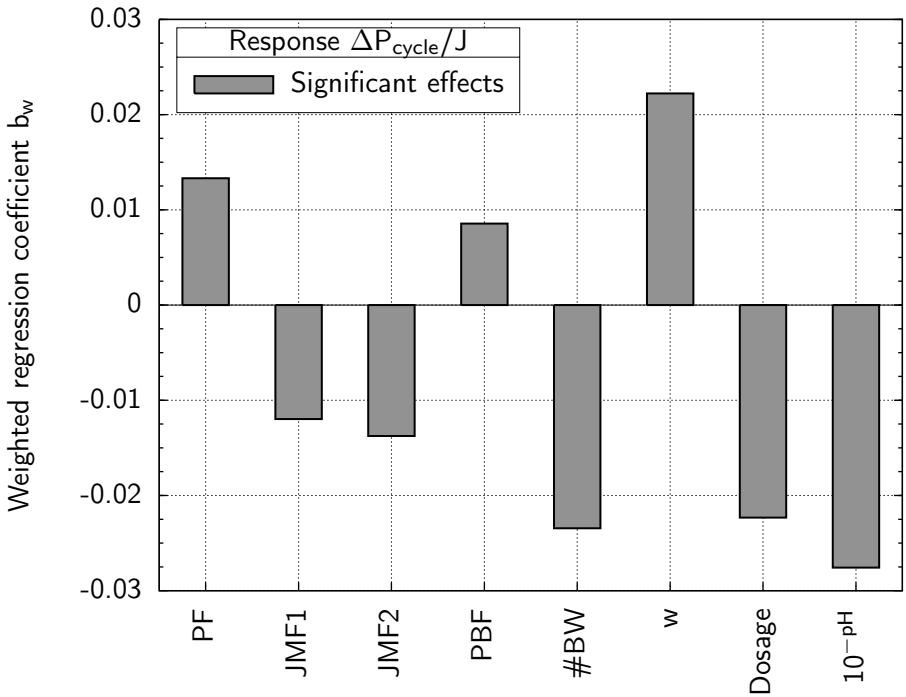

Figure 6.20: Relative influence of predictors on $\Delta P_{cycle}/J$.

A PLS model based on two PLS components was fitted to this response using the previously mentioned predictors, except flux. The regression results indicated that the response values obtained in Exps. P12 and P25 were outliers. Incidentally, the highest ΔP_{cycle}-values were measured in these two experiments. This gives rise to the assumption that operating conditions leading to high cake resistances exert non-linear influences that are not captured by the model. The high ΔP_{cycle}-value in Exp. P12 was due to long filtration cycles (1 hour). Since the data set contains no further experiments with equally long filtration cycles, P12 was excluded from regression. On the other hand, coagulation at pH 7 is the most likely explanation for the high pressure increase in Exp. P25. Despite the deviation, observation P25 was kept in the data set to retain information on pressure development at pH 7 and to complement P26.

The revised PLS model based on 25 observations explained 84% of the variance in the response. Coagulation pH, backwash frequency, water recovery, and coagulant dosage were the 4 strongest predictors describing 67% of the Y-variance (Fig. 6.20). This implies that the group of remaining predictors still carries a significant share of information. In principle, all of the 8 predictors

may be expected to influence R_c due to their effect on

- filtration time,
- cake layer thickness, or
- particle characteristics.

The revised PLS model also reflects this because the regression returns all predictors as significant. According to the b_w-values, flocculation using a PF or PBF increases cake resistance, while jet-mix flocculation leads to lower resistance in the cake. It may be hypothesized that the former flocculation conditions give denser cake structures due to smaller particle size. In case of the PF, the high shear forces prevent formation of larger flocs, while in the PBF floc size is limited due to particle erosion in the packed bed. As no such limitations exist in the jet-mix flocculators, more porous cake structures with lower resistance form due to larger floc size. The obvious correlation with cake layer thickness explains the strong influences of backwash frequency and water recovery. More frequent backwashing reduces the cake layer thickness; higher water recovery increases it due to higher particle concentration in the immersion tank. Furthermore, the model also predicts the strong inverse relationship between coagulant dosage and cake resistance. Although increasing dosage leads to higher sludge production and thus thicker cake layers, cake resistance decreases. This can be attributed to improved flocculation as commented earlier. Since the particle collision frequency increases with the particle concentration, larger aggregates are formed, which increases cake porosity. Pikkarainen *et al.* (2004) found a similar behaviour for iron-based coagulants. Finally, the PLS model also accounts for the notably higher ΔP_{cycle}-values measured at pH 7 (Exps. P25 and P26), which are likely to be due to denser cakes forming from the more voluminous sweep-flocs. Even though the pressure increase per filtration cycle is not a critical design parameter, its strong dependence on coagulation conditions is striking. Coagulation with PACl at pH 6–6.5 limits pressure development, while both lower and higher pH increase ΔP_{cycle} significantly (Fig. 6.13–6.14).

6.4.3 Limitations of multivariate analysis

Multivariate analysis is an empirical or data-based modelling method. The structure of empirical models is determined by an observed relationship among experimental data rather than by underlying physical, chemical, and biological principles. While empirical models can be useful for forecasting and describing

Table 6.7: Steps in developing empirical models

Step	Task description
1	Collect data
2	Specify a correlation structure between variables
3	Use a technique to find parameters maximising the correlation between data
4	Validate the model
5	If model is not satisfactory go to step 2

trends in behaviour, they are not necessarily mechanistically relevant. It must be underlined that the objective of using multivariate analysis in this study was mainly to assess the relative influence of predictors quantitatively, not to develop process models. The latter requires a thorough development procedure and a more extensive data set (Tab. 6.7).

PLS regression represents one of many different empirical approaches to analyze data. Since the structure of PLS models is based on linear contributions of predictors only (Eq. 6.5), complex mathematical relationships cannot be described. Evidently, this is a limitation of PLS models. On the other hand, major deviations from linearity between X and Y were not detected in any of the three models presented in Chapter 6.4. Other shortcomings that may be implicated in the PLS-approach:

Limited data set. Empirical modelling techniques depend strongly on the availability of representative data. In the present study, some operating parameters were varied during a few experiments only (e.g. water recovery and pH), others are under-represented in the experiments. This increases the uncertainty intervals of the respective predictors.

Narrow calibration range. For practical reasons, some operating parameters were varied within a relatively narrow margin. Extrapolation of response values outside the calibration range are thus prone to error. For instance, the PLS model would fail to forecast the high pressure increase rates observed below pH 6.

Flocculation was introduced as a "blackbox process". The regression coefficients obtained for the flocculation predictors are therefore of no physical

significance and their absolute values should not be compared with the other predictors. For flocculation, the sign of the coefficient and the significance of the predictor should be regarded as the most relevant result.

Residual Y-variance. The presented PLS models explained between 70% and 85% of the Y-variance. Although some variation in the data must be attributed to experimental error, a residual Y-variance of 15–30% indicates the existence of other, unknown factors influencing the response. As a result, some response values are described poorly by their respective predictor values.

Chapter 7

Conclusions

7.1 Revising hypotheses

The results presented in the previous chapter allow for a validity check of the hypotheses set forth a priori in Chapter 4:

A Operation without continuous air scouring is feasible.

In absence of continuous air scouring, the filtration pressure increases faster in each cycle due to stronger cake formation. Nonetheless the results showed that the long-term pressure increase due to hydraulically not-reversible fouling remains unaffected provided that backwashing is efficient. Furthermore, without continuous air scouring, particles settle in the immersion tank during each filtration cycle, which allows for more efficient sludge withdrawal. A rough estimation demonstrated that continuous air scouring consumes about 10 times the amount of energy used for permeate withdrawal and backwashing. Hence, using compressed air only to assist backwashes gives a major reduction in energy cost. The higher pressure increase per filtration cycle (ΔP_{cycle}) may be used advantageously as process monitoring parameter. For instance, coagulation failures will affect particle deposition strongly and shortly after the event. For a system with continuous air scouring, the differences in the development of ΔP_{cycle} may be less detectable due to reduced particle deposition. Hypothesis A is confirmed.

B Coagulant dosage requirements decrease.

The results did not give conclusive evidence to support this hypothesis. However, given that both aggregate characteristics and flocculation affected membrane performance, optimal coagulant dosages are likely to be in the same range

as for other coagulation-based filtration processes. Reducing coagulant dosages significantly below the optimal dosage results in coagulation conditions in the charge neutralization regime, where particle aggregation is limited. Furthermore, judging by the strongly increasing fouling propensity of particles forming below pH 6 (Fig. 6.14), coagulation in the charge neutralization regime should be avoided. Reducing the coagulant dosage 1 mg Al/L below the optimal dosage of 3 mg Al/L resulted in very low pressure increase rates for forward filtration but backwash pressures increased rapidly. This may be taken as a first indication of suboptimal performance.

An assessment of the molecular size distribution of NOM in the investigated raw water revealed that a low-pressure membrane will not retain uncoagulated organics to any significant extent. NOM removal thus depends entirely on the coagulant dosage. Since it is common to specify a target permeate quality in practical applications, coagulant savings cannot be expected when replacing media filtration with hollow-fibre membrane filtration.

C Chitosan is a suitable coagulant for pre-coagulation.

Chitosan neither met the expectations for NOM removal for the investigated raw water nor did its use seem favourable in combination with a polymeric membrane. At a dosage of 5 mg Chi/L, permeate colour and TOC did not meet the current guidelines for approval as hygienic barrier (Tab. 4.1). Given a current marked price of 12–20 EUR/kg for chitosan, a dosage of 5 mg/L invokes specific cost on the order of 0.1 EUR per m^3 treated water for coagulant consumption alone. Due to the charge dependency of chitosan, the coagulation pH should be kept in the acidic range, possibly even below 5, to achieve a reasonable removal of NOM, which in turn requires further chemical addition for pH control. It is doubtful whether such high chitosan dosages allow for a cost-efficient pre-treatment to a low-pressure membrane application. Even though certain cost savings may be expected for disposal of organic chitosan sludges instead of inorganic sludges, the notably poorer permeate quality practically rules out chitosan as coagulant for NOM-rich surface waters. The pressure increase rates measured on the membrane also suggest unfavourable interactions between the cationic polymer and the negatively charged membrane. Removing fouling layers by CIP was more time-consuming and elaborate than with metal-based coagulants. Hypothesis C is rejected.

D Flocculation has an impact on long-term fouling.

Flocculation could both exacerbate and reduce the pressure development due to hydraulically not-reversible fouling. Short flocculation times and turbulent

flow conditions in a pipe flocculator (G$\simeq$ 400 s^{-1}) resulted in higher pressure increase rates than flocculation at low G-values. Except for coagulant dosages higher than the optimal dosage, use of a packed-bed flocculator reduced pressure increase rates. In packed-bed flocculators, the forming suspension is routed through a complex geometry with a large surface for nucleation, which can improve precipitation kinetics particularly at lower temperatures. No significant difference between flocculation conditions could be established for coagulant dosages exceeding the optimal dosage. On the other hand, hydraulically not-reversible fouling increases strongly with the coagulant dosage, which renders coagulation at the optimal dosage followed by controlled flocculation at low G-value (<30 s^{-1}) more efficient for downstream O–I filtration. Hypothesis F is confirmed.

E Water recovery does not influence long-term fouling.

The results support this hypothesis partially. Reducing water recovery decreases the solids retention time in the immersion tank, i.e. solids are removed faster from the system. The pressure increase per filtration cycle decreases as a result of lower suspended solids concentrations in the immersion tank. For optimized coagulation conditions, no benefit of reducing water recovery became apparent. Long-term pressure increase rates were not significantly different between experiments at 85% and 95% recovery. Lower recovery could stabilize performance with respect to pressure increase rates. While notable differences between the filtration and backwash pressure increase rates occurred in comparable experiments at 95% recovery, no such effects were observed at 85% recovery. However, the discrepancies observed at 95% recovery were more likely to be due to inefficient sludge removal than to the higher recovery. Reducing water recovery may therefore mitigate adverse effects on pressure increase rates.

It is doubtful whether operation at lower recovery and recycling of settled retenate (cf. process scheme depicted in Fig. 4.3) will improve system performance per se. On the one hand, the membrane system may respond more stably in case of sudden variations upstream at the expense of higher plant complexity and footprint. Given the generally minor influence of water recovery for normal operating conditions, efforts should rather be made to ensure sound coagulation and efficient sludge withdrawal.

F The optimal coagulation conditions correspond to those for direct media filtration.

From point of view of aluminium residuals, coagulation in the pH range between 6 and 7 is most suitable for any NOM removal process relying on alu-

minium coagulants. Experiments showed that coagulation at pH 6–6.5 was most favourable with respect to long-term pressure increase on the membrane. In this pH range, direct media filters also achieve optimal performance in NOM-removal applications. Since coagulant dosages will essentially be the same for equivalent NOM removal, direct media filters and O–I hollow-fibres require similar coagulation conditions for optimal performance. This confirms Hypothesis F.

G Operation at low NOM concentrations does not decrease fouling rates.

The experimental results show that membrane pressure increases at similar rates for optimally coagulated raw waters with different NOM concentration. This implies that aggregate characteristics are the primary cause of hydraulically not-reversible fouling. Treatment effort and cost between different humic waters thus only differ in terms of coagulant consumption and sludge disposal. It may therefore be said that the potential for application of coagulation-based O–I systems is highest for NOM-rich surface waters. While the efficiency of most other treatment processes decreases at high particle loadings, the performance of an O–I membrane system will remain largely unaffected. Hypothesis G is confirmed.

7.2 Recommendations for operation

7.2.1 Coagulation

The results presented in this research mostly apply to surface water with elevated concentrations of natural organic matter. As discussed in Chapter 2.1.7, NOM has a dominant influence on coagulant demand and floc formation. On the other hand, since natural organics are ubiquitous in surface water, the results of this study are relevant also for applications aiming primarily at turbidity removal.

The efficiency of hydrolysing metal coagulants in terms of NOM removal and cost render them most suitable as pre-treatment chemicals. However, the possibility of precipitates exacerbating fouling on membranes and high metal residuals in the finished water have to be taken into account. Crucial to performance of metal-based coagulants is their continuous and rapid dispersion (flash mixing) at the dosing point. This should be carefully considered in pilot studies where the flow in coagulant dosing lines is low.

For aluminium-based coagulants, such as alum or PACl, optimal performance with respect to NOM removal, membrane performance, and aluminium residuals is achieved within a pH range of 6–6.5. Lower pH improves NOM removal but increases both aluminium residuals and pressure increase rates on the membrane. At higher coagulation pH mainly permeate quality deteriorates due to reduced coagulant efficiency. Optimization of the coagulant dosage is the key to good membrane performance. Overdosing coagulant in particular affects long-term membrane pressure development adversely. Pre-polymerized products may be preferable due to better performance at low temperatures, lower alkalinity consumption, and better flocculation behaviour.

Iron-based coagulants were not tested in this study but are common in drinking water applications based on hollow-fibre membranes. Notwithstanding the advantages of ferric coagulants, including lower cost, higher NOM removal potential, and lower metal solubility, their optimal pH for NOM coagulation falls within the pH range of reduced or depleted alkalinity (pH 4–5). Controlling pH is thus more challenging for ferric-based systems. The results of this study showed that a stable coagulation pH is vital to maintaining performance of the membrane unit. Due to the similarities in speciation chemistry, there is reason to believe that ferric- and aluminium-based coagulants exhibit similar behaviour in a coagulation/hollow-fibre applications. Hence, a ferric-based system may be prone to instabilities.

Chitosan cannot be recommended as coagulant in combination with O–I hollow-fibre filtration. Although chitosan is capable of achieving acceptable NOM removal efficiency at lower raw water colour (Saltnes *et al.* 2001), formation of recalcitrant fouling layers on the membranes will remain a problem. Similar problems must be expected for other cationic polymer coagulants.

As a first step, each application should include an assessment of the raw water to identify the optimal conditions for pre-treatment. Minimal use of chemicals is desirable both from an economical and the consumer's point of view. In this study, jar-test experiments were applied successfully to assess pretreatment conditions. Combinations of dosage and pH resulting in zeta potentials near zero or just below provided a good estimate for optimal coagulation conditions in case of metal-based coagulants. Although such preliminary testing does not allow to estimate fouling rates on an subsequent membrane rig, it provides essential data for optimizing the entire hybrid system in a pilot study.

In summary, the study showed that coagulation is crucial to successful operation of low-pressure O–I membranes. On the one hand, the performance of the membrane rig depends largely on optimal coagulation conditions; on

the other hand, the membrane will only act as physical barrier to viruses and NOM under well-controlled coagulation conditions.

7.2.2 Flocculation

Controlling floc aggregation can reduce pressure increase rates on an O–I hollow-fibre membranes provided that flocculators are designed for low velocity gradients ($G<30\ s^{-1}$). Flocculation at high G-values is of no avail and may even exacerbate pressure increase rates. The results of this study indicate that a packed-bed flocculator outperforms empty-tank or jet-mix flocculators for cold, low-turbidity waters. This effect may, however, be of minor importance for surface waters with higher turbidity.

Although flocculation contributes little to operating cost, the flocculation vessel and the resulting increase in footprint of the installation add to the investment cost. Short flocculation times are therefore preferable to keep flocculator sizes small. On the other hand, too short flocculation times may cause fast increases of the backwash pressure. The experiments in this study were based on a flocculation time of approximately 5 minutes, which may be too short under certain conditions, particularly for waters with low coagulant demand. Longer flocculator detention times are therefore recommended.

7.2.3 Outside-in membrane filtration

For drinking water applications, immersed O–I membrane systems should be operated without continuous air scouring during filtration to save energy. During backwashes, however, vigorous air scouring improves detachment of cake structures from the fibres. It must be noted that the airflow during backwashes was not optimized. Airflow rates lower than the applied 6–7 $m^3\ m^{-2}_{footprint}\ min^{-1}$ may therefore be sufficient. A diffusor mounted in or near the bottom module header can also be used effectively to disperse cleaning chemicals and remove foulants during a CIP.

Transmembrane pressures increase linearly as long as coagulation conditions remain stable and the membrane is backwashed with permeate in intervals. Flux design is subject to several conditions:

- The required membrane area for the installation and thus a part of the investment cost decrease with increasing design fluxes.

- Since the limiting pressure in O–I filtration is the backwash pressure, manufacturers normally specify a maximum backwash pressure to prevent fibre rupture (630–650 mbar for a ZeeWeed® system). Given the proportional relationship between transmembrane pressure and flux, the start-up pressure for a clean membrane increases with the flux. Hence, the pressure loss that the system can sustain as a result of hydraulically not-reversible fouling decreases on increasing design flux.

- For similar pre-treatment conditions, hydraulically not-reversible fouling increases with flux. Higher pressure increase rates shorten the system runtime and cause more frequent maintenance cleaning. The acceptable frequency of CIP-procedures is case-dependent. For O–I systems, CIP intervals of several months are common.

- High pressure increase rates render the membrane system more vulnerable to plant upsets such as coagulation failures.

- Seasonal variations in raw water conditions must be considered, particularly lower temperatures during winter time.

In addition, site-dependent conditions may exist, e.g. restricted use of cleaning chemicals, limited space availability, or demand for increased system redundance. Experience values serve to calculate first estimates of process design but normally flux-pressure performance data have to be collected in a pilot study on-site. In this study, fluxes up to 75 LMH were applied with moderate pressure increase rates. However, it must be borne in mind that studies conducted with bench-scale modules only provide guidance values for full-scale operation but do not serve for process design. In a full-scale installation, lower fluxes may be expected due to scale-up effects.

During backwashes, fluxes are normally higher than during filtration, at least for a certain period of time. Backwash flux optimization was not within the scope of this study. To avoid influences of inefficient backwashing on the long-term pressure increase for the most part, a high flux of 1.5 times the forward filtration flux was chosen for the backwash. Since permeate backwashing causes water losses, lower backwash fluxes are commonly applied in practice. Backwash intervals in the range of 30–60 minutes were sufficient for the investigated conditions. Shorter backwash cycles had little influence on the long-term pressure development. In most experiments, the pressure increase during filtration (ΔP_{cycle}) remained below 15 mbar. However, since the solids concentration in the immersion tank has a strong effect on ΔP_{cycle}, the frequency of backwashing will be largely case-dependent.

High achievable water recovery is one of the major advantages of O–I hollow-fibre filtration. A recovery of 95% is recommended as starting point for normal operation. While higher water recoveries may be applicable in low-solids applications, it must be borne in mind that suspended solids concentrations in the immersion tank increase rapidly beyond 95% recovery, which may cause problems with sludging of membranes. Particles that settle in the immersion tank should be withdrawn efficiently to avoid re-suspension of sludge during backwashes.

Soaking in a 250-ppm chlorine solution efficiently removed fouling layers formed by aluminium-based coagulants. No permanent loss in the membrane's pure water permeability was detected after long-term use. Chitosan fouling layers required minimum two cleaning steps for successful removal: first backwashing with a 1-ppm citric acid solution followed by soaking in a 250-ppm chlorine solution.

Membrane performance can be monitored easily based on the pressure increase rates for forward filtration and backwashing as described in Chapter 5.2.5. Furthermore, the pressure increase per filtration cycle (ΔP_{cycle}) serves as an early indicator for disturbances upstream of the membrane unit.

Chapter 8

Suggestions for further research

8.1 Verification of results in a field study

Field experiments are required to verify the results of this study on full-scale membrane modules. Flow in hollow-fibres is subject to significant pressure loss, which in case of O–I operated fibres results in axial flux maldistribution (Chang and Fane 2001). Since this affects operating pressures, results obtained with bench-scale modules do not translate directly into practice. During the course of this study, the author has been involved in field studies on coagulation with O–I hollow-fibre filtration. The adverse effects of inadequate coagulation and flocculation became frequently apparent also on membrane systems with other module geometries, which underscores the importance of further research for performance optimization.

8.2 Barrier assessment during coagulation failures

Low-pressure membranes achieve only limited virus removal without upstream coagulation. While virus removal is practically complete for coagulated raw waters (Fiksdal and Leiknes 2004, Matsushita *et al.* 2005), viruses may pass through the membrane during coagulation failures. It may be expected that an immersed system operating at high water recovery can compensate for short-term failure events for a certain period of time because viruses are adsorbed to suspended particles in the immersion tank. Over time, particles are washed out of the system and the barrier height for viruses converges towards the value for an uncoagulated feed. If parameters such as changes in the membrane response or permeate quality deterioration are used for performance monitoring,

coagulation failures are only detected after some time. Knowing the response function for virus removal during failure events would allow to assess the quality of straightforward process monitoring.

8.3 Raw water monitoring to optimize membrane performance

The study showed that membrane performance strongly depends on coagulation conditions. Maintaining stable and good coagulation is thus synonymous with optimal membrane performance and permeate quality. Flow-proportional dosing of coagulant is prevalent but prone to instabilities. Some techniques to monitor coagulation rely on measurements after coagulant addition, e.g. streaming potential monitoring. The applied sensors frequently experience a rapid deterioration of signal quality due to precipitates forming on outer surfaces, creeping currents, or other error sources and require frequent recalibration. Since coagulant demand is largely determined by NOM-characteristics in colour removal applications, a coagulation control unit based on an optical raw water sensor that measures light absorption values at wavelengths of 254 nm and/or 410 nm online would help to maintain stable coagulation conditions. Evidently, such a sensor has to cope with biofilm formation and raw water turbidity.

8.4 Pressure performance modelling

Membrane performance modelling is complex for many reasons. The influence of raw water conditions on membrane performance is intricate due to unknown membrane-solute or membrane-particle interactions, many operating parameters, process dependencies, etc. Conceiving mechanistical models is often time-consuming and requires extensive knowledge on process behaviour. The results presented in Chapter 6.4 show that empirical modelling methods are helpful in explaining complex behaviour. On the other hand, predictability is limited with multi-linear models even with large sets of data. Neural networks represent a powerful technique to model complex real-world processes because they are able to

- discover the nature of dependencies in a system;
- learn from experience in order to improve their performance and to adapt to changes in the environment;

- deal with incomplete or noisy data.

In situations where no mechanistic models exist, neural networks are especially effective. Since neural networks are able to approximate any function based on a given input structure, they can be used to predict a time-series of pressure performance for a membrane system from readily accessible process parameters. A neural network must be "trained" with measured data, for instance from a pilot study. For so-called *supervised training*, predictor and response values are provided, causing the network to adapt itself to the response. Results from such a modelling approach could be used to further investigate similarities and differences between applications with different raw waters.

Appendix A

Pathogenic organisms

Table A.1: Viral pathogens[1]

Agent	Size, nm	Capsid symmetry	Pathogenicity
Enteroviruses[2]	25–30	Icosahedral	Paralysis, meningitis, cardiomyopathy, colds, fever
Hepatitis A	27	Icosahedral	Infectious hepatitis
Norwalk and Norwalk-like	27–35	Spherical	Gastroenteritis
Astroviruses	28	Spherical	Gastroenteritis
Hepatitis E	27–34	Spherical	Acute hepatitis
Caliciviruses	32–38	Spherical	Gastroenteritis (in children)
Rotavirus	50–65	Icosahedral	Gastroenteritis
Adenoviruses	70–80	Icosahedral	Acute respiratory disease, gastroenteritis

[1] Sources: Wyn-Jones and Sellwood (2001), Baron (1996), Irving *et al.* (1996), World Health Organization (2006)

[2] Poliovirus, Coxsackie A and B viruses, ECHO viruses, EV68 to EV72

Table A.2: Size, shape, and pathogenicity of bacterial pathogens[1]

Agent	Size, µm (width × length)	Shape	Pathogenicity (depends on species)
Leptospira spp.	0.1 × 6–20	spiral-shaped	Leptospirosis
Pseudomonas aeruginosa[2]	0.5–0.8 × 1–3	rod-shaped	Skin rashes, outer ear infections
Francisella tularensis	0.2 × 0.3–0.7	cocco-bacilli	Tularemia
Campylobacter spp.	0.2–0.5 × 0.5–5	slender, spirally curved rods	Gastrointestinal disease
Mycobacterium spp.	0.2–0.6 × 1	slender, curved rods	Tuberculosis, leprosy
Aeromonas spp.[2]	0.3–1.0 × 1.0–3.5	straight rods or cocco-bacilli	Wound infections, septicaemia, diarrheal illness
Legionella pneumophila[2]	0.3–0.9 × 0.3–0.9	straight rods	"Legionaires' disease", "Pontiac" fever
Shigella spp.	0.3–1.0 × 1–6	rod-shaped	Bacillary dysentery
Yersinia enterocolitica[2]	0.5–0.8 × 1–3	short rods or cocco-bacilli	Acute febrile diarrhea
Vibrio cholerae	0.5–0.8 × 1.4–2.6	rod-shaped	Cholera, gastroenteritis
Helicobacter pylori	0.5–1.0 × 3	spiral-shaped	Gastritis, gastric and duodenal ulcers
Salmonella spp.	0.7–1.5 × 2–5	rod-shaped	Salmonellosis, typhoid and paratyphoid fever
Enterovirulent *Escherichia coli*	1.0–1.5 × 2–6	rod-shaped	Diarrhea, enteritis, fever

[1] Sources: Baron (1996), Irving *et al.* (1996), World Health Organization (2006)
[2] can proliferate in distribution systems

Table A.3: Size, shape, and pathogenicity of protozoal pathogens[1]

Agent	Size, µm (width × length)	Shape of infectious form	Pathogenicity
Microsporidia	1–4.5	Spores	Diarrhea, bronchitis, pneumonia, sinusitis, keratoconjunctivitis
Cryptosporidium parvum	3–7	Spherical or oval oocyst	Cryptosporidial diarrhoea
Giardia lamblia	6–9 × 8–12	Ovoid cyst	Giardiasis
Cyclospora cayetanensis	8–10	Round oocyst	Diarrhoea, nausea, fever
Naegleria fowleri	8–12	Spherical cyst	Primary amoebic meningoencephalitis
Entamoeba histolytica	10–16	Cyst	Acute or chronic diarrhoea, dysentery
Toxoplasma gondii	12 × 11	Oocyst	Flue-like illness, swollen lymphs
Acanthamoeba spp.	15–28	Spherical cyst	Encephalitis, ulcerating keratitis
Isospora belli	22–33 × 12–15	Elliptical cyst	Diarrhoea and abdominal pain
Ballantidium coli	50–55	Spherical or oval cyst	Severe diarrhoea, dysentery, intestinal ulcers

[1] Sources: Baron (1996), Irving *et al.* (1996)

Appendix B

Experimental data

Guide to the figures presented for each experiment (X denotes the id of the experiment, e.g. A01):

Figure X(a). Development of the operating pressure measured immediately after a backwash. Pressure data are normalized to a temperature of 20℃. Open squares (⊡) denote data points omitted for regression analysis. Regression data presented in the legend text entail slope of the curve (m), standard error of the slope (se), number of data points included (n), and the correlation coefficient (r^2).

Figure X(b). Development of the backwash pressure (highest pressure measured during backwash). Backwash pressure data are normalized to 20℃. Open squares (⊡) denote data points omitted from regression analysis. Regression parameters as above.

Figure X(c). Pressure increase during a cycle of forward filtration, i.e. between backwashes (ΔP_{cycle}), see also Fig. 5.5. Pressure data are normalized to 20℃.

Figure X(d). Suspended solids concentration (0.45 µm) measured in immersion tank immediately after a backwash (completely mixed tank contents).

Figure X(e). Colour and UV_{254} absorbance measured in raw water and permeate. Error bars indicate the highest and lowest values measured.

Figure X(f). Residual turbidity (see section 5.3) after coagulation (C), after flocculation (F), and in the immersion tank (M) after a backwash. Error bars indicate the highest and lowest values measured.

Experiment A01

Description

Reference values for coagulation with alum, high dosage.

Raw water

Colour	50 mg Pt/L
Average temperature	9.6℃

Pre-treatment

Coagulant	Aluminium sulphate
Specific dosage	5 mg Al/L
Average coagulation pH	6.1
Flocculation	PF

Membrane operating parameters

Filtration flux	J_f	60 L m^{-2} h^{-1}
Backwash flux	J_{bw}	90 L m^{-2} h^{-1}
Filtration cycle	t_f	29'30 min'sec
Backwash cycle	t_{bw}	00'30 min'sec
Water recovery	w	95%

Pressure increase rates obtained by regression

	Slope (mbar/d)		Intercept (mbar)	
	m	CI 95%	b	CI 95%
Filtration	3.72	± 0.40	77.41	± 0.50
Backwash	5.61	± 0.83	108.56	± 1.04

Comments

None.

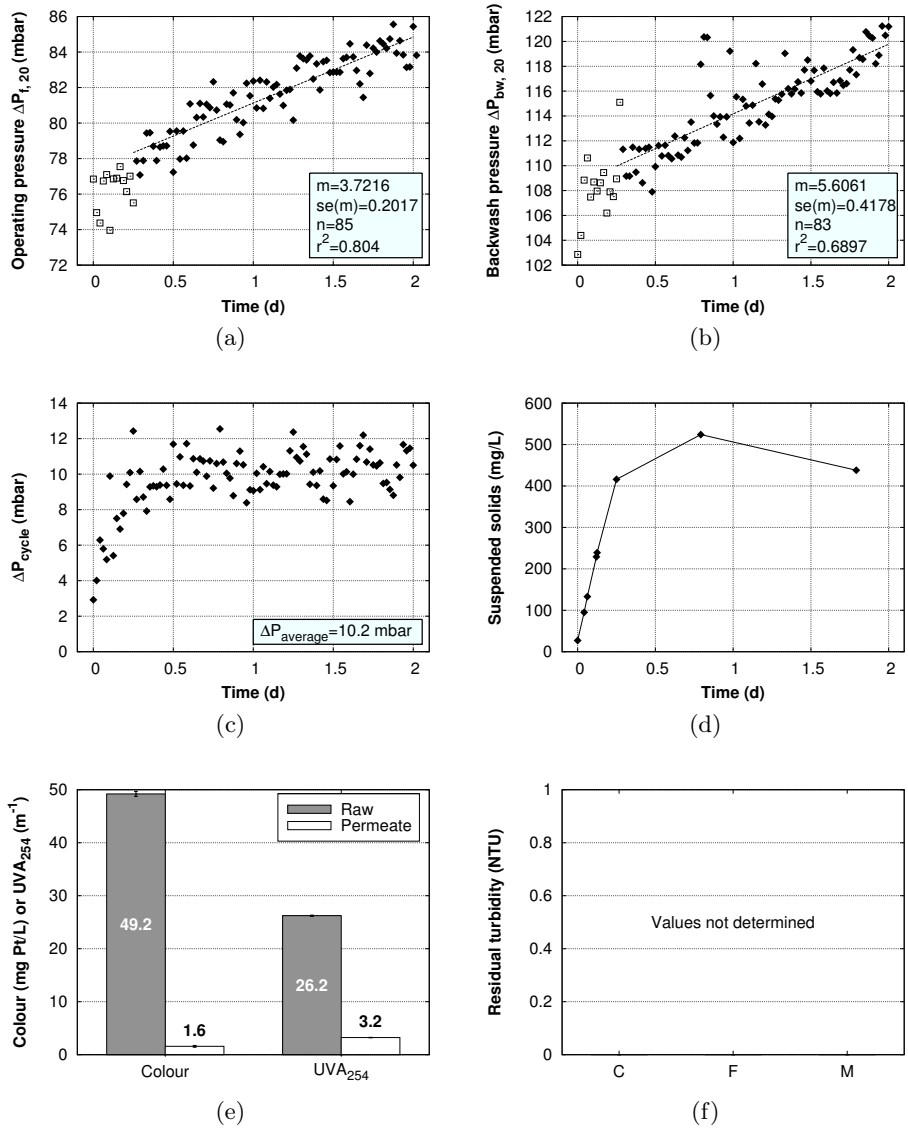

Figure A01: Overview of results for experiment A01. No residual turbidity values were determined during this experiment (f).

Experiment A02

Description

Reference values for coagulation with alum, optimal dosage.

Raw water

Colour	50 mg Pt/L
Average temperature	8.2℃

Pre-treatment

Coagulant	Aluminium sulphate
Specific dosage	3.5 mg Al/L
Average coagulation pH	6.2
Flocculation	PF

Membrane operating parameters

Filtration flux	J_f	60 L m^{-2} h^{-1}
Backwash flux	J_{bw}	90 L m^{-2} h^{-1}
Filtration cycle	t_f	29'30 min'sec
Backwash cycle	t_{bw}	00'30 min'sec
Water recovery	w	95%

Pressure increase rates obtained by regression

	Slope (mbar/d)		Intercept (mbar)	
	m	CI 95%	b	CI 95%
Filtration	3.91	± 0.25	75.16	± 0.30
Backwash	2.83	± 1.01	106.91	± 1.24

Comments

None.

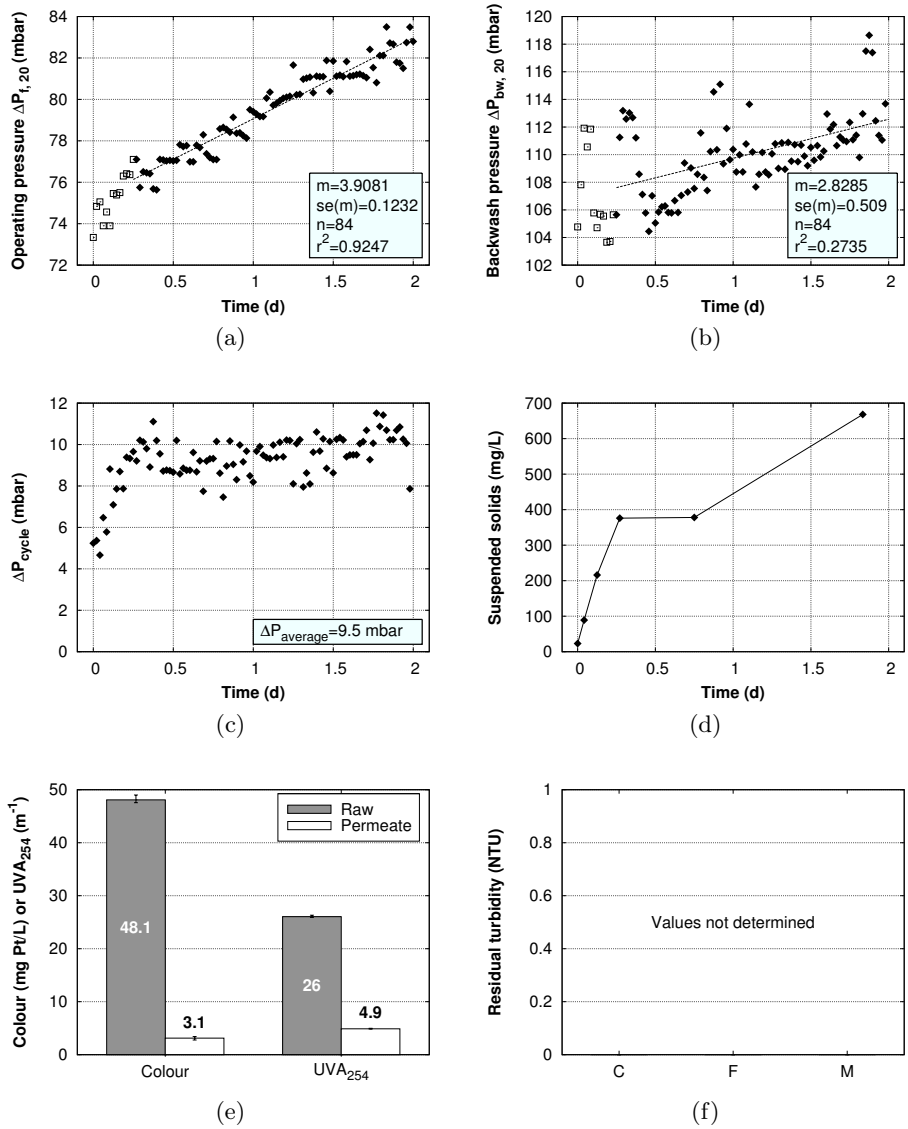

Figure A02: Overview of results for experiment A02. No residual turbidity values were determined during this experiment (f).

Experiment A03

Description

As A01, shorter filtration and backwash cycle lengths.

Raw water

Colour	50 mg Pt/L
Average temperature	9.3℃

Pre-treatment

Coagulant	Aluminium sulphate
Specific dosage	5 mg Al/L
Average coagulation pH	6.1
Flocculation	PF

Membrane operating parameters

Filtration flux	J_f	60 L m^{-2} h^{-1}
Backwash flux	J_{bw}	90 L m^{-2} h^{-1}
Filtration cycle	t_f	14'45 min'sec
Backwash cycle	t_{bw}	00'15 min'sec
Water recovery	w	95%

Pressure increase rates obtained by regression

	Slope (mbar/d)		Intercept (mbar)	
	m	CI 95%	b	CI 95%
Filtration	5.32	± 0.23	75.48	± 0.28
Backwash	6.94	± 0.72	104.76	± 0.89

Comments

None.

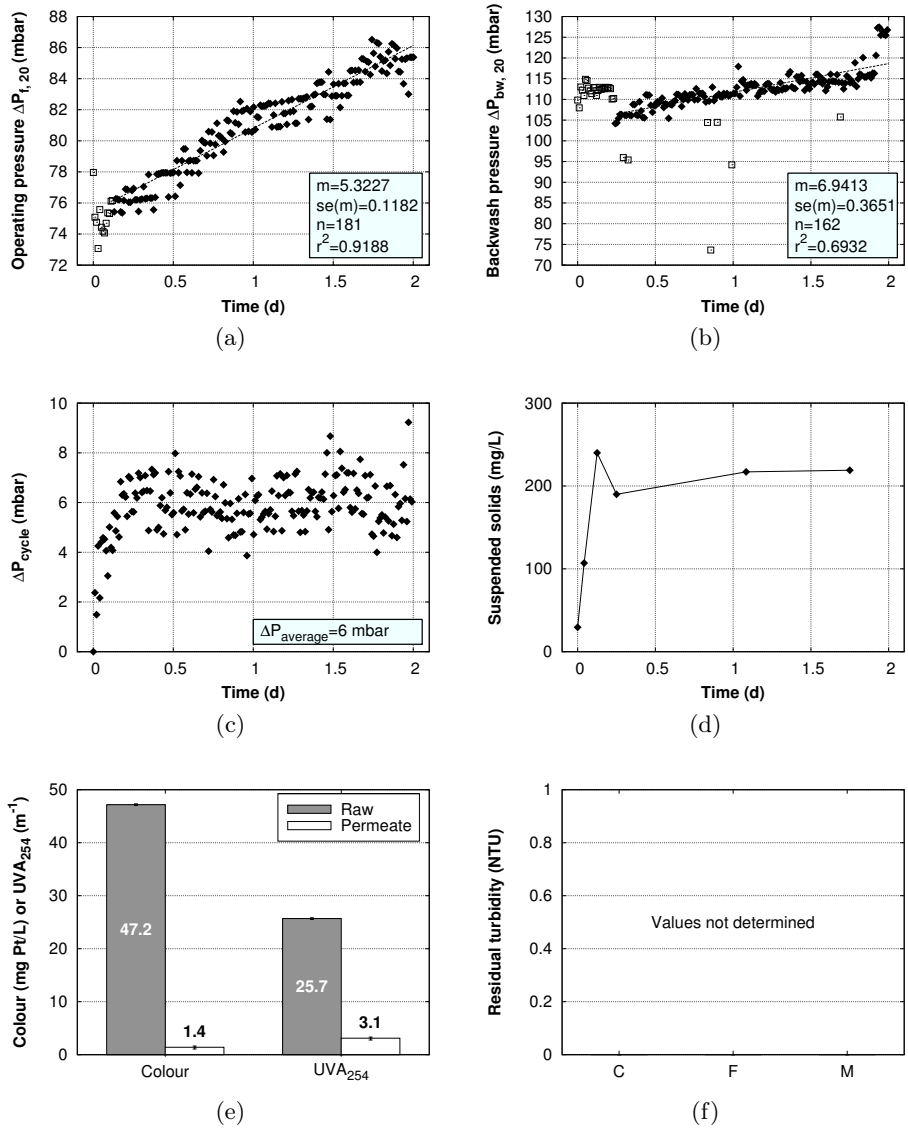

Figure A03: Overview of results for experiment A03. No residual turbidity values were determined during this experiment (f).

Experiment A04

Description

As A01, longer filtration and backwash cycle lengths.

Raw water

Colour	50 mg Pt/L
Average temperature	8.7℃

Pre-treatment

Coagulant	Aluminium sulphate
Specific dosage	5 mg Al/L
Average coagulation pH	6.1
Flocculation	PF

Membrane operating parameters

Filtration flux	J_f	60 L m^{-2} h^{-1}
Backwash flux	J_{bw}	90 L m^{-2} h^{-1}
Filtration cycle	t_f	59'00 min'sec
Backwash cycle	t_{bw}	01'00 min'sec
Water recovery	w	95%

Pressure increase rates obtained by regression

	Slope (mbar/d)		Intercept (mbar)	
	m	CI 95%	b	CI 95%
Filtration	3.50	± 0.75	75.79	± 0.93
Backwash	4.81	± 0.86	106.51	± 1.04

Comments

None.

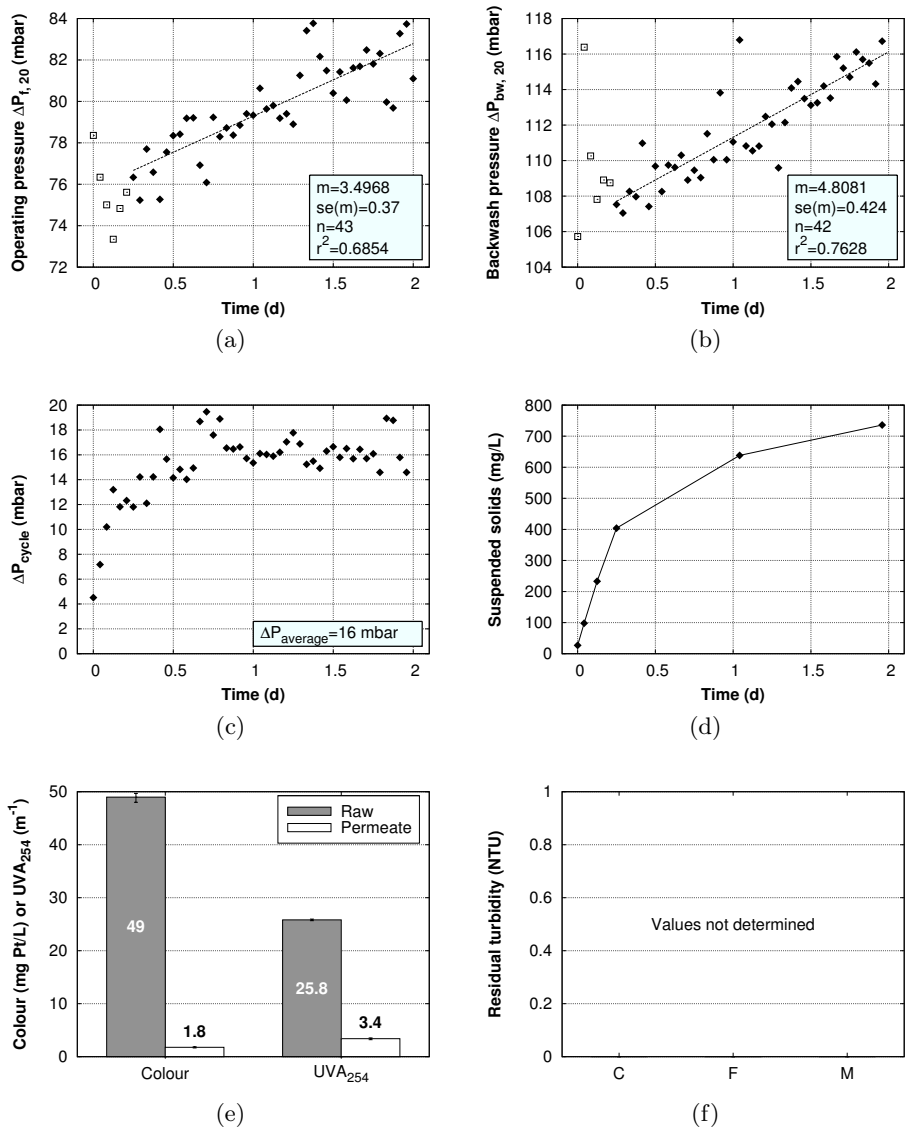

Figure A04: Overview of results for experiment A04. No residual turbidity values were determined during this experiment (f).

Experiment A05

Description

As A01, shorter duration of backwash cycle and increased hydraulic efficiency.

Raw water

Colour	50 mg Pt/L
Average temperature	7.9℃

Pre-treatment

Coagulant	Aluminium sulphate
Specific dosage	5 mg Al/L
Average coagulation pH	6.1
Flocculation	PF

Membrane operating parameters

Filtration flux	J_f	60 L m^{-2} h^{-1}
Backwash flux	J_{bw}	90 L m^{-2} h^{-1}
Filtration cycle	t_f	29'50 min'sec
Backwash cycle	t_{bw}	00'10 min'sec
Water recovery	w	95%

Pressure increase rates obtained by regression

	Slope (mbar/d)		Intercept (mbar)	
	m	CI 95%	b	CI 95%
Filtration	3.38	± 0.35	74.21	± 0.43
Backwash	2.06	± 1.50	108.05	± 1.84

Comments

None.

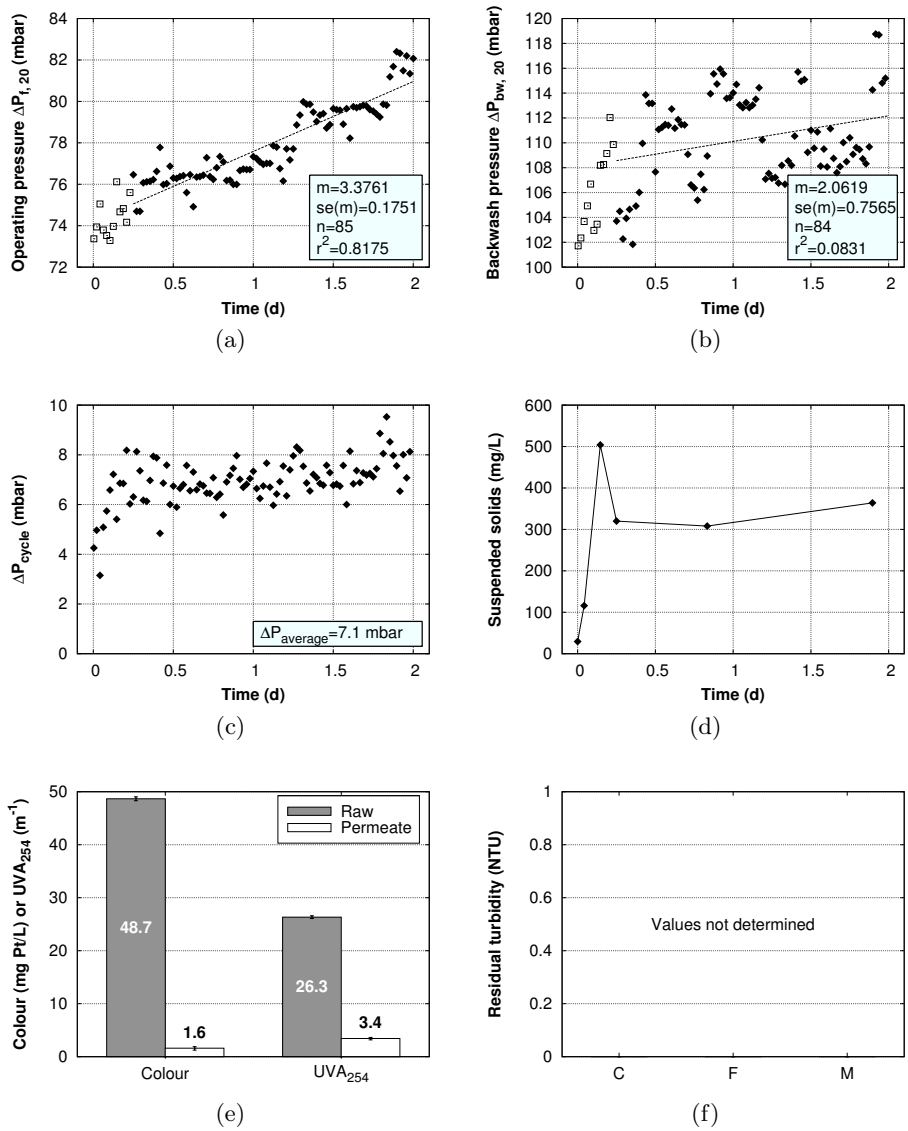

Figure A05: Overview of results for experiment A05. No residual turbidity values were determined during this experiment (f).

Experiment C01

Description

Reference values for coagulation with chitosan.

Raw water

Colour	50 mg Pt/L
Average temperature	10.6℃

Pre-treatment

Coagulant	Chitosan
Dosage	5 mg/L
Average coagulation pH	5.0
Flocculation	None (empty upflow tank 5 min detention time)

Membrane operating parameters

Filtration flux	J_f	60 L m^{-2} h^{-1}
Backwash flux	J_{bw}	90 L m^{-2} h^{-1}
Filtration cycle	t_f	29'30 min'sec
Backwash cycle	t_{bw}	00'30 min'sec
Water recovery	w	95%

Pressure increase rates obtained by regression

	Slope (mbar/d)		Intercept (mbar)	
	m	CI 95%	b	CI 95%
Filtration	2.50	± 0.24	80.01	± 0.33
Backwash	4.80	± 0.61	112.55	± 0.81

Comments

None.

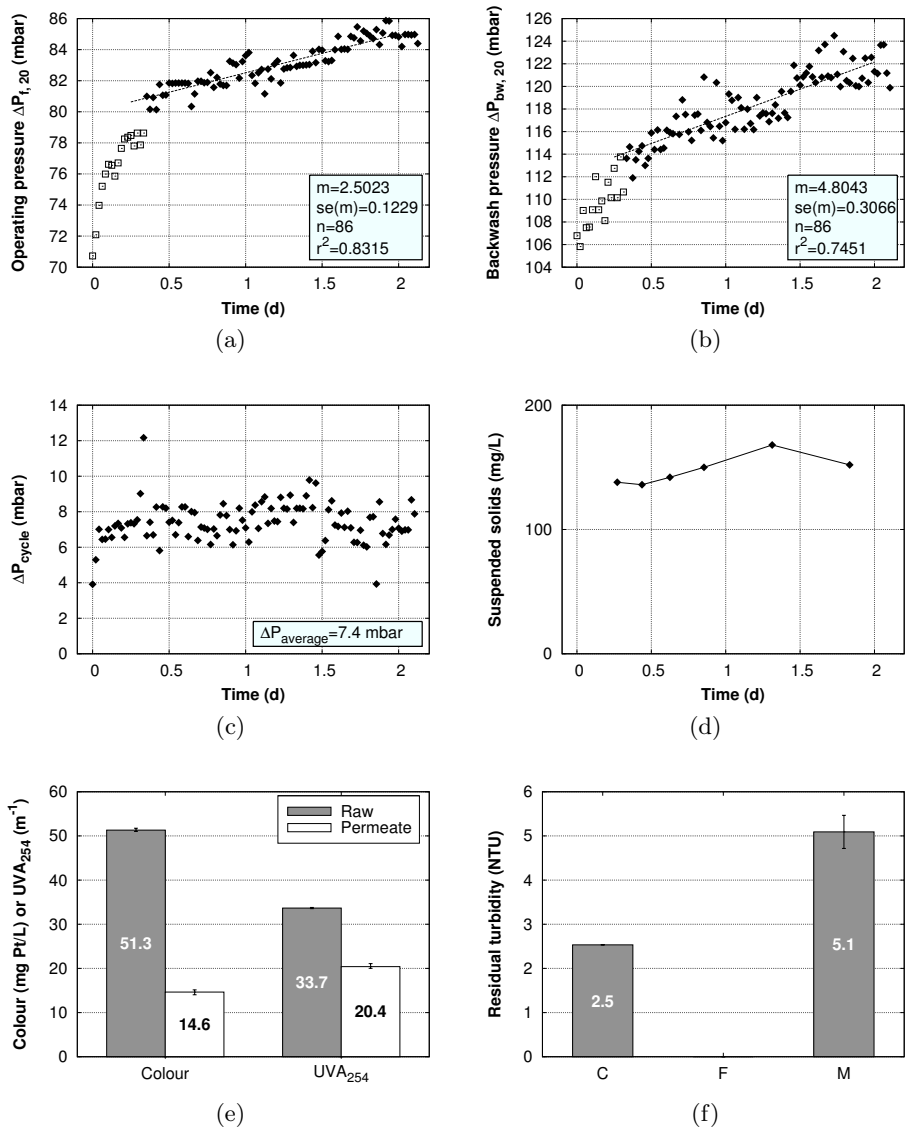

Figure C01: Overview of results for experiment C01.

Experiment P01

Description

Reference values for coagulation with PACl, high dosage.

Raw water

Colour	50 mg Pt/L
Average temperature	7.7℃

Pre-treatment

Coagulant	Polyaluminium chloride
Dosage	5 mg Al/L
Average coagulation pH	6.3
Flocculation	PF

Membrane operating parameters

Filtration flux	J_f	60 L m^{-2} h^{-1}
Backwash flux	J_{bw}	90 L m^{-2} h^{-1}
Filtration cycle	t_f	29'30 min'sec
Backwash cycle	t_{bw}	00'30 min'sec
Water recovery	w	95%

Pressure increase rates obtained by regression

	Slope (mbar/d)		Intercept (mbar)	
	m	CI 95%	b	CI 95%
Filtration	4.39	± 0.29	75.32	± 0.36
Backwash	6.89	± 1.13	106.04	± 1.39

Comments

None.

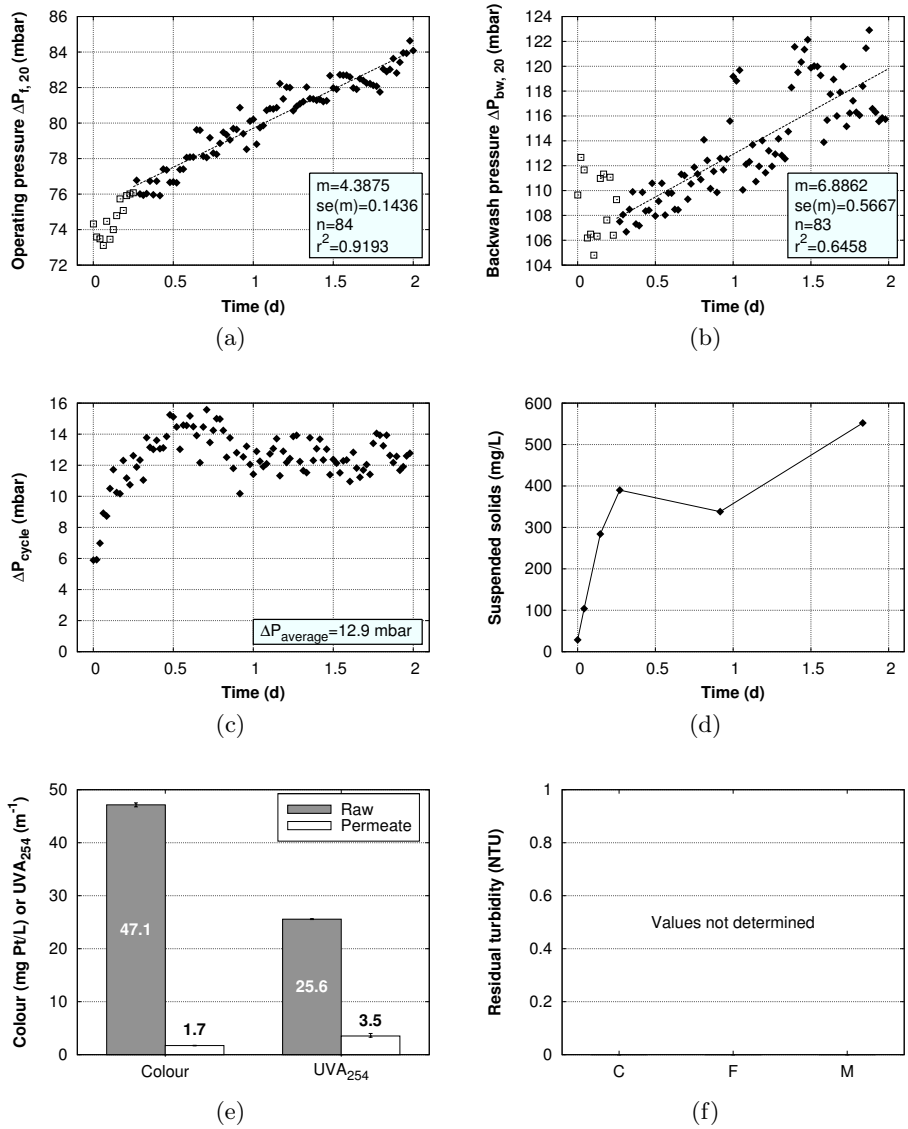

Figure P01: Overview of results for experiment P01. No residual turbidity values were determined during this experiment (f).

Experiment P02

Description

Reference values for coagulation with PACl, optimal dosage.

Raw water

Colour	50 mg Pt/L
Average temperature	7.2℃

Pre-treatment

Coagulant	Polyaluminium chloride
Dosage	3.5 mg Al/L
Average coagulation pH	6.3
Flocculation	PF

Membrane operating parameters

Filtration flux	J_f	60 L m^{-2} h^{-1}
Backwash flux	J_{bw}	90 L m^{-2} h^{-1}
Filtration cycle	t_f	29'30 min'sec
Backwash cycle	t_{bw}	00'30 min'sec
Water recovery	w	95%

Pressure increase rates obtained by regression

	Slope (mbar/d)		Intercept (mbar)	
	m	CI 95%	b	CI 95%
Filtration	3.57	± 0.27	78.69	± 0.33
Backwash	2.84	± 0.54	109.75	± 0.67

Comments

None.

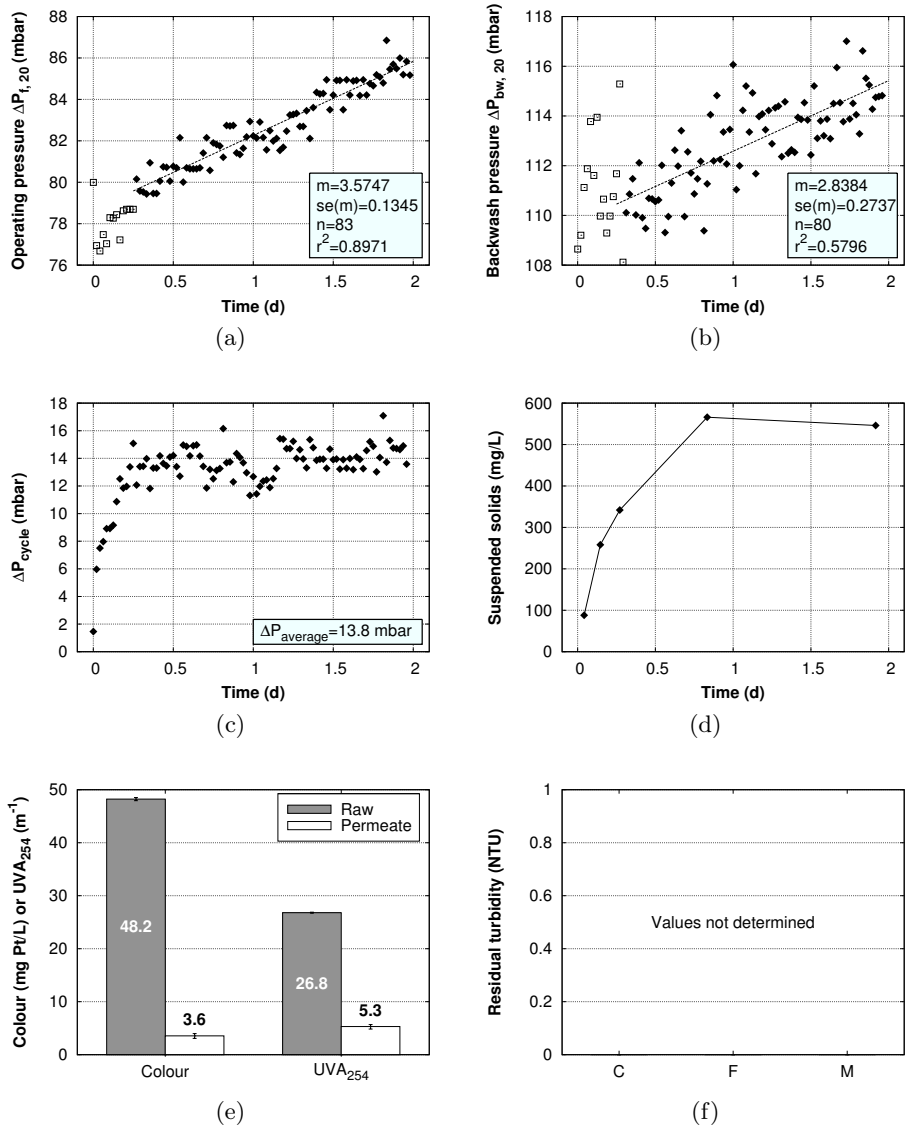

Figure P02: Overview of results for experiment P02. No residual turbidity values were determined during this experiment (f).

Experiment P03

Description

More frequent backwashing with shorter duration of backwash cycle.

Raw water

Colour	50 mg Pt/L
Average temperature	7.7℃

Pre-treatment

Coagulant	Polyaluminium chloride
Dosage	5 mg Al/L
Average coagulation pH	6.3
Flocculation	PF

Membrane operating parameters

Filtration flux	J_f	60 L m^{-2} h^{-1}
Backwash flux	J_{bw}	90 L m^{-2} h^{-1}
Filtration cycle	t_f	14'45 min'sec
Backwash cycle	t_{bw}	00'15 min'sec
Water recovery	w	95%

Pressure increase rates obtained by regression

	Slope (mbar/d)		Intercept (mbar)	
	m	CI 95%	b	CI 95%
Filtration	3.90	± 0.19	74.85	± 0.24
Backwash	5.68	± 0.27	105.55	± 0.32

Comments

None.

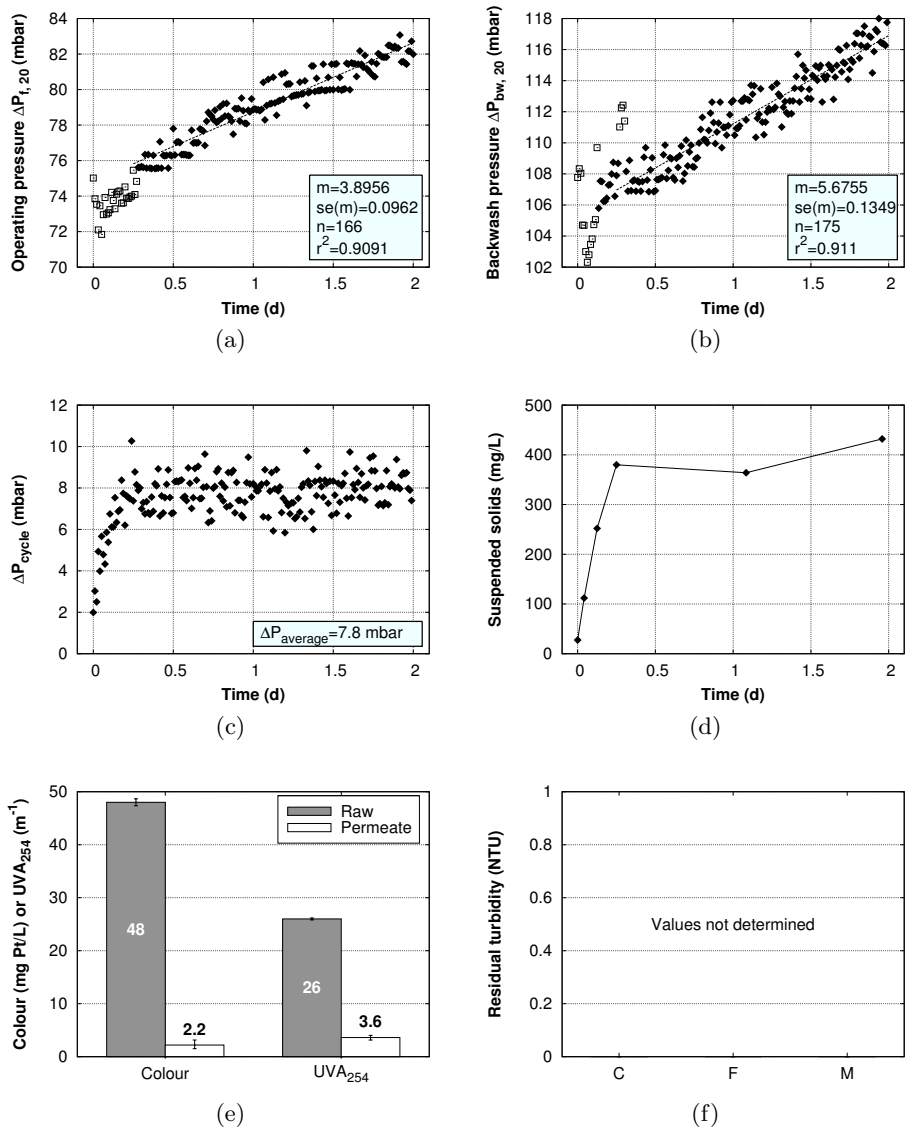

Figure P03: Overview of results for experiment P03. No residual turbidity values were determined during this experiment (f).

Experiment P04

Description

No flocculation, optimal Al-dosage.

Raw water

Colour	50 mg Pt/L
Average temperature	11.4℃

Pre-treatment

Coagulant	Polyaluminium chloride
Dosage	3 mg Al/L
Average coagulation pH	6.3
Flocculation	None

Membrane operating parameters

Filtration flux	J_f	60 L m^{-2} h^{-1}
Backwash flux	J_{bw}	90 L m^{-2} h^{-1}
Filtration cycle	t_f	29'30 min'sec
Backwash cycle	t_{bw}	00'30 min'sec
Water recovery	w	95%

Pressure increase rates obtained by regression

	Slope (mbar/d)		Intercept (mbar)	
	m	CI 95%	b	CI 95%
Filtration	2.32	± 0.23	75.13	± 0.31
Backwash	3.14	± 0.46	105.84	± 0.64

Comments

None.

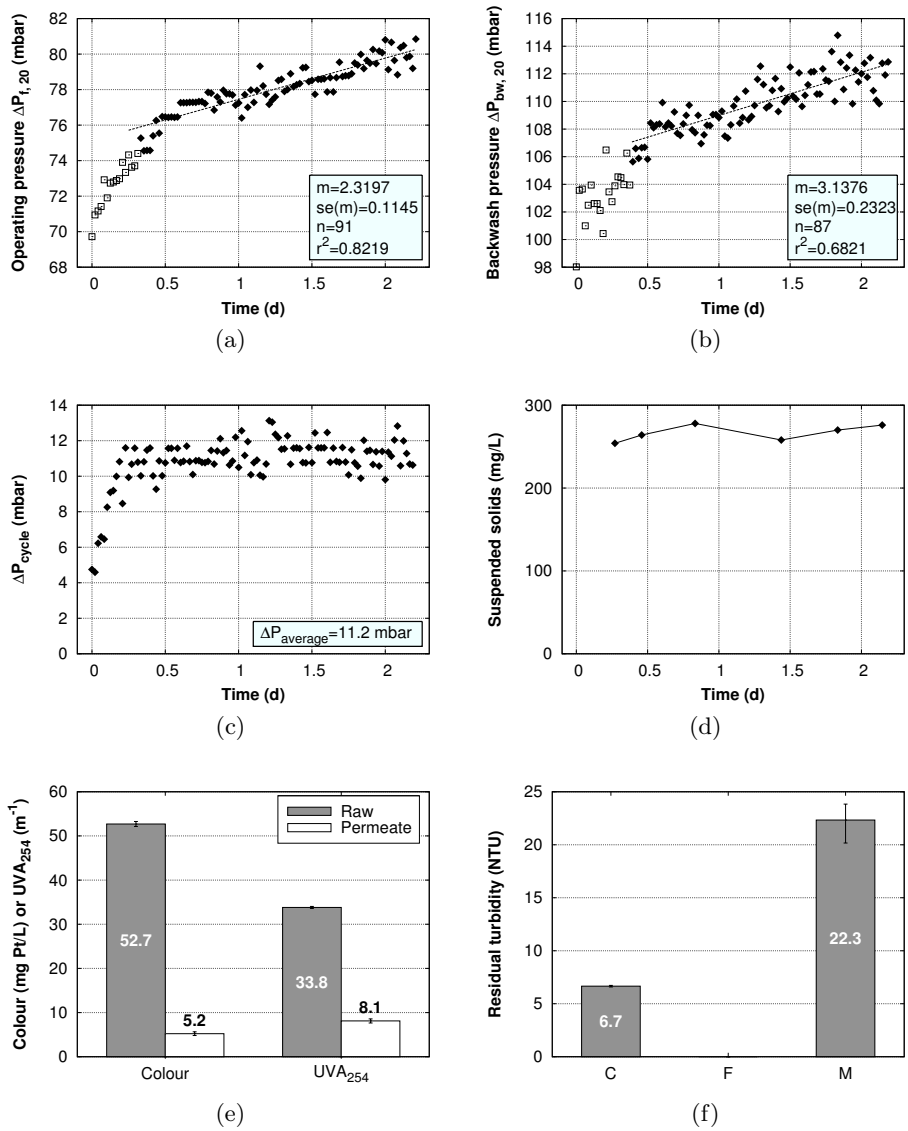

Figure P04: Overview of results for experiment P04.

Experiment P05

Description

No flocculation, increased Al-dosage.

Raw water

Colour	50 mg Pt/L
Average temperature	11.2℃

Pre-treatment

Coagulant	Polyaluminium chloride
Dosage	5 mg Al/L
Average coagulation pH	6.2
Flocculation	None

Membrane operating parameters

Filtration flux	J_f	60 L m^{-2} h^{-1}
Backwash flux	J_{bw}	90 L m^{-2} h^{-1}
Filtration cycle	t_f	29'30 min'sec
Backwash cycle	t_{bw}	00'30 min'sec
Water recovery	w	95%

Pressure increase rates obtained by regression

	Slope (mbar/d)		Intercept (mbar)	
	m	CI 95%	b	CI 95%
Filtration	3.92	± 0.21	68.74	± 0.27
Backwash	5.18	± 0.47	98.78	± 0.64

Comments

Decreased coagulation pH to 5.5 after 48 hours.

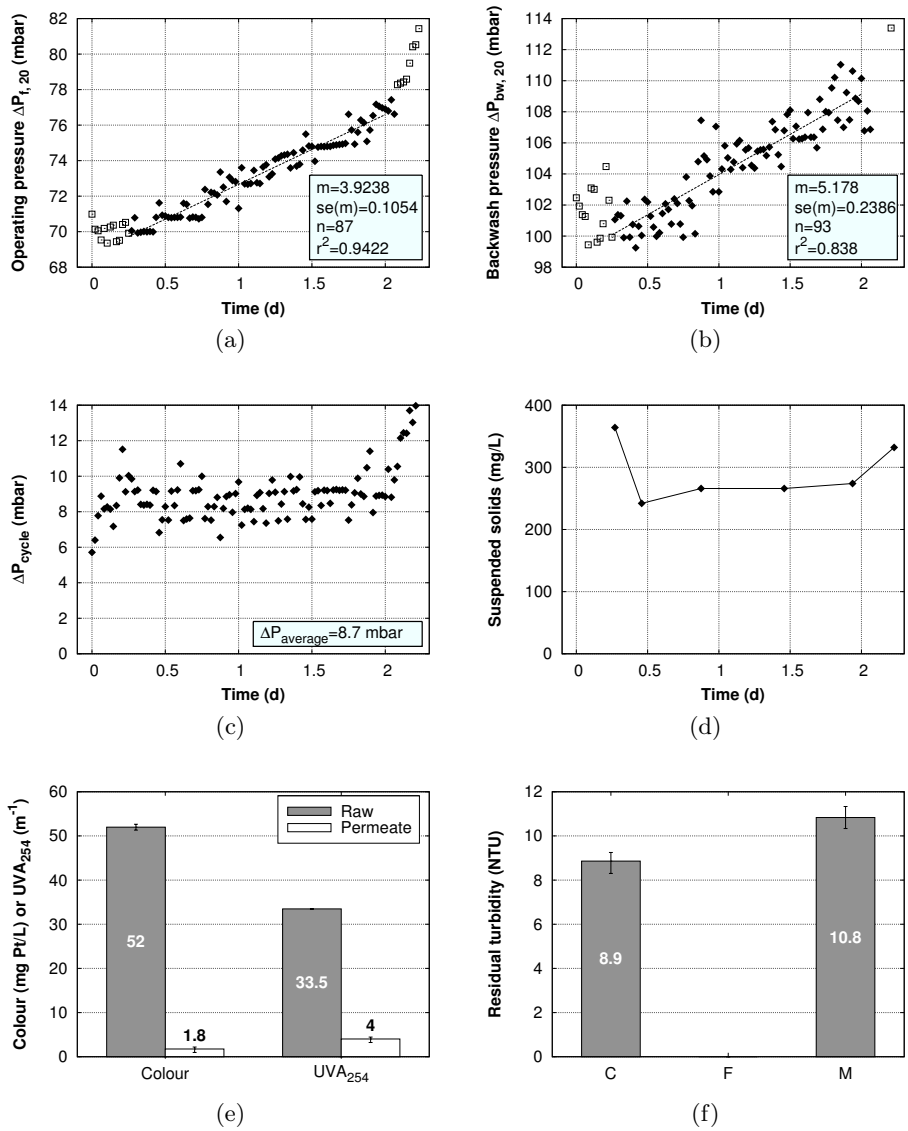

Figure P05: Overview of results for experiment P05.

Experiment P06

Description

Effect of jet-mix flocculator (design 1) at low filtration flux.

Raw water

Colour	50 mg Pt/L
Average temperature	8.1℃

Pre-treatment

Coagulant	Polyaluminium chloride
Dosage	5 mg Al/L
Average coagulation pH	6.3
Flocculation	JMF1

Membrane operating parameters

Filtration flux	J_f	45 L m^{-2} h^{-1}
Backwash flux	J_{bw}	68 L m^{-2} h^{-1}
Filtration cycle	t_f	29'30 min'sec
Backwash cycle	t_{bw}	00'30 min'sec
Water recovery	w	95%

Pressure increase rates obtained by regression

	Slope (mbar/d)		Intercept (mbar)	
	m	CI 95%	b	CI 95%
Filtration	2.13	± 0.24	55.23	± 0.33
Backwash	2.49	± 0.43	82.45	± 0.57

Comments

None.

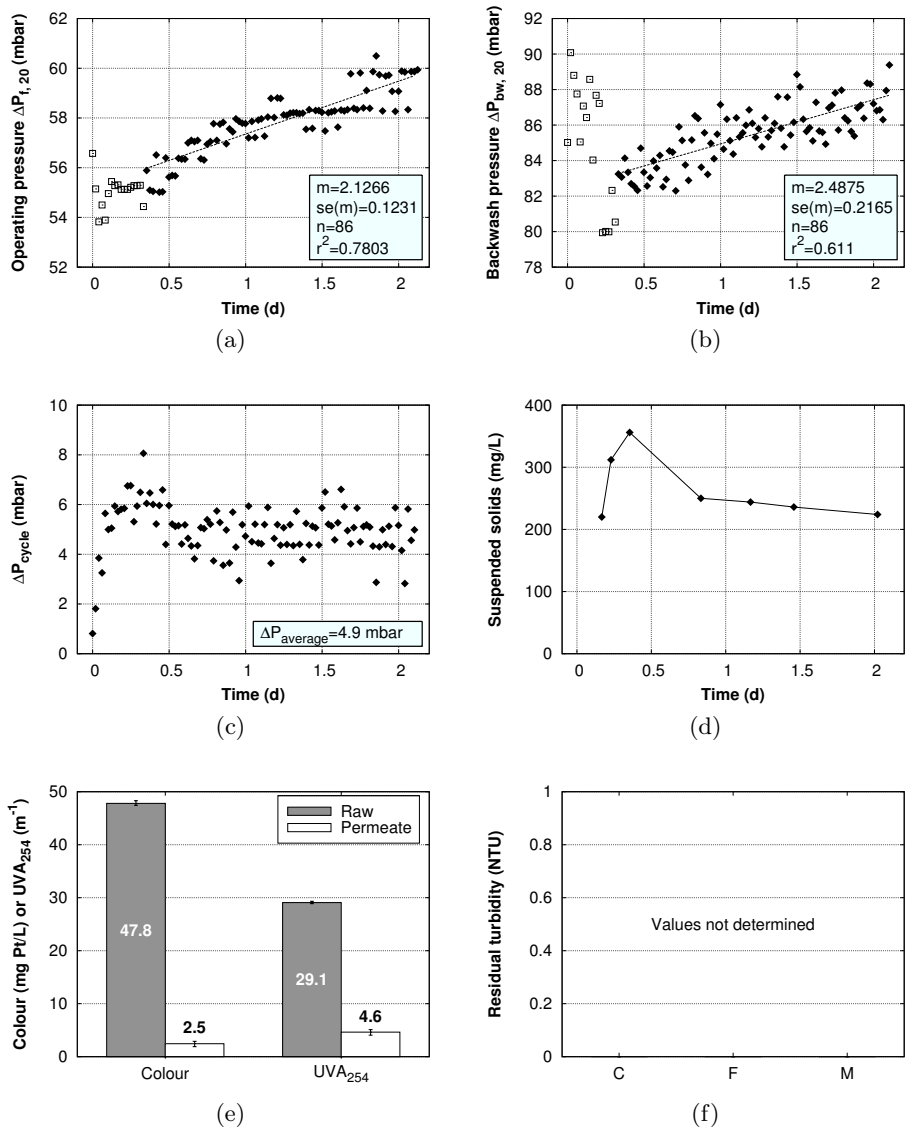

Figure P06: Overview of results for experiment P06. No residual turbidity values were determined during this experiment (f)

Experiment P07

Description

As P01 and P05 but with jet-mix flocculator (design 1).

Raw water

Colour	50 mg Pt/L
Average temperature	7.3℃

Pre-treatment

Coagulant	Polyaluminium chloride
Dosage	5 mg Al/L
Average coagulation pH	6.3
Flocculation	JMF1

Membrane operating parameters

Filtration flux	J_f	60 L m^{-2} h^{-1}
Backwash flux	J_{bw}	90 L m^{-2} h^{-1}
Filtration cycle	t_f	29'30 min'sec
Backwash cycle	t_{bw}	00'30 min'sec
Water recovery	w	95%

Pressure increase rates obtained by regression

	Slope (mbar/d)		Intercept (mbar)	
	m	CI 95%	b	CI 95%
Filtration	4.34	± 0.28	84.29	± 0.33
Backwash	3.93	± 0.33	125.61	± 0.40

Comments

None.

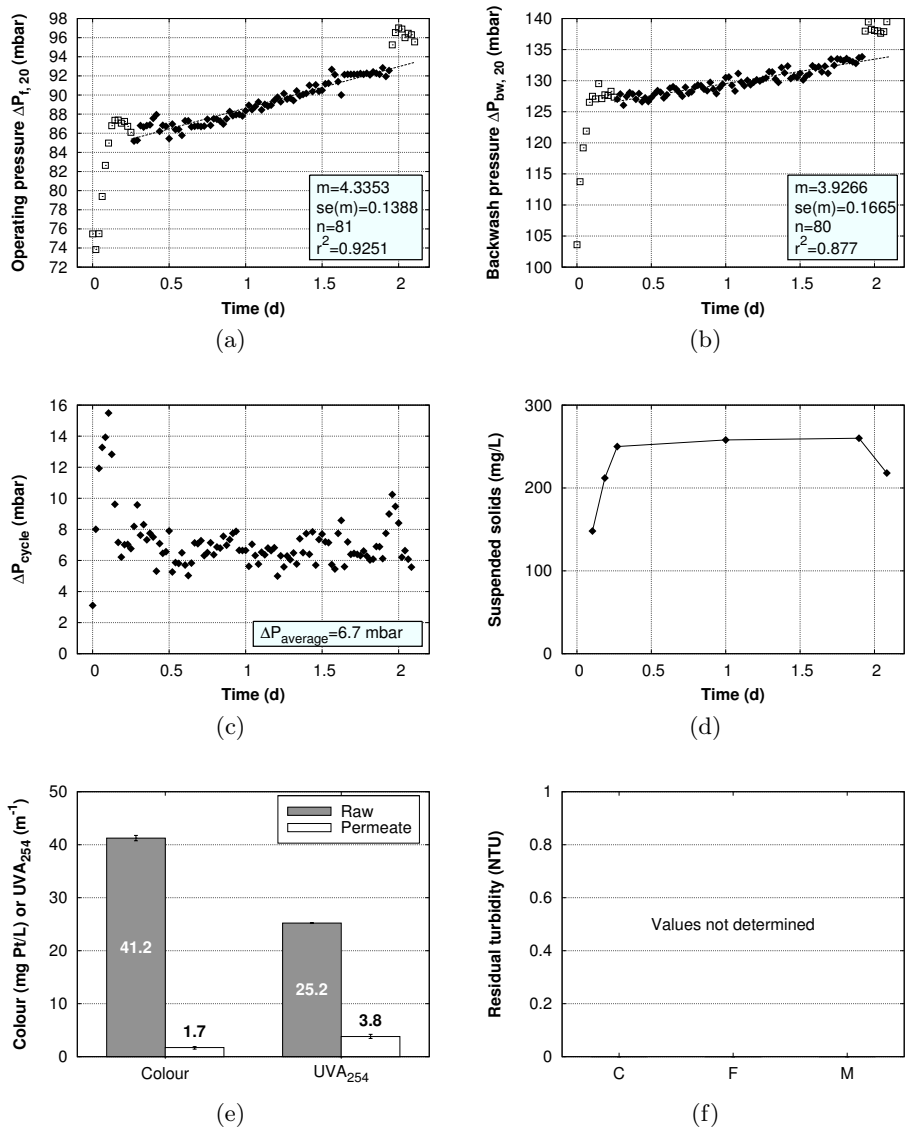

Figure P07: Overview of results for experiment P07. No residual turbidity values were determined during this experiment (f)

Experiment P08

Description

Jet-mix flocculator, high flux.

Raw water

Colour	50 mg Pt/L
Average temperature	7.5℃

Pre-treatment

Coagulant	Polyaluminium chloride
Dosage	5 mg Al/L
Average coagulation pH	6.3
Flocculation	JMF1

Membrane operating parameters

Filtration flux	J_f	75 L m^{-2} h^{-1}
Backwash flux	J_{bw}	105 L m^{-2} h^{-1}
Filtration cycle	t_f	29'30 min'sec
Backwash cycle	t_{bw}	00'30 min'sec
Water recovery	w	95%

Pressure increase rates obtained by regression

	Slope (mbar/d)		Intercept (mbar)	
	m	CI 95%	b	CI 95%
Filtration	6.09	± 0.29	91.19	± 0.37
Backwash	4.42	± 0.43	114.23	± 0.55

Comments

None.

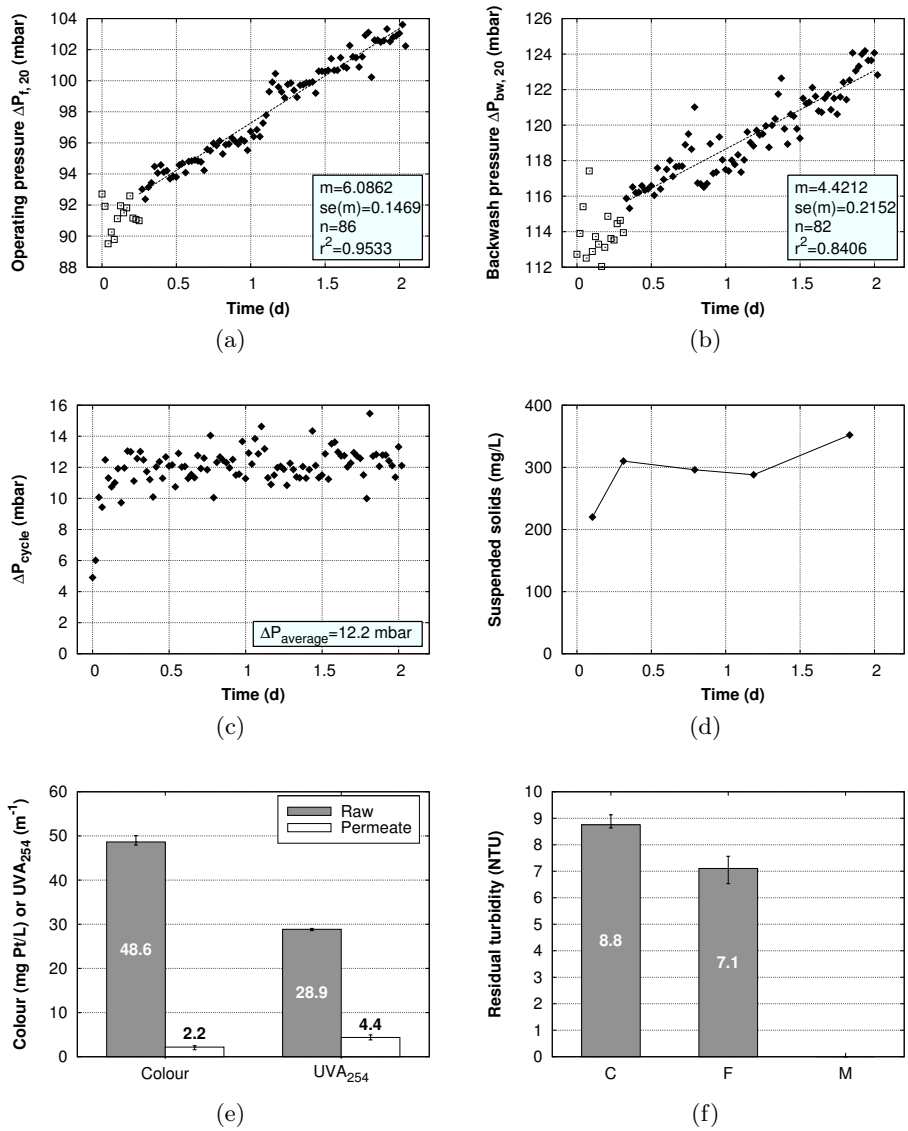

Figure P08: Overview of results for experiment P08.

Experiment P09

Description

Combined pipe and jet-mix flocculator.

Raw water

Colour	50 mg Pt/L
Average temperature	7.9℃

Pre-treatment

Coagulant	Polyaluminium chloride
Dosage	5 mg Al/L
Average coagulation pH	6.3
Flocculation	PF+JMF1

Membrane operating parameters

Filtration flux	J_f	60 L m^{-2} h^{-1}
Backwash flux	J_{bw}	90 L m^{-2} h^{-1}
Filtration cycle	t_f	29'30 min'sec
Backwash cycle	t_{bw}	00'30 min'sec
Water recovery	w	95%

Pressure increase rates obtained by regression

	Slope (mbar/d)		Intercept (mbar)	
	m	CI 95%	b	CI 95%
Filtration	3.30	± 0.17	73.67	± 0.21
Backwash	4.22	± 1.12	108.33	± 1.44

Comments

None.

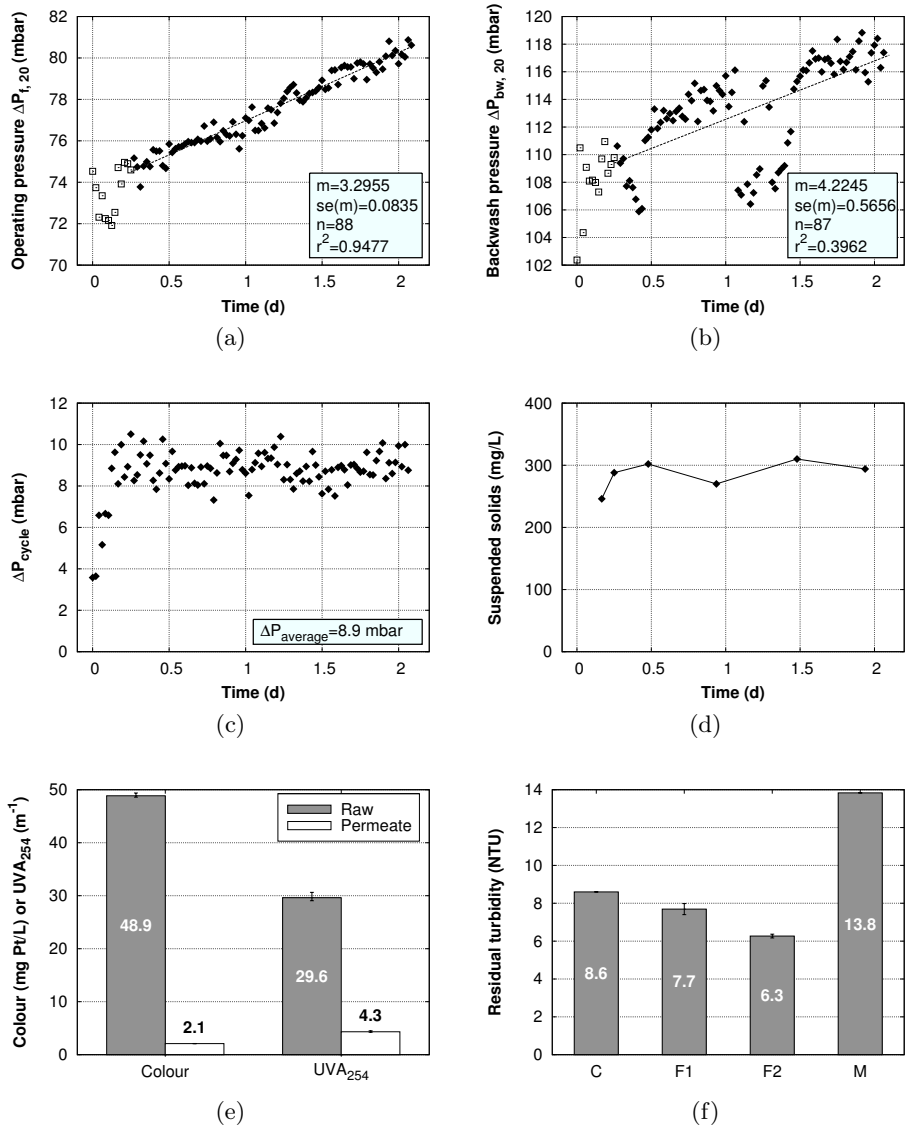

Figure P09: Overview of results for experiment P09. Residual turbidity (f): F1=after PF; F2=after JMF1

Experiment P10

Description

Optimal Al-dosage, jet-mix flocculator design 2, reduced backwash cycle length.

Raw water

Colour	50 mg Pt/L
Average temperature	11.3℃

Pre-treatment

Coagulant	Polyaluminium chloride
Dosage	3 mg Al/L
Average coagulation pH	6.3
Flocculation	JMF2

Membrane operating parameters

Filtration flux	J_f	60 L m^{-2} h^{-1}
Backwash flux	J_{bw}	90 L m^{-2} h^{-1}
Filtration cycle	t_f	14'45 min'sec
Backwash cycle	t_{bw}	00'15 min'sec
Water recovery	w	95%

Pressure increase rates obtained by regression

	Slope (mbar/d)		Intercept (mbar)	
	m	CI 95%	b	CI 95%
Filtration	2.60	± 0.20	74.39	± 0.25
Backwash	1.36	± 0.28	116.63	± 0.36

Comments

None.

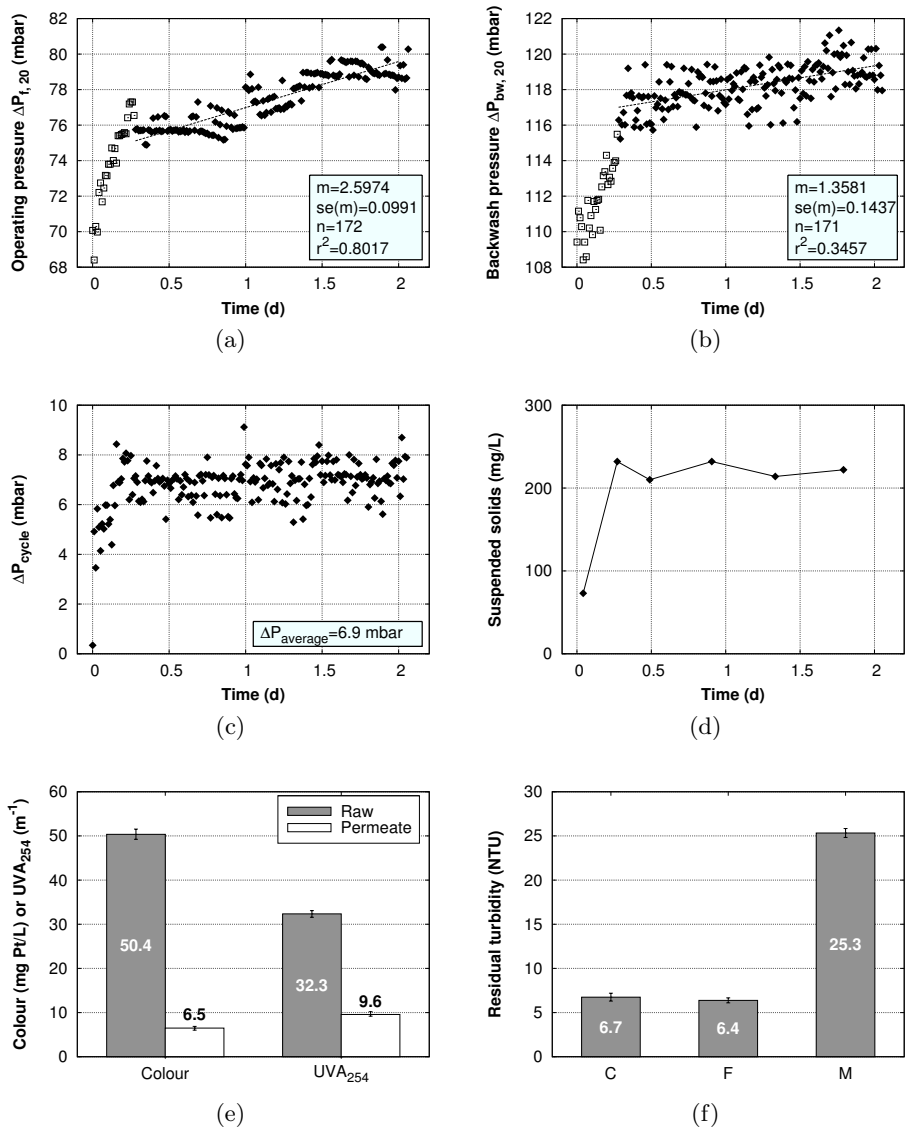

Figure P10: Overview of results for experiment P10

Experiment P11

Description

As P10, normal backwash interval and length.

Raw water

Colour	50 mg Pt/L
Average temperature	9.9℃

Pre-treatment

Coagulant	Polyaluminium chloride
Dosage	3 mg Al/L
Average coagulation pH	6.4
Flocculation	JMF2

Membrane operating parameters

Filtration flux	J_f	60 L m^{-2} h^{-1}
Backwash flux	J_{bw}	90 L m^{-2} h^{-1}
Filtration cycle	t_f	29'30 min'sec
Backwash cycle	t_{bw}	00'30 min'sec
Water recovery	w	95%

Pressure increase rates obtained by regression

	Slope (mbar/d)		Intercept (mbar)	
	m	CI 95%	b	CI 95%
Filtration	1.55	± 0.25	78.56	± 0.32
Backwash	3.33	± 0.57	111.40	± 0.71

Comments

None.

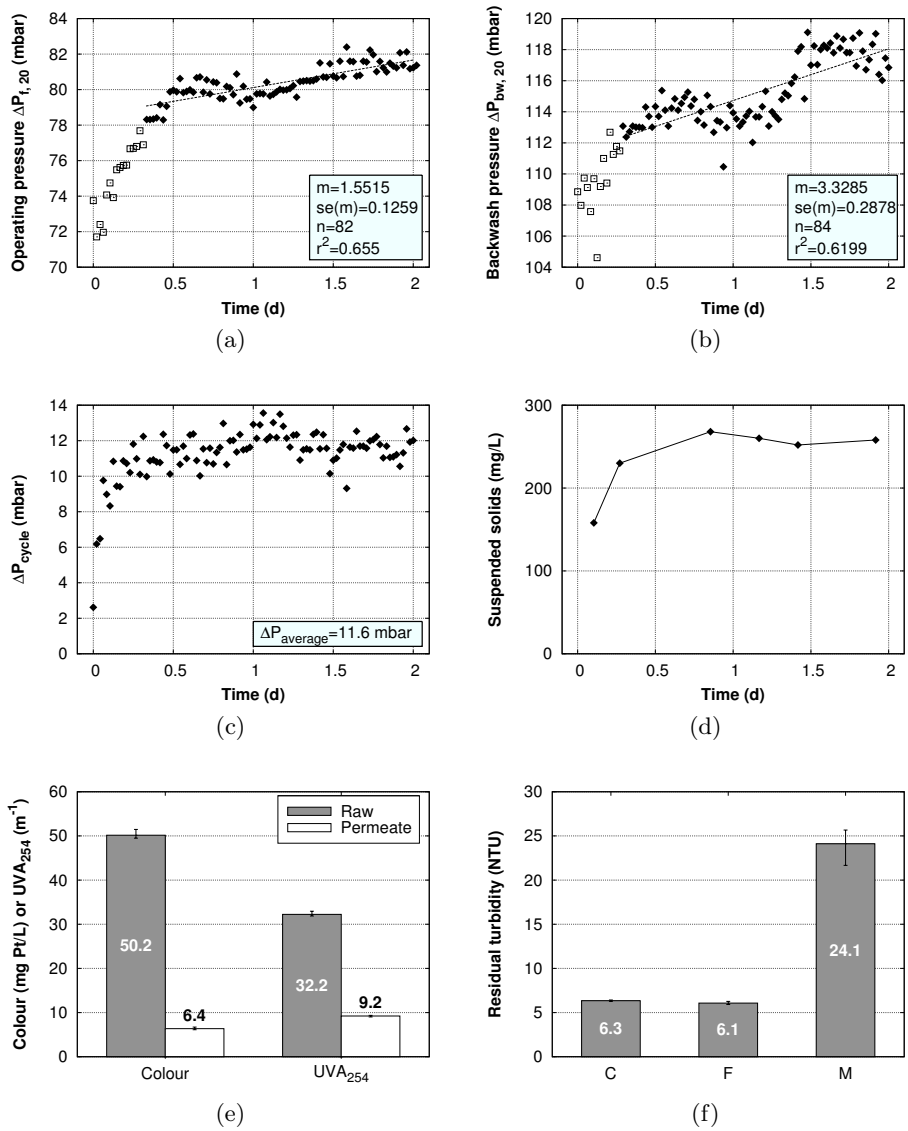

Figure P11: Overview of results for experiment P11

Experiment P12

Description

As P10, less frequent and longer backwash cycles.

Raw water

Colour	50 mg Pt/L
Average temperature	10.8℃

Pre-treatment

Coagulant	Polyaluminium chloride
Dosage	3 mg Al/L
Average coagulation pH	6.3
Flocculation	JMF2

Membrane operating parameters

Filtration flux	J_f	60 L m^{-2} h^{-1}
Backwash flux	J_{bw}	90 L m^{-2} h^{-1}
Filtration cycle	t_f	59'00 min'sec
Backwash cycle	t_{bw}	01'00 min'sec
Water recovery	w	95%

Pressure increase rates obtained by regression

	Slope (mbar/d)		Intercept (mbar)	
	m	CI 95%	b	CI 95%
Filtration	0.86	± 0.41	77.54	± 0.53
Backwash	1.84	± 0.58	114.81	± 0.73

Comments

None.

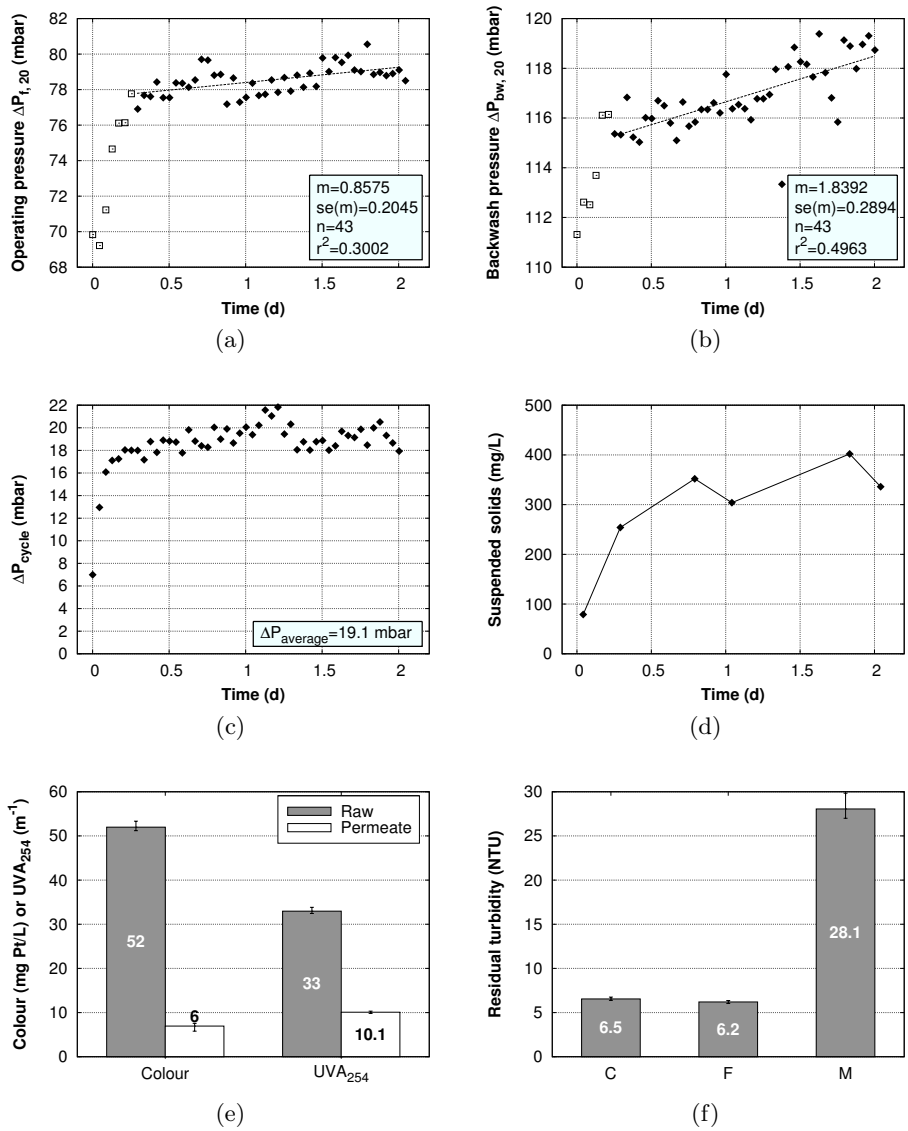

Figure P12: Overview of results for experiment P12

Experiment P13

Description

As P10, higher coagulant dosage.

Raw water

Colour	50 mg Pt/L
Average temperature	9.8℃

Pre-treatment

Coagulant	Polyaluminium chloride
Dosage	5 mg Al/L
Average coagulation pH	6.3
Flocculation	JMF2

Membrane operating parameters

Filtration flux	J_f	60 L m^{-2} h^{-1}
Backwash flux	J_{bw}	90 L m^{-2} h^{-1}
Filtration cycle	t_f	29'30 min'sec
Backwash cycle	t_{bw}	00'30 min'sec
Water recovery	w	95%

Pressure increase rates obtained by regression

	Slope (mbar/d)		Intercept (mbar)	
	m	CI 95%	b	CI 95%
Filtration	4.24	± 0.28	74.05	± 0.36
Backwash	4.55	± 0.97	103.84	± 1.21

Comments

Results from replicate experimental run:

	Slope (mbar/d)		Intercept (mbar)	
	m	CI 95%	b	CI 95%
Filtration	4.63	± 0.32	71.69	± 0.39
Backwash	4.49	± 0.42	108.80	± 0.51

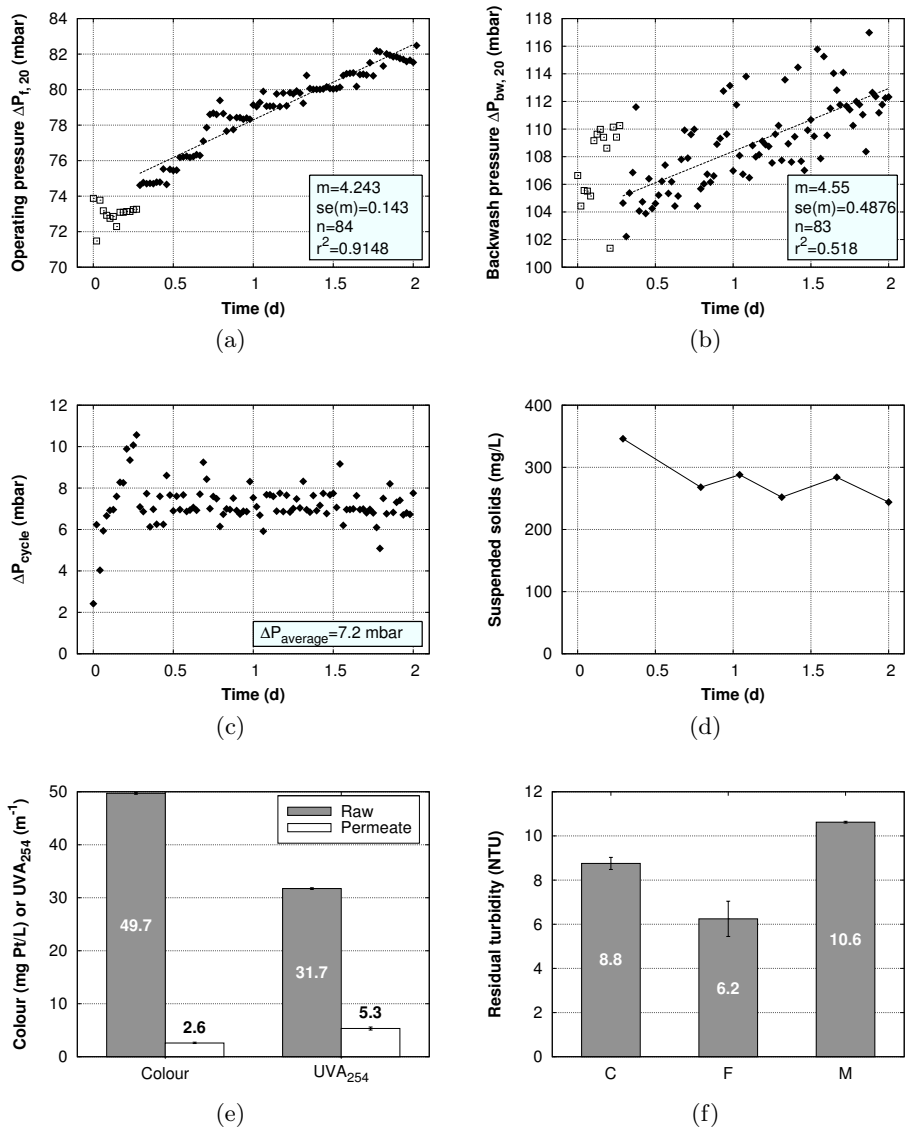

Figure P13: Overview of results for experiment P13

Experiment P14

Description

Jet-mix flocculator, optimal Al-dosage, low flux.

Raw water

Colour	50 mg Pt/L
Average temperature	11.5℃

Pre-treatment

Coagulant	Polyaluminium chloride
Dosage	3 mg Al/L
Average coagulation pH	6.4
Flocculation	JMF2

Membrane operating parameters

Filtration flux	J_f	45 L m^{-2} h^{-1}
Backwash flux	J_{bw}	68 L m^{-2} h^{-1}
Filtration cycle	t_f	29'30 min'sec
Backwash cycle	t_{bw}	00'30 min'sec
Water recovery	w	95%

Pressure increase rates obtained by regression

	Slope (mbar/d)		Intercept (mbar)	
	m	CI 95%	b	CI 95%
Filtration	1.51	± 0.22	53.72	± 0.29
Backwash	0.71	± 0.50	82.15	± 0.64

Comments

None.

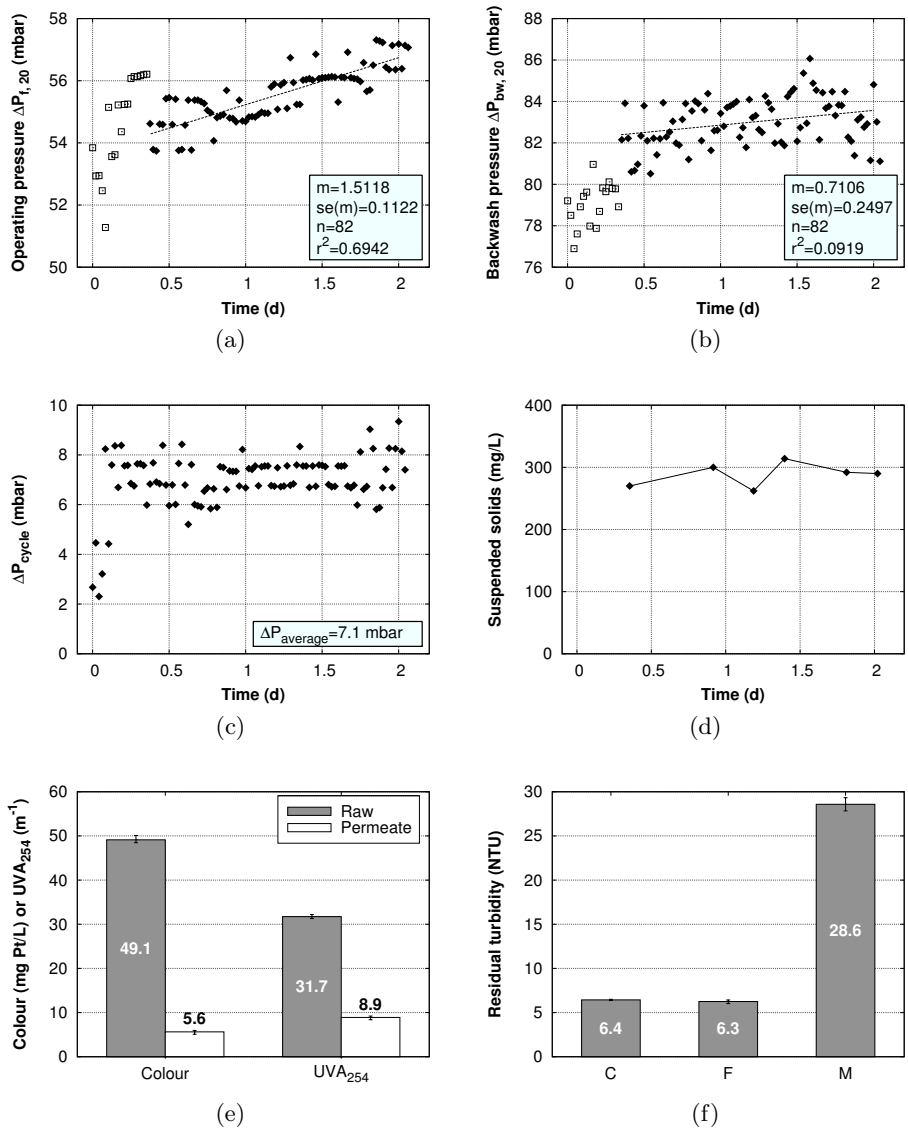

Figure P14: Overview of results for experiment P14

Experiment P15

Description

Packed-bed flocculator, optimal Al-dosage, low flux, long cycles.

Raw water

Colour	50 mg Pt/L
Average temperature	12.1℃

Pre-treatment

Coagulant	Polyaluminium chloride
Dosage	3 mg Al/L
Average coagulation pH	6.3
Flocculation	PBF

Membrane operating parameters

Filtration flux	J_f	45 L m^{-2} h^{-1}
Backwash flux	J_{bw}	68 L m^{-2} h^{-1}
Filtration cycle	t_f	59'00 min'sec
Backwash cycle	t_{bw}	01'00 min'sec
Water recovery	w	95%

Pressure increase rates obtained by regression

	Slope (mbar/d)		Intercept (mbar)	
	m	CI 95%	b	CI 95%
Filtration	0.66	± 0.34	54.92	± 0.49
Backwash	1.89	± 0.48	91.08	± 0.64

Comments

None.

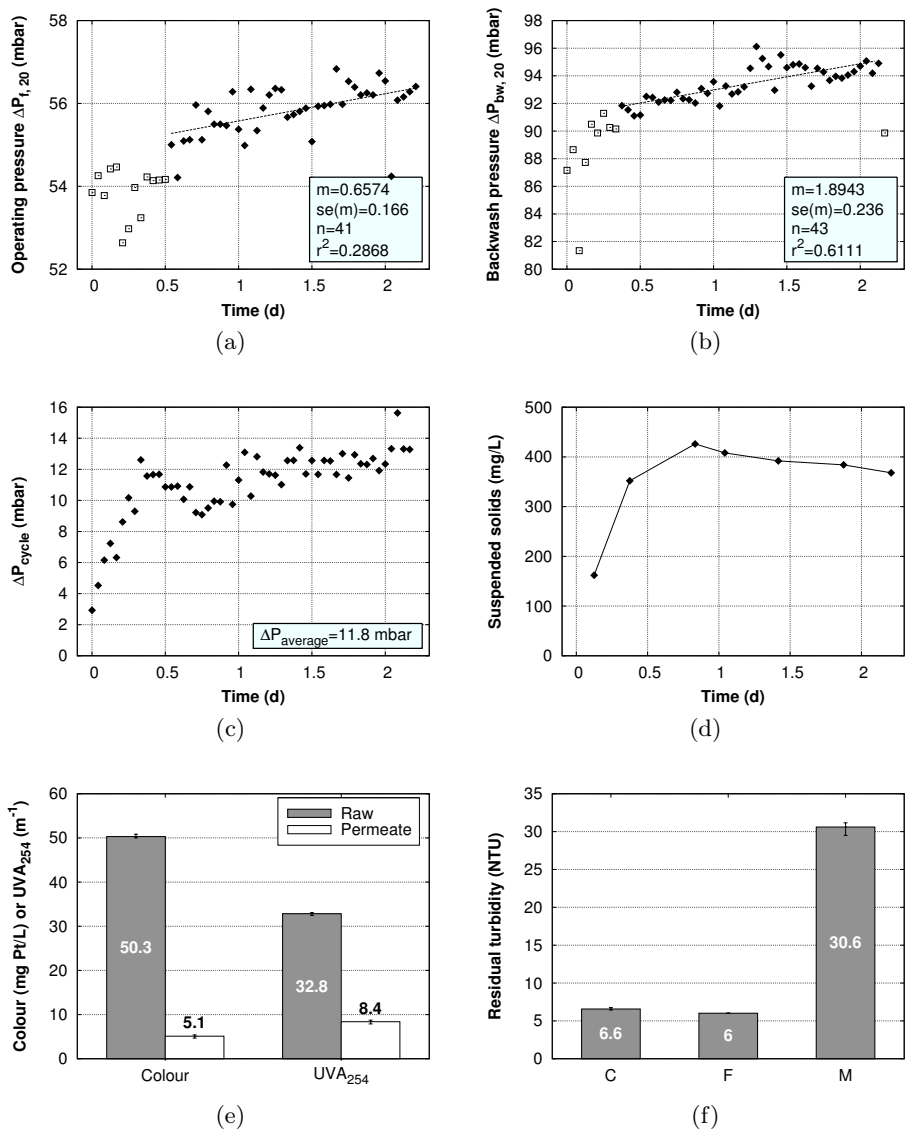

Figure P15: Overview of results for experiment P15

Experiment P16

Description

Packed-bed flocculator, optimal Al-dosage, normal flux.

Raw water

Colour	50 mg Pt/L
Average temperature	12.1℃

Pre-treatment

Coagulant	Polyaluminium chloride
Dosage	3 mg Al/L
Average coagulation pH	6.2
Flocculation	PBF

Membrane operating parameters

Filtration flux	J_f	60 L m^{-2} h^{-1}
Backwash flux	J_{bw}	90 L m^{-2} h^{-1}
Filtration cycle	t_f	29'30 min'sec
Backwash cycle	t_{bw}	00'30 min'sec
Water recovery	w	95%

Pressure increase rates obtained by regression

	Slope (mbar/d)		Intercept (mbar)	
	m	CI 95%	b	CI 95%
Filtration	0.37	± 0.38	79.53	± 0.49
Backwash	1.98	± 0.33	122.39	± 0.41

Comments

None.

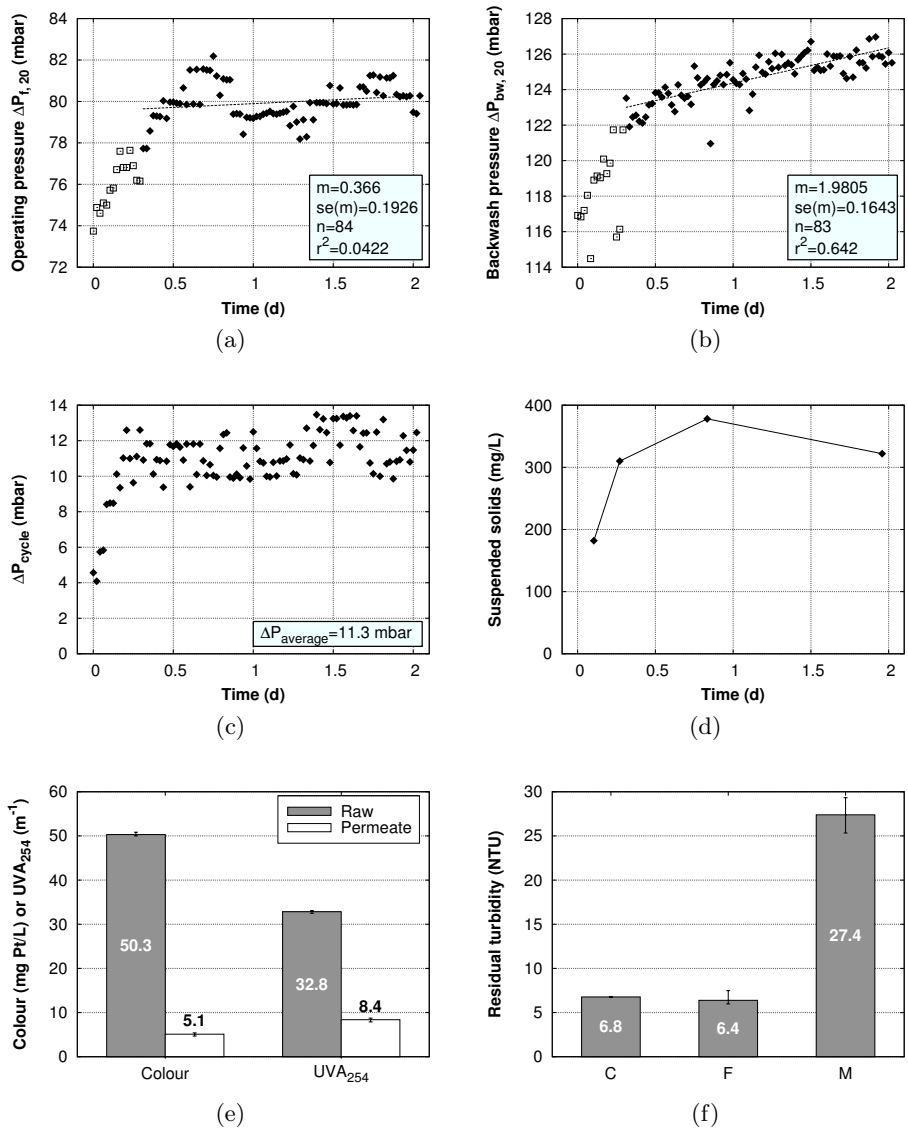

Figure P16: Overview of results for experiment P16

Experiment P17

Description

Packed-bed flocculator, optimal Al-dosage, high flux.

Raw water

Colour	50 mg Pt/L
Average temperature	8.9℃

Pre-treatment

Coagulant	Polyaluminium chloride
Dosage	3 mg Al/L
Average coagulation pH	6.2
Flocculation	PBF

Membrane operating parameters

Filtration flux	J_f	75 L m^{-2} h^{-1}
Backwash flux	J_{bw}	105 L m^{-2} h^{-1}
Filtration cycle	t_f	29'30 min'sec
Backwash cycle	t_{bw}	00'30 min'sec
Water recovery	w	95%

Pressure increase rates obtained by regression

	Slope (mbar/d)		Intercept (mbar)	
	m	CI 95%	b	CI 95%
Filtration	3.08	± 0.21	96.97	± 0.27
Backwash	-0.33	± 1.07	129.73	± 1.37

Comments

None.

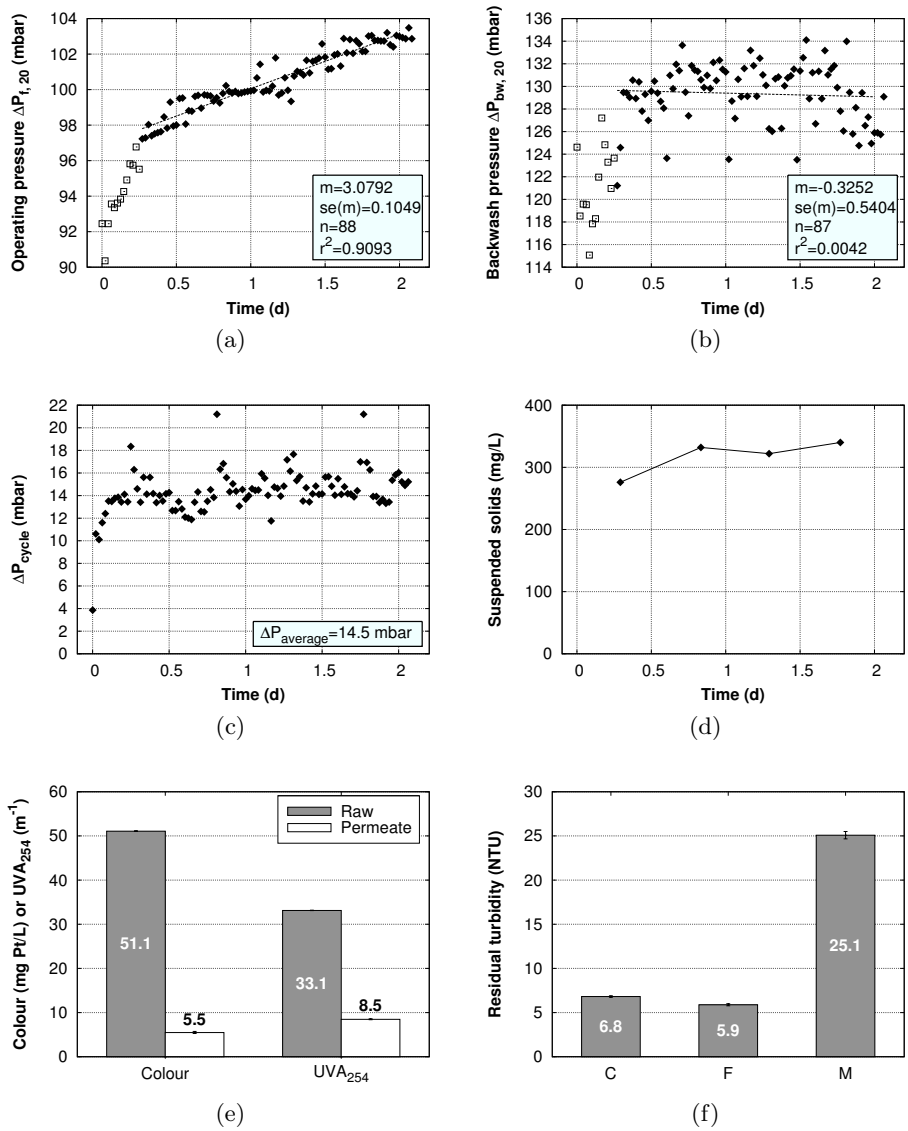

Figure P17: Overview of results for experiment P17

Experiment P18

Description

Packed-bed flocculator, high Al-dosage, short cycles.

Raw water

Colour	50 mg Pt/L
Average temperature	12.2℃

Pre-treatment

Coagulant	Polyaluminium chloride
Dosage	5 mg Al/L
Average coagulation pH	6.2
Flocculation	PBF

Membrane operating parameters

Filtration flux	J_f	60 L m^{-2} h^{-1}
Backwash flux	J_{bw}	90 L m^{-2} h^{-1}
Filtration cycle	t_f	14'45 min'sec
Backwash cycle	t_{bw}	00'15 min'sec
Water recovery	w	95%

Pressure increase rates obtained by regression

	Slope (mbar/d)		Intercept (mbar)	
	m	CI 95%	b	CI 95%
Filtration	1.87	± 0.22	72.94	± 0.28
Backwash	5.08	± 0.26	114.32	± 0.33

Comments

None.

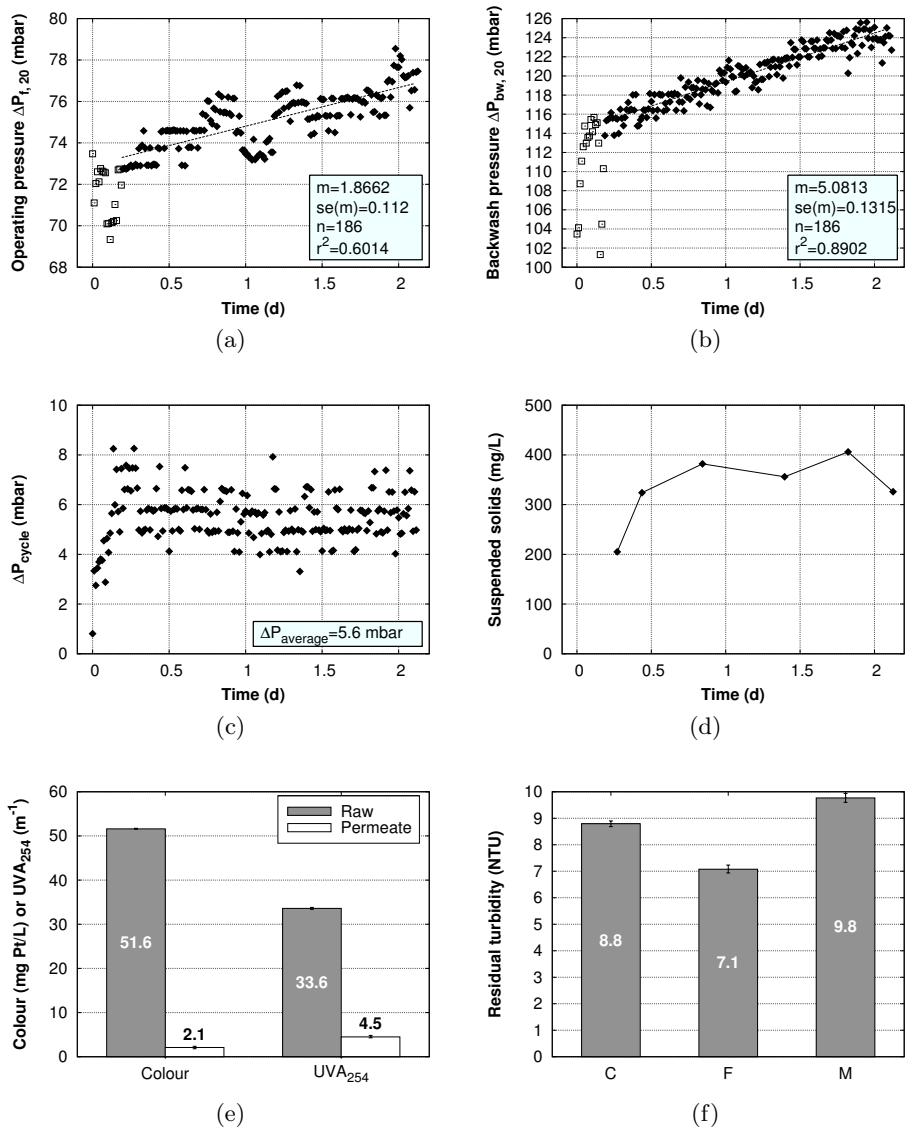

Figure P18: Overview of results for experiment P18

Experiment P19

Description

Packed-bed flocculator, high Al-dosage, normal cycles.

Raw water

Colour	50 mg Pt/L
Average temperature	11.3℃

Pre-treatment

Coagulant	Polyaluminium chloride
Dosage	5 mg Al/L
Average coagulation pH	6.1
Flocculation	PBF

Membrane operating parameters

Filtration flux	J_f	60 L m^{-2} h^{-1}
Backwash flux	J_{bw}	90 L m^{-2} h^{-1}
Filtration cycle	t_f	29'30 min'sec
Backwash cycle	t_{bw}	00'30 min'sec
Water recovery	w	95%

Pressure increase rates obtained by regression

	Slope (mbar/d)		Intercept (mbar)	
	m	CI 95%	b	CI 95%
Filtration	3.68	± 0.46	72.62	± 0.59
Backwash	6.16	± 0.69	103.07	± 0.92

Comments

None.

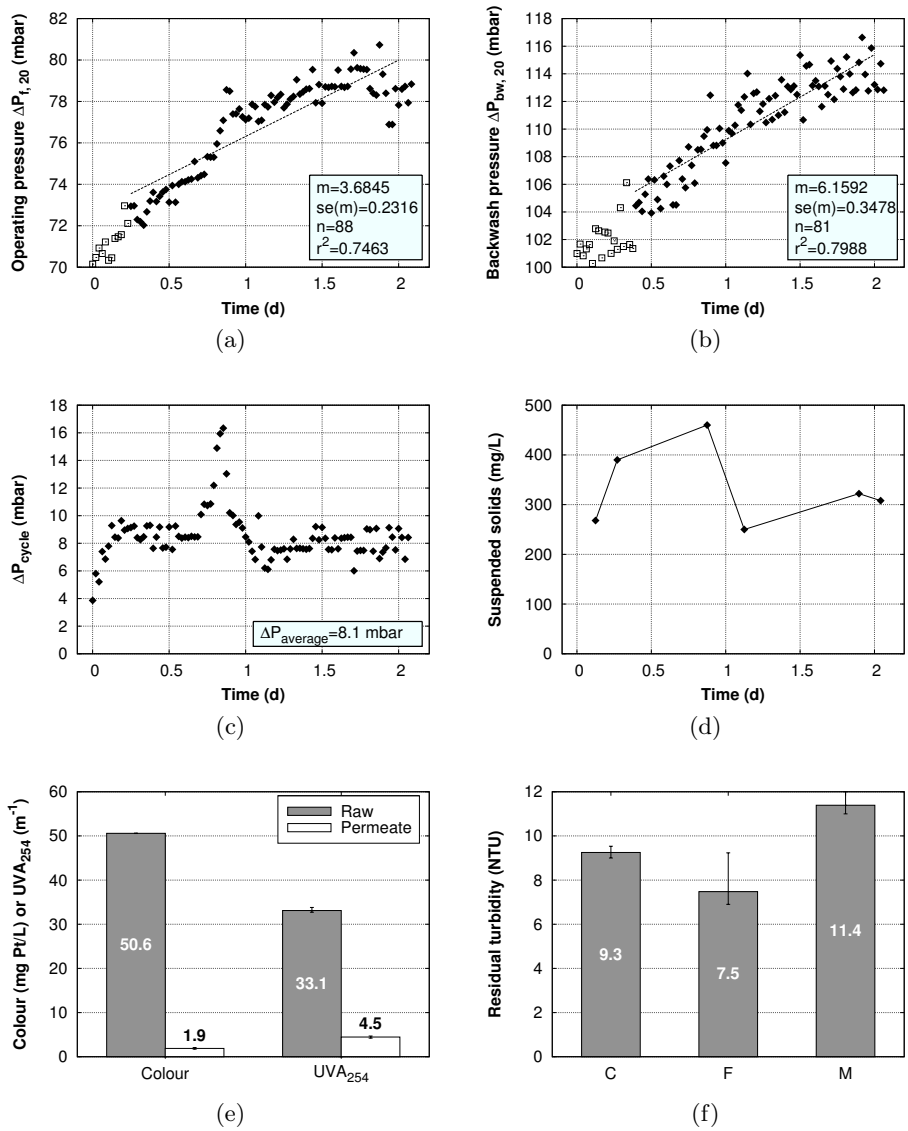

Figure P19: Overview of results for experiment P19

Experiment P20

Description

Packed-bed flocculator, low Al-dosage, normal cycles.

Raw water

Colour	50 mg Pt/L
Average temperature	11.7℃

Pre-treatment

Coagulant	Polyaluminium chloride
Dosage	2 mg Al/L
Average coagulation pH	6.2
Flocculation	PBF

Membrane operating parameters

Filtration flux	J_f	60 L m^{-2} h^{-1}
Backwash flux	J_{bw}	90 L m^{-2} h^{-1}
Filtration cycle	t_f	29'30 min'sec
Backwash cycle	t_{bw}	00'30 min'sec
Water recovery	w	95%

Pressure increase rates obtained by regression

	Slope (mbar/d)		Intercept (mbar)	
	m	CI 95%	b	CI 95%
Filtration	0.02	± 0.35	80.45	± 0.44
Backwash	7.34	± 1.03	106.62	± 1.29

Comments

None.

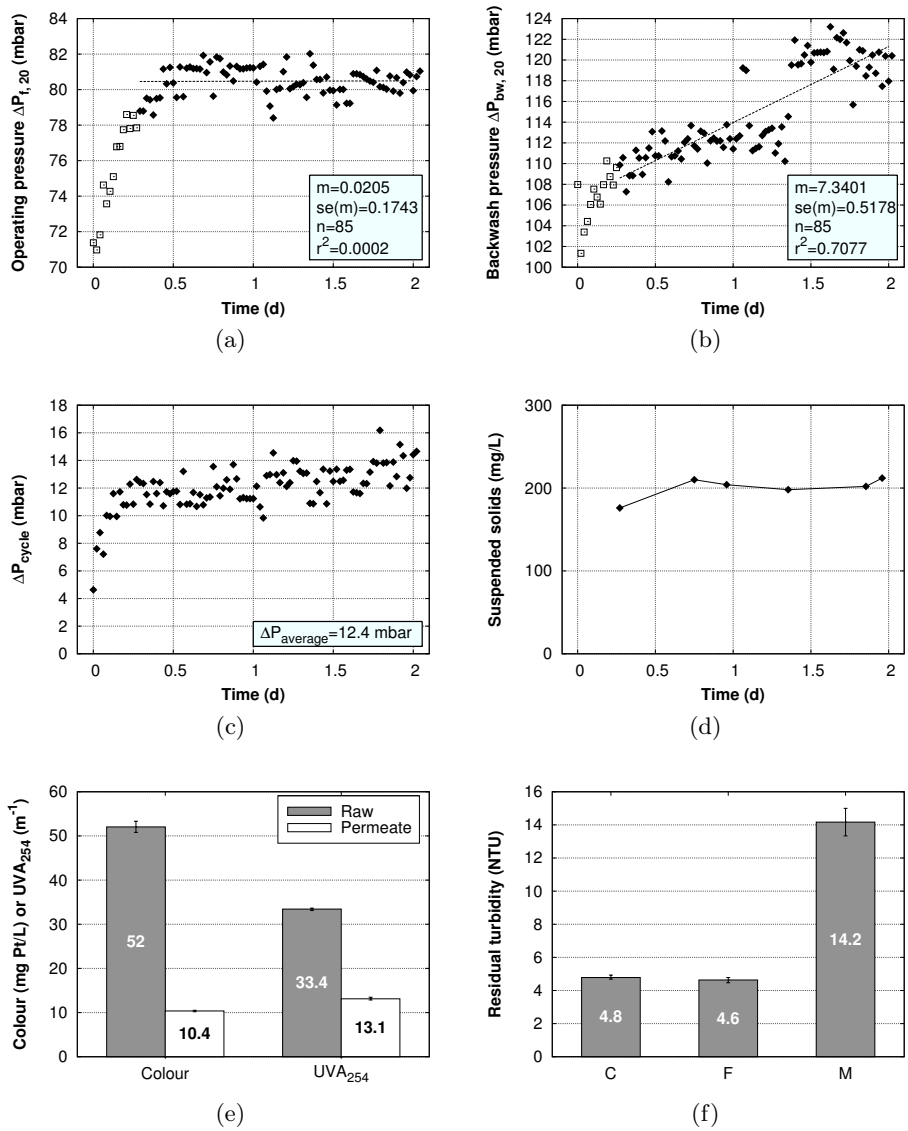

Figure P20: Overview of results for experiment P20

Experiment P21

Description

Packed-bed flocculator, optimal Al-dosage, lower water recovery.

Raw water

Colour	50 mg Pt/L
Average temperature	12.2℃

Pre-treatment

Coagulant	Polyaluminium chloride
Dosage	3 mg Al/L
Average coagulation pH	6.2
Flocculation	PBF

Membrane operating parameters

Filtration flux	J_f	60 L m^{-2} h^{-1}
Backwash flux	J_{bw}	90 L m^{-2} h^{-1}
Filtration cycle	t_f	29'30 min'sec
Backwash cycle	t_{bw}	00'30 min'sec
Water recovery	w	85%

Pressure increase rates obtained by regression

	Slope (mbar/d)		Intercept (mbar)	
	m	CI 95%	b	CI 95%
Filtration	2.35	± 0.15	76.39	± 0.30
Backwash	1.16	± 0.29	118.06	± 0.61

Comments

None.

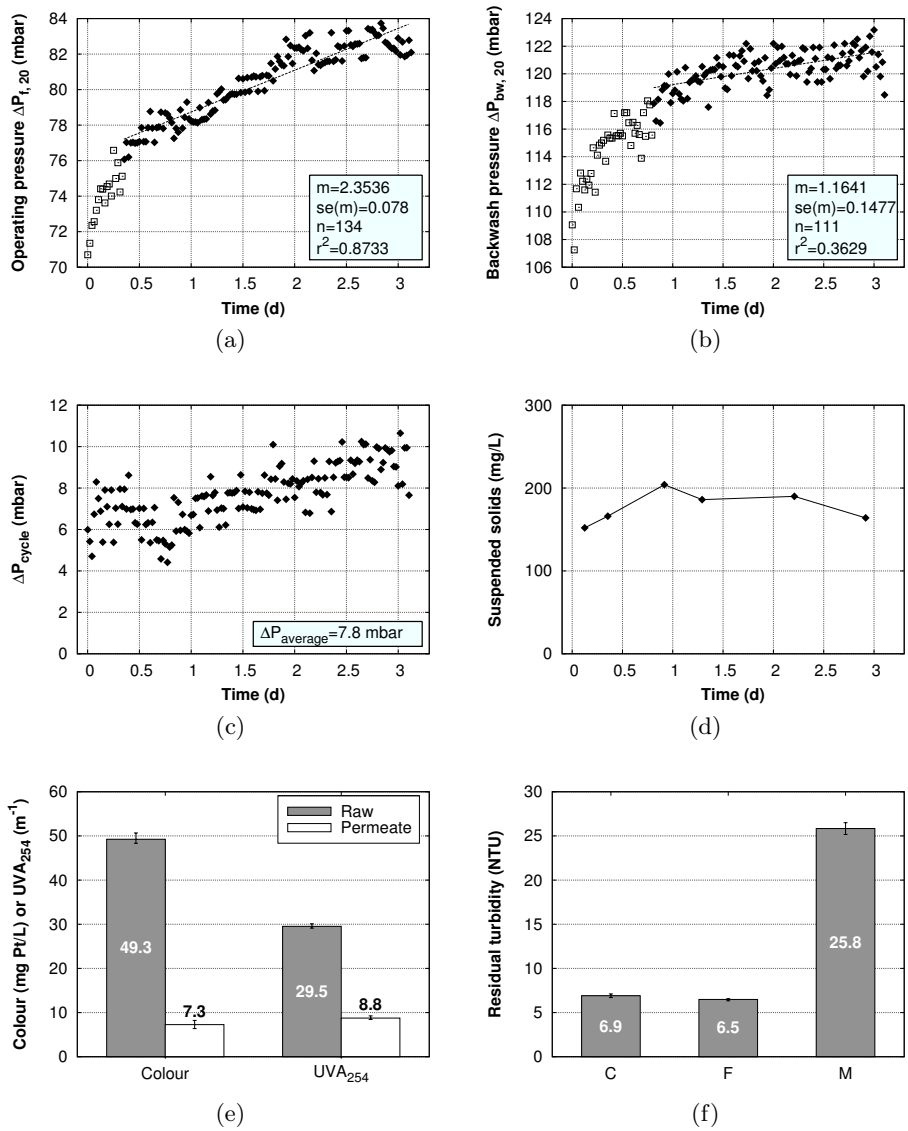

Figure P21: Overview of results for experiment P21

Experiment P22

Description

Packed-bed flocculator, high Al-dosage, lower water recovery.

Raw water

Colour	50 mg Pt/L
Average temperature	12.2℃

Pre-treatment

Coagulant	Polyaluminium chloride
Dosage	5 mg Al/L
Average coagulation pH	6.3
Flocculation	PBF

Membrane operating parameters

Filtration flux	J_f	60 L m^{-2} h^{-1}
Backwash flux	J_{bw}	90 L m^{-2} h^{-1}
Filtration cycle	t_f	29'30 min'sec
Backwash cycle	t_{bw}	00'30 min'sec
Water recovery	w	85%

Pressure increase rates obtained by regression

	Slope (mbar/d)		Intercept (mbar)	
	m	CI 95%	b	CI 95%
Filtration	3.72	± 0.16	70.04	± 0.29
Backwash	3.50	± 0.24	110.44	± 0.41

Comments

None.

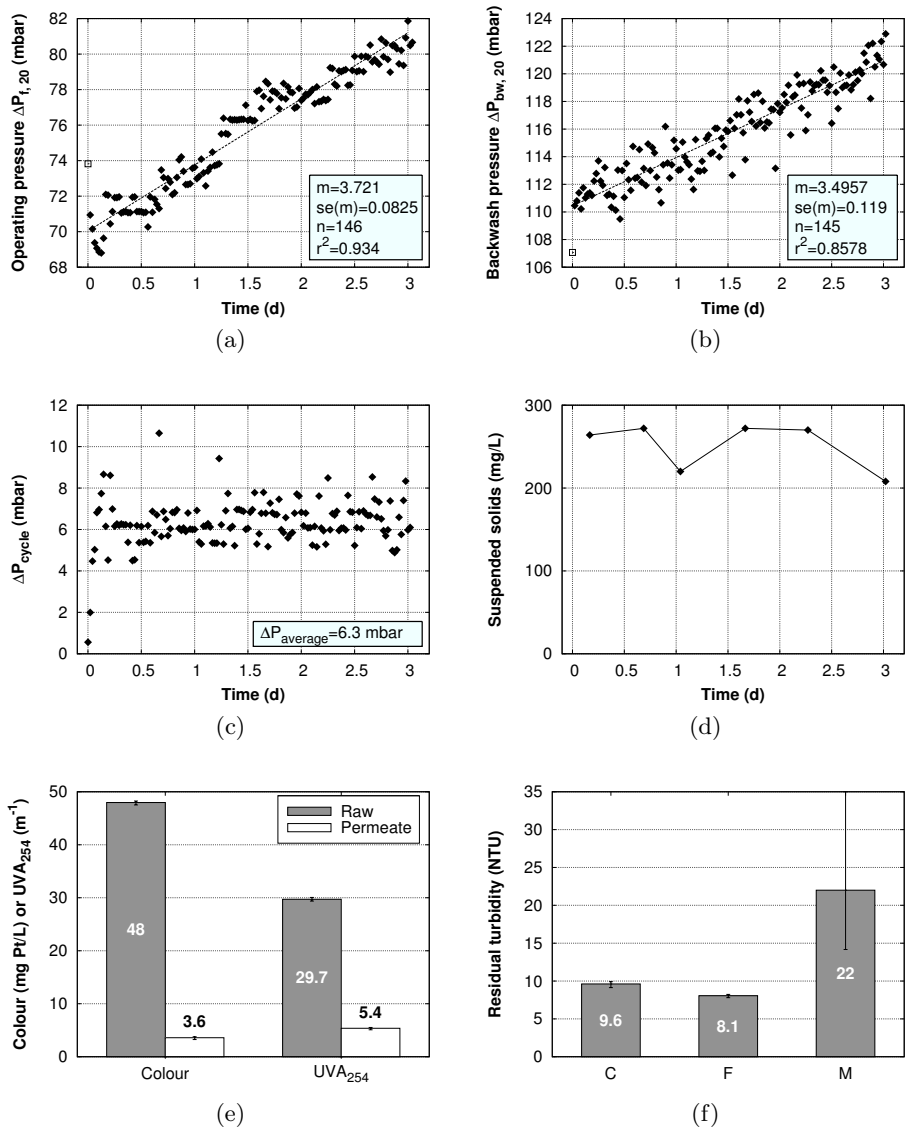

Figure P22: Overview of results for experiment P22

Experiment P23

Description

As P21, high flux.

Raw water

Colour	50 mg Pt/L
Average temperature	11.5℃

Pre-treatment

Coagulant	Polyaluminium chloride
Dosage	3 mg Al/L
Average coagulation pH	6.2
Flocculation	PBF

Membrane operating parameters

Filtration flux	J_f	75 L m^{-2} h^{-1}
Backwash flux	J_{bw}	105 L m^{-2} h^{-1}
Filtration cycle	t_f	29'30 min'sec
Backwash cycle	t_{bw}	00'30 min'sec
Water recovery	w	85%

Pressure increase rates obtained by regression

	Slope (mbar/d)		Intercept (mbar)	
	m	CI 95%	b	CI 95%
Filtration	3.10	± 0.20	94.54	± 0.37
Backwash	3.41	± 0.28	128.62	± 0.49

Comments

None.

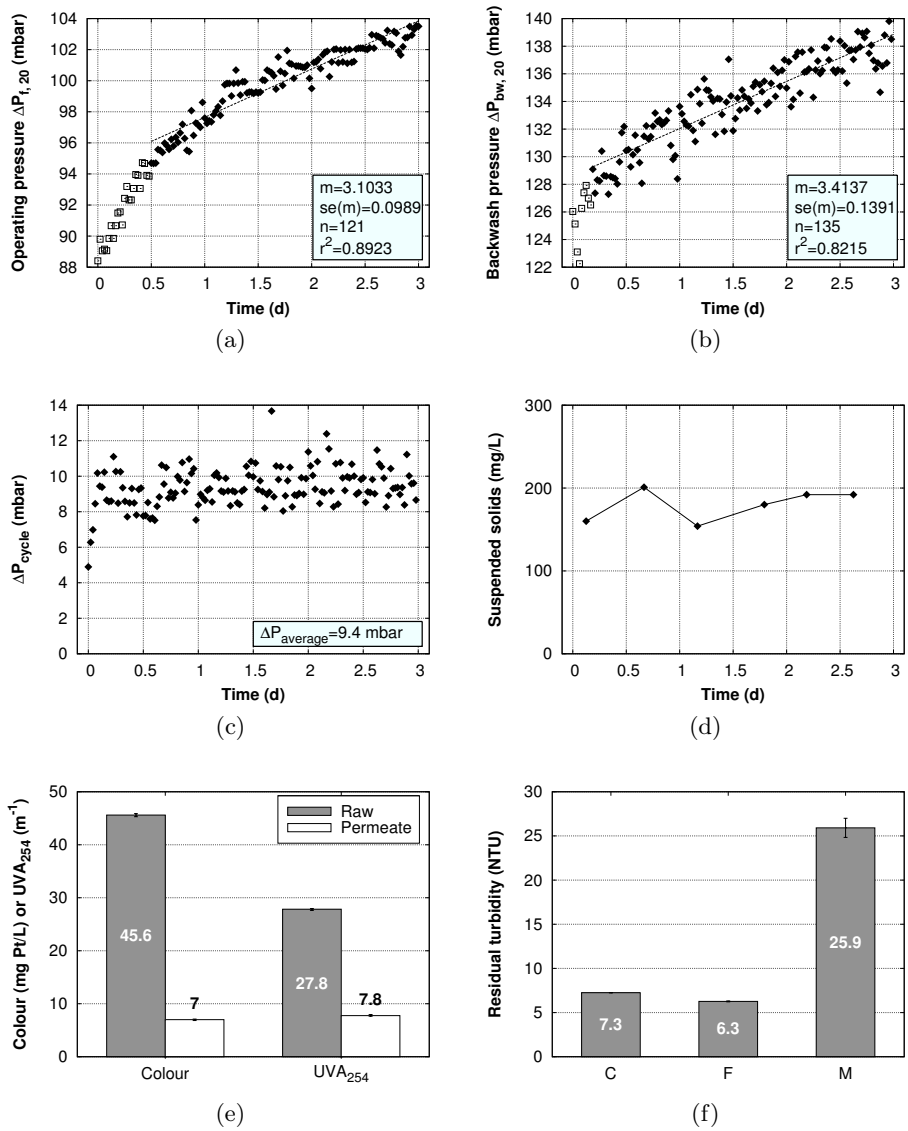

Figure P23: Overview of results for experiment P23

Experiment P24

Description

As P22, high flux.

Raw water

Colour	50 mg Pt/L
Average temperature	10.7℃

Pre-treatment

Coagulant	Polyaluminium chloride
Dosage	5 mg Al/L
Average coagulation pH	6.2
Flocculation	PBF

Membrane operating parameters

Filtration flux	J_f	75 L m^{-2} h^{-1}
Backwash flux	J_{bw}	105 L m^{-2} h^{-1}
Filtration cycle	t_f	29'30 min'sec
Backwash cycle	t_{bw}	00'30 min'sec
Water recovery	w	85%

Pressure increase rates obtained by regression

	Slope (mbar/d)		Intercept (mbar)	
	m	CI 95%	b	CI 95%
Filtration	3.88	± 0.16	90.67	± 0.29
Backwash	3.83	± 0.45	127.40	± 0.80

Comments

None.

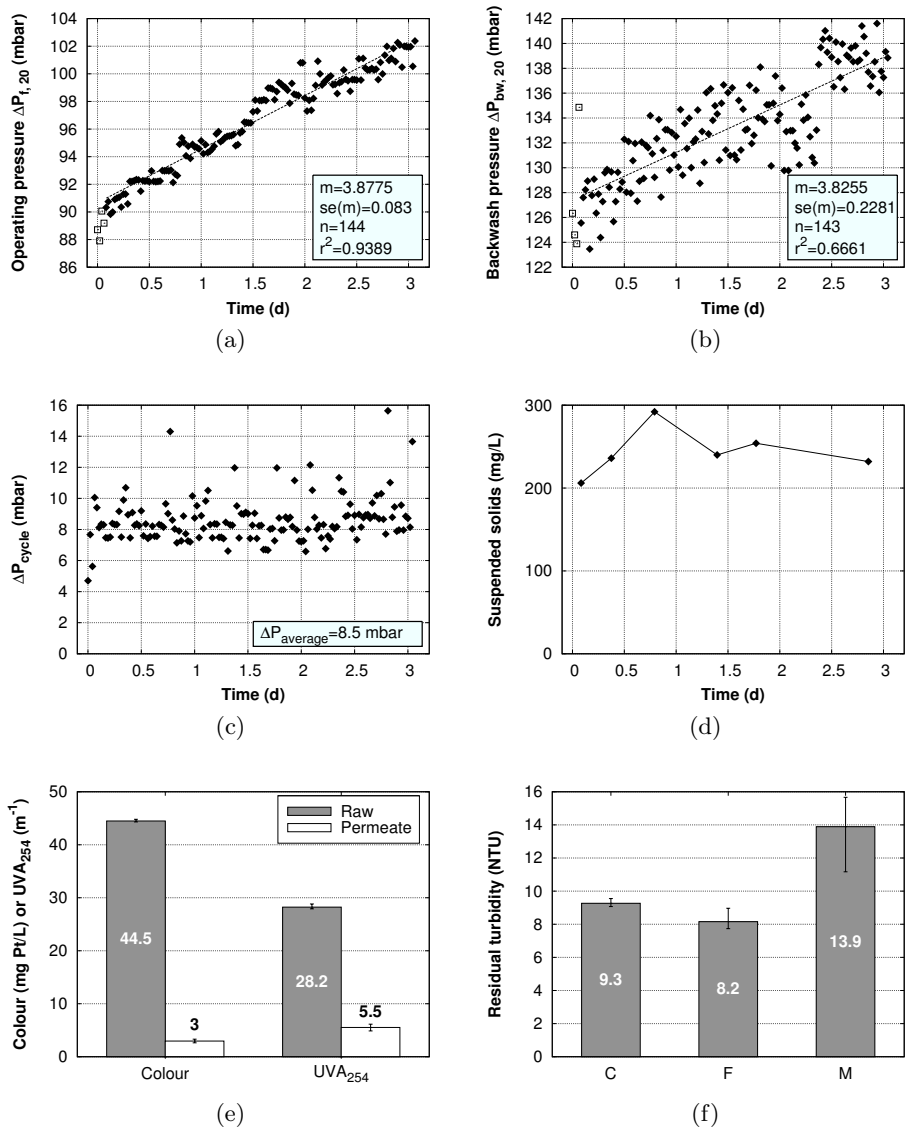

Figure P24: Overview of results for experiment P24

Experiment P25

Description

As P16, coagulation pH 7.

Raw water

Colour	50 mg Pt/L
Average temperature	10.5℃

Pre-treatment

Coagulant	Polyaluminium chloride
Dosage	3 mg Al/L
Average coagulation pH	7.0
Flocculation	PBF

Membrane operating parameters

Filtration flux	J_f	60 L m^{-2} h^{-1}
Backwash flux	J_{bw}	90 L m^{-2} h^{-1}
Filtration cycle	t_f	29'30 min'sec
Backwash cycle	t_{bw}	00'30 min'sec
Water recovery	w	95%

Pressure increase rates obtained by regression

	Slope (mbar/d)		Intercept (mbar)	
	m	CI 95%	b	CI 95%
Filtration	0.29	± 0.34	85.25	± 0.65
Backwash	2.31	± 0.41	122.04	± 0.76

Comments

None.

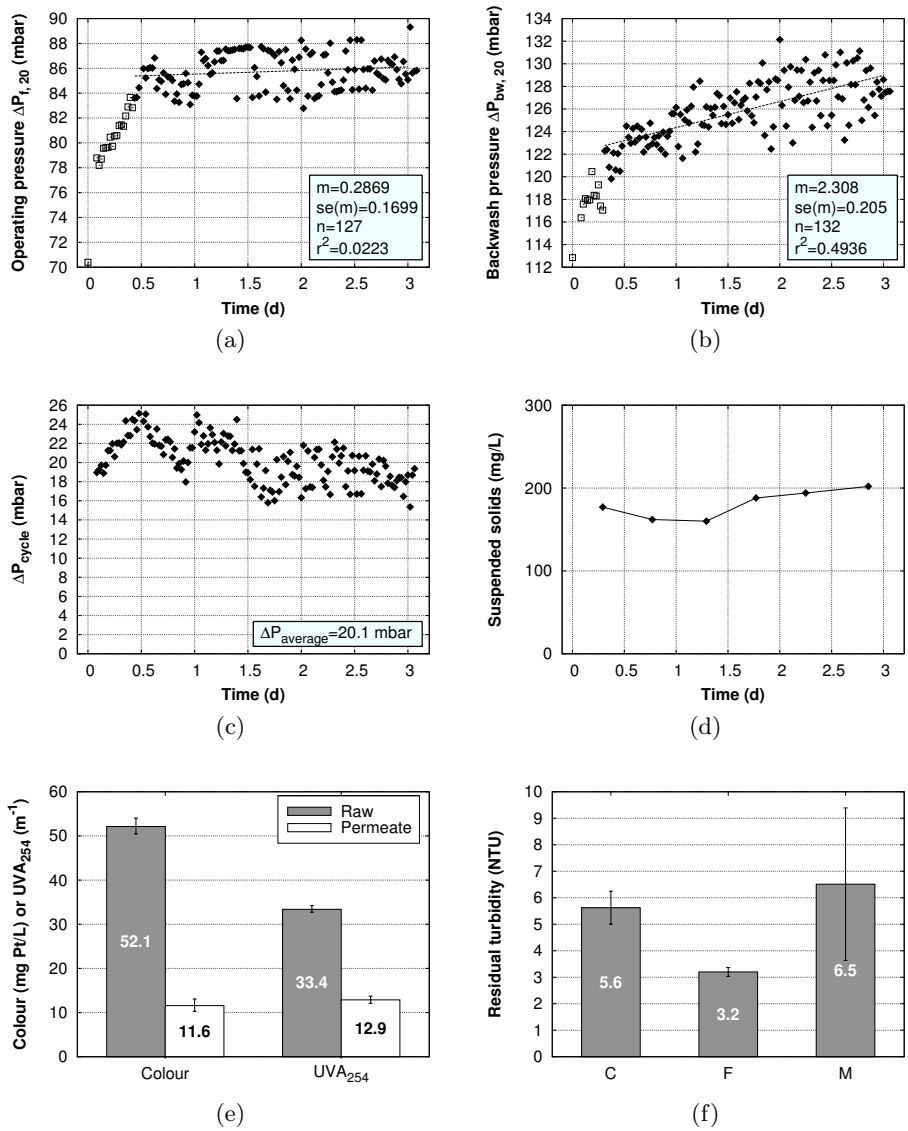

Figure P25: Overview of results for experiment P25

Experiment P26

Description

As P19, coagulation pH 7.

Raw water

Colour	50 mg Pt/L
Average temperature	9.6℃

Pre-treatment

Coagulant	Polyaluminium chloride
Dosage	5 mg Al/L
Average coagulation pH	7.0
Flocculation	PBF

Membrane operating parameters

Filtration flux	J_f	60 L m^{-2} h^{-1}
Backwash flux	J_{bw}	90 L m^{-2} h^{-1}
Filtration cycle	t_f	29'30 min'sec
Backwash cycle	t_{bw}	00'30 min'sec
Water recovery	w	95%

Pressure increase rates obtained by regression

	Slope (mbar/d)		Intercept (mbar)	
	m	CI 95%	b	CI 95%
Filtration	1.75	± 0.17	71.49	± 0.32
Backwash	2.76	± 0.35	109.17	± 0.66

Comments

None.

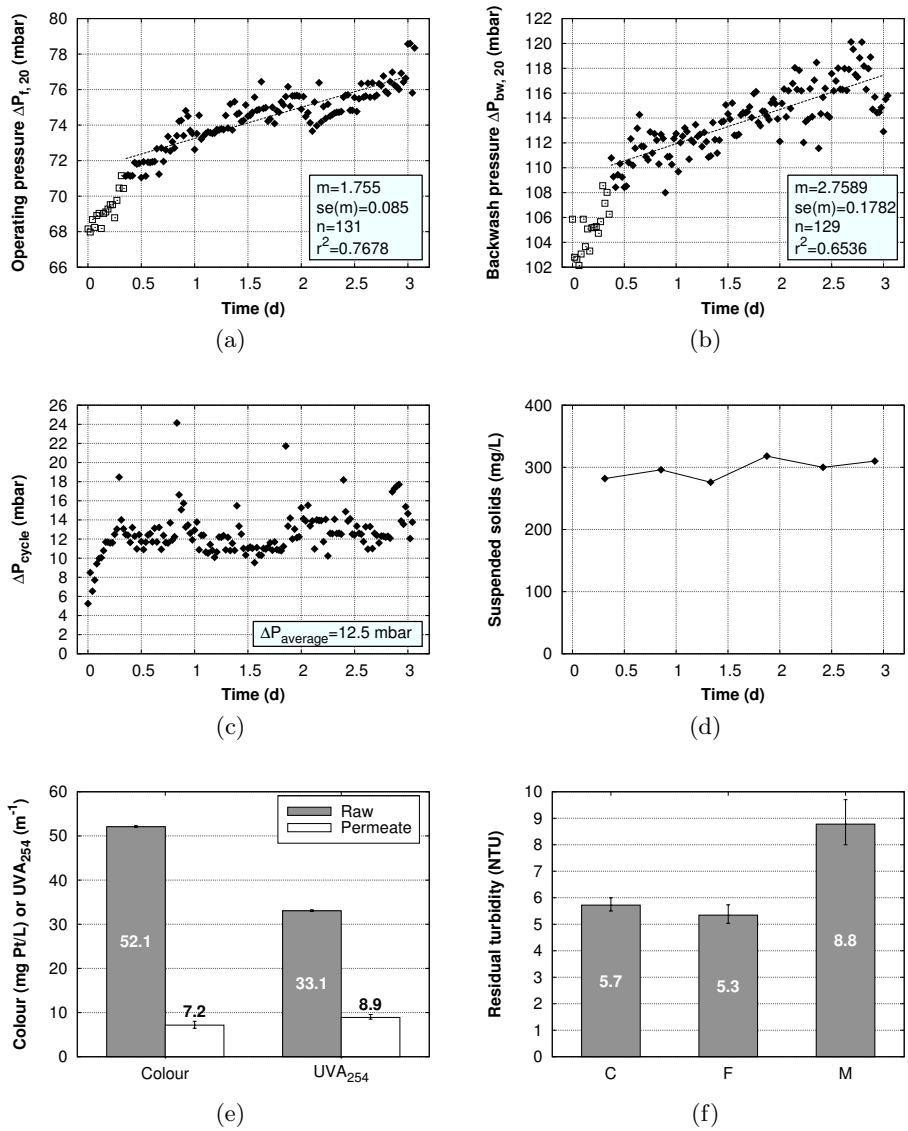

Figure P26: Overview of results for experiment P26

Experiment P27

Description

Reference values for reduced raw water colour.

Raw water

Colour	30 mg Pt/L
Average temperature	8.6℃

Pre-treatment

Coagulant	Polyaluminium chloride
Dosage	1.5 mg Al/L
Average coagulation pH	6.2
Flocculation	PBF

Membrane operating parameters

Filtration flux	J_f	60 L m^{-2} h^{-1}
Backwash flux	J_{bw}	90 L m^{-2} h^{-1}
Filtration cycle	t_f	29'30 min'sec
Backwash cycle	t_{bw}	00'30 min'sec
Water recovery	w	95%

Pressure increase rates obtained by regression

	Slope (mbar/d)		Intercept (mbar)	
	m	CI 95%	b	CI 95%
Filtration	3.04	± 0.11	70.40	± 0.19
Backwash	3.69	± 0.29	109.73	± 0.49

Comments

None.

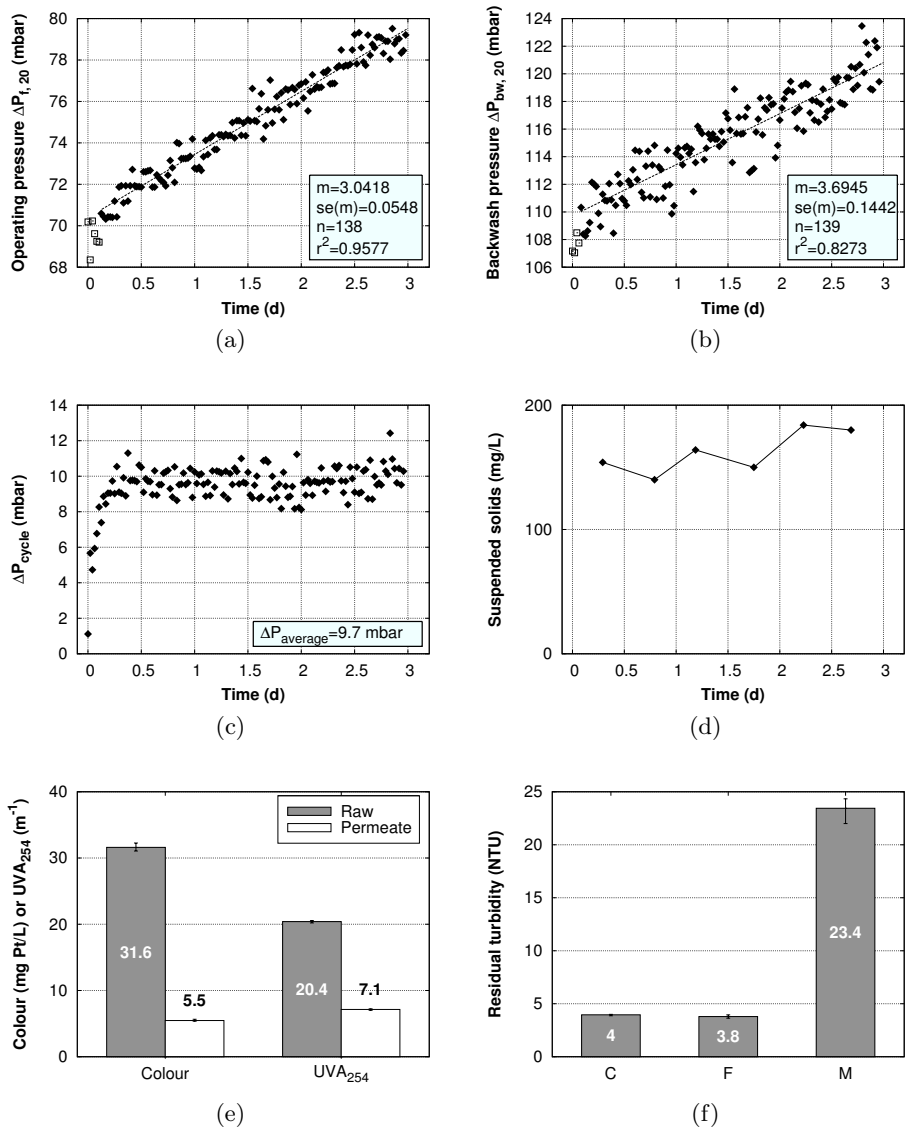

Figure P27: Overview of results for experiment P27

Experiment P28

Description

Reference values for reduced raw water colour.

Raw water

Colour	30 mg Pt/L
Average temperature	9.1℃

Pre-treatment

Coagulant	Polyaluminium chloride
Dosage	2 mg Al/L
Average coagulation pH	6.2
Flocculation	PBF

Membrane operating parameters

Filtration flux	J_f	60 L m^{-2} h^{-1}
Backwash flux	J_{bw}	90 L m^{-2} h^{-1}
Filtration cycle	t_f	29'30 min'sec
Backwash cycle	t_{bw}	00'30 min'sec
Water recovery	w	95%

Pressure increase rates obtained by regression

	Slope (mbar/d)		Intercept (mbar)	
	m	CI 95%	b	CI 95%
Filtration	2.37	± 0.10	70.98	± 0.20
Backwash	3.73	± 0.33	109.58	± 0.62

Comments

None.

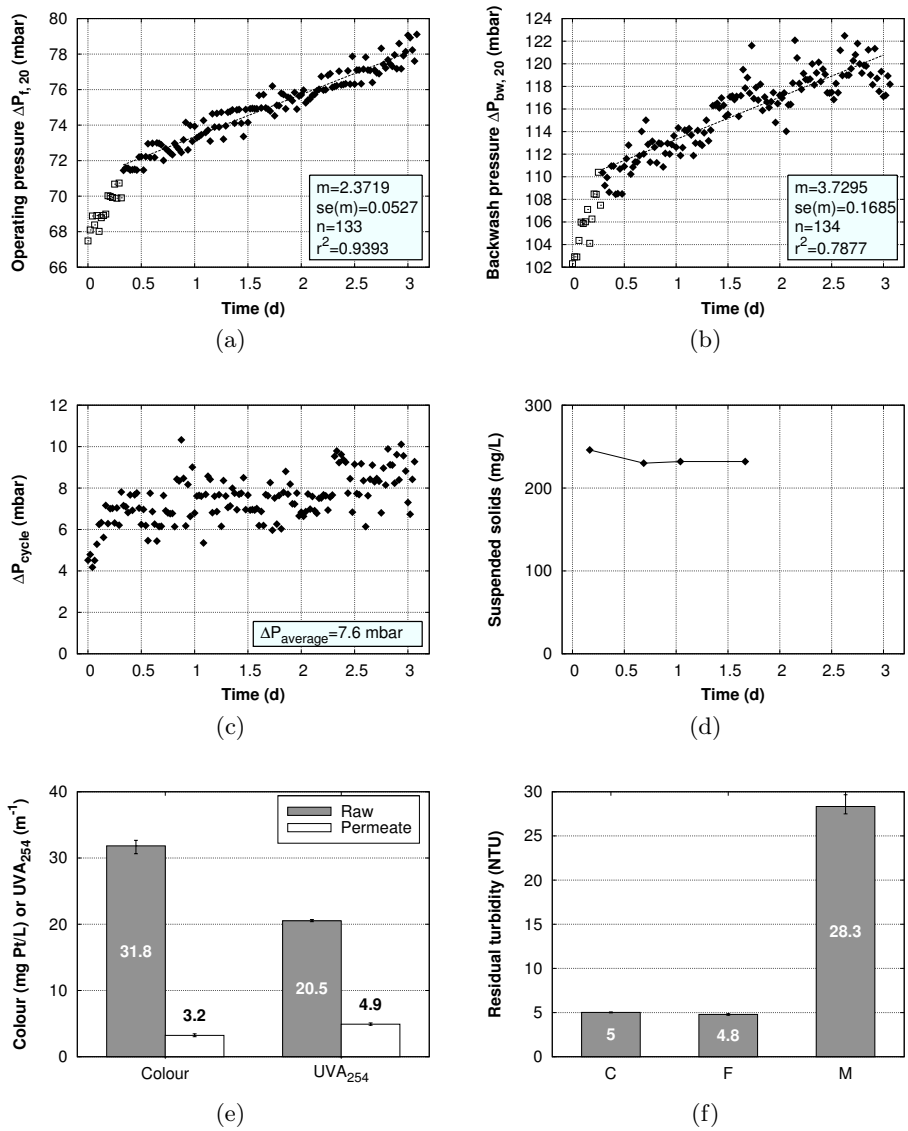

Figure P28: Overview of results for experiment P28

Appendix C

PLS modelling data

This chapter summarizes the background results from multivariate data analysis discussed in Chapter 6. Table C.7 presents the complete predictor matrix and the response vectors used for regression calculations. For each model, the modelling conditions and obtained regression coefficients are presented in tabular form. As explained in Chapter 6.4, the response Y is approximated by the function

$$Y = b_0 + \sum_i s_i \, b_{w,i} \, X_i$$

where b_0 is the intercept, s are the weighting factors, b_w the weighted regression coefficients, and X the predictor values. The quality of fit is given in terms of

- the explained Y-variance,
- the root-mean square error, and
- the predicted versus measured plot.

Two PLS models are presented for each of the pressure increase rates: the "general model" is based on all 9 predictors independent of their significance; the "revised model" is based on the significant predictors only.

C.1 Filtration pressure

Modelling conditions

Observations:	All (P01–P26)	
Predictor variables:	General model:	all
	Revised model:	PBF, Al-dosage, w, flux, $[H^+]$
Response variable:	m_f	
PLS components:	1	
Validation method:	Full cross validation	
Weighting:	Predictors:	all 1/SDev
	Response:	1.0 (no weighting)
Centering:	yes	

Table C.1: Explained Y-variance m_f and rms error

	General model	Revised model
All predictors	73%	81%
Flux and Al-dosage alone	53%	64%
Root-mean-square error	0.744	0.618

Table C.2: PLS regression coefficients for m_f

Predictor	Weighting factor s	General model b_w	Revised model b_w
PF	2.718	0.295	0
JMF1	2.718	0.34	0
JMF2	2.488	−0.157	0
PBF	1.967	−0.348	−0.512
Al-dosage	0.941	0.64	0.941
#BW	1.367	0.15	0
w	27.178	−0.156	−0.23
Flux	0.126	0.422	0.621
$[H^+]$	$6.54 \cdot 10^6$	0.217	0.32
Intercept b_0	–	−0.05	−0.401

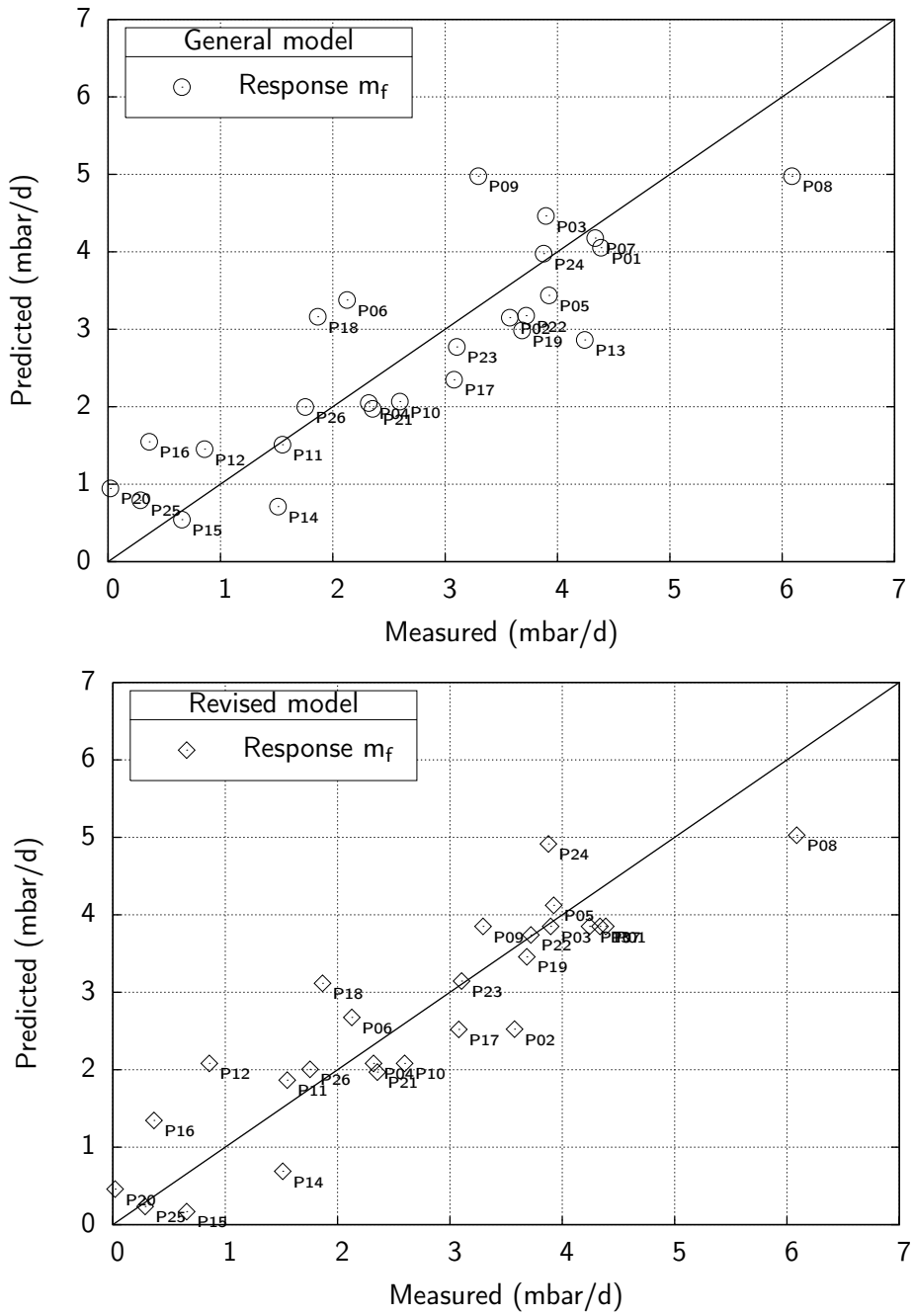

Figure C.1: Predicted versus measured plots for 2 PLS models approximating the filtration pressure increase rate m_f.

C.2 Backwash pressure

Modelling conditions

Observations:	All, except P17 and P20	
Predictor variables:	General model:	all
	Revised model:	PF, Al-dosage, w, flux, $[H^+]$
Response variable:	m_{bw}	
PLS components:	1	
Validation method:	Full cross validation	
Weighting:	Predictors:	all 1/SDev
	Response:	1.0
Centering:	yes	

Table C.3: Explained Y-variance m_{bw} and rms error

	General model	Revised model
All predictors	66%	72%
Flux and Al-dosage alone	57%	59%
Root-mean-square error	0.889	0.798

Table C.4: PLS regression coefficients for m_{bw}

Predictor	Weighting factor s	General model b_w	Revised model b_w
PF	2.627	0.387	0.52
JMF1	2.627	0.085	0
JMF2	2.411	−0.33	0
PBF	1.986	−0.118	0
Al-dosage	1.0	0.693	0.93
#BW	1.313	0.222	0
w	26.268	0.124	0.167
Flux	0.131	0.324	0.435
$[H^+]$	$6.412 \cdot 10^6$	0.262	0.352
Intercept b_0	–	−6.426	−9.251

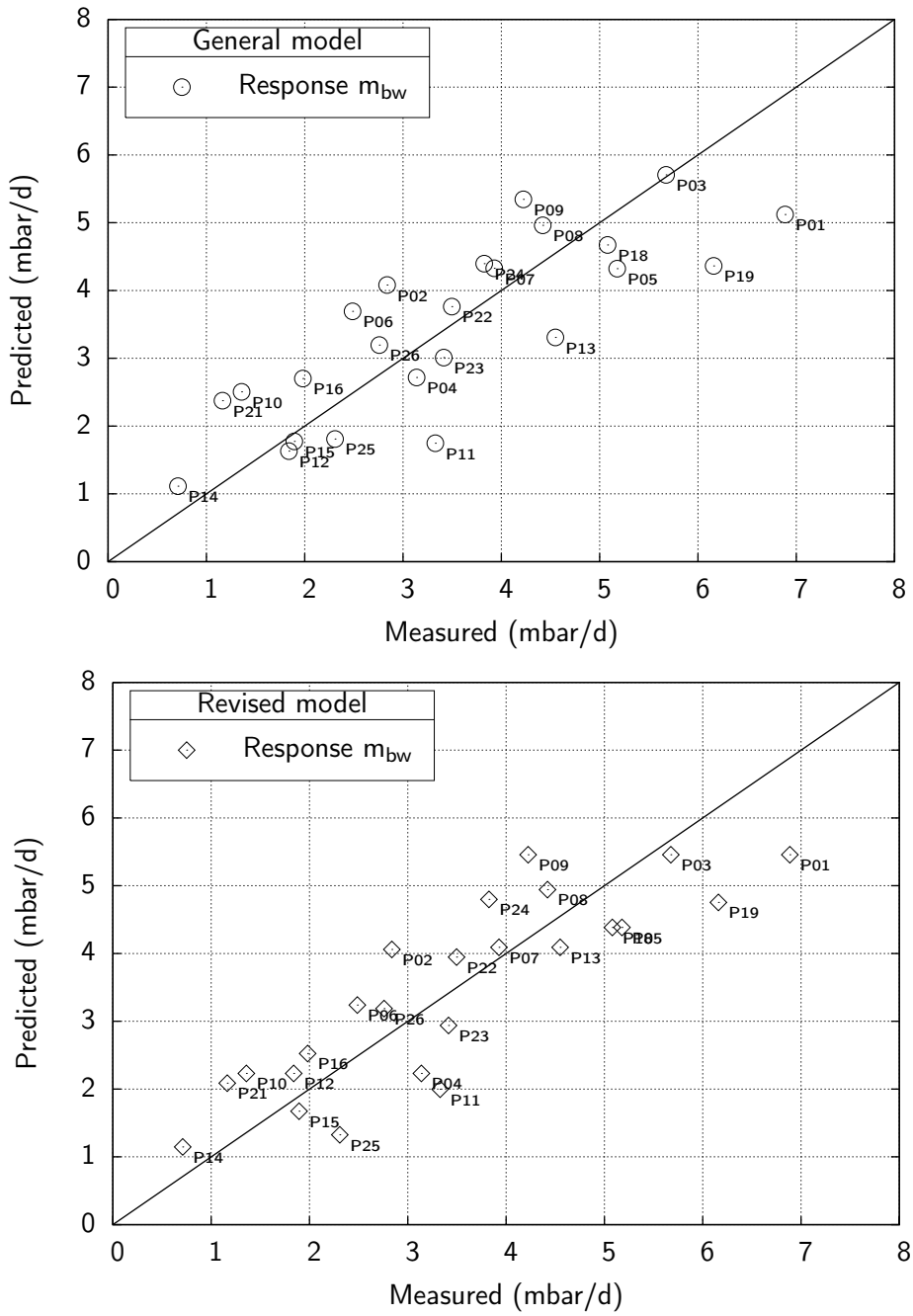

Figure C.2: Predicted versus measured plots for 2 PLS models approximating the backwash pressure increase rate m_{bw}

C.3 Pressure increase per filtration cycle

Observations:	All, except P12	
Predictor variables:	All, except flux	
Response variable:	$\Delta P_{cycle}/J$	
PLS components:	2	
Validation method:	Full cross validation	
Weighting:	Predictors:	all 1/SDev
	Response:	1.0
Centering:	yes	

Table C.5: Explained Y-variance $\Delta P_{cycle}/J$ and rms error

All predictors	84%
$[H^+]$, #BW, w, and Al-dosage alone	67%
Root-mean-square error	$1.806 \cdot 10^{-2}$

Table C.6: PLS regression coefficients for $\Delta P_{cycle}/J$

Predictor	Weighting factor s	Regression coefficient b_w
PF	2.673	$1.332 \cdot 10^{-2}$
JMF1	2.673	$-1.197 \cdot 10^{-2}$
JMF2	2.673	$-1.376 \cdot 10^{-2}$
PBF	1.961	$8.553 \cdot 10^{-3}$
Al-dosage	0.939	$-2.233 \cdot 10^{-2}$
#BW	1.414	$-2.345 \cdot 10^{-2}$
w	26.726	$2.233 \cdot 10^{-2}$
$[H^+]$	$6.411 \cdot 10^6$	$-2.758 \cdot 10^{-2}$
Intercept b_0	–	−0.143

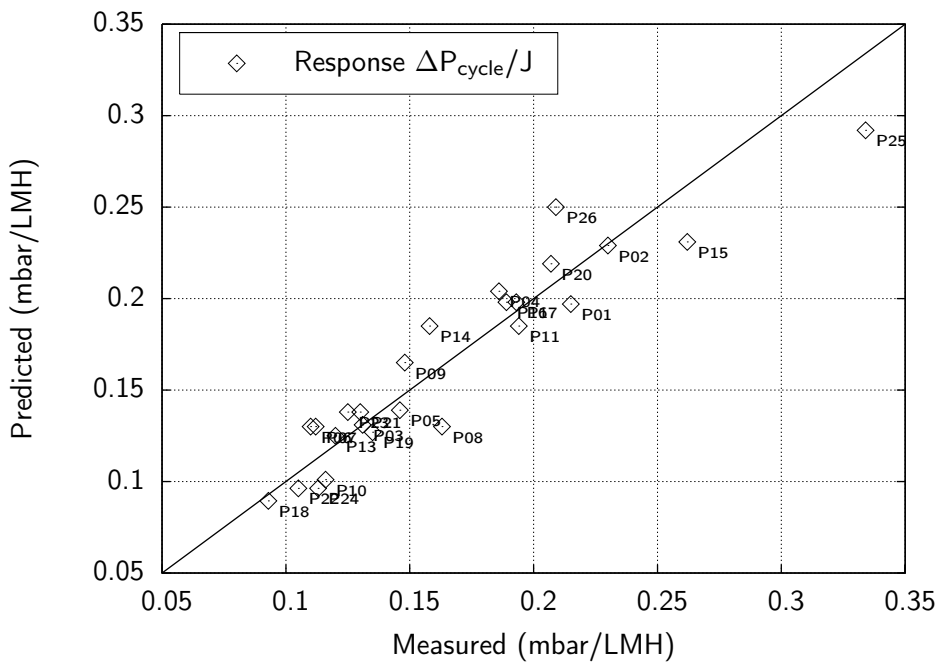

Figure C.3: Predicted versus measured plot for a PLS model approximating the response $\Delta P_{cycle}/J$.

Table C.7: Data matrix for multivariate analysis (i=26 observations, k=10 predictors)

Exp	*Predictor variables*									*Response variables*		
i	PF	JMF1	JMF2	PBF	Al-dosage	#BW[a]	w[b]	Flux	$[H^+]$ [c]	m_f	m_{bw}	$\Delta P_{cycle}/J$
P01	1	0	0	0	5.0	2	0.95	60	5.012	4.387	6.886	0.215
P02	1	0	0	0	3.5	2	0.95	60	5.012	3.575	2.838	0.230
P03	1	0	0	0	5.0	4	0.95	60	5.012	3.896	5.676	0.131
P04	0	0	0	0	3.0	2	0.95	60	5.012	2.320	3.134	0.186
P05	0	0	0	0	5.0	2	0.95	60	6.310	3.924	5.178	0.146
P06	0	1	0	0	5.0	2	0.95	45	5.012	2.127	2.487	0.110
P07	0	1	0	0	5.0	2	0.95	60	5.012	4.335	3.927	0.112
P08	0	1	0	0	5.0	2	0.95	75	5.012	6.086	4.421	0.163
P09	1	1	0	0	5.0	2	0.95	60	5.012	3.295	4.224	0.148
P10	0	0	1	0	3.0	4	0.95	60	5.012	2.597	1.358	0.116
P11	0	0	1	0	3.0	2	0.95	60	3.981	1.552	3.328	0.194
P12	0	0	1	0	3.0	1	0.95	60	5.012	0.858	1.839	–[d]
P13	0	0	1	0	5.0	2	0.95	60	5.012	4.243	4.550	0.120
P14	0	0	1	0	3.0	2	0.95	45	3.981	1.512	0.711	0.158
P15	0	0	0	1	3.0	1	0.95	45	6.310	0.657	1.894	0.262
P16	0	0	0	1	3.0	2	0.95	60	6.310	0.366	1.981	0.189

continued on next page

Table C.7: Data matrix for multivariate analysis (continued from previous page)

Exp	*Predictor variables*									*Response variables*		
i	PF	JMF1	JMF2	PBF	Al-dosage	#BW[a]	w[b]	Flux	$[H^+]$ [c]	m_f	m_{bw}	$\Delta P_{cycle}/J$
P17	0	0	0	1	3.0	2	0.95	75	6.310	3.079	–[d]	0.193
P18	0	0	0	1	5.0	4	0.95	60	6.310	1.866	5.081	0.093
P19	0	0	0	1	5.0	2	0.95	60	7.943	3.684	6.159	0.135
P20	0	0	0	1	2.0	2	0.95	60	6.310	0.021	–[d]	0.207
P21	0	0	0	1	3.0	2	0.85	60	6.310	2.354	1.164	0.130
P22	0	0	0	1	5.0	2	0.85	60	6.310	3.721	3.496	0.105
P23	0	0	0	1	3.0	2	0.85	75	6.310	3.103	3.414	0.125
P24	0	0	0	1	5.0	2	0.85	75	6.310	3.877	3.826	0.113
P25	0	0	0	1	3.0	2	0.95	60	1.000	0.287	2.308	0.334
P26	0	0	0	1	5.0	2	0.95	60	1.000	1.755	2.759	0.209

[a] Backwash frequency as number of backwashes per hour
[b] Water recovery
[c] $[H^+]=10^{-pH}$ instead of pH
[d] Removed outlier

Appendix D

Membrane specifications

Table D.1: Zenon ZW-10 specifications

Membrane/fibre		
Outside diameter	mm	2
General type	–	supported, hydrophilic
Nominal pore size	µm	0.04[a]
Module		
Effective membrane surface area	m^2	0.93
Module length	cm	69.2
Module diameter	cm	11
Active fibre length	cm	56
Approx. number of fibres	–	300
Hold-up volume	mL	130
System		
System Process Flow	L/d	400–2 000
Membrane configuration	–	integral immersed
Immersion tank volume[b]	L	20
Backpulse Tank Volume	L	15

[a] no pore larger than 0.1 µm
[b] custom-made

Table D.2: Zenon ZW-10 operating ranges

Max. permeation pressure	mbar	600
Operating transmembrane pressure	mbar	70–550
Permeate flow range	L/h	18–72
Typical permeate flow	L/h	42
Max. backpulse pressure	mbar	700
Max. scouring air flow rate	m^3/h	7.2
Max. operating Temperature	℃	40
Max. cleaning temperature	℃	40
Operating pH range	–	5–9
Cleaning pH range	–	2–10.5
Max. free chlorine exposure	ppm-hours	1 000 000
Max. free chlorine concentration	ppm	1 000
Max. feed suspended solids	mg/L	25 000

Appendix E

Photographs

(a) Top header (b) Bottom header

Figure E.1: Module headers with fibre bundle immersed in distilled water. Inclined plate settler visible in the bottom.

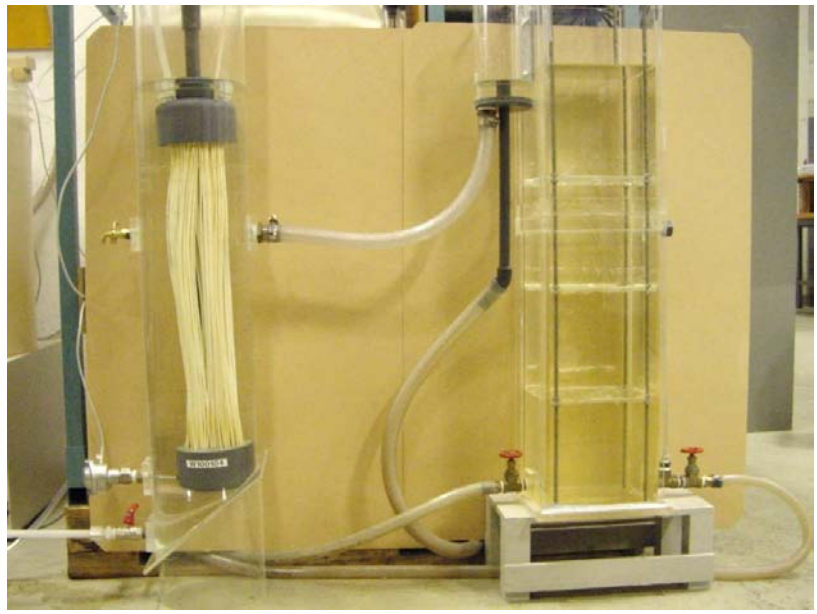

(a) Immersion tank and flocculator

(b) Coagulant dosing station and air blower (left)

Figure E.2: Views of the pilot plant.

Appendix F

Abstract in Norwegian

Sammendrag

Behandling av drikkevann med lavtrykk-hulfibermembraner blir stadig mer utbredt som erstatning for tradisjonell separasjonsteknologi. Forbehandling med koagulering kan redusere beleggdannelse på membraner og gjør det mulig å fjerne kolloider og oppløste stoffer mindre enn membranens porer. Integrering av membransystemer med koagulering kan derimot også redusere systemytelse dersom partikler med ugunstige egenskaper dannes. Dette blir særlig viktig ved koagulering av humusholdig vann fordi dannelse av humusaggregater avhenger i stor grad egenskapene av råvannet.

Hensikten med det eksperimentelle arbeidet var å finne optimale driftsbetingelser for koagulering, flokkulering og membranseparasjon for behandling av overflatevann med høy humusinnhold. Aluminiumbaserte koagulanter og kitosan ble brukt i forbehandlingen. Etter dosering av koagulant ble suspensjonen flokkulert i rør, jet-mix eller kompaktlagsflokkulator med kort oppholdstid. Partiklene ble separert med et ultrafiltreringssystem basert på polymeriske hulfibermembraner. Strømningsretningen gjennom hulfibrene var fra utsiden og inn.

Resultatene viser at optimalisering av koaguleringstrinnet er avgjørende for vellykket drift av membransystemet. En aluminiumdose på 3 mg Al/L og en koagulerings-pH i området 6–6.5 ga optimal behandling av vann med fargetall 50 mg Pt/L i forhold til permeatkvalitet, membrandrift og metallresidualer. Høyere koagulantdose eller lav koagulerings-pH førte til økt dannelse av belegg som ikke lot seg fjerne ved enkel tilbakevasking. Kitosan ga ikke tilfredsstil-

lende resultater med hensyn til permeatkvalitet og dannet et belegg som var vanskelig å fjerne.

Kontrollert flokkulering gir en redusert rate for trykkøkning i membranen dersom flokkuleringstrinnet dimensjoneres for lave G-verdier ($G<30\ s^{-1}$). Kompaktlagsflokkulatoren oppnådde bedre resultater enn de øvrige flokkulatorene. En flokkuleringstid lengre enn 5 minutter bør velges for å unngå at trykket for tilbakevasking øker raskere enn filtreringstrykket.

Membransystemet ble driftet med flukser mellom 45 og 75 LMH under filtrering, mens fluksen ble økt med 50% under tilbakevasking. Forsøkene viser at filtrering uten innbobling av luft i bunnen av membranen er mulig. Kraftig innbobling av luft ble imidlertid brukt under tilbakevasking for å forbedre løsrivelse av belegg. Gode resultater ble oppnådd med filtreringssykluser på 30–60 minutter etterfulgt av tilbakevasking i ca. 30 sekunder. Økende koagulantdose og fluks bidro sterkest til dannelse av ikke tilbakevaskbart belegg. Vannutbyttet over membranen påvirket trykkutviklingen av membranen i liten grad, men raskt uttak av slam fra membrantanken viste seg å være viktig. Ved behandling av råvann med lavere humuskonsentrasjon forble trykkutvikling i membranen tilnærmet uendret. Anvendelsespotensialet for koagulering etterfulgt av hulfiberfiltrering med utside–in membraner er derfor høyest for overflatevann med høyt innhold av naturorganisk materiale.

References

Anselme, C. and E. P. Jacobs (1996). Ultrafiltration. In: *Water Treatment Membrane Processes* (J. Mallevialle, P. E. Odendaal and M. R. Wiesner, eds.), pp. 10.1–10.88. McGraw-Hill, New York.

Aptel, P. and C. A. Buckley (1996). Categories of membrane operations. In: *Water Treatment Membrane Processes* (J. Mallevialle, P. E. Odendaal and M. R. Wiesner, eds.), pp. 2.1–2.24. McGraw-Hill, New York.

Baron, S. (1996). *Medical Microbiology (4th ed.)*. The University of Texas, Medical Branch, Galveston, TX, USA.

Belfort, G., R. H. Davis and A. L Zydney (1994). The behaviour of suspensions and macromolecular solutions in crossflow microfiltration. *J. Membr. Sci.* **96**(1–2), 1–58.

Bian, R., Y. Watanabe, N. Tambo and G. Ozawa (1999). Removal of humic substances by UF and NF membrane systems. *Water Sci. Technol.* **40**(9), 121–129.

Boerlage, S. F. E., M. D. Kennedy, M. R. Dickson, D. E. Y. El-Hodali and J. C. Schippers (2002). The modified fouling index using ultrafiltration membranes (MFI-UF): characterisation, filtration mechanisms and proposed reference membrane. *J. Membr. Sci.* **197**(1–2), 1–21.

Bolto, B. (1995). Soluble polymers in water purification. *Prog. Polym. Sci.* **20**(6), 987–1041.

Bolto, B. A., D. R. Dixon, R. J. Eldridge and S. J. King (1998). The use of cationic polymers as primary coagulants in water treatment. In: *Chemical Water and Wastewater Treatment V* (H. H. Hahn, E. Hoffmann and H. Ødegaard, eds.), pp. 173–185. Springer, Berlin.

Bolto, B., D. Dixon, R. Eldridge and S. King (2001). Cationic polymer and clay or metal oxide combinations for natural organic matter removal. *Water Res.* **35**(11), 2669–2676.

Broo, A. E., N. Berghult and T. Hedberg (1999). Copper corrosion in water distribution systems - the influence of natural organic matter (NOM) on the solubility of copper corrosion products. *Corros. Sci.* **40**(9), 1479–1489.

California Department of Health Services (2001). Alternative Filtration Technology Demonstration Report, ed. R.H. Sakaji, June 2001 Draft.

Camel, V. and A. Bermond (1998). The use of ozone and associated oxidation processes in drinking water treatment. *Water Res.* **32**(11), 3208–3222.

Camp, T. R. and P. C. Stein (1943). Velocity gradient and internal work in fluid motion. *J. Boston Soc. Civ. Engrs.* **30**(4), 219–237.

Carroll, T. and N. A. Booker (2000). Axial features in the fouling of hollow-fibre membranes. *J. Membr. Sci.* **168**(1–2), 203–212.

Carroll, T., S. King, S. R. Gray, B. A. Bolto and N. A. Booker (2000). The fouling of microfiltration membranes by NOM after coagulation treatment. *Water Res.* **34**(11), 2861–2868.

Chang, S., A. G. Fane and S. Vigneswaran (2002). Modeling and optimizing submerged hollow fiber membrane modules. *AIChE J.* **48**(10), 2203–2212.

Chang, S. and A. G. Fane (2000*a*). Characteristics of microfiltration of suspensions with inter-fiber two-phase flow. *J. Chem. Technol. Biotechnol.* **75**(7), 533–540.

Chang, S. and A. G. Fane (2000*b*). Filtration of biomass with axial inter-fibre upward slug flow: performance and mecanisms. *J. Membr. Sci.* **180**(1), 57–68.

Chang, S. and A. G. Fane (2001). The effect of fibre diameter on filtration and flux distribution – relevance to submerged hollow fibre modules. *J. Membr. Sci.* **184**(2), 221–231.

Chellam, S. and J. G. Jacangelo (1998). Existence of critical recovery and impacts of operational mode on potable water microfiltration. *J. Environ. Eng.-ASCE* **124**(12), 1211–1219.

Chen, V., A. G. Fane, S. S. Madaeni and I. G. Wenten (1997). Particle deposition during membrane filtration of colloids: transition between concentration polarization and cake formation. *J. Membr. Sci.* **125**(1), 109–122.

Cheryan, M. (1998). *Ultrafiltration and Microfiltration Handbook*. Technomic Publishing Company, Pennsylvania, USA.

Cho, J., G. Amy and J. Pellegrino (1999). Membrane filtration of natural organic matter: initial comparison of rejection and flux decline characteristics with ultrafiltration and nanofiltration membranes. *Water Res.* **33**(11), 2517–2526.

Choksuchart, P., M. Héran and A. Grasmick (2002). Ultrafiltration enhanced by coagulation in an immersed membrane system. *Desalination* **145**(1–3), 265–272.

Cornel, P. K., R. S. Summers and P. V. Roberts (1986). Diffusion of humic acid in dilute aqueous solutions. *J. Coll. Interf. Sci.* **110**(1), 149–164.

Côté, P., D. Mourato, C. Güngerich, J. Russel and E. Houghton (1998). Immersed membrane filtration for the production of drinking water: Case studies. *Desalination* **117**(1–3), 181–188.

Dirksen, J. A. and T. A. Ring (1990). Fundamentals of crystallization: Kinetic effects on particle size distributions and morphology. *Chem. Eng. Sci.* **46**(10), 2389–2427.

Duan, J. and J. Gregory (2003). Coagulation by hydrolysing metal salts. *Adv. Coll. Interf. Sci.* **100–102**, 475–502.

Edzwald, J. K. and J. E. Tobiason (1999). Enhanced coagulation: US requirements and a broader view. *Water Sci. Technol.* **40**(9), 63–70.

Egeberg, P. K., A. A. Christy and M. Eikenes (2002). The molecular size of natural organic matter (NOM) determined by diffusivimetry and seven other methods. *Water Res.* **36**(4), 925–932.

Eikebrokk, B. (1999). Coagulation-direct filtration of soft, low alkalinity humic waters. *Water Sci. Technol.* **40**(9), 55–62.

Emelko, M. B., P. M Huck and Douglas I. P. (2003). *Cryptosporidium* and microsphere removal during late in-cycle filtration. *J. Am. Water Works Assoc.* **95**(5), 173–182.

Engebretson, R. R. and R. von Wandruszka (1994). Microorganization in dissolved humic acids. *Environ. Sci. Technol.* **28**(11), 1934–1941.

Fan, L., J. L. Harris, F. A. Roddick and N. A. Booker (2004). Influence of the characteristics of natural organic matter on the fouling of microfiltration membranes. *Water Res.* **35**(18), 4455–4463.

Farahbakhsh, K., S. S. Adham and Smith D. W. (2003). Monitoring the integrity of low-pressure membranes. *J. Am. Water Works Assoc.* **95**(6), 95–107.

Fettig, J. (1999). Removal of humic substances by adsorption/ion exchange. *Water Sci. Technol.* **40**(9), 173–182.

Field, R. W., D. Wu, J. A. Howell and B. B. Gupta (1995). Critical flux concept for microfiltration fouling. *J. Membr. Sci.* **100**(3), 259–272.

Fiksdal, L. and T. Leiknes (2004). The effect of coagulation with MF/UF membrane filtration for the removal of virus in drinking water. *J. Membr. Sci.* **279**(1–2), 364–371.

Gallard, H. and U. von Gunten (2002). Chlorination of natural organic matter: kinetics of chlorination and of THM formation. *Water Res.* **36**(1), 65–74.

Gerba, C. P., N. Nwachuku and K. R. Riley (2003). Disinfection resistance of waterborne pathogens on the United States Environmental Protection Agency's Contaminant Candidate List (CCL). *J. Water Supply Res. Technol.-AQUA* **52**(2), 81–94.

Ghosh, K. and M. Schnitzer (1980). Macromolecular structures of humic substances. *Soil Sci.* **129**(5), 266–276.

Gregor, J. E., C. J. Nokes and Fenton E. (1997). Optimising natural organic matter removal from low turbidity waters by controlled pH adjustment of aluminium coagulation. *Water Res.* **31**(12), 2949–2958.

Gregory, J. and V. Dupont (2001). Properties of flocs produced by water treatment coagulants. *Water Sci. Technol.* **44**(10), 231–236.

Grohmann, A. (1985). Flocculation in pipes: design and operation. In: *Chemical Water and Wastewater Treatment* (A. Grohmann, H. H. Hahn and R. Klute, eds.), pp. 113–131. Gustav Fischer Verlag, Stuttgart, Germany.

Han, M. Y. and D. F. Lawler (1992). The (relative) insignificance of G in flocculation. *J. Am. Water Works Assoc.* **84**(10), 79–91.

Heinicke, G., T. Hedberg and M. Hermansson (2000). Biological pre-treatment for improved removal of manganese. In: *Chemical Water and Wastewater Treatment VI* (H. H. Hahn, E. Hoffmann and H. Ødegaard, eds.), pp. 201–210. Springer, Berlin.

Hem, L. J. and H. Efraimsen (2001). Assimilable organic carbon in molecular weight fractions of natural organic matter. *Water Res.* **35**(4), 1106–1110.

Herath, G., K. Yamamoto and T. Urase (1999). Removal of viruses by microfiltration membranes at different solution environments. *Water Sci. Technol.* **40**(4–5), 331–338.

Hillis, P. (2006). Enhanced coagulation, flocculation and immersed ultrafiltration for treatment of low alkalinity and highly coloured upland water. *J. Water Supply Res. Technol.-AQUA* **55**(7–8), 549–558.

Hiraide, M. (1992). Heavy-metals complexed with humic substances in fresh water. *Anal. Sci.* **8**(4), 453–459.

Hong, S. and M. Elimelech (1997). Chemical and physical aspects of natural organic matter (NOM) fouling of nanofiltration membranes. *J. Membr. Sci.* **132**(2–3), 159–181.

Hongve, D. and G. Akesson (1996). Spectrophotometric determination of water colour in Hazen units. *Water Res.* **30**(11), 2771–2775.

Hou, K., C. P. Gerba, S. M. Goyal and K. S. Zerda (1980). Capture of latex beads, bacteria, endotoxin, and viruses by charge-modified filters. *App. Environ. Microbiol.* **40**, 892–896.

Howe, K. and M. M. Clark (2002). *Coagulation pretreatment for membrane filtration*. AWWA and AWWA Research Foundation, Denver CO, USA.

Howell, J. A. (1995). Sub-critical flux operation of microfiltration. *J. Membr. Sci.* **107**(1–2), 165–171.

Irving, T. E., J. de Louvois and Nichols G. L. (1996). Fact sheets on emerging waterborne pathogens: Final report to the Department of the Environment. AWWA Research Foundation Report No: DWI 4248/1.

Jacangelo, J. G., S. S. Adham and J. M. Laîné (1995). Mechanism of *Cryptosporidium*, *Giardia*, and MS2 virus removal by MF and UF. *J. Am. Water Works Assoc.* **87**(9), 107–121.

Jack, A. M. and M. M. Clark (1998). Using PAC–UF to treat a low-quality surface water. *J. Am. Water Works Assoc.* **90**(11), 83–95.

Jang, N. Y., Y. Watanabe and S. Minegishi (2005). Performance of ultrafiltration membrane process combined with coagulaton/sedimentation. *Water Sci. Technol.* **51**(6–7), 209–219.

Jensen, J. N. (2001). Approach to steady state in completely mixed flow reactors. *J. Environ. Eng.-ASCE* **127**(1), 13–13.

Jones, K. L. and C. R. O'Melia (2001). Ultrafiltration of protein and humic substances: effect of solution chemistry on fouling and flux decline. *J. Membr. Sci.* **193**(2), 163–173.

Jucker, C. and M. M. Clark (1994). Adsorption of aquatic humic substances on hydrophobic ultrafiltration membranes. *J. Membr. Sci.* **97**(1), 37–52.

Judd, S. (2002). Submerged membrane bioreactors: flat plate or hollow fibre? *Filtr. Sep.* **39**(5), 30–31.

Judd, S. J. and P. Hillis (2001). Optimisation of combined coagulation and microfiltration for water treatment. *Water Res.* **35**(12), 2895–2904.

Kam, S.-K. and J. Gregory (2001). The interaction of humic substances with cationic polyelectrolytes. *Water Res.* **35**(15), 3557–3566.

Karimi, A. A., J. C. Vickers and R. F. Harasick (1999). Microfiltration goes Hollywood: the Los Angeles experience. *J. Am. Water Works Assoc.* **91**(6), 90–103.

Kawamura, S. (1991). Effectiveness of natural polyelectrolytes in water treatment. *J. Am. Water Works Assoc.* **83**(10), 88–91.

Kawamura, S. (2000). Initial (flash) mixing by water jet diffusion. *J. Water Supply Res. Technol.-AQUA* **49**(6), 307–319.

van der Kooij, D., J. S. Vrouwenvelder and H. R. Veenendaal (2003). Elucidation and control of biofilm formation processes in water treatment and distribution using the unified biofilm approach. *Water Sci. Technol.* **47**(5), 83–90.

Korpijärvi, J., E. Laine and H. Ahlsted (2000). Using CFD in the study of mixing in coagulation and flocculation. In: *Chemical Water and Wastewater Treatment VI* (H. H. Hahn, E. Hoffmann and H. Ødegaard, eds.), pp. 89–99. Springer, Berlin.

Krogh, T. and T. Hofshagen (1998). Hygieniske barrierer (in Norwegian). *Norsk Veterinærtidsskrift* **110**(10), 578–584.

Kvinnesland, T. (2003). Coagulation and flocculation of dissolved organic substances with organic polymers. PhD thesis, Norwegian University of Science and Technology, Department of Hydraulic and Environmental Engineering.

Kwon, D. Y., S. Vigneswaran, A. G. Fane and R. Ben Aïm (2000). Experimental determination of critical flux in cross-flow microfiltration. *Sep. Purif. Technol.* **19**(3), 157–242.

Lahoussine-Turcaud, V., M. R. Wiesner, J. Y. Bottero and J. Mallevialle (1990). Coagulation pretreatment for ultrafiltration of a surface water. *J. Am. Water Works Assoc.* **82**(12), 76–81.

Laîné, J. M., J. P. Hagstrom, M. M. Clark and J. Mallevialle (1989). Effects of ultrafiltration membrane composition. *J. Am. Water Works Assoc.* **81**(11), 61–67.

Le Clech, P., B. Jefferson, I. S. Chang and S. J. Judd (2003). Critical flux determination by the flux-step method in a submerged membrane bioreactor. *J. Membr. Sci.* **227**(1–2), 81–93.

Lee, J.-D., S.-H. Lee, M.-H. Jo, Park P.-K., Lee C.-H. and Kwak J.-W. (2000). Effect of coagulation conditions on membrane filtration characteristics in coagulation-microfiltration process for water treatment. *Environ. Sci. Technol.* **34**(17), 3780–3788.

Lee, N., G. Amy, J.-P. Croué and H. Buisson (2004). Identification and understanding of fouling in low-pressure membrane (MF/UF) filtration by natural organic matter (NOM). *Water Res.* **38**(20), 4511–4523.

Leenheer, J. A. (1994). Chemistry of dissolved organic matter in rivers, lakes, and reservoirs. *Adv. Chem. Ser.* **237**, 195–221.

Lerch, A., S. Panglisch and R. Gimbel (2005). Research experiences in direct potable water treatment using coagulation/ultrafiltration. *Water Sci. Technol.* **51**(6–7), 221–229.

Lin, C. F., T. Y. Lin and O. J. Hao (2000). Effects of humic substance characteristics on UF performance. *Water Res.* **34**(4), 1097–1106.

Logan, B. E. and Q. Jiang (1991). Molecular size distributions of dissolved organic matter. *J. Environ. Eng.-ASCE* **116**(6), 1046–1062.

Maartens, A., P. Swart and E. P. Jacobs (1999). Feed-water pretreatment: methods to reduce membrane fouling by natural organic matter. *J. Membr. Sci.* **163**(1), 51–62.

Madaeni, S. S., A. G. Fane and G. S. Grohmann (1995). Virus removal from water and wastewater using membranes. *J. Membr. Sci.* **102**, 65–75.

Malmrose, P. (2003). Committee report: Residuals management for low-pressure membranes. *J. Am. Water Works Assoc.* **95**(6), 68–82.

Marshall, A. D., P. A. Munrob and G. Trägårdh (1993). The effect of protein fouling in microfiltration and ultrafiltration on permeate flux, protein retention and selectivity: A literature review. *Desalination* **91**(1), 65–108.

Martens, H. and T. Næs (1989). *Multivariate Calibration*. John Wiley & Sons, New York.

Matsushita, T., Y. Matsui, N. Shirasaki and Y. Kato (2005). Effect of membrane pore size, coagulation time, and coagulant dose on virus removal by a coagulation-ceramic microfiltration hybrid system. *Desalination* **178**(1–3), 21–26.

Meier-Haack, J., N. A. Booker and T. Carroll (2003). A permeability-controlled microfiltration membrane for reduced fouling in drinking water treatment. *Water Res.* **37**(3), 585–588.

Metsämuuronen, S., J. Howell and M. Nyström (2002). Critical flux in ultrafiltration of myoglobin and baker's yeast. *J. Membr. Sci.* **196**(1), 13–25.

Morris, R. D., A. M. Audet, I. F. Angelillo, T. C. Chalmers and F. Mosteller (1992). Chlorination, chlorination by-products, and cancer: a meta-analysis. *J. Am. Public Health* **82**(7), 955–963.

Mulder, M. (1998). *Basic Principles of Membrane Technology (2nd ed.)*. Kluwer Academic Publishers, Dordrecht.

Norwegian Ministry of Health and Care Services (2001). Forskrift om vannforsyning og drikkevann (Drikkevannsforskriften). FOR-2001-12-04-1372, effective date 2002-01-01.

Österberg, R., I. Lindqvist and K. Mortensen (1993). Particle size of humic acid. *Soil Sci. Soc. Am. J.* **57**(1), 283–285.

Peuchot, M. M. and R. Ben Aïm (1992). Improvement of crossflow microfiltration performances with flocculation. *J. Membr. Sci.* **68**(3), 241–248.

Pikkarainen, A. T., S. J. Judd, J. Jokela and L. Gillberg (2004). Precoagulation for microfiltration of an upland surface water. *Water Res.* **38**(2), 455–465.

Ratnaweera, H., E. Gjessing and E. Oug (1999). Influence of physical-chemical characteristics of natural organic matter (NOM) on coagulation properties: An analysis of eight norwegian water sources. *Water Sci. Technol.* **40**(9), 89–95.

Rautenbach, R. and R. Albrecht (1989). *Membrane Processes*. John Wiley & Sons, New York.

Ridgway, H. F. and H. C. Flemming (1996). Membrane biofouling. In: *Water Treatment Membrane Processes* (J. Mallevialle, P. E. Odendaal and M. R. Wiesner, eds.), pp. 6.1–6.62. McGraw-Hill, New York.

Saltnes, T., H. Ødegaard and B. Eikebrokk (2001). Metal residuals in drinking water (in Norwegian). *Vann* **36**(3), 253–258.

Schäfer, A. I., A. G. Fane and T. D. Waite (2001). Cost factors and chemical pretreatment effects in the membrane filtration of waters containing natural organic matter. *Water Res.* **35**(6), 1509–1517.

Schäfer, A. I., U. Schwicker, M. M. Fischer, A. G. Fane and T. D. Waite (2000). Microfiltration of colloids and natural organic matter. *J. Membr. Sci.* **171**(2), 151–172.

Schoenen, D. (2002). Role of disinfection in suppressing the spread of pathogens with drinking water: possibilities and limitations. *Water Res.* **36**(15), 3874–3888.

Shaw, P. J., H. de Haan and R. I. Jones (1994). Applicability and reliability of gel-filtration to study aquatic humic substances revisited - the effects of pH on molecular size distributions. *Environ. Int.* **15**(8), 753–764.

Shen, Y.-H. and B. A. Dempsey (1998). Synthesis and speciation of polyaluminum chloride for water treatment. *Environ. Int.* **24**(8), 899–910.

Singer, P. C. (1999). Humic substances as precursors for potentially harmful disinfection by-products. *Water Sci. Technol.* **40**(9), 25–30.

Sobrinho, J. A. H., L. T. Thiem and E. A. Alkhatib (1996). Optimizing submerged jet flocculator performance. *J. Am. Water Works Assoc.* **88**(8), 81–92.

Stevenson, F. J. (1994). *Humus Chemistry. Genesis, Composition, Reactions.* 2nd ed.. John Wiley & Sons, New York.

Strand, T., B. Lind and G. Thommesen (1998). Naturlig radioaktivitet i husholdningsvann fra borebrønner i Norge (in Norwegian). *Norsk Veterinærtidsskrift* **110**(10), 662–665.

Suchecka, T., W. Pieatkiewicz and T. R. Sosnowski (2005). Is the cell retention by MF membrane absolutely safe–a hypothetical model for cell deformation in a membrane pore. *J. Membr. Sci.* **250**(1–2), 135–140.

Sundaramoorthy, K., A. Brügger, S. Panglisch, A. Lerch and R. Gimbel (2005). Studies on the minimisation of NOM fouling of MF/UF membranes with the help of a submerged "single" capillary membrane apparatus. *Desalination* **179**(1–3), 355–367.

Tarabara, V. V., R. M. Hovinga and M. R. Wiesner (2002). Constant transmembrane pressure vs. constant permeate flux: Effect of particle size on crossflow membrane filtration. *Environ. Eng. Sci.* **19**(6), 343–355.

Taylor, J. S. and R. R. Wiesner (1999). Membranes. In: *Water Quality & Treatment* (R. D. Letterman, ed.), fifth edition, pp. 11.1–11.71. McGraw-Hill, New York.

Theron, J. and T. E. Cloete (2002). Emerging waterborne infections: contributing factors, agents, and detection tools. *Crit. Rev. Microbiol.* **28**(1), 1–26.

Thomas, D. N., S. J Judd and N. Fawcett (1999). Flocculation modelling: a review. *Water Res.* **33**(7), 1579–1592.

Thorsen, T. (1999). Fundamental studies on membrane filtration of coloured surface water. PhD thesis, Norwegian University of Science and Technology, Department of Hydraulic and Environmental Engineering.

Thurman, E. M. (1985). *Organic Geochemistry of Natural Waters.* Nijhoff/Jank Publishers, Dordrecht, The Netherlands.

Tiller, C. L. and C. R. O'Melia (1993). Natural organic matter and colloidal stability: models and measurements. *Colloids Surf. A* **73**, 89–102.

Urase, T., K. Yamamoto and S. Ohgaki (1996). Effect of pore structure of membranes and module configuration on virus retention. *J. Membr. Sci.* **115**(1), 21–29.

US EPA (1998). National primary drinking water regulations: disinfectants and disinfection by-products; final rule. *Federal Register* **63**(241), 69390–69476.

US EPA (2005). Membrane Filtration Guidance Manual. Office of Water, EPA 815-R-06-009 November 2005. United States Environmental Protection Agency.

Van Benschoten, J. E. and J. K. Edzwald (1990*a*). Chemical aspects of coagulation using aluminum salts: I. Hydrolytic reactions of alum and polyaluminum chloride. *Water Res.* **24**(12), 1519–1526.

Van Benschoten, J. E. and J. K. Edzwald (1990*b*). Chemical aspects of coagulation using aluminum salts: II. Coagulation of fulvic acid using alum and polyaluminum chloride. *Water Res.* **24**(12), 1527–1535.

Veerapaneni, S., D. Brejchová, D.C. Schmelling, F. F. Nazzal and M. R. Wiesner (1992). Pilot evaluation of ceramic membranes in surface water treatment with coagulation pretreatment. *Water Sci. Technol.* **26**(9–11), 2285–2288.

Vogelsang, C. (2001). Precipitation of humic substances with chitosan - use of zeta potential to study coagulation mechanisms (in Norwegian). *Vann* **36**(4), 308–318.

Voßenkaul, K. and S. Schäfer (2002). Development of a new capillary module for water production and wastewater treatment. In: *Proc. IWA, AWWA, JWWA, EDS 5th Conference on Membranes in Drinking and Industrial Water Production (MDIW), Mühlheim (Ruhr), Germany, 22–26 September 2002.*

Watanabe, Y. and H. Yonekawa (2007). Flocculation and its role in membrane filtration process including the fractal approach in floc structure. In: *Proc. IWA International Conference on Particle Separation, Toulouse, France, 9–12 July 2007.*

Watanabe, Y., S. Kasahara and Y. Iwasaki (1998). Enhanced flocculation/sedimentation process by a jet mixed separator. *Water Sci. Technol.* **37**(10), 55–67.

Wetterau, G. E., M. M. Clark and C. Anselme (1996). A dynamic model for predicting fouling effects during the ultrafiltration of a groundwater. *J. Membr. Sci.* **185**(2), 185–204.

Wiesner, M. R. and S. Chellam (1999). The promise of membrane technology. *Environ. Sci. Technol.* **33**(17), 360 A–366 A.

Wiesner, M. R., M. M. Clark and J. Mallevialle (1989). Membrane filtration of coagulated suspensions. *J. Environ. Eng.-ASCE* **115**(1), 20–40.

World Health Organization (2006). Guidelines for Drinking Water Quality (3rd edition). Internet: http://www.who.int/.

Wyn-Jones, A. P. and J. Sellwood (2001). Enteric viruses in the aquatic environment. *J. Appl. Microbiol.* **91**(6), 945–962.

Yoon, S. H., C. H. Lee, K. J. Kim and A. G. Fane (1998). Effect of calcium ion on the fouling of nanofilter by humic acid in drinking water production. *Water Res.* **32**(7), 2180–2186.

Yuan, W. and A. L. Zydney (1999*a*). Effects of solution environment on humic acid fouling during microfiltration. *Desalination* **122**(1), 63–76.

Yuan, W. and A. L. Zydney (1999*b*). Humic acid fouling during microfiltration. *J. Membr. Sci.* **157**(1), 1–12.

Zenon (2005). Personal communication.

Zouboulis, A. I. and G. Traskas (2005). Comparable evaluation of various commercially available aluminium-based coagulants for the treatment of surface water and for the post-treatment of urban wastewater. *J. Chem. Technol. Biotechnol.* **80**(10), 1136–1147.

Ødegaard, H., B. Eikebrokk and R. Storhaug (1999). Processes for the removal of humic substances from water - an overview based on Norwegian experiences. *Water Sci. Technol.* **40**(9), 37–46.